BARRIER AVOIDANCE CONTROL FOR HIGH-ORDER SYSTEM WITH COMPLEX STATE CONSTRAINTS AND ITS APPLICATION TO DOWN-HOLE DRILLING

A Dissertation

by

TIAN, DONGZUO

Submitted to the Graduate and Professional School of
Texas A&M University
in partial fulfillment of the requirements for the degree of

DOCTOR OF PHILOSOPHY

Chair of Committee,	Xingyong Song
Committee Members,	Prabhakar Pagilla
	Bryan Rasmussen
	Wei Zhan
Head of Department,	Andreas Polycarpou

December 2021

Major Subject: Mechanical Engineering

ABSTRACT

This thesis investigates a novel state-constrained control technique, namely 'Barrier Avoidance Control', that can be applied to a high-order system to address state barriers of complex shape, and then applies this control method to a downhole drilling system to avoid drilling at undesired operating conditions.

Drilling is one of the most critical processes in the exploration and production of shale oil & gas, enhanced geothermal energy, and minerals. Control of the drilling process is challenging due to the underactuated feature of a long drill string, large uncertainty in the downhole environments, and the nonlinear and nonsmooth nature of the bit-rock interaction that can cause severe vibrations. These harmful vibrations, such as stick-slip and bit bouncing, will be largely exacerbated if not properly controlled, since the oscillation will be transported by the wave propagation and reflection along the drill string. In addition, the tendencies of using directional/horizontal wells with deeper and more complex drilling environments further complicate the drilling control. The coupling of vibration modes in the directional/horizontal drilling can make certain regions in the state space, which correspond to particular working conditions, undesirable in the drilling operation. Thus, drilling process needs to avoid these undesired regimes, so as not to experience slow drilling rate, significant vibration, safety problems, and drilling system failure. State barrier avoidance is not only necessary for the steady state, but is also critical during control transients.

In this thesis, we will introduce the state barrier avoidance control theories to keep the system states away from the undesired state regime in both steady state and transients. Since existing methods on state barrier avoidance control cannot be directly applied to directional drilling applications, therefore, a novel barrier avoidance method is proposed, which can be applied to high-order systems and address state barriers with complex shapes. This new control method is then applied to directional drilling, whose effectiveness is demonstrated through both simulation and experimental results.

Here, the logic flow of this thesis is organized as follows: 1) Firstly, one of the most commonly

used state-constrained control methods, namely the integral barrier Lyapunov function based control, is applied to the drilling control. The dynamic model contains a lumped-parameter drill string model and a bit-rock interaction governed by a delay-differential equation. A customized model transformation is employed to enable the barrier control design. However, it is found that this method can be applied to a system described by a lower-order model such as the vertical drilling scenario, but it is hard to be implemented to the higher-order model that is suitable for directional drilling. 2) Because of this, we propose a novel barrier avoidance control scheme, where a diffeomorphic transformation projects the constrained region in the original space into a radially large region in the new space, and converts the state-constrained control problem into a nonconstrained problem. The method can offer large flexibility in the barrier avoidance control design, and thus is more promising to address control of a higher-order control system. 3) As the empirical results of the field tests show the desired operating zone of the drilling inherently behaves in a complex shape, the corresponding state constraint can be found in a complex barrier region. However, none of the existing studies on barrier avoidance control investigates the complex barrier case. Therefore, a new method is proposed to address the complex state constraints based on the transformation-based barrier avoidance framework. The method is then applied to the directional drilling control, and its effectiveness is evaluated through comprehensive simulation results. 4) Finally, we validate the state-constrained drilling control in an experimental study in a hardware-in-the-loop framework, which contains a lab-scale drill rig with a real size polycrystalline diamond compact bit, and drill string simulation in a real-time environment. The experiment setup captures severe vibration modes through the contact of the drill bit to the rock sample. The barrier avoidance control is next applied to this lab-scale drill rig testbed. The testing results validate the effectiveness and robustness of the proposed state-constrained controller, providing proof of implementing this barrier avoidance control technique to full-scale drill rigs in the field.

DEDICATION

To my family and friends, my greatest support.

ACKNOWLEDGMENTS

Foremost, I would like to express my sincere gratitude to my advisor Professor Xingyong Song for the continuous support of my Ph.D.'s study and research, for his patience, motivation, enthusiasm, and immense knowledge. He helps me in all the time of research and writing of this thesis. His wisdom ignites my mind and broadens my views. Only with his advice and guidance that I can go so far in my field of study.

Besides my advisor, I would like to thank the rest of my thesis committee: Professor Prabhakar Pagilla, Professor Bryan Rasmussen, and Professor Wei Zhan, for your insightful comments, and hard questions.

My sincere thanks also go to my labmates, Chong Ke, Zihang Zhang, Abhishek Paramasivan, Masood Ghasemi, Mohammadali Kargar, Sai Sudeep Reddy, and Tohid Sardarmehni. I will always remember the days that we worked together and shared our happiness and sorrowfulness. Moreover, I shall thank my dear girlfriend Xiaoqian Jia. You are the shine in my life, and your care and support help me get through those tough days and finish my thesis in such good manners

Last but not least, I would like to thank my family: my parents Xia Wang and Qiang Tian, for giving birth to me in the first place and supporting me spiritually throughout my life.

CONTRIBUTORS AND FUNDING SOURCES

Contributors

This work was supported by a thesis (or) dissertation committee consisting of Prof. Xingyong Song, Prof. Prabhakar Pagilla and Prof. Bryan Rasmussen of the Department of Mechanical Engineering and Prof. Wei Zhan of the Department of Engineering Technology and Industrial Distribution.

All other work conducted for the thesis (or) dissertation was completed by the student independently.

Funding Sources

Graduate study was partially supported by the National Academy of Sciences (NAS) GRP Early Career Research Fellow Award and American Chemical Society PRF Doctoral Young Investigator Award.

NOMENCLATURE

BHA	Bottom Hole Assembly
LWD	Logging While Drilling
MWD	Measurement While Drilling
MPT	Mud Pulse Telemetry
PDC	Polycrystalline Diamond Compact
DoC	Depth-of-Cut
RPM	Revolutions Per Minute
ROP	Rate of Penetration
WOB	Weight-on-Bit
BLF	Barrier Lyapunov Function
iBLF	Integral Barrier Lyapunov Function
MPC	Model Predictive Control
CLBF	Control Lyapunov-Barrier Function
NN	Neural Network
DDE	Delay Differential Equation
EID	Equivalent Input Disturbance
PDE	Partial Differential Equation
SMC	Sliding Mode Control
LHP	Left Half Plane
BIBO	Bounded-Input-Bounded-Output
QLF	Quadratic Lyapunov Function
DOF	Degree-of-Freedom

LPV	Linear Parameter Varying
LMI	Linear Matrix Inequality
RA	Region of Attraction
EGS	Enhanced Geothermal System
HIL	Hardware-in-the-Loop

TABLE OF CONTENTS

Page

LIST OF FIGURES

FIGURE Page

LIST OF TABLES

TABLE Page

1. INTRODUCTION AND LITERATURE REVIEW

1.1 Background

Drilling is a cutting process that uses a drill bit to cut a hole of circular cross-section in solid materials. Commonly, the use of a large-scale drilling system in the field is to extract natural resources, such as water, oil, natural gas, mineral resources, and geothermal energy. In history, the first oil well in record is back to AD 347 in China, and these wells were up to 800 feet deep, where a drill bit is attached to the bamboo poles to produce salt with a byproduct of oil [2, 3]. In the following few centuries, petroleum and natural gas had been explored and extracted in ancient China and Japan. It is until the mid-19th century that modern history began with the refining of paraffin from crude oil by a Scottish chemist James Young [4]. In the United States, the modern oil industry began in the year 1859 in Titusville, Pennsylvania, where the business man Edwin L. Drake drilled the first oil well in the documented history [5]. In the 20th century, the second industrial revolution accelerated the development of the oil and gas industry, which became the major supplier of energy due to the invention of the automobile and the establishment of the petrochemical industry [6].

In recent years, the exploration of natural gas, crude oil, and geothermal energy from shale formations has become a quickly expanding trend in onshore domestic energy resource exploration. The vast extraction of the new shale oil and gas reservoirs stimulates the drilling activity to a 25-year record high [7]. The predicted turning point of oil production level by Hubert Theory [8], and the increasing needs of crude oil and gas for energy consumption, chemical industries, fertilizers, and plastics, have accelerated the development of down-hole extraction technologies. Because of the unconventional geological environment and the deep formation of the shale, the shale energy resource has not been fully investigated and explored until three decades ago. Currently, as the revolution of the directional/horizontal drilling and hydraulic fracturing technology, the energy resources at the shale formation become available. Nevertheless, due to the price-oriented market

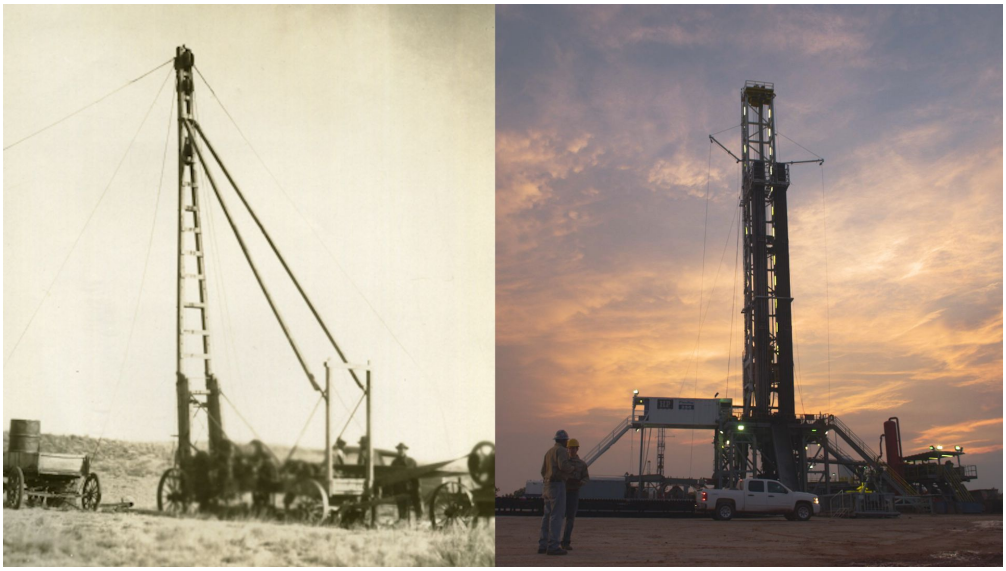

Figure 1.1: Historical and modern drilling rigs

and the complex down-hole environment, the challenges and uncertainties still remain in the exploration of shale energy resources. Therefore, a robust and reliable drilling operation is critical in this field, which attracts a surge of research studies.

To better understand the problem and challenges of down-hole drilling, the schematic of a typical drilling rig is depicted in Fig. 1.2, in which a full scale drilling system consists of the following components:

1) **Power system**: To carry out the drilling work, a power system provides all the necessary power for drawworks, mud pumps, and rotary table. Usually, the local combustion generators are installed to generate power from diesel engines. A normal drilling rig requires 1000-3000 horsepower to maintain the drilling operation. The energy efficiency of the system can be largely affected by the temperature and the down-hole environment.

2) **Hoisting and rotary system**: At the top drive, hoisting system can lift and lower the drill pipe and casing to complete the well, through the operation of draw works, derrick, tackle & block, and dead line anchor. The rotary system drives the pipe & bit rotation, consisting of

swivel, kelly, rotary drive, and rotary table. The draw works and rotary drive are typically using high-voltage AC induction motors.

3) **Drill pipe and casing**: Drill pipes are durable steel pipes that conduct the force to the drill bit. Multiple sections of drill pipes are screwed together to assemble the main body of the drill string. The outer tube is called casing that stablizes the wellbore. Casing can protect the layers of soil and prevent all the groundwater from being contaminated by the drilling mud and fraction fluids.

4) **Bottom hole assembly and drill bit**: Bottom hole assembly (BHA) is the lowest part of the drill string that attaches the drill bit to the drill pipe. The assembly includes drill collars, stabilizers, reamers, shocks, and hole-openers. The logging while drilling (LWD) / measurement while drilling (MWD) tools for formation evaluation are usually installed as parts of BHA. The drill bit contacts and breaks the rock formation at the bottom wellbore. Two types of the drill bits are commonly in use: a roller cutter bit to crush the formation, and a fixed cutter bit to scrape the formation using polycrystalline diamond cutter (PDC). The PDC bit can provide higher rate of penetration (ROP) but is less durable than a roller cutter bit.

5) **Circulating system**: The mud pump will circulate the drilling mud from a mud reservior called mud pit, to the bottom well. The drilling mud is able to lubricate and cool the drill bit and bring the rock cuttings to the surface through the annulus between drill pipe and the wall. This mud can also carry the MWD information to the surface through the mud pulse telemetry (MPT) technique.

6) **Well control & monitoring system**: Due to the extremely high pressure of the reservior (can be several thousand psi) and the potential danger that it can cause, the well control & monitoring system such as blowout preventer must be installed at the top of the wellbore. If there is a sudden pressure change in the well that pushes the formation fluid up to the surface, blowout preventer will be closed and seal the well from blowout.

1.2 Motivation and Current Research Trends

With the emergence of shale oil and gas and growing energy exploration in both onshore and offshore, the drilling operation is becoming increasingly challenging. Given the needs for drilling deeper wells in more complex downhole geological environments, accurate modeling and reliable steering are highly demanded to increase the ROP while reducing the abnormal drilling conditions. Due to the improper mechanical design and the inaccurate control strategy, severe vibrations can arise and spread along the whole drill string, which will result in damage to the drilling tools, especially on the drill bit. The replacement of the drill bit can be costly and require a full stop of the overall operation, which largely increases the down-time. For a more complex system such as a large scale directional/horizontal drilling setting, the conventional drilling operation relying solely on the human driller's experience is likely to result in drilling failure. Thus, a fully/semi automatical drilling control with advanced control technology is highly desired in the modern down-hole drilling system.

This motivates recent trends of drilling research on: 1) the modeling of the drill string and bit-rock interaction, 2) the analysis of the significant downhole vibrations, 3) advanced real-time control of the drilling system to mitigate these harmful vibrations, to keep track of the pre-defined drilling trajectory, and to enhance the production safety.

1.2.1 Modeling of the Drilling System Dynamics

As shown schematicly in Fig. 1.2, the drilling process has several unique features that distinguish its dynamics from other mechanical operations.

a) **Large axial-to-radius ratio of the drill string**: The drill string can be over ten thousand feet long from the ground to the bottom of the wellbore, while the diameter of the drill pipe is usually less than 10 inches.

b) **Nonlinear and nonsmooth nature of the boundary condition**: The drill string can contact with wellbore at both drill pipe and drill bit. In particular, the major nonlinearities including bifurcations and periodic orbits will arise at the bottom end's bit-rock interaction.

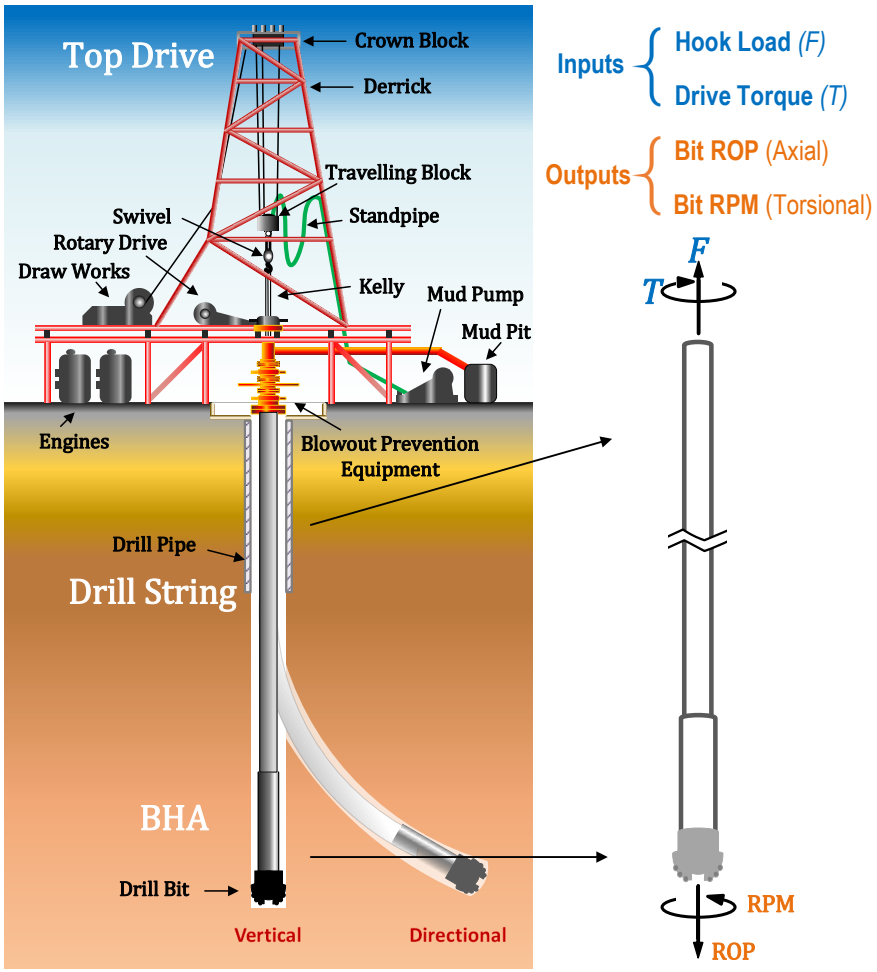

Figure 1.2: Schematic of a vertical/directional down-hole drilling system

c) **Highly underactuated dynamics**: Usually the actuation of a drilling system is only provided at the top drive. Due to the structural flexibility of the large scale drill string, the number of actuators/inputs is less than the degree-of-freedom (DOF).

Because of these features, the reasearch studies of drilling system's modeling mainly focus on the following two portions: modeling of the drill string and modeling of the drill bit.

1.2.1.1 Modeling of the Drill String

In many previous studies of the drilling string's modeling, only torsional dynamics are considered with a simplified system dynamics [9, 10, 11, 12]. In these studies, the model used for

the dynamic motion is only dependent on the torsional state variables and assumes a constant or averaging axial rate of penetration. As discussed in [13, 14, 15], the torsional and axial dynamics are indeed coupled, in particular, through the bit-rock interaction from the bottom wellbore. A thorough analysis is proposed in the same work, to precisely re-produce both axial and torsional vibrations using the coupled dynamics. Therefore, such a coupled rate-independent model can better describe the drilling system's behavior.

On the other hand, the lumped parameter system is widely used for the modeling of the down-hole drilling. The spring-mass-damper model is a classic type of model for a low order lumped parameter system. A low-dimention model with coupled axial-torsional dynamics was firstly proposed in [16, 17], and further modified into a dimensionless form in [18]. Due to the limited bandwidth of low-order model, a high-order spring-mass-damper model can better capture different dynamic modes in a large frequency range [19]. Furthermore, a finite-element-method (FEM) model can create a large number of the nodes to numerically solve differential equations using mathematical tools, providing more accurate results for a complex geometry of the drilling system, including the directional and horizontal settings with a curved drill string [20, 21, 22, 23, 24]. With the development of the powerful computational software, the FEM approach becomes available as a high-fidelity modeling tool in both academia research and commercial use.

1.2.1.2 Modeling of the Bit-rock Interaction

Some major harmful vibration modes, such as axial/torsional stick-slip, lateral out-of-balance whirl, and bit-bouncing, are induced by the bit-rock interaction. A well understanding of this interaction model is critical to the modeling and controls of the down-hole drilling. In the literature, limited to only considering the torsional dynamics, a number of studies use a simplified Coulomb friction models under empirical modifications for different operating scenarios [9, 10]. Even though these models can successfully simulate the stick-slip behavior, however, they fail to be extended to other types of vibration modes. Also, this type of model is only suitable for the a roller cutter bit instead of a PDC bit.

In order to capture different dynamic and vibration modes of the drilling process, a more accu-

rate bit-rock interaction model is needed. In this effort, the blade-rock cutting model considered both sharp and worn cutter's conditons is first proposed by [25, 26, 27], and later experimentally verified by [28]. The model is based on the depth-of-cut (DoC) of the drill bit blade, and can describe multiple phases of the drilling process. The delay differential equation (DDE) is introduced to such a model by [13, 15], to precisely capture the DoC using a coupled axial-torsional dynamics. The research [29, 30, 31] further expand the blade-rock cutting model to a more complex scheme, where axial, torsional, and lateral motions are all considered. This approach can generate axial/torsional stick-slip, lateral out-of-balance whirl, and bit-bouncing behaviors.

1.2.2 Vibration Suppression of the Drilling Process

Due to improper bit selection and intricate wellbore conditions, different types of harmful vibrations can occur, including bit-bouncing, axial/torsional stick-slip phenomenon, and lateral out-of-balance whirl motion. These vibrations, especially emerging at the BHA, are excited by the bit–rock interactions, mud hydrodynamics and BHA eccentricity, and will transport throughout the entire drill string, which can increase drilling power consumption, reduce efficiency of drilling process, and even cause drilling failure due to fatigue. For example, severe oscillations can damage the PDC bit, and the replacement of a new PDC bit requires a complete stop of the drilling operation, which increases the time and labor cost. In most drilling systems, the actuators generating axial force and torsional torque are located at the top drive on the surface. Since the length of drill string connecting the top drive and the BHA can be over several thousand feet that results in relatively low effective stiffness and underactuation, the prevention of these severe oscillation modes becomes challenging. The vibration suppresion of the drilling process can be divided into two major categries, including passtive vibration suppression and active vibration suppression. The passive suppression method is grouped into three approaches, i.e. bit selection and redesign, optimization of the BHA, and the use of downhole tools [32], and these mechanical/structural designs need to be implemented before the drilling operation. To ensure the safety and performance during the drilling operation, the active suppression method, i.e., the control system design, is required. Next, some state-of-the-art studies for the active drilling control are listed as follows.

1.2.2.1 Linear Control Design

The linear control techniques for the drilling dynamics usually have lower computation cost and can be directly implemented to the field tests due to their robustness. Since the bit-rock interaction and the drill pipe-wellbore contact are inherently nonlinear, the implemtation of the linear controller will require one of the three oprerations: linearization of the system, cancelling of the nonlinear term, or regarding the nonlinear term as uncertainties.

In the literature, the linear control design for a drilling sytem includes, but not limits to: Jansen and Steen (1995) used frequency analysis to increase the resultant damping force through the tuning of the actuation motor [33]. Serrarens et al. (1998) developed an H_∞-contoller to mitigate torsional vibrations in a scaled experimental setup [34]. Karkoub et al. (2010) applied the μ-synthesis method to attenuate the model uncertainty and down-hole disturbance [35]. Harris, Açıkmese, and Oort (2014) introduced an linear matrix inequality (LMI) based approach to reject the disturbance with input constaints [36]. Ke and Song (2019) proposed an equivalent input disturbance (EID) method for the distributed parameter system derived from partial differential equations (PDE) [37]. Nessjoen et al. (2011) implemented the PI controller by modeling the torsional dynamics as a transmission line model [38].

1.2.2.2 Nonlinear Control Design

The nonlinear control methods for the drilling dynamics need a higher computation cost and a more accurate modeling. For the practical point of view, due to the great complexity of the nonlinear model, the nonlinear controller usually requires the real-time steering within a shorter time step. With the increasing computation capability of the embedded controller for industrial use, the nonlinear control for a more complex drilling dynamics becomes available.

In the literature, the nonlinear control design for a drilling sytem includes, but not limits to: Navarro-López and Licéaga-Castro (2009) introduced the sliding mode control (SMC) to the torsional dynamics, while addressing the non-smoothness of the bit-rock contact through the choice of a sliding surface [10]. Ghasemi and Song (2017) extended the use of SMC to a coupled axial-

torsional dynamics with the full state feedback [39]. Abdulgalil and Siguerdidjane (2005) applied the backstepping approach to the drilling system for the first time [40]. A hybrid backstepping sliding mode controller is implemented in the drilling process by Mendil, Kidouche and Doghmane (2021), with the comparison of using a backstepping or sliding mode controller solely [41]. Numerical solvers are also combined with the drilling control, through the genetic algorithm based control (Karkoub, Abdel-Magid and Balachandran 2009) [42], and dynamics programming method (Feng, Zhang and Chen 2017) [43].

1.3 Research Objectives and Literature Survey on Barrier Avoidance Control

Many advanced control techniques has been successfully implemented to the down-hole drilling system, as discussed in Section 1.2.2. However, these control methodologies either just fulfill the stability in the local sense using nonlinear control/linearization techniques, or regard the nonlinear bit-rock reaction terms as disturbances. Since the undesired vibrations' mechanics are not captured or modeled in these existing control approaches, the harmful oscillations can still occur during the transients. On the other hand, the bit-rock interaction models to characterize these harmful vibrations can be complex and highly nonlinear. The existing control techniques are limited to address such intricated nonlinearities. These factors let the control design for the drilling system become a non-trivial task. Therefore, we pose the main objective in this study:

Use active control design to stablize the down-hole drilling system while ensuring the mitigation of severe vibration modes.

For the above research objective of this thesis, we will inquire into applying the constrained control method to the drilling process. Since the harmful oscillation modes are more likely to occur in the non-optimal working regimes in the drilling process [1, 32] (as shown in Fig. 1.3), the control with state constraints are critical and can ensure safety and smooth operations. For example, for torsional/axial stick-slip behavior, the stick phase can only occur when the bit's velocity falls to zero, and thus a constraint ensuring the bit velocity always be greater than zero will prevent the stick phase and the damaging vibrations.

In the literature, a number of the well-known studies on the constrained control subject have

been proposed. Model predictive control (MPC) can be used to constrain states, but it requires solving a nonlinear numerical optimization in real-time [44, 45]. Studies [46, 47] used a reference governor method by modulating the control reference, but constantly changing the reference is not always allowed and it also requires numerically solving a nonlinear optimization online. A control Lyapunov-barrier function (CLBF) based method was introduced in [48]. However, finding such a function, that not only requires a level set to cover the barrier region but also contains an attractive basin, can be very difficult for practical systems. Recently, as being first introduced in [49] and further extended by [50, 51, 52, 53, 54], the barrier Lyapunov function (BLF) based method has been introduced in solving the constrained control porblem, which embeds an extra term in the original Lyapunov function. Such a function yields a value that approaches infinity whenever the state approaches the boundary, and thus can keep the state from entering the undesired regime.

In the past decade, the BLF based approaches have been intensively studied in the literature, including application to a Neural Network (NN) control [55], a switched system [56], a pure-feedback system [57], and an unknown control direction system [58]. Besides, the BLF has been implemented to a number of physical systems, such as attitude tracking control of multiple space-crafts [59], positioning control of a flexible crane system [60], boundary control for a flexible marine riser with vessel dynamics [61], and vibration mitigation of a down-hole drilling system via active control [62]. However, many times, finding a stabilizing controller with a BLF can be challenging, since the control design is based on a Lyapunov function of a specific form containing the high magnitude barrier term. Thus, most control design using BLF in literature [50, 51, 53] is carried out for systems in strict feedback forms using a backstepping-based approach (This way the barrier for each state can be addressed one by one, making it more promising to find a feasible solution). Nevertheless, this limits the type of systems in which this BLF method can be applied.

In this work, we will apply the BLF approach in the downhole drilling system first, and then establish a novel state-constrained control method called barrier avoidance control, that can tackle the limitations of using the BLF. The research objectives are then given as:

i) We will first implement the BLF approach into a drilling system with a low DOF drill string

model. Since the BLF requires a strict feedback form, a state transformation of the drilling's dynamic model is first investigated. Besides, the state-dependent delay in the bit-rock interaction model is taken into account. Due to the lack of well-established studies on this state-dependent delay, we will explore an advanced control method to address this issue.

ii) The BLF approach has several limitations. For the drilling system, especially, the high-order lumped-parameter drill string model cannot be transformed into a strict feedback form, which is not suitable for the BLF design. Thus, we aim to find a novel state-constrained control method that can break the barrier of this limitation. This way, the state-constrained control becomes available for a high DOF drill string model.

iii) As depicted in Fig. 1.3, the optimum operating region of the drilling process has a complex shape in bit's axial and torsional dimensions. Most efforts in state-constrained control only consider a hyperrectangle shape, and a study that can explicitly address the complex state constraints is still limited. We will develope a systematic way to exceed this limitation and remove the conservativeness of the drilling control.

iv) Since the directional drilling requires a high-order system model, we adopt the FEM model for the drill string's dynamics. Unlike vertical drilling, the drill string of a directional drilling system not only contacts the bottom wellbore, but also interacts with a drill pipes along the string. This interaction can be highly nonlinear, resulting in a great complexity in the nonlinear control design. In this work, we aim to perform a custermized model order reduction for the directional driling to enable the feedback control design.

v) Due to the extermely large size of a full-size drill rig, it is not feasible to directly accommodate an actual testbed to any facilities. As a remedy, the hardware-in-the-loop (HIL) provides a platform that can replace a portion of the physical system with real-time simulations, and this way the actual drill rig can be converted into a size that fits into a lab environment. This will enable the commissioning of our constrained control technique into a close-to-real drilling process.

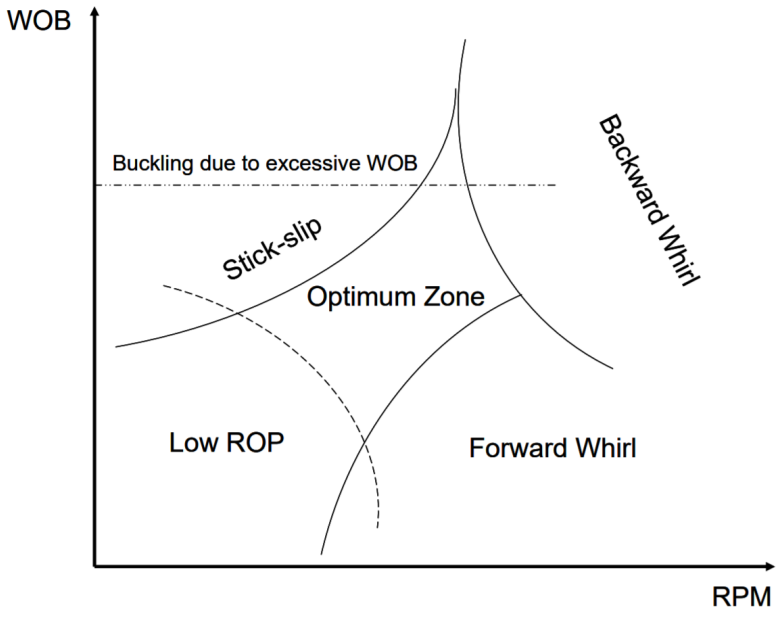

Figure 1.3: Schematic delineation of optimum zone (reprinted with permission) [1]

1.4 Dissertation Organization and Overview

In summary, this thesis proposes the dynamics analysis, system modeling and control design of a downhole drilling system, and also presents a new state-constrained control synthesis approach for general nonlinear systems. Firstly, the iBLF based method is implemented to a low DOF lumped parameter drilling system dynamics model in Chapter 2, to mitigate the harmful vibrations. Chapter 3 investigates a novel state-barrier avoidance control techniques based on diffeomorphic transformation theoretically. This approach largely extends the choice of nonlinear control strategies for a state-constrained control problem. Due to the limitation of the hyperrectangle shape of the state-barriers in the previous efforts, Chapter 4 comes up with a systematic way to address the complex state constraints using the novel barrier avoidance control scheme. Following this guideline, Chapter 5 applies the barrier avoidance based LPV method to a high-order FEM model of a directional drilling system, considering a empirical state constraints of the bit's motion in a complex shape. Finally, Chapter 6 presents a experimental drill rig in a HIL platform, and

validates the proposed contrained control techniques for active vibration mitigation purpose.

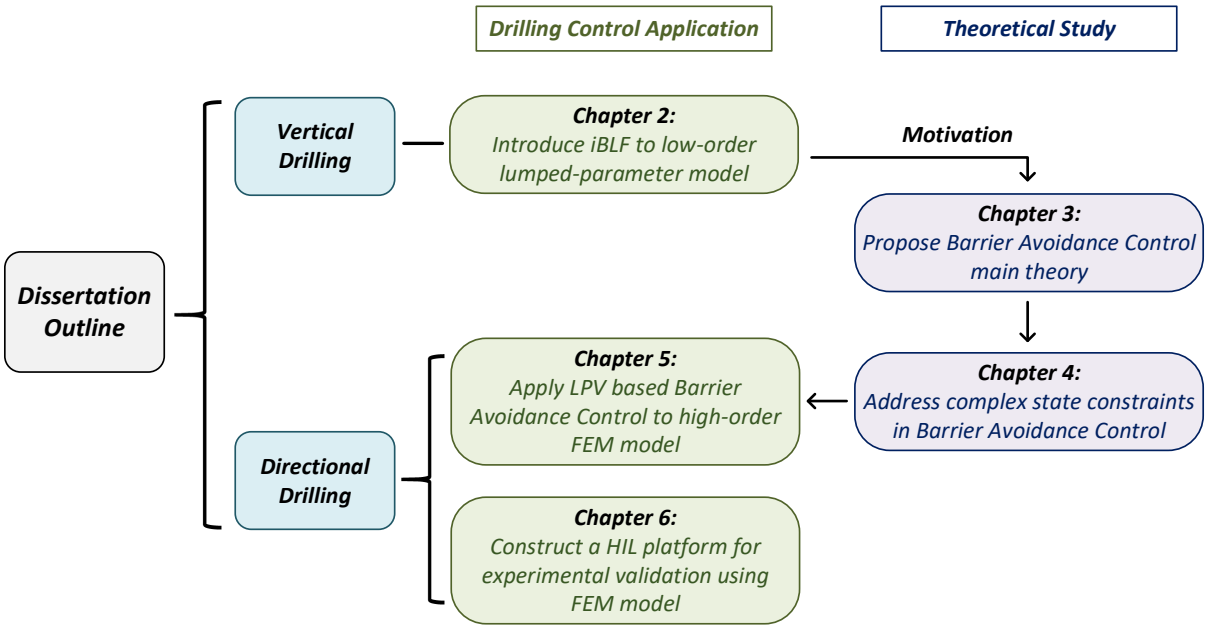

Figure 1.4: Dissertation structure

The outline and structure of the dissertation is shown in Fig. 1.4, and the organization of the thesis will be presented in detailed as follows.

1.4.1 Chapter 2

In this chapter, the integral type BLF based control method is introduced to a vertical downhole drilling system for the vibration elimination. Because of complex downhole environments and underactuated, nonlinear, and nonsmooth features of the drilling dynamics, control synthesis of the drilling system is a challenging task. In this section, we propose a novel nonlinear control design for set-point tracking of the torsional velocity and axial rate of penetration, for a vertical drilling system with coupled axial and torsional dynamics and a velocity-independent bit-rock interaction model. To eliminate damaging oscillations such as stick-slip, the barrier function is introduced in the Lyapunov candidate to ensure smooth motion of the drill bit, and to avoid having drilling

operate in undesired working conditions. Meanwhile, the stability, boundedness and convergence properties with respect to system states are proved. To this end, simulation results of case studies are given to evaluate the efficacy and robustness of the proposed control approach.

1.4.2 Chapter 3

In this chapter, we propose the state barrier avoidance control methodology using a diffeomorphic transformation based approach. In previous studies, BLF method is oftentimes embedded in a backstepping scheme, which greatly limits the flexibility to choose other nonlinear techniques. Instead, this section presents a novel design method for state constrained control problem in a state space. This is achieved through a diffeomorphic transformation, which projects the constrained region in the original space into a radially large region in the new space. By this transformation, the state-constrained control problem is converted into a non-constrained problem, and thus significantly increases the flexibility of the control design options compared with existing state-constrained control methods. Three case studies including sliding mode control, backstepping control, and LPV control are given at the end to demonstrate the effectiveness of the proposed method.

1.4.3 Chapter 4

In this chapter, for the state-constrained control problem with complex barrier regions, we present an effective construction method of the state transformation for the barrier avoidance control design. The diffeomorphic transformation in barrier avoidance control converts a constrained control problem into an unconstrained one, and enables the nonlinear control design in the new coordinates. However, a systematic way to construct such a transformation under a non-hyperrectangular barrier shape has never been explored in the literature. This chapter provides a guideline to choose this diffeomorphic transformation in a cascade manner for a class of complex barrier regions. In the case studies, the proposed method is applied to a high-order double integrator system using sliding mode control, and also to a uncertain strict-feedback system using adaptive backstepping control.

1.4.4 Chapter 5

In this chapter, we investigate a setpoint tracking problem of a downhole directional drilling process via a nonlinear state constrained control approach, for the objective of vibration mitigation using active control. The coupled dynamics of axial and torsional dimensions are incorporated in the FEM based drill string model together with a velocity-independent bit-rock interaction model. A model order reduction is performed for the drill string model to ensure the controlliablity, and enables the control design for its error dynamics. With the undesired region of the drilling formulated into the state constraints, the state barrier avoidance control technique embeds these constraints into the LPV plant of the drilling system, to prevent the severe vibrations under feedback control. The simulation results are provided at the end to evaluate the efficacy of the proposed algorithm, through the comparison and analysis of different case studies.

1.4.5 Chapter 6

In this chapter, we formulate a HIL experimental testbed for a full-scale down-hole drilling system, including a physical BHA and a real-time simulation of the drill string model. The physical BHA consists of motion sensors that collects the measurements of the bit, and a real PDC bit in contact with the rock sample. The drill string model is programmed in an embedded environment using a FEM model in the simulation. The integration of these two subsystems enables the feedback control design, using system identification for an accurate system dynamic model and an observer for the real-time state estimation. The barrier avoidance controller is combined with a H_∞ based LPV method, to tolerate the disturbances from the bit-rock interaction. The experimental results prove the fidelity of the proposed algorithm, through a series of performance tests using both open-loop and closed-loop control.

2. CONTROL OF A VERTICAL DOWNHOLE DRILLING SYSTEM USING AN INTEGRAL BARRIER LYAPUNOV FUNCTION BASED METHOD

2.1 Introduction

Drilling is one of the most critical processes for wellbore creation and downhole energy extraction in the field of oil & gas production. As depicted in Fig. 2.1, the drilling system is of a very large scale (can be over 10000 feet) with a complex nonlinear boundary condition on the drill bit. Due to improper bit selection and intricate wellbore conditions, different types of harmful vibrations can occur, including torsional and axial stick-slip phenomenon, and lateral out-of-balance whirl motion. These vibrations, especially emerging at the bottom-hole assembly (BHA), will transport throughout the entire drill string, which can increase drilling power consumption, reduce efficiency of drilling process, and even cause drilling failure due to fatigue. In most drilling systems, the actuators generating axial force and torsional torque are located at the top drive on the surface. Since the drill string connecting the top drive and the BHA can be thousands of feet long, which results in relatively low effective stiffness, the control design becomes challenging. Thus, increasing attentions have been paid to modeling of the drill string and bit-rock interaction, analysis of the stick-slip behavior and other vibrations, and control to mitigate these harmful vibrations.

Most existing studies on drilling control only focus on control of the torsional dynamics [9, 10, 11, 12]. However, as pointed out [25, 28, 14, 13, 15], the torsional and axial dynamics of the drilling system are coupled due to the complex bit-rock interaction, and the control should indeed consider both dimensions together in the design. In this chapter, we will address the drilling control for both torsional and axial dynamics based on the coupled dynamics model. One critical control objective is to have drilling avoid undesired operating conditions such as stick-slip, where the drill bit can get stuck and then suddenly accelerate to a high speed. Operating at those conditions can result in failure mode for drilling and deteriorate the drilling rate. Most existing studies on the

feedback control design to mitigate the vibration are achieved by just tracking a pre-defined reference, and assume that stick-slip can be prevented if the reference is tracked. This includes, but not limits to, sliding mode control [10], backstepping control [40], equivalent input disturbance based control [63], genetic algorithm based control [42] and dynamics programming method [43], etc. However, these control methodologies either just fulfill the stability in the local sense using nonlinear control/linearization techniques, or regard the nonlinear bit-rock reaction terms as disturbances. During the tracking transient and also when having disturbance, stick-slip can still occur, which will make the drilling dynamics highly nonlinear and complex. A method that can explicitly prevent drilling control from falling into those undesired operating modes is critical but was not researched before. In this chapter, we will resolve this problem by embedding the operating constraints into the control design using an integral Barrier Lyapunov Function (iBLF) approach [53], so the dynamical states can be ensured to avoid those undesired operating regimes when the control is active.

The main contributions of this study are in twofold. First, a state transformation of error states is applied to the drilling system, and the system states are converted into internal and external parts. A strict feedback form is obtained for the external dynamics to allow the backstepping based iBLF control design. A sufficient condition for the control design is given to ensure asymptotical stability of the external dynamics. For the internal states, we prove the boundedness and convergence properties instead of asymptotic stability, due to the limitation imposed by a nonlinear time-delayed model description of the bit-rock interaction. The second contribution is that we directly investigate the nonlinear bit-rock interaction described by a delay differential equation (DDE) with a state-dependent delay in the control design without any approximations. In the literature, theoretical analysis on the state-dependent delay in such a model is limited. In [15], the model with state-dependent delay is converted into a linearized model with a constant delay to enable control design, but it is sensitive to variation of the operating point. Other studies address this issue using an approximation of the depth-of-cut (DoC) model [64], which is only valid when having a relatively high torsional velocity. In this chapter, by using a state transformation, we obtain the exact upper

and lower bounds of the terms with state-dependent delays in the bit-rock interaction model. The bounds are then explicitly incorporated into the control design through a discontinuous term and no approximations are needed.

The outline of this chapter is as follows. In Section 2.2, the drilling system dynamics model and the boundary conditions are discussed, and the error dynamics for this model is derived. Section 2.3 exhibits the internal and external dynamics through model transformation, and then presents the control design using an integral Barrier Lyapunov Function to eliminate the stick-slip behavior, where asymptotic stability, boundedness and convergent properties for the corresponding system states are shown. Finally, simulation results are presented in Section 2.4.

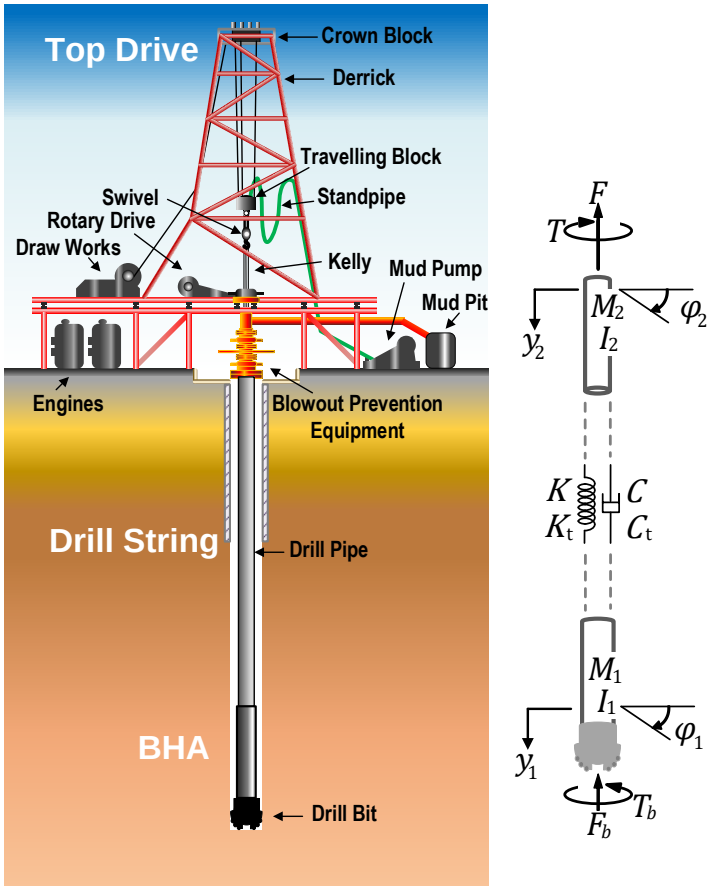

Figure 2.1: Drill string schematic

2.2 Dynamics Model of Vertical Drilling System

The critical dynamics typically considered in a vertical down-hole drilling system are torsional and axial dynamics. We present a lumped-parameter drilling system dynamics model based on [15]. In this model, the axial and torsional dynamics are coupled through the boundary condition, i.e., the bit-rock interaction. We introduce the model of drill string and bit-rock interaction respectively, and provide the error dynamics in the following sub-sections.

2.2.1 Model of Drill String

In the previous studies, different approaches for the modeling of the drilling system have been proposed [20]. Among them, the low order lumped-parameter models are widely used for control design, comparing with other models such as the higher-order lumped-parameter model [9] and the distributed parameter model with neutral type time delay [65, 66]. Discussed in [67], the low-order lumped-parameter model can perform similar numerical behavior in the dominant modes compared with a more complex finite-element model for a vertical drilling system. Thus, in this chapter, a lumped parameter model is used for the vertical drilling system, as depicted in Fig. 2.1. Here, a top rotatory drive and an axial motor are used to provide the control inputs of torsional torque and axial force. A long drill string transmits power from surface to the down-hole bit. The polycrystalline diamond compact (PDC) drill bit at the bottom end of the BHA has direct contact with the rock. In the modeling, we mainly consider two portions: the lower portion of the drill string and the BHA, the top drive and the upper drill string, whose masses and inertias are denoted by M_1, M_2 and I_1, I_2 as shown in Fig. 2.1. For the axial dynamics, the stiffness and damping coefficients between the two portions are modeled as K and C, and for the torsional dynamics we denote the stiffness and damping coefficients as K_t and C_t. The hook load F and the torsional driving torque T are employed on the top drive. Besides, the bit-rock interaction on the bottom end has high nonlinearity, and endures the reaction force F_b and torque T_b on the bit, coupling the axial and torsional dynamics. It is worth noting that, the friction between drill string and the wellbore is negligible, compared with other forces [39]. Therefore, we have equations of motion for the drill

string as

$$
\begin{aligned}
M_1\ddot{y}_1(t) =& C(\dot{y}_2(t) - \dot{y}_1(t)) + K(y_2(t) - y_1(t)) - F_b(t) + M_1 g \\
M_2\ddot{y}_2(t) =& -C(\dot{y}_2(t) - \dot{y}_1(t)) - K(y_2(t) - y_1(t)) - F(t) + M_2 g \\
I_1\ddot{\phi}_1(t) =& C_t(\dot{\phi}_2(t) - \dot{\phi}_1(t)) + K_t(\phi_2(t) - \phi_1(t)) - T_b(t) \\
I_2\ddot{\phi}_2(t) =& -C_t(\dot{\phi}_2(t) - \dot{\phi}_1(t)) - K_t(\phi_2(t) - \phi_1(t)) + T(t)
\end{aligned} \tag{2.1}
$$

where $y_i(t)$ and $\phi_i(t)$, $i = 1, 2$ are the axial and torsional displacements of M_i, $i = 1, 2$ respectively.

In this study, the objective is to have the bit axial velocity $\dot{y}_1(t)$ and torsional velocity $\dot{\phi}_1(t)$ track the desired constant velocities $v_d > 0$ and $\omega_d > 0$ respectively, and at the same time avoid undesired state regimes during operation. We first define the error states as

$$
\begin{aligned}
\chi_1(t) &\triangleq y_1(t) - y_{1d}(t), \quad \tilde{v}_1(t) \triangleq \dot{y}_1(t) - v_d \\
\chi_2(t) &\triangleq y_2(t) - y_{2d}(t), \quad \tilde{v}_2(t) \triangleq \dot{y}_2(t) - v_d \\
\theta_1(t) &\triangleq \phi_1(t) - \phi_{1d}(t), \quad \tilde{\omega}_1(t) \triangleq \dot{\phi}_1(t) - \omega_d \\
\theta_2(t) &\triangleq \phi_2(t) - \phi_{2d}(t), \quad \tilde{\omega}_2(t) \triangleq \dot{\phi}_2(t) - \omega_d
\end{aligned} \tag{2.2}
$$

where $y_{1d}(t)$, $y_{2d}(t)$ are the desired axial displacements for M_1, M_2, and $\phi_{1d}(t)$, $\phi_{2d}(t)$ are their desired torsional displacements, defined as

$$
\begin{aligned}
y_{1d}(t) &= y_{2d}(t) + \frac{M_1}{K} g - \frac{1}{K} F_{bd}, \quad y_{2d}(t) = v_d t \\
\phi_{1d}(t) &= \phi_{2d}(t) - \frac{1}{K_t} T_{bd}, \quad \phi_{2d}(t) = \omega_d t
\end{aligned} \tag{2.3}
$$

with $F_{bd} > 0$ as the desired force on the bit and $T_{bd} > 0$ as the desired torque on the bit, which can be calculated using the bit-rock interaction model in the next sub-section.

2.2.2 Model of Bit-rock Interaction

The boundary force and torque are determined by the bit-rock interaction between the drill bit and the bottom of the wellbore. This interaction forms a coupled dynamics between the axial and torsional dimensions [15], and has multiple regimes as shown in [28]. The torsional torque and axial force at the bit induced by the bit-rock interaction can be decomposed into two components as:

$$\begin{aligned} F_b &= F_f + F_c \\ T_b &= T_f + T_c \end{aligned} \tag{2.4}$$

where the subscripts 'f' and 'c' denote the frictional component and cutting component of the reaction, respectively. The friction component is introduced from the underside of contact between bit and rock, and its magnitude depends on a physical variable called depth-of-cut $D(t)$, which is the instantaneous depth of contact between the bit blade and the rock surface to be cut. It can be modeled as [15]

$$D(t) = n(y_1(t) - y_1(t - \tau(t))) \tag{2.5}$$

The depth-of-cut $D(t)$ depends on the current position of the blade and the rock profile cut by the previous blade, and n is the number of the blades. Here, $\tau(t)$ is a state-dependent delay, which describes the time interval between two successive blades reaching the same torsional position, as shown in Fig. 2.2. This delay $\tau(t)$ is constrained by

$$\frac{2\pi}{n} = \phi_1(t) - \phi_1(t - \tau(t)) \tag{2.6}$$

Definition 1. *For any state $\nu(t)$, we define the subscript τ for $\nu(t)$, as $\nu_\tau(t) \triangleq \nu(t - \tau(t))$.*

To express depth-of-cut $D(t)$ with the error state variables, we substitute $\chi_1(t)$, $\chi_{1\tau}(t)$, $\theta_1(t)$,

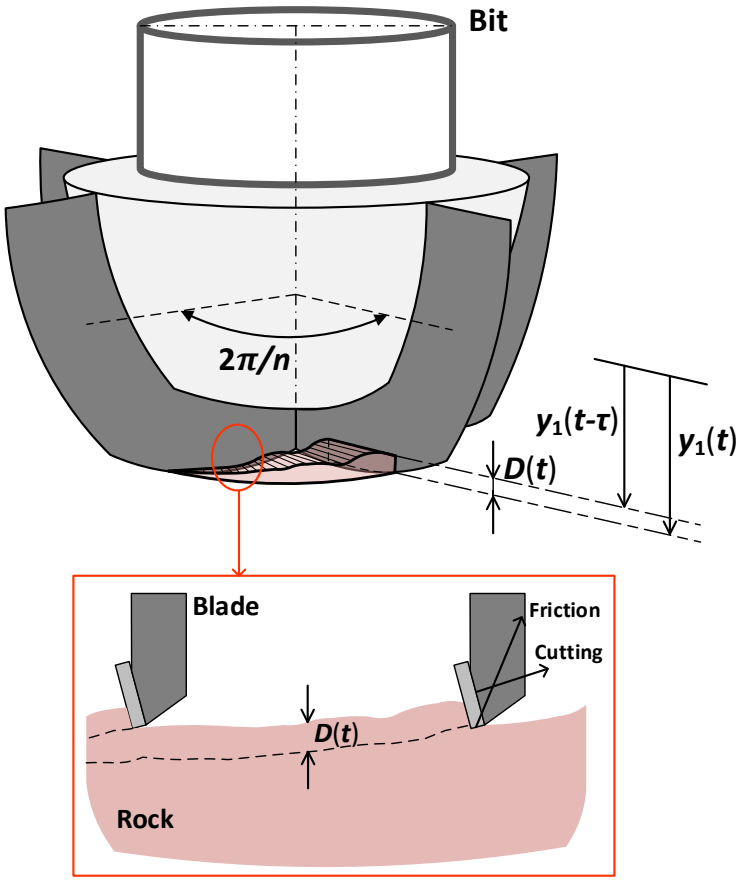

Figure 2.2: Bit-rock interaction model

$\theta_{1\tau}(t)$ into (2.5) and (2.6)

$$D(t) = n(\chi_1(t) - \chi_{1\tau}(t) + v_d\tau(t)), \tag{2.7}$$

$$\frac{2\pi}{n} = \theta_1(t) - \theta_{1\tau}(t) + \omega_d\tau(t) \tag{2.8}$$

Eliminating $\tau(t)$ in (2.7) and (2.8) gives

$$D(t) = 2\pi\frac{v_d}{\omega_d} + n(\chi_1(t) - \chi_{1\tau}(t)) - n\frac{v_d}{\omega_d}(\theta_1(t) - \theta_{1\tau}(t)) \tag{2.9}$$

In (2.9), if the error states $\chi_1(t)$, $\chi_{1\tau}(t)$, $\theta_1(t)$, $\theta_{1\tau}(t)$ are set to zero, we define the desired depth-

of-cut as

$$D_d \triangleq 2\pi \frac{v_d}{\omega_d} \tag{2.10}$$

Characterized by the value of the depth-of-cut, we consider two phases in bit-rock interaction as phase I and II. In **phase I**, the depth-of-cut $D(t)$ is small, while the increase of $D(t)$ affects both the cutting and frictional components. The length of the bit wear-flat is proportional to $D(t)$. We have the expressions of reaction force and torque as [28]

$$\begin{aligned} F_{b1}(t) &= a\sigma\kappa D(t) + a\zeta\vartheta D(t) \\ T_{b1}(t) &= \frac{1}{2}a^2\mu\gamma\sigma\kappa D(t) + \frac{1}{2}a^2\vartheta D(t) \end{aligned} \tag{2.11}$$

where F_{bi} and T_{bi} $i = 1, 2$ are the reaction force and torque in different phases, a denotes the radius of drill bit, σ is the maximum normal contact stress, κ represents the rate of variance of the contact length (typically a number in $[1, 10]$), ϑ accounts for the intrinsic specific energy required to remove a unit volume of rock, μ is the coefficient of friction at the wear-flat, γ represents the orientation and distribution of the contact forces on bit, and ζ is a characteristic number in $[0.5, 0.8]$.

In **phase II**, as the depth-of-cut $D(t)$ becomes larger and the friction component is fully mobilized, the contact force will not increase anymore and the variance of the cutting component becomes dominant correlating to the change of $D(t)$. Let F_b^* and T_b^* denote the reaction force and torque at the transition of the two phases, and we have D^* denote the depth-of-cut at this transition point. The reactions in this phase are given by

$$\begin{aligned} F_{b2}(t) &= F_b^* + a\zeta\vartheta(D(t) - D^*) \\ T_{b2}(t) &= T_b^* + \frac{1}{2}a^2\vartheta(D(t) - D^*) \end{aligned} \tag{2.12}$$

Combining these two drilling regimes, we express the reaction force and torque corresponding

to the depth-of-cut $D(t)$ as a generic form as

$$
\begin{aligned}
F_b^{dy}(t) &= F_{b1}(t)(1 - U(D(t) - D^*)) + F_{b2}(t)U(D(t) - D^*) \\
T_b^{dy}(t) &= T_{b1}(t)(1 - U(D(t) - D^*)) + T_{b2}(t)U(D(t) - D^*)
\end{aligned} \tag{2.13}
$$

where $U(\cdot)$ represents the unit step function, and the superscript 'dy' stands for 'dynamic' (under conditions $\dot{y}_1 > 0, \dot{\phi}_1 > 0$). Note that the desired force on the bit F_{bd} and desired torque on the bit T_{bd} are calculated by substituting the desired depth-of-cut (2.10) into (2.13).

However, the two drilling regimes phase I and II expressed in (2.13) are valid only when the drilling is operated in a desired mode, i.e. $D \geq 0$, $\dot{y}_1 > 0$, $\dot{\phi}_1 \neq 0$. If these conditions are not satisfied, the drilling dynamics become more complex [39]. First, if the depth-of-cut $D < 0$, the bit is not in contact with the bottom of wellbore, and the interaction force F_b and torque T_b become zero. Second, if $\dot{y}_1 < 0$, the force on the bit will be zero. Finally, when the bit gets stuck in either axial or torsional dimension, i.e., $\dot{y}_1 = 0$ or $\dot{\phi}_1 = 0$, the force or torque on the bit can be determined using the force/torque balance as well as a static/dynamic friction model. For example, considering the case of $\dot{\phi}_1 = 0$, the Coulomb friction model is adopted for the expression of torque on the bit $T_b(t)$

$$
T_b = \begin{cases} \min\{T_r, T_b^{dy}\} & \dot{\phi}_1 = 0 \\ T_b^{dy} & \dot{\phi}_1 \neq 0 \end{cases} \tag{2.14}
$$

where T_b^{dy} is given in (2.13) and $T_r = C_t\dot{\phi}_2(t) + K_t(\phi_2(t) - \phi_1(t))$. As shown in Fig. 2.3, in the stick phase $\dot{\phi}_1 = 0$, the torque balance is maintained by static friction when $T_r \leq T_b^{dy}$. Once $T_r > T_b^{dy}$, the transition of stick phase to slip phase will arise. Also, the similar Coulomb friction model is introduced for the force on the bit F_b.

It is worth noting that, because of the switching between forward and reverse rotation, stick-slip behavior, bit bouncing, rock porosity and irregular rock geometry, the force and torque on the bit will behave non-smoothly, which will induce a complicated nonlinear dynamics. Thus, in this

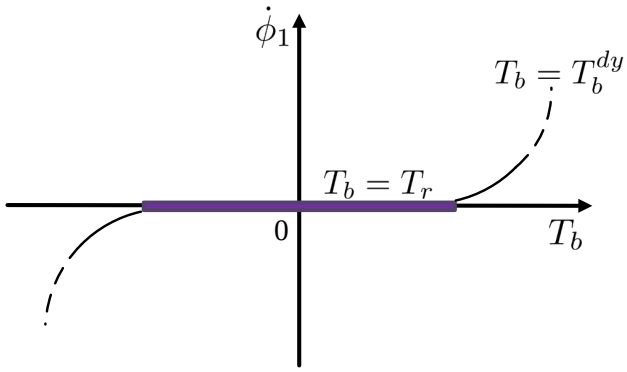

Figure 2.3: Coulomb friction model for torque on bit T_b

study, one of the key control objectives is to have the drilling avoid entering these non-smooth phases, using an iBLF based approach.

2.2.3 Error Dynamics

Having the models of both drill string and bit-rock interaction well described, the error dynamics for a set-point tracking problem are provided. Define the state vector $\boldsymbol{x} = [\ \chi_1,\ \tilde{v}_1,\ \chi_2,\ \tilde{v}_2,\ \theta_1,\ \tilde{\omega}_1,\ \theta_2,\ \tilde{\omega}_2\ ]^T$. The error dynamics are written as

$$
\begin{aligned}
\dot{x}_1(t) =& x_2(t) \\
\dot{x}_2(t) =& -\frac{K}{M_1}x_1(t) - \frac{C}{M_1}x_2(t) + \frac{K}{M_1}x_3(t) + \frac{C}{M_1}x_4(t) - H_1(x_1(t), x_{1\tau}(t), x_5(t), x_{5\tau}(t)) \\
\dot{x}_3(t) =& x_4(t) \\
\dot{x}_4(t) =& \frac{K}{M_2}x_1(t) + \frac{C}{M_2}x_2(t) - \frac{K}{M_2}x_3(t) - \frac{C}{M_2}x_4(t) + u_1(t) \\
\dot{x}_5(t) =& x_6(t) \\
\dot{x}_6(t) =& -\frac{K_t}{I_1}x_5(t) - \frac{C_t}{I_1}x_6(t) + \frac{K_t}{I_1}x_7(t) + \frac{C_t}{I_1}x_8(t) - H_2(x_1(t), x_{1\tau}(t), x_5(t), x_{5\tau}(t)) \\
\dot{x}_7(t) =& x_8(t) \\
\dot{x}_8(t) =& \frac{K_t}{I_2}x_5(t) + \frac{C_t}{I_2}x_6(t) - \frac{K_t}{I_2}x_7(t) - \frac{C_t}{I_2}x_8(t) + u_2(t)
\end{aligned}
\tag{2.15}
$$

where u_1 and u_2 are the virtual control inputs defined as

$$u_1(t) = \frac{1}{M_2}((M_1 + M_2)g - F(t) - F_{bd})$$
$$u_2(t) = \frac{1}{I_2}(T(t) - T_{bd}) \tag{2.16}$$

The nonlinear terms H_1 and H_2 are defined as

$$H_1(x_1(t), x_{1\tau}(t), x_5(t), x_{5\tau}(t)) \triangleq \frac{1}{M_1}(F_b(t) - F_{bd})$$
$$H_2(x_1(t), x_{1\tau}(t), x_5(t), x_{5\tau}(t)) \triangleq \frac{1}{I_1}(T_b(t) - T_{bd}) \tag{2.17}$$

The initial conditions are given as $x_i(0) = x_{i0}, i = 1, 2, ..., 8$ and $x_i(t) = \varpi_i(t), i = 1, 2, ..., 8$ for $t \in [-\tau(0), 0)$.

Since the bit's reaction force $F_b(t)$ and torque $T_b(t)$ only depend on depth-of-cut $D(t)$, and $D(t)$ depends on $\chi_1(t)$, $\chi_{1\tau}(t)$, $\theta_1(t)$, $\theta_{1\tau}(t)$ as per (2.9), (2.13) and (2.17), we denote H_1 and H_2 as functions of $x_1(t)$, $x_{1\tau}(t)$, $x_5(t)$, $x_{5\tau}(t)$.

2.3 Main Results

Following the drilling system dynamics model (2.15) and the bit-rock interaction model (2.5), (2.6) and (2.13), this study aims to design a controller using Barrier Lyapunov Function (BLF) for both axial and torsional dynamics to prevent the states of drilling system from falling into undesired regimes. This is usually to avoid occurrence of the drill bit stick-slip vibration and to have the torsional and axial drilling velocity be consistently positive and follow a desired trajectory.

2.3.1 Model Transformation of the Drilling System

The control design using iBLF is embedded in the framework of the backstepping approach, where a strict feedback form is required [53]. Note that, the error dynamics model of the drilling system (2.15) is not in a strict feedback form. Therefore, we conduct a customized model transformation for the error dynamics to enable the backstepping based control design.

In this study, the state transformation follows a routine of feedback linearization/input-output linearization, where a normal form decomposes the system into an internal part and an external part through the Lie derivatives of the output. The external part is stabilized by the control inputs, while the internal part is made unobservable by the same control [68]. Consider two virtual outputs for the system (2.15)

$$h_1(t) = x_1(t), \quad h_2(t) = x_5(t) \tag{2.18}$$

The relative degree with respect to the two outputs $h_1(t), h_2(t)$ is $\{3, 3\}$. Then, new system coordinates in a manner similar to an MIMO normal form are constructed as shown in (2.19), where the original system states $\boldsymbol{x}$ are transformed into an internal part $\boldsymbol{\eta} = [\ \eta_1, \eta_2\ ]^T$, and an external part $\boldsymbol{\xi} = [\ \xi_1, \xi_2, \xi_3, \xi_4, \xi_5, \xi_6\ ]^T$. Note that, we choose $\frac{d\xi_1(t)}{dt} = \xi_2(t)$, $\frac{d\xi_2(t)}{dt} = \xi_3(t)$ and $\frac{d\xi_4(t)}{dt} = \xi_5(t)$, $\frac{d\xi_5(t)}{dt} = \xi_6(t)$.

$$\begin{bmatrix} x_3(t) \\ x_7(t) \\ x_1(t) \\ x_2(t) \\ -\frac{K}{M_1}x_1(t) - \frac{C}{M_1}x_2(t) + \frac{K}{M_1}x_3(t) + \frac{C}{M_1}x_4(t) - H_1(x_1(t), x_{1\tau}(t), x_5(t), x_{5\tau}(t)) \\ x_5(t) \\ x_6(t) \\ -\frac{K_t}{I_1}x_5(t) - \frac{C_t}{I_1}x_6(t) + \frac{K_t}{I_1}x_7(t) + \frac{C_t}{I_1}x_8(t) - H_2(x_1(t), x_{1\tau}(t), x_5(t), x_{5\tau}(t)) \end{bmatrix} = \begin{bmatrix} \eta_1(t) \\ \eta_2(t) \\ \xi_1(t) \\ \xi_2(t) \\ \xi_3(t) \\ \xi_4(t) \\ \xi_5(t) \\ \xi_6(t) \end{bmatrix} \tag{2.19}$$

The error dynamics (2.15) are therefore transformed as

$$\begin{aligned} \dot{\eta}_1(t) =& \frac{M_1}{C}\Big(\frac{K}{M_1}\xi_1(t) + \frac{C}{M_1}\xi_2(t) - \frac{K}{M_1}\eta_1(t) + \xi_3(t) + H_1(\xi_1(t), \xi_{1\tau}(t), \xi_4(t), \xi_{4\tau}(t))\Big) \\ \dot{\eta}_2(t) =& \frac{I_1}{C_t}\Big(\frac{K_t}{I_1}\xi_4(t) + \frac{C_t}{I_1}\xi_5(t) - \frac{K_t}{I_1}\eta_2(t) + \xi_6(t) + H_2(\xi_1(t), \xi_{1\tau}(t), \xi_4(t), \xi_{4\tau}(t))\Big) \end{aligned} \tag{2.20}$$

$$
\begin{aligned}
\dot{\xi}_1(t) =& \xi_2(t) \\
\dot{\xi}_2(t) =& \xi_3(t) \\
\dot{\xi}_3(t) =& -\frac{K}{M_1}x_2(t) - \frac{C}{M_1}\xi_3(t) + \frac{K}{M_1}x_4(t) + \frac{C}{M_1}\Big(\frac{K}{M_2}x_1(t) + \frac{C}{M_2}x_2(t) - \frac{K}{M_2}x_3(t) - \frac{C}{M_2}x_4(t) \\
& + u_1(t)\Big) - \frac{dH_1(\xi_1(t), \xi_{1\tau}(t), \xi_4(t), \xi_{4\tau}(t))}{dt} \qquad (2.21) \\
\dot{\xi}_4(t) =& \xi_5(t) \\
\dot{\xi}_5(t) =& \xi_6(t) \\
\dot{\xi}_6(t) =& -\frac{K_t}{I_1}x_6(t) - \frac{C_t}{I_1}\xi_6(t) + \frac{K_t}{I_1}x_8(t) + \frac{C_t}{I_1}\Big(\frac{K_t}{I_2}x_5(t) + \frac{C_t}{I_2}x_6(t) - \frac{K_t}{I_2}x_7(t) - \frac{C_t}{I_2}x_8(t) \\
& + u_2(t)\Big) - \frac{dH_2(\xi_1(t), \xi_{1\tau}(t), \xi_4(t), \xi_{4\tau}(t))}{dt} \qquad (2.22)
\end{aligned}
$$

where (2.20) is the internal dynamics, and the external dynamics contains two sub-systems: axial dynamics (2.21) and torsional dynamics (2.22), which are both in the strict feedback form.

2.3.2 Control Design Using iBLF

Before introducing the control design, two assumptions are made first.

A1. The downhole information of the system states is available in real-time. This can be achieved by two methods. First, the high-speed telemetry has been heavily researched and applied to the drilling system in recent years [69]. The copper-wire based telemetry can offer a faster signal transmission than the previously used mud pulse method, to transfer the measurements of strain sensor or accelerometer installed along the drill string. Second, even under a large transmission delay of the down-hole measurement, the system states can still be observed using an integrated state estimator [70], which has great robustness under transmission noise.

A2. With a discontinuous controller provided in this study, the solutions are understood in the Filippov sense [71].

As claimed to be the essential contribution in this study, the BLF is introduced, where constraints are coped with the control design. Next, the definition of BLF is provided.

Definition 2. *(K. P. Tee et al., 2009 [50]) For a system $\dot{x} = f(x)$, a Barrier Lyapunov Function*

(BLF) is a scalar function $V(x)$ defined on an open region $\mathcal{D}$ containing the origin, which is continuous, positive definite, and has continuous first-order partial derivatives at every point of $\mathcal{D}$. It satisfies $V(x) \to \infty$ as x approaches the boundary of $\mathcal{D}$, and $V(x) \leq b$ along the solution of $\dot{x} = f(x)$ for $x(0) \in \mathcal{D}$ and certain constant $b > 0$.

To employ the integral type BLF in the control design for the external dynamics (2.21) and (2.22), we first specify the state constraints as

$$|\xi_2| < k_v, \quad |\xi_5| < k_\omega \tag{2.23}$$

with k_v and k_ω as positive constants satisfying $k_v < v_d$ and $k_\omega < \omega_d$. These two conditions ensure that $\dot{y}_1 > 0, \dot{\phi}_1 > 0$, and therefore the drilling states are blocked away from the barrier set by these two constraints and avoided entering the undesired operating region (such as stick-slip mode), as discussed in Section 2.2.2. The remaining step is how to ensure the two constraints on the error states are always met through control design, even during the transients.

For system (2.21) and (2.22), we propose the Barrier Lyapunov Function candidate consisting of both axial and torsional dynamics

$$\begin{aligned} V(\boldsymbol{z}, \boldsymbol{\alpha}) &= V_a(\boldsymbol{z}, \boldsymbol{\alpha}) + V_t(\boldsymbol{z}, \boldsymbol{\alpha}) \\ V_a(\boldsymbol{z}, \boldsymbol{\alpha}) &= \frac{1}{2} z_1^2 + V_v(z_2, \alpha_1) + \frac{1}{2} z_3^2 \\ V_t(\boldsymbol{z}, \boldsymbol{\alpha}) &= \frac{1}{2} z_4^2 + V_\omega(z_5, \alpha_4) + \frac{1}{2} z_6^2 \end{aligned} \tag{2.24}$$

where

$$\begin{aligned} V_v(z_2, \alpha_1) &= \int_0^{z_2} \frac{\varsigma k_v^2}{k_v^2 - (\varsigma + \alpha_1)^2} d\varsigma \\ V_\omega(z_5, \alpha_4) &= \int_0^{z_5} \frac{\varsigma k_\omega^2}{k_\omega^2 - (\varsigma + \alpha_4)^2} d\varsigma \end{aligned} \tag{2.25}$$

We define z_i as

$$z_1 = \xi_1, \quad z_2 = \xi_2 - \alpha_1, \quad z_3 = \xi_3 - \alpha_2$$
$$z_4 = \xi_4, \quad z_5 = \xi_5 - \alpha_4, \quad z_6 = \xi_6 - \alpha_5 \tag{2.26}$$

Note that, in (2.25), if the states approach the undesired operating regime, i.e., $|\xi_2| \to k_v$ and $|\xi_5| \to k_\omega$, the integrals will approach infinity at their upper limits, and the Lyapunov function (2.24) can result in an infinity value, and thus can effectively have the states avoid entering the undesired operating conditions. The stabilizing functions $\alpha_{1,2}$ and $\alpha_{4,5}$ are continuously differentiable functions satisfying $|\alpha_1| \leq A_v < k_v$ and $|\alpha_4| \leq A_\omega < k_\omega$ for positive constants A_v and A_ω. As defined in (2.25), V_v and V_ω are positive definite, continuously differentiable, and satisfy the decrescent condition when $|\xi_2| < k_v$ and $|\xi_5| < k_\omega$, given as

$$\frac{z_2^2}{2} \leq V_v \leq z_2^2 \int_0^1 \frac{\beta k_v^2}{k_v^2 - (\beta z_2 + \text{sgn}(z_2) A_v)^2} d\beta$$
$$\frac{z_5^2}{2} \leq V_\omega \leq z_5^2 \int_0^1 \frac{\beta k_\omega^2}{k_\omega^2 - (\beta z_5 + \text{sgn}(z_5) A_\omega)^2} d\beta \tag{2.27}$$

Also, the following conditions hold (see *Lemma 1* in [53])

$$V_v \leq \frac{k_v^2 z_2^2}{k_v^2 - \xi_2^2}, \quad V_\omega \leq \frac{k_\omega^2 z_5^2}{k_\omega^2 - \xi_5^2} \tag{2.28}$$

Next, we use the backstepping procedure to design the controller for the axial dynamics (2.21) first, and then a similar approach can be applied to the torsional dynamics (2.22).

Step 1: In the first step, we have $V_{a1} = \frac{1}{2} z_1^2$, and its time-derivative is given as

$$\dot{V}_{a1} = z_1 (z_2 + \alpha_1) \tag{2.29}$$

The stabilizing function is chosen as $\alpha_1 = -p_1 z_1$, where p_1 is a positive constant control gain,

yielding

$$\dot{V}_{a1} = -p_1 z_1^2 + z_1 z_2 \tag{2.30}$$

Step 2: Next, we consider $V_{a2} = \frac{1}{2} z_1^2 + V_v$. The time-derivative of V_{a2} is given as

$$\dot{V}_{a2} = -p_1 z_1^2 + z_1 z_2 + \frac{k_v^2 z_2}{k_v^2 - \xi_2^2}(z_3 + \alpha_2 - \dot{\alpha}_1) + \frac{\partial V_{a2}}{\partial \alpha_1}\dot{\alpha}_1 \tag{2.31}$$

where

$$\frac{\partial V_{a2}}{\partial \alpha_1} = z_2 \left(\frac{k_v^2}{k_v^2 - \xi_2^2} - \varrho_2(z_2, \alpha_1) \right) \tag{2.32}$$

$$\begin{aligned} \varrho_2(z_2, \alpha_1) &= \int_0^1 \frac{k_v^2}{k_v^2 - (\beta z_2 + \alpha_1)^2} d\beta \\ &= \frac{k_v^2}{2 z_2} \ln \frac{(k_v + z_2 + \alpha_1)(k_v - \alpha_1)}{(k_v - z_2 - \alpha_1)(k_v + \alpha_1)} \end{aligned} \tag{2.33}$$

The partial derivative of $\varrho_2(z_2, \alpha_1)$ is written as

$$\frac{\partial \varrho_2}{\partial z_2} = \frac{1}{z_2}\left(\frac{k_v^2}{k_v^2 - (z_2 + \alpha_1)^2} - \varrho_2\right) \tag{2.34}$$

$$\frac{\partial \varrho_2}{\partial \alpha_1} = \frac{k_v^2 (z_2 + 2\alpha_1)}{(k_v^2 - (z_2 + \alpha_1)^2)(k_v^2 - \alpha_1^2)} \tag{2.35}$$

As per L'Hôpital's rule [72], the following limits are derived as

$$\lim_{z_2 \to 0} \varrho_2(z_2, \alpha_1) = \frac{k_v^2}{k_v^2 - \alpha_1^2} \tag{2.36}$$

$$\lim_{z_2 \to 0} \frac{\partial \varrho_2}{\partial z_2} = \frac{k_v^2 \alpha_1}{(k_v^2 - \alpha_1^2)^2} \tag{2.37}$$

From (2.33), (2.34), (2.35), (2.36) and (2.37), we showed that ϱ_2, $\frac{\partial \varrho_2}{\partial z_2}$ and $\frac{\partial \varrho_2}{\partial \alpha_1}$ are well-defined in the neighborhood of $z_2 = 0$, if $|\alpha_1| < k_v$.

The stabilizing function is chosen as

$$\alpha_2 = \frac{k_v^2 - \xi_2^2}{k_v^2}(-z_1 + \varrho_2 \dot{\alpha}_1) - p_2 z_2 \tag{2.38}$$

where p_2 is a positive constant control gain, rendering

$$\dot{V}_{a2} = -p_1 z_1^2 - p_2 \frac{k_v^2 z_2^2}{k_v^2 - \xi_2^2} + \frac{k_v^2 z_2 z_3}{k_v^2 - \xi_2^2} \tag{2.39}$$

Step 3: In the last step, we consider $V_a = \frac{1}{2} z_1^2 + V_v + \frac{1}{2} z_3^2$, and its time-derivative is written as

$$\dot{V}_a = -p_1 z_1^2 - p_2 \frac{k_v^2 z_2^2}{k_v^2 - \xi_2^2} + \frac{k_v^2 z_2 z_3}{k_v^2 - \xi_2^2} + z_3(\dot{\xi}_3 - \dot{\alpha}_2) \tag{2.40}$$

Since $\frac{\partial \varrho_2}{\partial z_2}$ and $\frac{\partial \varrho_2}{\partial \alpha_1}$ are well defined, $\dot{\alpha}_2$ is also well defined in the neighborhood of $z_2 = 0$.

Before presenting the control law, we first address the nonlinear term $\frac{dH_1}{dt}$ in system's equation (2.21). From (2.17), we observe that H_1 has dependence of $x_{1\tau}$ and $x_{5\tau}$, where the delay $\tau(t)$ is an implicit function of the state $\boldsymbol{x}$. Thus, the value of the delayed states $x_{1\tau}$ and $x_{5\tau}$ cannot be directly used in the control design, and the nonlinear term $\frac{dH_1}{dt}$ cannot be directly canceled. A remedy to this is to consider $\frac{dH_1}{dt}$ as an uncertainty, whose bounds can be derived as follows. Since H_1 is a function of the depth-of-cut D, we have $\frac{dH_1}{dt}$ written by

$$\frac{dH_1}{dt} = \frac{dH_1}{dD}\frac{dD}{dt} \tag{2.41}$$

Using (2.13), we can see that the lower bound of $\frac{dH_1}{dD}$ is larger than 0, and the upper bound is a positive constant as

$$B_{H_1} \triangleq \frac{1}{M_1}(a\varsigma\kappa + a\zeta\vartheta). \tag{2.42}$$

The other factor $\frac{dD}{dt}$ is given by the following operations. We take time-derivative of both (2.5) and

(2.6) as

$$\frac{dD}{dt} = n\Big(\dot{y}_1(t) - \Big(1 - \frac{d\tau(t)}{dt}\Big)\dot{y}_{1\tau}(t)\Big) \tag{2.43}$$

$$0 = \dot{\phi}_1(t) - \Big(1 - \frac{d\tau(t)}{dt}\Big)\dot{\phi}_{1\tau}(t) \tag{2.44}$$

Eliminating $\Big(1 - \frac{d\tau(t)}{dt}\Big)$ in (2.43) and (2.44) gives

$$\begin{aligned}\frac{dD}{dt} &= n\Big(\dot{y}_1(t) - \frac{\dot{\phi}_1(t)}{\dot{\phi}_{1\tau}(t)}\dot{y}_{1\tau}(t)\Big) \\ &= n\Big((v_d + \xi_2(t)) - \frac{\omega_d + \xi_5(t)}{\omega_d + \xi_{5\tau}(t)}(v_d + \xi_{2\tau}(t))\Big)\end{aligned} \tag{2.45}$$

Considering the constraints $|\xi_2(t)| < k_v$ and $|\xi_5(t)| < k_\omega$, we can infer that $|\xi_{2\tau}(t)| < k_v$ and $|\xi_{5\tau}(t)| < k_\omega$, and then the upper and lower bounds of $\frac{dD}{dt}$ are denoted by constants B_D^+ and B_D^- respectively, as

$$\begin{aligned}B_D^+ &\triangleq n\Big((v_d + k_v) - \frac{\omega_d - k_\omega}{\omega_d + k_\omega}(v_d - k_v)\Big) > 0 \\ B_D^- &\triangleq n\Big((v_d - k_v) - \frac{\omega_d + k_\omega}{\omega_d - k_\omega}(v_d + k_v)\Big) < 0\end{aligned} \tag{2.46}$$

Combining (2.42) and (2.46) gives the upper and lower bounds of $\frac{dH_1}{dt}$ as $B_{H_1} \cdot B_D^+$ and $B_{H_1} \cdot B_D^-$.

Thus, given the bounds of uncertainty for the nonlinear term as derived above, the control input is then designed as

$$\begin{aligned}u_1 =& \frac{M_1}{C}\Big(\dot{\alpha}_2 - \frac{k_v^2 z_2}{k_v^2 - \xi_2^2} - p_3 z_3 + \frac{K}{M_1}x_2 + \frac{C}{M_1}\xi_3 - \frac{K}{M_1}x_4\Big) - \frac{K}{M_2}x_1 \\ &- \frac{C}{M_2}x_2 + \frac{K}{M_2}x_3 + \frac{C}{M_2}x_4 - \frac{M_1}{C}B_{H_1}\psi(z_3)\text{sgn}(z_3)\end{aligned} \tag{2.47}$$

where p_3 is a positive constant control gain, and the function $\psi(z_i)$ is defined as

$$\psi(z_i) = \begin{cases} -B_D^- & z_i \geq 0 \\ B_D^+ & z_i < 0 \end{cases} \tag{2.48}$$

Substituting u_1 into (2.40) yields

$$\dot{V}_a = -p_1 z_1^2 - p_2 \frac{k_v^2 z_2^2}{k_v^2 - \xi_2^2} - p_3 z_3^2 - z_3 \Big(B_{H_1} \psi(z_3) \text{sgn}(z_3) + \frac{dH_1}{dt} \Big) \tag{2.49}$$

where $z_3 \Big(B_{H_1} \psi(z_3) \text{sgn}(z_3) + \frac{dH_1}{dt} \Big) \geq 0$ if $|\xi_2| < k_v$.

For the torsional dynamics (2.22), similar procedures as **Steps 1-3** can be applied. To design the controller, we choose p_4, p_5 and p_6 to be positive constant control gains, and the stabilizing function is designed as

$$\alpha_4 = -p_4 \xi_4, \quad \alpha_5 = \frac{k_\omega^2 - \xi_5^2}{k_\omega^2} (-z_4 + \varrho_5 \dot{\alpha}_4) - p_5 z_5 \tag{2.50}$$

where ϱ_5 is given by

$$\begin{aligned} \varrho_5(z_5, \alpha_4) &= \int_0^1 \frac{k_\omega^2}{k_\omega^2 - (\beta z_5 + \alpha_4)^2} d\beta \\ &= \frac{k_\omega^2}{2 z_5} \ln \frac{(k_\omega + z_5 + \alpha_4)(k_\omega - \alpha_4)}{(k_\omega - z_5 - \alpha_4)(k_\omega + \alpha_4)} \end{aligned} \tag{2.51}$$

Also, we have the upper bound for $\frac{dH_2}{dt}$, as

$$B_{H_2} \triangleq \frac{1}{I_1} (\frac{1}{2} a^2 \mu \gamma \sigma \kappa + \frac{1}{2} a^2 \vartheta) \tag{2.52}$$

The control input u_2 is designed as

$$\begin{aligned} u_2(t) =& \frac{I_1}{C_t}\Big(\dot{\alpha}_5 - \frac{k_\omega^2 z_5}{k_\omega^2 - \xi_5^2} - p_6 z_6 + \frac{K_t}{I_1}x_6 + \frac{C_t}{I_1} - \frac{K_t}{I_1}x_8\Big) - \frac{K_t}{I_2}x_5 \\ & - \frac{C_t}{I_2}x_6 + \frac{K_t}{I_2}x_7 + \frac{C_t}{I_2}x_8 - \frac{I_1}{C_t}B_{H_2}\psi(z_6)\text{sgn}(z_6) \end{aligned} \tag{2.53}$$

where ϱ_5, $\frac{\partial \varrho_5}{\partial z_5}$, $\frac{\partial \varrho_5}{\partial \alpha_4}$ and $\dot{\alpha}_5$ are well-defined in the neighborhood of $z_5 = 0$, if $|\alpha_4| < k_\omega$.

Now we take time-derivative of the Lyapunov function $V_t = \frac{1}{2}z_4^2 + V_\omega + \frac{1}{2}z_6^2$, given by

$$\dot{V}_t = - p_4 z_4^2 - p_5 \frac{k_\omega^2 z_5^2}{k_\omega^2 - \xi_5^2} - p_6 z_6^2 - z_6\Big(B_{H_2}\psi(z_6)\text{sgn}(z_6) + \frac{dH_2}{dt}\Big) \tag{2.54}$$

where the factor $z_6\Big(B_{H_2}\psi(z_6)\text{sgn}(z_6) + \frac{dH_2}{dt}\Big) \geq 0$ if $|\xi_5| < k_\omega$.

Then, considering both axial and torsional dynamics, the time-derivative of the Lyapunov function V defined in (2.24) is

$$\dot{V} = \dot{V}_a + \dot{V}_t \tag{2.55}$$

Using the fact of (2.28), the following inequalities are obtained

$$\dot{V}_a \leq -\rho_a V_a, \quad \dot{V}_t \leq -\rho_t V_t \tag{2.56}$$

where $\rho_a = 2\min\{p_i\}, i = 1, 2, 3$ and $\rho_t = 2\min\{p_i\}, i = 4, 5, 6$, if (2.23) is satisfied. From (2.55) and (2.56), we have

$$\dot{V} \leq -\rho V \tag{2.57}$$

where $\rho = 2\min\{p_i\}, i = 1, 2, ..., 6$.

Now we have the closed-loop system for both axial and torsional dynamics in $\boldsymbol{z}$ domain as

$$
\begin{aligned}
\dot{z}_1 &= -p_1 z_1 + z_2 \\
\dot{z}_2 &= -p_1^2 z_1 + (p_1 - p_2) z_2 + z_3 + \frac{k_v^2 - \xi_2^2}{k_v^2}(-z_1 + \varrho_2 \dot{\alpha}_1) \\
\dot{z}_3 &= -\frac{k_v^2 z_2}{k_v^2 - \xi_2^2} - p_3 z_3 - \left(B_{H_1} \psi(z_3) \text{sgn}(z_3) + \frac{dH_1}{dt} \right) \\
\dot{z}_4 &= -p_4 z_4 + z_5 \\
\dot{z}_5 &= -p_4^2 z_4 + (p_4 - p_5) z_5 + z_6 + \frac{k_\omega^2 - \xi_5^2}{k_\omega^2}(-z_4 + \varrho_5 \dot{\alpha}_4) \\
\dot{z}_6 &= -\frac{k_\omega^2 z_5}{k_\omega^2 - \xi_5^2} - p_6 z_6 - \left(B_{H_2} \psi(z_6) \text{sgn}(z_6) + \frac{dH_2}{dt} \right)
\end{aligned} \tag{2.58}
$$

Since $\boldsymbol{z}$ and $\boldsymbol{\alpha}$ are the functions of $\boldsymbol{\xi}$, the closed loop system of this external dynamics can be written in $\boldsymbol{\xi}$ domain as

$$
\dot{\boldsymbol{\xi}} = f(\boldsymbol{\xi}, \boldsymbol{\xi}_\tau) \tag{2.59}
$$

where $f(\boldsymbol{\xi}, \boldsymbol{\xi}_\tau)$ is non-Lipschitz in $\boldsymbol{\xi}$ due to the functions $\text{sgn}(\cdot)$ and $\psi(\cdot)$, and is Lipschitz in $\boldsymbol{\xi}_\tau$.

Next, with the constructed close-loop system, we establish the following results to show the main results of this study.

Theorem 1. *Consider the error dynamics* (2.15) *under control* (2.47) *and* (2.53)*, with the initial condition in the set* $\Omega = \{\boldsymbol{\xi} \in \mathbb{R}^8 : |\xi_2| < k_v, |\xi_5| < k_\omega\}$*. If*

$$
p_1 \sqrt{2V_a|_{t=0}} < k_v, \quad p_4 \sqrt{2V_t|_{t=0}} < k_\omega \tag{2.60}
$$

then the following statements hold:

i) The backstepping errors $z_i(t)$ decrease exponentially to 0, satisfying

$$\begin{aligned} |z_i(t)| \leq & \sqrt{2V_a|_{t=0}}\, e^{-\frac{\rho_a t}{2}}, \quad i = 1, 2, 3 \\ |z_i(t)| \leq & \sqrt{2V_t|_{t=0}}\, e^{-\frac{\rho_t t}{2}}, \quad i = 4, 5, 6, \ \forall t > 0 \end{aligned} \tag{2.61}$$

ii) The states $\boldsymbol{\xi}(t)$ stay in Ω for all $t > 0$.

iii) In $\boldsymbol{x}$ domain, the states $x_1(t)$, $x_2(t)$, $x_5(t)$, $x_6(t)$ are asymptotically stable at 0, and the states $x_3(t)$, $x_4(t)$, $x_7(t)$, $x_8(t)$ are bounded and convergent to 0.

iv) The stabilizing functions $\alpha_{1,2}$, $\alpha_{4,5}$ and control inputs $u_{1,2}$ are bounded for all $t > 0$.

Proof:

i) Using (2.56), we obtain $V_a|_t \leq V_a|_{t=0} e^{-\rho_a t}$ and $V_t|_t \leq V_t|_{t=0} e^{-\rho_t t}$. From (2.27), we have $V_a|_t \geq \sum_{i=1}^{3} z_i^2/2$ and $V_t|_t \geq \sum_{i=4}^{6} z_i^2/2$. Thus, combining them gives $z_i^2(t) \leq 2V_a|_{t=0} e^{-\rho_a t}$ for $i = 1, 2, 3$ and $z_i^2(t) \leq 2V_t|_{t=0} e^{-\rho_t t}$ for $i = 4, 5, 6$.

ii) We assume that at certain $t = t_n$, $\boldsymbol{\xi}(t)$ is at the boundary of Ω for the first time, i.e. $|\xi_2(t_n)| = k_v$ or $|\xi_5(t_n)| = k_\omega$. It can be inferred that $|\xi_{2\tau}(t_n)| < k_v$ and $|\xi_{5\tau}(t_n)| < k_\omega$, since $\xi_{2\tau}(t_n) = \xi_2(t_n - \tau(t_n))$ and $\xi_{5\tau}(t_n) = \xi_5(t_n - \tau(t_n))$. Thus, the bounds defined in (2.46) are valid, and the conditions (2.56) and (2.57) are not violated. When the initial condition is in Ω, from (2.57) we have

$$V|_{t=t_n} \leq V|_{t=0} \tag{2.62}$$

Employ integration by part for $V_v|_{t=t_n}$ and $V_w|_{t=t_n}$

$$\begin{aligned} V_v|_{t=t_n} =& \frac{k_v}{2} \int_0^{z_2} \varsigma \Big(\frac{1}{k_v - (\varsigma + \alpha_1)} + \frac{1}{(\varsigma + \alpha_1) + k_v} \Big) d\varsigma \\ =& \frac{k_v}{2} \Big((\alpha_1(t_n) + k_v) \ln \frac{\alpha_1(t_n) + k_v}{\xi_2(t_n) + k_v} + (k_v - \alpha_1(t_n)) \ln \frac{k_v - \alpha_1(t_n)}{k_v - \xi_2(t_n)} \Big) \end{aligned}$$

$$
\begin{aligned}
V_\omega|_{t=t_n} =& \frac{k_\omega}{2}\int_0^{z_5} \varsigma\Big(\frac{1}{k_\omega-(\varsigma+\alpha_4)}+\frac{1}{(\varsigma+\alpha_4)+k_\omega}\Big)d\varsigma \\
=& \frac{k_\omega}{2}\Big((\alpha_4(t_n)+k_\omega)\ln\frac{\alpha_4(t_n)+k_\omega}{\xi_5(t_n)+k_\omega}+(k_\omega-\alpha_4(t_n))\ln\frac{k_\omega-\alpha_4(t_n)}{k_\omega-\xi_5(t_n)}\Big)
\end{aligned} \tag{2.63}
$$

If either $|\xi_2(t_n)| = k_v$ or $|\xi_5(t_n)| = k_\omega$ holds, $V_v|_{t=t_n}$ or $V_\omega|_{t=t_n}$ will be unbounded, and $V|_{t=t_n}$ becomes unbounded, contradicting (2.62). Therefore, we conclude that $\boldsymbol{\xi}(t)$ remains in Ω for all $t > 0$.

iii) First, we will show that states $x_1(t)$, $x_2(t)$, $x_5(t)$, $x_6(t)$ are asymptotically stable at 0. Considering the Lyapunov function $V(\boldsymbol{z},\boldsymbol{\alpha})$ in (2.24), since $\boldsymbol{z}$ and $\boldsymbol{\alpha}$ are the functions of $\boldsymbol{\xi}$, it can be verified that

$$
\begin{aligned}
&V(\boldsymbol{z},\boldsymbol{\alpha}) = 0, \quad \text{if } \boldsymbol{\xi} = 0 \\
&V(\boldsymbol{z},\boldsymbol{\alpha}) > 0, \quad \text{if } \boldsymbol{\xi} \in \Omega - \{0\}
\end{aligned} \tag{2.64}
$$

Now, we can choose $V(\boldsymbol{z},\boldsymbol{\alpha})$ as a Lyapunov candidate for $\boldsymbol{\xi}$, denoted by $V(\boldsymbol{\xi})$. It is worth noting that, since the governing equation (2.59) is non-Lipschitz in $\boldsymbol{\xi}$, the solution of the closed-loop system is understood in Filippov sense, and the validity of $V(\boldsymbol{\xi})$ can be checked using the extended Lyapunov stability theorems [73], which shows the Lyapunov stability of the states $\boldsymbol{\xi}$. Moreover, the convergence of the states $\boldsymbol{\xi}$ is proven as follows. The time-derivative of $V(\boldsymbol{\xi})$ satisfies

$$
\dot{V}(\boldsymbol{\xi}) = \dot{V}_a + \dot{V}_t \leq 0 \tag{2.65}
$$

We define $W(t)$ as

$$
\begin{aligned}
W(t) = -(\dot{V}_a + \dot{V}_t) =& p_1 z_1^2 + p_2\frac{k_v^2 z_2^2}{k_v^2-\xi_2^2} + p_3 z_3^2 + z_3\Big(B_{H_1}\text{sgn}(z_3)\psi(z_3)+\frac{dH_1}{dt}\Big) \\
&+ p_4 z_4^2 + p_5\frac{k_\omega^2 z_5^2}{k_\omega^2-\xi_5^2} + p_6 z_6^2 + z_6\Big(B_{H_2}\text{sgn}(z_6)\psi(z_6)+\frac{dH_2}{dt}\Big) \\
=& -\dot{V}(\boldsymbol{\xi}(t))
\end{aligned} \tag{2.66}
$$

Integrating both sides

$$\int_0^t W(\tau)d\tau = V(\boldsymbol{\xi}(0)) - V(\boldsymbol{\xi}(t)) \tag{2.67}$$

As $V(\boldsymbol{\xi}(0))$ is bounded and $V(\boldsymbol{\xi}(t))$ is non-increasing and bounded, we conclude

$$\lim_{t\to\infty} \int_0^t W(\tau)d\tau \leq \infty \tag{2.68}$$

Due to the fact that $W(t)$ is uniformly continuous, using Barbalat's Lemma [74] we have

$$\lim_{t\to\infty} W(t) = 0 \tag{2.69}$$

It shows that $\boldsymbol{z}$ converge to zero as $t \to \infty$, and it can be verified that $\boldsymbol{\xi}$ also converge to zero as $t \to \infty$. Therefore, the states $\boldsymbol{\xi}$ are asymptotically stable at 0. Given the definition of state transformation (2.19), we conclude that the states $x_1(t)$, $x_2(t)$, $x_5(t)$, $x_6(t)$ are asymptotically stable at 0.

Next, we will show that the states $x_3(t)$, $x_4(t)$, $x_7(t)$, $x_8(t)$ are bounded and convergent to 0. Rewrite the first row of (2.20) as

$$\dot{\eta}_1(t) = -\, b\eta_1(t) + l(t) \tag{2.70}$$

where $b = \frac{K}{C}$, and $l(t) = \frac{M_1}{C}\Big(\frac{K}{M_1}\xi_1(t) + \frac{C}{M_1}\xi_2(t) + \xi_3(t) + H_1(\xi_1(t), \xi_{1\tau}(t), \xi_4(t), \xi_{4\tau}(t))\Big)$.

Due to the fact that $\frac{d(t-\tau)}{dt} = \frac{\dot{\phi}_1}{\dot{\phi}_{1\tau}} > 0$ from (2.44), the delayed states $\xi_{1\tau(t)}$ and $\xi_{4\tau(t)}$ are bounded and convergent to 0. By the definition of H_1 in (2.9), (2.13) and (2.17), we have H_1 be bounded and convergent to 0. Also, since the states $\xi_1(t)$, $\xi_2(t)$ and $\xi_3(t)$ are asymptotically stable, we infer that $l(t)$ is bounded and convergent to 0. In (2.70), the signals $l(t)$ and $\eta_1(t)$ can be regarded as the input and output of the first-order linear system with a LHP pole. We can conclude that $\eta_1(t)$ is bounded as a result of the bounded-input-bounded-output (BIBO) property. Moreover, to show

that $\eta_1(t)$ is convergent to 0, we first derive the solution of η_1 as

$$\eta_1(t) = \eta_1(0)e^{-bt} + \int_0^t e^{-b(t-\tau)} l(\tau) d\tau \tag{2.71}$$

where $\eta_1(0)e^{-bt}$ is convergent to 0. Next, we show that $\int_0^t e^{b(t-\tau)} l(\tau) d\tau$ is convergent to 0. Given that $|l(t)|$ is bounded by $B_l > 0$, we specify an ϵ, and consider the fact that $\forall \epsilon^* = b\epsilon/2 > 0$, $\exists \overline{T} > 0$ such that $|l(t)| < \epsilon^*$ for $t > \overline{T}$. Then we choose

$$\widetilde{T} = \max\left\{\overline{T}, \overline{T} + \frac{1}{b} \ln \frac{2B_l}{b\epsilon}\right\} \tag{2.72}$$

For $\forall t > \widetilde{T}$, we have

$$\begin{aligned}
\left| \int_0^t e^{-b(t-\tau)} l(\tau) d\tau \right| &= \left| \int_0^{\overline{T}} e^{-b(t-\tau)} l(\tau) d\tau + \int_{\overline{T}}^t e^{-b(t-\tau)} l(\tau) d\tau \right| \\
&\leq \int_0^{\overline{T}} e^{-b(t-\tau)} \Big| l(\tau) \Big| d\tau + \int_{\overline{T}}^t e^{-b(t-\tau)} \Big| l(\tau) \Big| d\tau \\
&\leq \frac{B_l}{b} e^{-bt} (e^{b\overline{T}} - 1) + \frac{\epsilon}{2} (1 - e^{b(\overline{T}-t)}) \\
&\leq \frac{B_l}{b} e^{b(\overline{T}-t)} + \frac{\epsilon}{2} \\
&\leq \frac{B_l}{b} e^{b(\overline{T} - (\overline{T} + \frac{1}{b} \ln \frac{2B_l}{b\epsilon}))} + \frac{\epsilon}{2} \\
&= \epsilon
\end{aligned} \tag{2.73}$$

Thus, we can conclude that $\eta_1(t)$ satisfies

$$|\eta_1(t)| \leq B_{\eta_1} \text{ for } t \in [0, +\infty), \quad \lim_{t \to \infty} \eta_1(t) = 0 \tag{2.74}$$

where B_{η_1} is a positive constant. Moreover, from (2.70), we get

$$|\dot{\eta}_1(t)| \leq B_{\dot{\eta}_1} \text{ for } t \in [0, +\infty), \quad \lim_{t \to \infty} \dot{\eta}_1(t) = 0 \tag{2.75}$$

where $B_{\dot{\eta}_1}$ is a positive constant. Therefore, $x_3(t)$ and $x_4(t)$ are bounded and convergent to 0, given the fact that $x_3(t) = \eta_1(t)$ and $x_4(t) = \dot{\eta}_1(t)$. Moreover, $x_7(t)$ and $x_8(t)$ also have the boundedness and convergence properties, by applying the similar analysis for the second row of (2.20).

iv) From (2.60), (2.61) and the definition of α_1 and α_4, the following inequalities hold.

$$
\begin{aligned}
|\alpha_1| = p_1|z_1| &\leq p_1\sqrt{2V_a|_{t=0}}\, e^{-\frac{\rho_a t}{2}} \leq p_1\sqrt{2V_a|_{t=0}} < k_v \\
|\alpha_4| = p_4|z_4| &\leq p_4\sqrt{2V_t|_{t=0}}\, e^{-\frac{\rho_t t}{2}} \leq p_4\sqrt{2V_t|_{t=0}} < k_\omega
\end{aligned} \tag{2.76}
$$

Under these conditions, we have ϱ_2, ϱ_5 and their partial derivatives well-defined if $\boldsymbol{\xi} \in \Omega$, and then the stabilizing functions $\alpha_{1,2}$, $\alpha_{4,5}$ are bounded. Also, the errors $\boldsymbol{z}$ have exponentially decreasing bounds as shown in (2.61), and the states $\boldsymbol{x}$ are bounded as proven in (iii). Therefore, given control law (2.47) and (2.53), the inputs $u_{1,2}$ are bounded. ■

Remark 1. *In Theorem 1 (iii), the states of bit $x_1(t)$, $x_2(t)$, $x_5(t)$, $x_6(t)$ corresponds to the external states $\boldsymbol{\xi}$, and the states of top drive $x_3(t)$, $x_4(t)$, $x_7(t)$, $x_8(t)$ corresponds to the internal states $\boldsymbol{\eta}$. However, due to the existence of the time-delayed term $x_{1\tau}(t)$ and $x_{5\tau}(t)$, the state transformation* (2.19) *is not a diffeomorphism. The equivalence of the original coordinates $\boldsymbol{x}$ and the new coordinates $[\boldsymbol{\eta}^T\ \boldsymbol{\xi}^T]^T$ is not established. Therefore, once the external dynamics is asymptotically stable through the control design, we cannot conclude the asymptotic stability of the internal dynamics using the standard inference of the normal form [75, 76]. Alternatively, in this study we proved the boundedness and convergence of the states $x_3(t)$, $x_4(t)$, $x_7(t)$, $x_8(t)$ instead of asymptotic stability, which can be practically applied to the drilling system control.*

2.4 Simulation Results

We conduct a series of simulations in this section to show the effectiveness of the controller designed in Section 2.3. First, we implement the open-loop control by giving constant velocities on top drive. Next, the responses of the drilling system with the iBLF controller are provided. Then, the comparison to a quadratic Lyapunov function (QLF) based approach is shown through simulations. Also, the robustness of the proposed controller is analyzed at the end.

2.4.1 Open-loop Control

For the first case study, the axial and torsional velocities of the top part of the drill string are enforced to be constants. This strategy is currently commonly used in practice in the drilling industry. This is essential to stabilize the top drive velocities to be constants, with the intent of having the drill bit and drill string follow the top part as well. The parameters of the drill string and bit-rock interaction are given in Table 2.1 and Table 2.2, following [77, 78, 28] with minor modifications.

Table 2.1: Parameters of Drill String

M_1	44187 kg	I_1	1685 kgm^2
M_2	29028 kg	I_2	1178 kgm^2
C	34400 Ns/m	C_t	49.5 Nms/rad
K	353000 N/m	K_t	495 Nm/rad

Table 2.2: Parameters of Bit-Rock Interaction

ϑ	77e6 Pa	$\gamma \cdot \mu$	0.7
ζ	0.64	n	5
κ	5	σ	6.2572e7 Pa
a	0.15 m	D^*	1.8721e-4 m

However, such a simple control strategy can sometimes cause significant vibrations in the drilling field as shown in Fig. 2.4(a). It is clear that the stick-slip limit cycles can arise in both axial and torsional dimensions, and the axial dynamics exhibit fast dynamics compared to the torsional one, conforming to the results discussed in [15]. Also, the peak value of the axial velocity is up to 8 times of its desired value (1 mm/s), and the peak value of the torsional velocity becomes twice of its desired value (4 rad/s).

Next, we set a large disturbance in the bit-rock interaction by introducing uncertainties to the intrinsic specific energy parameter ϑ. With the white Gaussian noise added in this term, we can observe greater vibrations in both axial and torsional dimensions. In addition to the stick-slip phenomenon, the velocities can drop below zero and behave axial loss-of-contact and torsional reverse motion, as shown in Fig. 2.4(b). Therefore, a systematic control design is critical for drilling applications to avoid such damaging vibrations.

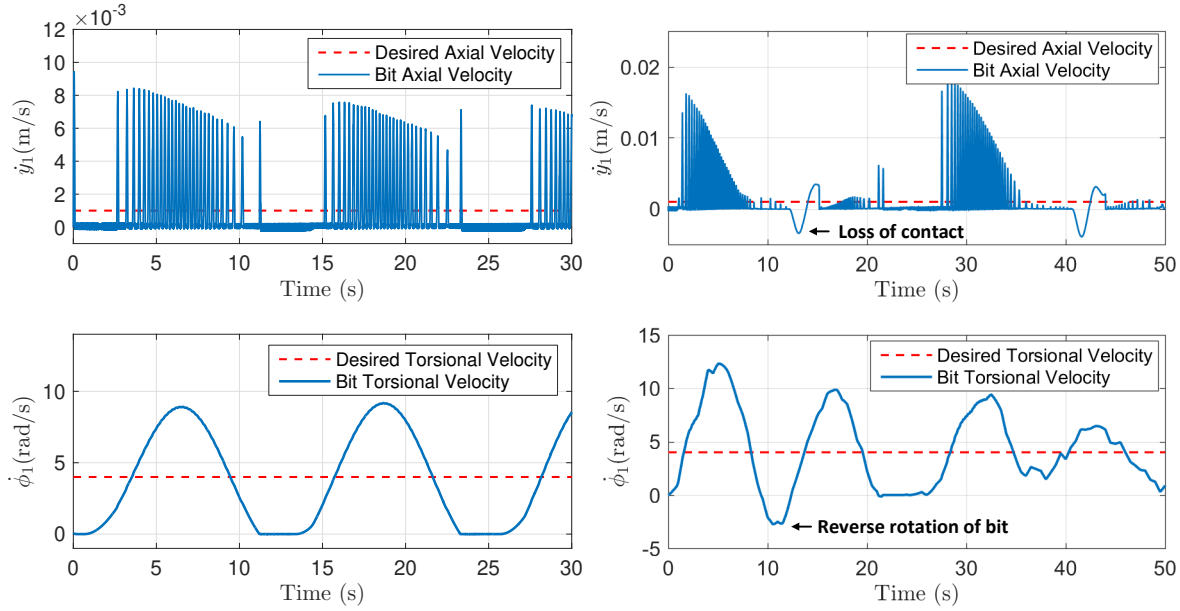

Figure 2.4: Responses of bit's axial and torsional velocities $\dot{y}_1$ and $\dot{\phi}_1$ with constant axial and torsional velocities on top drive: a) Constant ϑ value, b) Disturbance in ϑ value

2.4.2 Closed-loop Control Using iBLF

For the second case study, we apply the proposed algorithm for control design. Again the parameters of the drilling system are shown in Table 2.1 and Table 2.2. The desired axial and torsional velocities are set as $v_{d1} = 1$ mm/s and $\omega_{d1} = 4$ rad/s for the first 30 seconds, and then we switch the desired velocities to $v_{d2} = 1.5$ mm/s and $\omega_{d2} = 5$ rad/s for the next 30 seconds. In

the design of iBLF, we set the constraints for bit's axial and torsional velocities as $k_v = 0.9v_{d1}$ and $k_\omega = 0.5\omega_{d1}$ respectively during the whole simulation time. Moreover, the control gains are chosen as $p_1 = 0.0055$, $p_2 = 1$, $p_3 = 1$, $p_4 = 0.42$, $p_5 = 0.05$, $p_6 = 0.05$ such that the condition (2.60) is satisfied. In the control law $u_{1,2}$ in (2.47) and (2.53), the signum function sgn(z_3) and sgn(z_6) are substituted with tanh(z_3/ϵ_1) and tanh(z_3/ϵ_2), $\epsilon_{1,2} > 0$ for a smoother transient. The initial condition $\boldsymbol{x}(0)$ is given as

$$\begin{aligned} \boldsymbol{x}^T(0) =& [0, -0.05v_{d1}, 0, -0.05v_{d1}, 0, -0.3\omega_{d1}, 0, -0.3\omega_{d1}] \\ \text{and} \quad & \varpi_1(t) \equiv 0, \quad \varpi_2(t) \equiv -0.05v_{d1} \\ & \varpi_5(t) \equiv 0, \quad \varpi_6(t) \equiv -0.3\omega_{d1}, \quad t \in [-\tau(0), 0) \end{aligned}$$

where $\boldsymbol{\xi}(0) \in \Omega$ in this setting. At $t = 0$, we assume that the bit is just in touch with the rock, with the depth-of-cut $D(0)$ being equal to 0. Also, the white Gaussian noise is introduced in the bit's dynamics, representing uncertainties in the down-hole environment. In Fig. 2.5, the bit's axial and torsional velocities stay within the intervals 0.1 mm/s $< \dot{y}_1 <$ 1.9 mm/s and 2 rad/s $< \dot{\phi}_1 <$ 6 rad/s for the first 30 seconds and 0.6 mm/s $< \dot{y}_1 <$ 2.4 mm/s and 3 rad/s $< \dot{\phi}_1 <$ 7 rad/s for the last 30 seconds, corresponding to the given constraints in iBLF design. The dashed lines depict the upper and lower bounds of the constraints. The bit's axial and torsional velocities are kept above zero, avoiding the bit to enter the stick phase. Besides, Fig. 2.6 presents the boundedness and convergence properties of the states $\dot{y}_2$ and $\dot{\phi}_2$ with respect to the internal dynamics under a switching of desired velocities. The drill bit's depth-of-cut is depicted in Fig. 2.7, showing that the bit-rock interaction enters Phase II from Phase I and converges to the desired value in Phase II, and the switching of desired velocities can largely disturb the depth-of-cut at $t = 30$ sec. Also, we draw the control inputs, i.e., top drive's force and torque F and T, in Fig. 2.8. At $t = 0$ sec, the control inputs can rise up to a high magnitude, which is mainly caused by the initial condition setting in the numerical simulation. This situation is less likely to occur in practice since it denotes the instant when the bit just touches the rock surface, and the depth-of-cut is 0. In the real application, the

feedback control oftentimes takes effect when the operating parameters, such as torsional RPM and axial weight-on-bit, change significantly. Such a condition can be simulated by the switching of desired velocities at $t = 30$ sec. Here, the magnitude of the control is smaller compared with the $t = 0$ sec instant, which is feasible in practice.

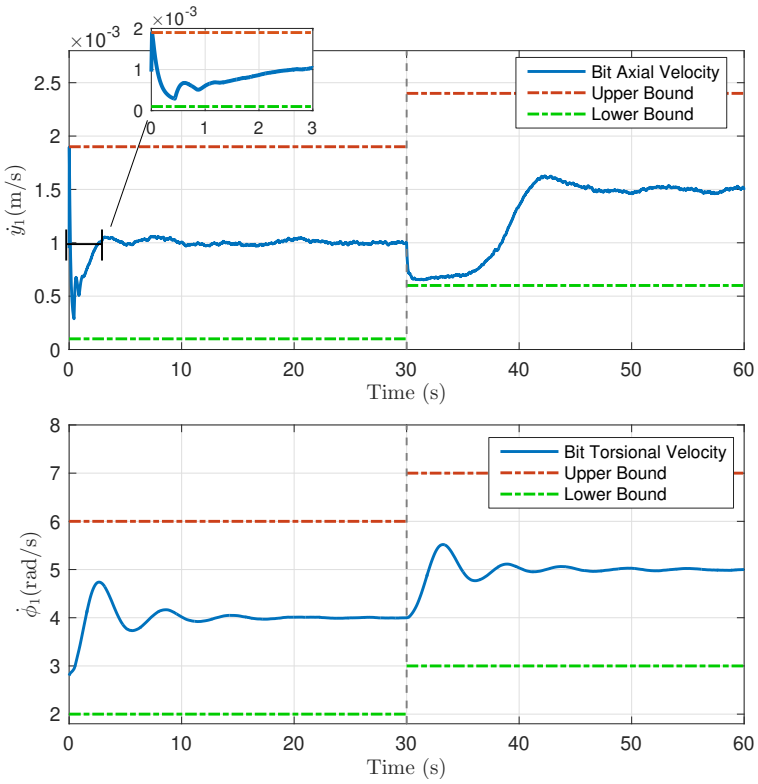

Figure 2.5: Time history of bit's axial and torsional velocities $\dot{y}_1$ and $\dot{\phi}_1$ with a switching of desired velocities (0-30 seconds: $v_{d1} = 1$ mm/s, $\omega_{d1} = 4$ rad/s; 30-60 seconds: $v_{d2} = 1.5$ mm/s, $\omega_{d2} = 5$ rad/s)

Next, to prove that the goal of barrier avoidance is indeed achieved comparing with other unconstrained control strategies, instead, we apply a backstepping control in a regular QLF form (without the Barrier terms V_v and V_ω in (2.25)). In Fig. 2.9, under the same initial conditions, the bit's responses using QLF controller can be stablized and forced to the desired rates ($v_{d1} = 1$ mm/s, $\omega_{d1} = 4$ rad/s during the whole simulation time). However, the barriers are violated and stick-slip

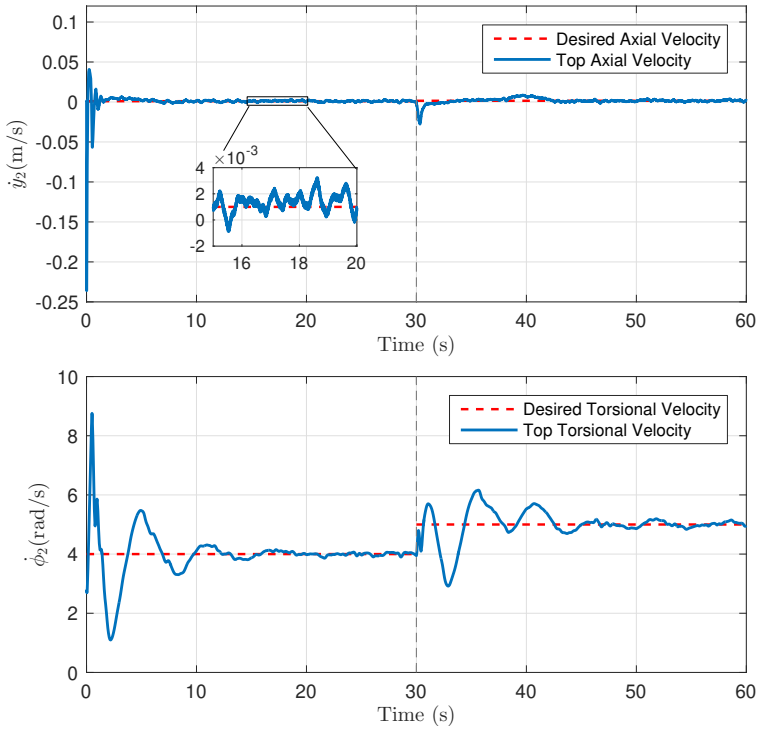

Figure 2.6: Time history of top drive's axial and torsional velocities $\dot{y}_2$ and $\dot{\phi}_2$ with a switching of desired velocities (0-30 seconds: $v_{d1} = 1$ mm/s, $\omega_{d1} = 4$ rad/s; 30-60 seconds: $v_{d2} = 1.5$ mm/s, $\omega_{d2} = 5$ rad/s)

phenomenons arise in both axial and torsional dimensions during the transient, in which the iBLF control will get rid of such oscillations.

To exam the robustness, we validate the control performance over a range of the intrinsic specific energy parameter ϑ, with the perturbance range 50%-150% of its nominal value 77 MPa. The responses of bit's axial velocities are shown in Fig. 2.10 (with the desired velocities $v_{d1} = 1$ mm/s, $\omega_{d1} = 4$ rad/s during the whole simulation time), where the state constraints are not transgressed under the variance of the perturbed ϑ.

To conclude, the simulation results highlight the barriers that are imposed on the bit's axial and torsional velocities through the control design using iBLF, and thus the constraints on the states are not violated. It can be seen that the stick-slip behavior is indeed eliminated as compared to the first case study, illustrating the performance and robustness of the proposed controller for a vertical

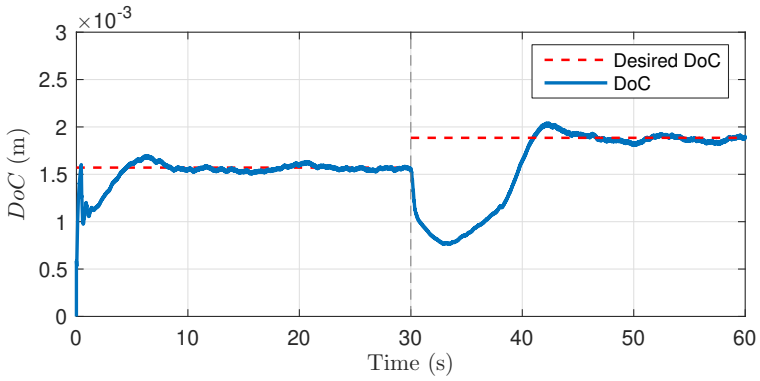

Figure 2.7: Time history of depth-of-cut $D(t)$ with a switching of desired velocities (0-30 seconds: $v_{d1} = 1$ mm/s, $\omega_{d1} = 4$ rad/s; 30-60 seconds: $v_{d2} = 1.5$ mm/s, $\omega_{d2} = 5$ rad/s)

drilling system.

2.5 Conclusion

The control design to avoid drilling system to operate in undesired conditions based on barrier Lyapunov functions is studied in this chapter. It is based on a model with coupled axial and torsional dynamics through the bit-rock interaction constrained by a DDE, which is transformed into internal and external dynamics using an input-output decoupling approach. The iBLF is implemented in a framework of backstepping, where explicit constraints on system states are embedded in the design of the Lyapunov function. In the numerical simulations, effectiveness of the proposed controller is validated through comparison of open-loop and closed-loop case studies. Furthermore, the state-constrained control strategy proposed in this study can be extended to a general class of control problems of regenerative process with state-dependent time delays, such as machine tool chatter [79, 80], which have not been explored before.

In the future study, we plan to investigate the state-constrained/iBLF control for directional drilling systems. A more sophisticated dynamics model incorporating the curved trajectory and the lateral motion will be used in the control design. The impact on the state constrained control on the trajectory tracking, rate of penetration regulation and vibration mitigation will be studied.

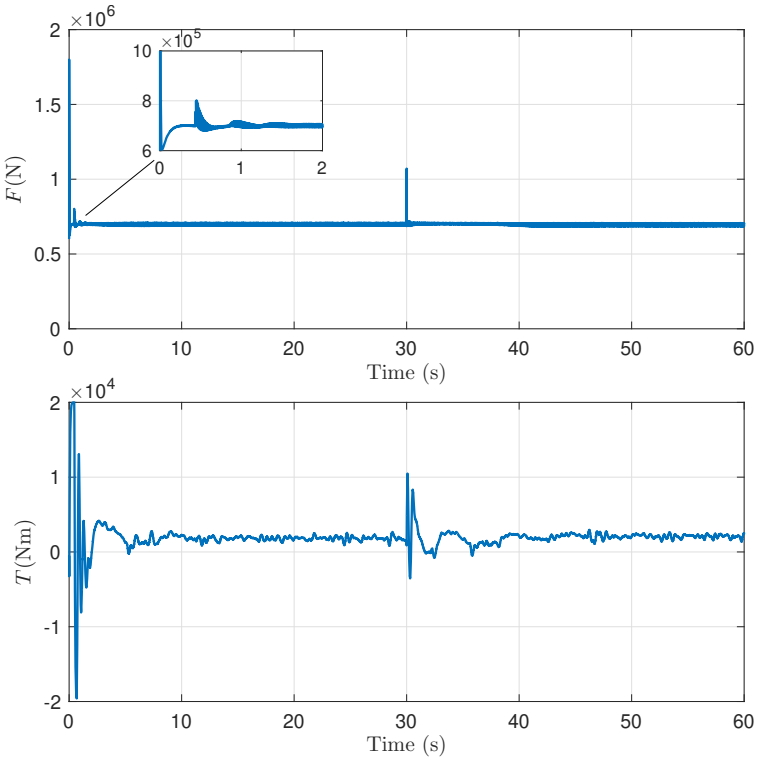

Figure 2.8: Time history of top drive's force F and torque T with a switching of desired velocities (0-30 seconds: $v_{d1} = 1$ mm/s, $\omega_{d1} = 4$ rad/s; 30-60 seconds: $v_{d2} = 1.5$ mm/s, $\omega_{d2} = 5$ rad/s)

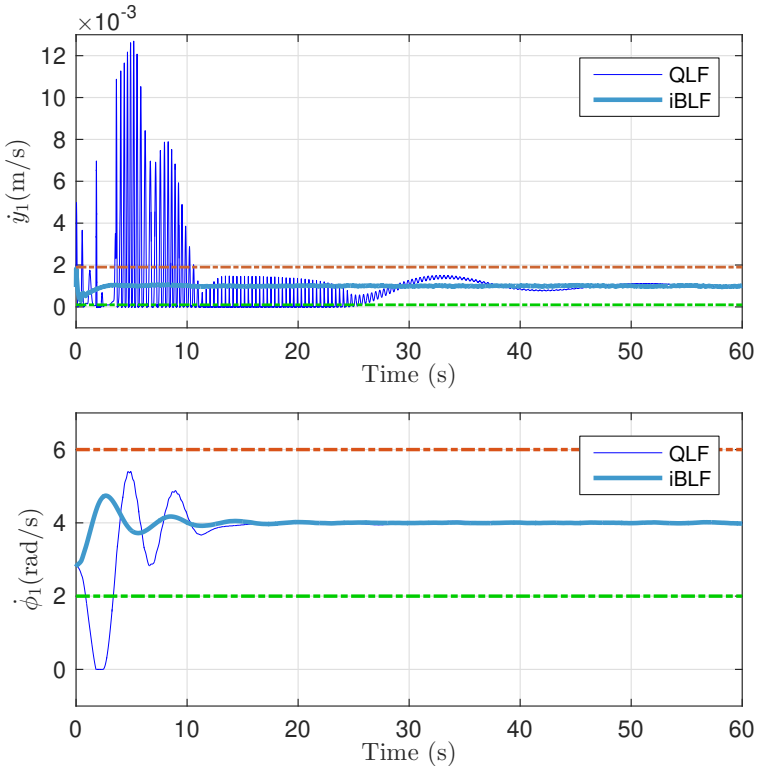

Figure 2.9: Comparison of iBLF and QLF methods with the responses of bit's axial and torisional velocities with the desired velocities $v_{d1} = 1$ mm/s, $\omega_{d1} = 4$ rad/s

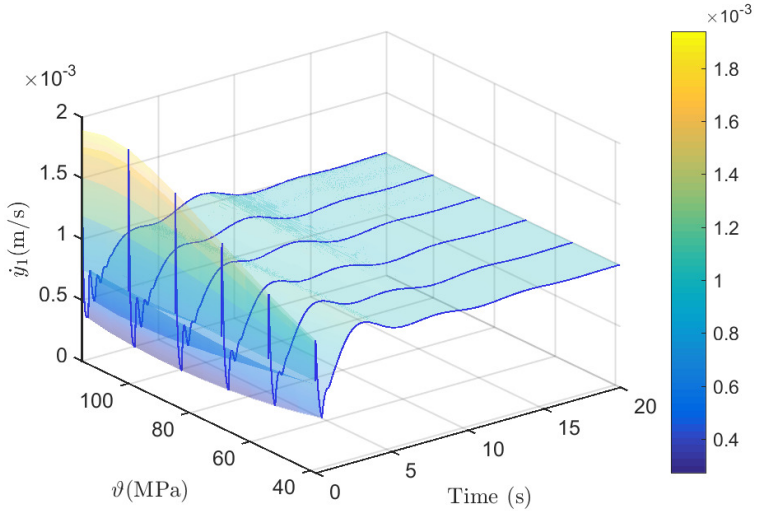

Figure 2.10: Bit's axial velocities with parameter perturbance of ϑ (50% to 150%) with the desired velocities $v_{d1} = 1$ mm/s, $\omega_{d1} = 4$ rad/s

3. STATE BARRIER AVOIDANCE CONTROL DESIGN USING A DIFFEOMORPHIC TRANSFORMATION BASED METHOD

3.1 Introduction

State constrained control or state-barrier avoidance control has recently attracted much attention in the field of nonlinear control systems. The problem is to constrain the system states to avoid undesired operating regions or barriers during convergence. In practice, constraints can arise as an inherent characteristic of systems, such as robot manipulators [81] and electrostatic microactuators [82], or can be deliberately chosen to improve the performance of systems, such as a marine riser [61], a crane system [60], a multi-spacecraft system [59], and a downhole drilling system [83].

In this chapter, we propose a new state-barrier avoidance control method based on state-space transformation. As shown in Fig. 3.1, the original state space on the left will be transformed into a new space through a diffeomorphic transformation. The barrier will be mapped to infinity or a region far from the origin of the new space. In the new space, as long as we can design a controller ensuring stability in the radially bounded region, the control will ensure avoidance of the barrier in the new space and therefore the same can be achieved in the original space. In other words, the barrier avoidance control is translated into a regular control design in the new space. This conversion can bring in an important benefit. It converts the state-constrained problem to an unconstrained one, and avoids the requirement of having the control design based on a Lyapunov function of a specific form, the limiting factor that restricts many control schemes to be used. For example, it is difficult to use a sliding mode control scheme in the existing BLF based design, since the design requires a single overall Lyapunov function containing all the barrier terms to be available, while the sliding mode scheme requires two phases (reaching and sliding) and the control design cannot be done with a single Lyapunov function. Nevertheless, as will be shown with a case study, using our new framework, it is convenient to use a sliding mode approach to

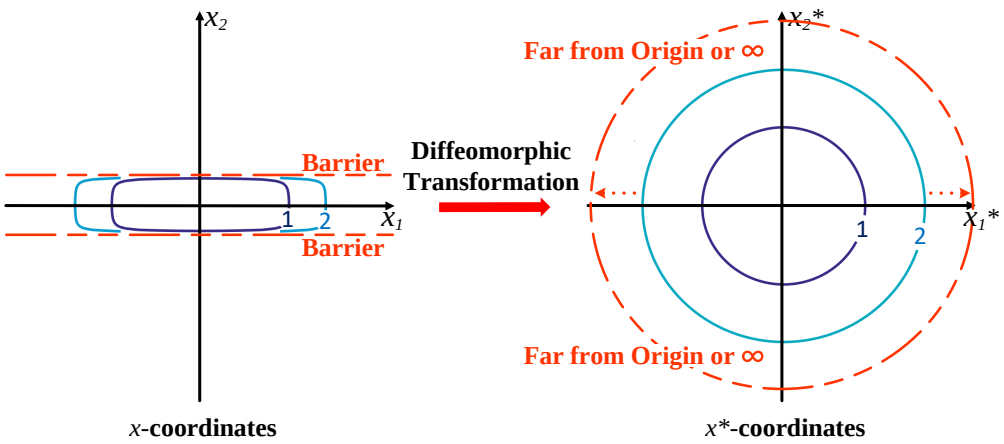

Figure 3.1: Diffeomorphic transformation from x-coordinates (original space) to x^*-coordinates (new space). The barrier in the original space is projected far from the origin or to infinity in the new space.

design a barrier avoidance controller. Thus, the new method opens up opportunities for addressing barrier avoidance using many well established nonlinear control techniques.

The rest of this chapter is organized as follows. In Section 3.2, we formulate the barrier avoidance control problem for a nonlinear system, and provide mathematical preliminaries on the sufficient conditions for the invariance of the stability properties under state transformation. Section 3.3 presents the main results of this study, where a diffeomorphic transformation based method is proposed to achieve the barrier avoidance and to maintain the stability properties. Finally, Section 3.4, Section 3.5, and Section 3.6 exhibit three case studies using sliding mode control, backstepping control, and LPV control techniques, respectively, applying to different classes of nonlinear systems. Simulations results are shown to prove efficacy of the proposed method.

3.2 Problem Formulation and Preliminaries

Consider the problem of designing a barrier avoidance controller $u = K(x)$ for the nonlinear system Σ_{ol}:

$$\Sigma_{ol} : \dot{x} = h_{ol}(x, u) \tag{3.1}$$

where $x \in \mathbb{R}^n$ and the initial condition $x(0) = x_0$. The closed-loop system $\Sigma : \dot{x} = h_{ol}(x, K(x)) = h(x)$ is locally Lipschitz in x, ensuring the uniqueness of the solution. Defining the safety region as $\mathcal{D} \subset \mathbb{R}^n$, the objective is:

System Σ is stable (asymptotically/exponentially stable) at the origin $x = 0$ and the states do not cross the barrier set by the boundary of $\mathcal{D}$.

Under a smooth non-degenerate change of coordinates $x^* = \Phi(x)$, $x \in \Omega$, the closed-loop system Σ is transformed into the new coordinates. The original system and the transformed system are denoted as:

$$\Sigma : \quad \dot{x} = h(x), \qquad x \in \Omega \subseteq \mathbb{R}^n \tag{3.2}$$

$$\Sigma^* : \quad \dot{x}^* = h^*(x^*), \quad x^* \in \Phi(\Omega) \subseteq \mathbb{R}^n \tag{3.3}$$

Given the initial conditions for Σ and Σ^* as x_0 and $x_0^* = \Phi(x_0)$ respectively, we denote the solutions of Σ and Σ^* as $x_S(t)$ and $x_S^*(t)$ for $t \in [0, \infty)$. The following two Lemmas provide conditions to maintain stability under the change of coordinates.

Lemma 1. *Consider a desired trajectory $x_d(t) \in \Omega$ and $x_d^*(t) = \Phi(x_d(t)) \in \Phi(\Omega)$. Define the errors as*

$$z(t) = x_S(t) - x_d(t), \quad z^*(t) = x_S^*(t) - x_d^*(t) \tag{3.4}$$

If there exist constants $\sigma > 0$ and $\bar{L} > 0$ such that

$$\|z^*(t)\| < \sigma \quad \textit{and} \quad \|z(t)\| \leq \bar{L}\|z^*(t)\| \tag{3.5}$$

for all $t \in [0, \infty)$ and $x^* \in \Phi(\Omega)$, then the stability (asymptotical/exponential stability) of $z^*(t)$ at $z^* = 0$ can infer the stability of $z(t)$ at $z = 0$. In particular, when $x_d^*(t) = c^*$ and $x_d(t) = \Phi^{-1}(c^*) = c$ (c, c^* are constants) and for all $t \in [0, \infty)$, the stability of $x_S^*(t)$ at $x_S^* = c^*$ can infer the stability of $x_S(t)$ at $x_S = c$.

Proof: We first specify an arbitrary $\bar{\epsilon} > 0$ to have $\|z(t)\| < \bar{\epsilon}$ for all $t \in [0, \infty)$ and choose a positive constant $\epsilon < \min[\bar{\epsilon}/\bar{L}, \sigma]$. Given the stability of $z^*(t)$, there exists a $\delta(\epsilon) > 0$ such that

$$\|x_S^*(0) - x_d^*(0)\| < \delta \quad \Rightarrow \quad \|x_S^*(t) - x_d^*(t)\| < \epsilon \tag{3.6}$$

for all $t \in [0, \infty)$. Since the mapping $x^* = \Phi(x)$ is smooth and is Lipschitz in Ω, then there exists a constant $L > 0$ such that

$$\|x_S^*(0) - x_d^*(0)\| \leq L\|x_S(0) - x_d(0)\| \tag{3.7}$$

Choosing $\bar{\delta} = \delta/L$, we can rewrite it as $\bar{\delta} = \bar{\delta}(\bar{\epsilon})$, since $\bar{\delta}$ depends on $\bar{\epsilon}$. If $\|x_S(0) - x_d(0)\| < \bar{\delta}$ holds, we have $\|x_S^*(0) - x_d^*(0)\| \leq L\bar{\delta} < \delta$ as per (3.7). Moreover, it can be implied that $\|x_S^*(t) - x_d^*(t)\| < \epsilon < \bar{\epsilon}/\bar{L}$ as a result of (3.6).

Therefore, using the condition (3.5), we can conclude that for any $\bar{\epsilon} > 0$, there exists a $\bar{\delta} = \bar{\delta}(\bar{\epsilon})$ such that

$$\|x_S(t) - x_d(t)\| \leq \bar{L}\|x_S^*(t) - x_d^*(t)\| < \bar{\epsilon} \tag{3.8}$$

whenever $\|x_S(0) - x_d(0)\| < \bar{\delta}$ holds. This completes the proof of stability for $z(t)$.

Besides, considering the asymptotical stability of $z^*(t)$, an additional condition is given as

$$\lim_{t\to\infty}(x_S^*(t) - x_d^*(t)) = 0 \tag{3.9}$$

By the inequality (3.8), the following condition holds

$$\lim_{t\to\infty}(x_S(t) - x_d(t)) = 0 \tag{3.10}$$

We conclude that $z(t)$ is asymptotically stable at 0.

Next, considering the exponential stability of $z^*(t)$, an additional condition is given as: there

exists $\delta > 0$, $\mu > 0$ and $P > 0$ such that

$$\|x_S^*(t) - x_d^*(t)\| \leq P\|x_S^*(0) - x_d^*(0)\|e^{-\mu t} \tag{3.11}$$

Using the facts of (3.5), (3.7) and (3.11), it gives

$$\begin{aligned}\|x_S(t) - x_d(t)\| &\leq \bar{L}\|x_S^*(t) - x_d^*(t)\| \\ &\leq \bar{L}P\|x_S^*(0) - x_d^*(0)\|e^{-\mu t} \\ &\leq L\bar{L}P\|x_S(0) - x_d(0)\|e^{-\mu t}\end{aligned} \tag{3.12}$$

We conclude that $z(t)$ is exponentially stable at 0. ■

Lemma 2. *Given the definition of $z(t)$ and $z^*(t)$ in Lemma 1, if $\Phi : \Omega \to \Phi(\Omega)$ is a diffeomorphism, and there exists an $\bar{\sigma} > 0$ such that a closed $\bar{\sigma}$-neighborhood of an arbitrary point $x_S^*(t)$, $t \in [0, \infty)$, is a subset of $\Phi(\Omega)$, then there exist constants $0 < \sigma \leq \bar{\sigma}$ and $M > 0$ such that*

$$\|z^*(t)\| < \sigma \quad \textit{and} \quad \|z(t)\| \leq M\|z^*(t)\| \tag{3.13}$$

for all $t \in [0, \infty)$ and $x^* \in \Phi(\Omega)$.

Proof: We specify $0 < \sigma \leq \bar{\sigma}$ and have $\|x_S^*(t) - x_d^*(t)\| < \sigma$ for $t \in [0, \infty)$. Define a set $\mathcal{U}_\sigma$ as

$$\mathcal{U}_\sigma \triangleq \bigcup_{t\in[0,\infty)} \left\{x^* \in \mathbb{R}^n \;\middle|\; \|x_S^*(t) - x^*\| \leq \sigma\right\} \tag{3.14}$$

Here, $\mathcal{U}_\sigma$ is a compact set and satisfies $\mathcal{U}_\sigma \subseteq \mathcal{U}_{\bar{\sigma}} \subset \Phi(\Omega)$ and $x_d^*(t) \in \mathcal{U}_\sigma$ for $t \in [0, \infty)$.

The diffeomorphism Φ^{-1} has the Lipschitz property on the compact convex set $\mathcal{Q}$ at certain $t = \tau$.

$$\mathcal{Q}_{\tau,\sigma} \triangleq \left\{x^* \in \mathbb{R}^n \;\middle|\; \|x_S^*(\tau) - x^*\| \leq \sigma\right\} \tag{3.15}$$

The Lipschitz constant on the set $\mathcal{Q}_{\tau,\sigma}$ satisfies

$$L_{\mathcal{Q}_{\tau,\sigma}} = \sup_{\mathcal{Q}_{\tau,\sigma}} \left\| \frac{\partial \Phi^{-1}}{\partial x^*} \right\| \leq \sup_{\mathcal{U}_\sigma} \left\| \frac{\partial \Phi^{-1}}{\partial x^*} \right\| = M \tag{3.16}$$

Thus, for all $\tau \in [0, \infty)$ we have

$$\|x_S(\tau) - x_d(\tau)\| \leq M \|x_S^*(\tau) - x_d^*(\tau)\| \tag{3.17}$$

This completes the proof. ■

3.3 Barrier Avoidance Control with the Diffeomorphic Transformation

To achieve the control objective as discussed in Section 3.2, we propose a diffeomorphic state transformation based barrier avoidance control method as the following.

Theorem 2. *Consider the closed-loop system Σ (defined in* (3.2)*) and a given open set $\mathcal{D}$. The boundary of $\mathcal{D}$ is noted as $\partial\mathcal{D}$, which is the barrier to avoid. If a diffeomorphism $x^* = \Phi(x)$ transforms the system Σ into Σ^* (defined in* (3.3)*) and satisfies:*

1) The transformation $x^* = \Phi(x)$ maps $\mathcal{D}$ into $\mathbb{R}^n$ in x^*-coordinates. The boundary $\partial\mathcal{D}$ is mapped to the points at infinity, and the origin $x = 0$ is mapped to the origin $x^* = 0$;

2) The system Σ^* is globally stable (globally asymptotically/exponentially stable) at $x^* = 0$.

Whenever the initial condition $x \in \mathcal{D}$, the following statements hold:

a) The states $x(t)$ stay in $\mathcal{D}$ for all $t \in [0, \infty)$, and avoid reaching the barrier $\partial\mathcal{D}$;

b) The system Σ is stable (asymptotically/exponentially stable) at $x = 0$ with the attractive region identical to $\mathcal{D}$.

Specially, when the condition 2) is modified as

2) The solution $x_S^*(t)$ is locally stable (locally asymptotically/exponentially stable) at $x^* = 0$.

Then the following statements hold:

a) The solution $x_S(t)$ stay in $\mathcal{D}$ for all $t \in [0, \infty)$;

b) The system Σ^* is locally stable (locally asymptotically/exponentially stable) at $x = 0$.

Proof: In x-coordinates, each point $x \in \mathcal{D}$ is projected to non-infinity point in x^*-coordinates. Since Σ^* is stable, the states $x^*(t)$ are bounded, and do not reach infinity. Due to the fact that $x^* = \Phi(x)$ is a bijection, the states $x(t)$ will stay in $\mathcal{D}$ for all $t \in [0, \infty)$, and will not reach the boundary $\partial\mathcal{D}$.

The projection $x^* = \Phi(x)$ maps $\mathcal{D}$ into $\mathbb{R}^n$, and in $\mathbb{R}^n$ the closed $\bar{\sigma}$-neighborhood of any trajectory will belong to $\mathbb{R}^n$ for $\bar{\sigma} > 0$. According to Lemma 1 and Lemma 2, stability (asymptotical/exponential stability) will be maintained under the state transformation from x^*-coordinates to x-coordinates. Since global stability is achieved in x^* coordinates, the attractive region in x-coordinates is idential to $\mathcal{D}$.

The local stabilities case is derived in a similar way. ■

Remark 2. *In the existing barrier avoidance methods [50, 51, 54], the forward invariance of the set $\mathcal{D}$ (barrier avoidance of $\partial\mathcal{D}$) and the stability are ensured by choosing a barrier Lyapunov function (BLF) $V(x)$ which satisfies the following two conditions:*

1) $V(x) \to \infty$ as $x \to \partial\mathcal{D}$;

2) $V(0) = 0$, $V(x) > 0$ for $x \in \mathcal{D}/\{0\}$ and $\dot{V}(x) \leq 0$ for $x \in \mathcal{D}$.

However, the design of BLF requires a careful selection of Lyapunov candidate to meet the two conditions at the same time, and many times it is non-trivial to find such a BLF or hard to design a controller based on such a Lyapunov function of a specific form. In this study, our method proposed in Theorem 2 decompose the control design into two steps:

i) Find a diffeomorphism $x^* = \Phi(x)$ satisfying the conditions given in Theorem 2;

ii) Design a controller in the new coordinates to globally stabilize the transformed system Σ^*. Specially, we can use a Lyapunov-based approach for Σ^*, i.e., choosing a Lyapunov function $V(x^*)$ satisfying the radially unbounded condition $\|x^*\| \to \infty \;\Rightarrow\; V(x^*) \to \infty$.

The method converts a state constrained control problem to a non-constrained problem, which allows greater flexibility in the control design and thus can be more promising to reach a design solution.

In the next two sections, case studies are given to demonstrate the effectiveness of the proposed algorithm.

3.4 Case Study I: Sliding Mode Control with Barrier Avoidance

3.4.1 Control Design

For the first case study, we design the barrier avoidance controller based on a sliding mode scheme. This shows an essential benefit of the proposed control method. Unlike the existing barrier Lyapunov function (BLF) based control design method, our design is not based on a single Lyapunov function of a specific form, and thus can be used under the sliding mode scheme which requires two phases (sliding and reaching). This offers more flexibility in the control design options. We consider a nonlinear double integrator as:

$$\begin{aligned} \dot{x}_1 &= x_2 \\ \dot{x}_2 &= f(x) + g(x)u + \delta(x,u) \end{aligned} \tag{3.18}$$

where $f(x)$, $g(x)$ and $\delta(x,u)$ are sufficiently smooth, and $\delta(x,u)$, $g(x)$ are unknown, satisfying $g(x) \geq g_0 > 0$. The safety region $\mathcal{D}$ is defined by

$$\mathcal{D} = \left\{ x \in \mathbb{R}^2 \,\middle|\, |x_1| < k_1, |x_2| < k_2 \right\} \tag{3.19}$$

where $k_{1,2} > 0$. The diffeomorphic transformation is chosen by

$$\begin{aligned} x_1^* &= \tan(\beta_1 x_1), \quad \beta_1 = \pi/(2k_1) \\ x_2^* &= \tan(\beta_1 x_1), \quad \beta_2 = \pi/(2k_2) \end{aligned} \tag{3.20}$$

The system (3.18) in the new coordinates is written as

$$\begin{aligned} \dot{x}_1^* &= \beta_1 \beta_2^{-1} (1 + x_1^{*2}) \tan^{-1} x_2^* \\ \dot{x}_2^* &= \beta_2 (1 + x_2^{*2})(f(x) + g(x)u + \delta(x, u)) \end{aligned} \tag{3.21}$$

Design the sliding manifold as $s = x_1^* + x_2^*$. We have the system dynamics on the sliding surface $s = 0$ as

$$\dot{x}_1^* = -\beta_1 \beta_2^{-1} (1 + x_1^{*2}) \tan^{-1} x_1^* \tag{3.22}$$

where x_1^* is globally exponentially stable at $x_1^* = 0$. Then taking time-derivative of s gives

$$\dot{s} = \beta_1 \beta_2^{-1} (1 + x_1^{*2}) \tan^{-1} x_2^* + \beta_2 (1 + x_2^{*2})(f(x) + g(x)u + \delta(x, u)) \tag{3.23}$$

We choose the control u as

$$u = \frac{1}{\hat{g}(x)} \left(-f(x) - \frac{\beta_1 (1 + x_1^{*2}) \tan^{-1} x_2^*}{\beta_2^2 (1 + x_2^{*2})} \right) + v \tag{3.24}$$

where $\hat{g}(x)$ is the nominal model of $g(x)$, and v is the virtual control input. Plugging (3.24) into (3.23) gives

$$\dot{s} = \beta_2 (1 + x_2^{*2}) g(x) v + \Delta(x^*, u) \tag{3.25}$$

where Δ is an uncertainty term defined as

$$\Delta(x^*, u) = \beta_2(1 + x_2^{*2})\delta(x, u) + \left(1 - \frac{g(x)}{\hat{g}(x)}\right)\left(\beta_2(1 + x_2^{*2})f(x) + \frac{\beta_1}{\beta_2}(1 + x_1^{*2})\tan^{-1} x_2^*\right) \tag{3.26}$$

For a continuous function $\varrho(x^*) > 0$, we assume that

$$\left|\frac{\Delta(x^*, u)}{\beta_2(1 + x_2^{*2})g(x)}\right| \leq \varrho(x^*) \tag{3.27}$$

Then we design the virtual control input v as

$$v = -\psi(x^*)\text{sat}\left(\frac{s}{\epsilon}\right) \tag{3.28}$$

where sat$(\cdot)$ denotes the saturation function and $\psi(x^*) \geq \varrho(x^*) + \psi_0$, for $\psi_0 > 0$. Next, choosing the Lyapunov function $V_s = 1/2s^2$, in the region $|s| > \epsilon$ we can obtain

$$\begin{aligned}
\dot{V}_s = s\dot{s} &\leq \beta_2(1 + x_2^{*2})g(x)(sv + |s|\varrho(x^*)) \\
&\leq \beta_2(1 + x_2^{*2})g(x)(-|s|\psi(x^*) + |s|\varrho(x^*)) \\
&\leq -\beta_2(1 + x_2^{*2})g_0\psi_0|s| \\
&\leq -\beta_2 g_0\psi_0|s| < 0
\end{aligned} \tag{3.29}$$

Also, having the Lyapunov function $V_0 = 1/2x_1^{*2}$, we can always find class $\mathcal{K}$ functions ϕ_1, ϕ_2, ϕ_3 and γ such that

$$\phi_1(|x_1^*|) \leq V_0 \leq \phi_2(|x_1^*|) \tag{3.30}$$

$$\dot{V}_0 = \beta_1\beta_2^{-1}(1 + x_1^{*2})\tan^{-1}(-x_1^* + s) \leq -\phi_3(|x_1^*|), \quad \forall\ |x_1^*| \geq \gamma(|s|) \tag{3.31}$$

Since V_0 is radially unbounded and the above conditions hold globally, we establish the following theorem to give a sufficient condition for the barrier avoidance control objective.

Theorem 3. *Consider the systems* (3.18) *and* (3.21)*. If we choose the control* u *given by* (3.24) *and* (3.28)*, satisfying the condition* (3.27) *globally and* $\varrho(0) = 0$*, then there exists* $\epsilon^* > 0$ *such that, for* $0 < \epsilon < \epsilon^*$*, the origin of system* (3.21) *is globally asymptotically stable, and the origin of system* (3.18) *is asymptotically stable with the attractive region* $\mathcal{D}$ *given in* (3.19)*.*

Proof: For a positive constant c, we have

$$|s| \leq c \;\Rightarrow\; \dot{V}_0 \leq -\phi_3(|x_1^*|), \quad \text{for } |x_1^*| \geq \gamma(c) \tag{3.32}$$

We define a class $\mathcal{K}$ function ϕ by

$$\phi(r) = \phi_2(\gamma(r)) \tag{3.33}$$

Then, we derive the following

$$\begin{aligned} V_0(x_1^*) \geq \phi(c) \;&\Rightarrow\; V_0(x_1^*) \geq \phi_2(\gamma(c)) \\ &\Rightarrow\; \phi_2(|x_1^*|) \geq \phi_2(\gamma(c)) \\ &\Rightarrow\; |x_1^*| \geq \gamma(c) \\ &\Rightarrow\; \dot{V}_0 \leq -\phi_3(|x_1^*|) \leq -\phi_3(\gamma(c)) \end{aligned} \tag{3.34}$$

Thus, $\dot{V}_0$ is negative on the boundary $V_0(x_1^*) = c_0$. When $c_0 \geq \phi(c)$, the set

$$\mathcal{P} = \{V_0(x_1^*) \leq c_0\} \times \{|s| \leq c\} \tag{3.35}$$

is positively invariant whenever $c > \epsilon$. Since $\dot{V}_0 \leq -\phi_3(\epsilon)$ for all $V_0(x_1^*) \geq \phi(\epsilon)$, the trajectories

will reach the positively invariant set

$$\mathcal{P}_\epsilon = \{V_0(x_1^*) \leq \phi(\epsilon)\} \times \{|s| \leq \epsilon\} \tag{3.36}$$

Due to the fact that $V_0(x_1^*)$ is radially unbounded, the set $\mathcal{P}$ includes any initial conditions. All trajectories that start in $\mathcal{P}$ will enter $\mathcal{P}_\epsilon$ within finite time. Inside $\mathcal{P}_\epsilon$, the closed-loop system is expressed as

$$\begin{aligned} \dot{x}_1^* &= \beta_1\beta_2^{-1}(1 + x_1^{*2}) \tan^{-1}(-x_1^* + s) \\ \dot{s} &= -\beta_2(1 + x_2^{*2})g(x)\psi(x^*)\frac{s}{\epsilon} + \Delta(x^*, u) \end{aligned} \tag{3.37}$$

There exist positive constants c_1, c_2, c_3 and c_4 such that

$$\begin{aligned} c_1|x_1^*|^2 \leq V_0(x_1^*) \leq c_2|x_1^*|^2 \\ \frac{\partial V_0}{\partial x_1^*}\beta_1\beta_2^{-1}(1 + x_1^{*2}) \tan^{-1}(-x_1^*) \leq -c_3|x_1^*|^2 \\ \left|\frac{\partial V_0}{\partial x_1^*}\right| \leq c_4|x_1^*| \end{aligned} \tag{3.38}$$

in the neighborhood of $x_1^* = 0$. By the smoothness of $\tan^{-1}(\cdot)$ and Δ, we can choose positive constants p_1, p_2 and p_3 such that

$$\begin{aligned} |\beta_1\beta_2^{-1}(1 + x_1^{*2}) \tan^{-1}(-x_1^* + s)\beta_1\beta_2^{-1}(1 + x_1^{*2}) \tan^{-1}(-x_1^*)| \leq p_1|s| \\ |\Delta| \leq p_2|x_1^*| + p_3|s| \end{aligned} \tag{3.39}$$

in the neighborhood of $(x_1^*, s) = (0, 0)$. Choose the Lyapunov candidate as

$$V = V_0 + V_s \tag{3.40}$$

It is shown that

$$\dot{V} \leq -c_3|x_1^*|^2+(c_4p_1+p_2)|x_1^*||s|+p_3|s|^2-\frac{\beta_2 g_0\psi_0}{\epsilon}|s|^2 \leq 0 \tag{3.41}$$

holds for sufficiently small ϵ. ■

3.4.2 Simulation Results

Consider an example of a cart with a nonlinear spring moving on a plane [84]

$$\begin{aligned}\dot{x}_1(t) &= x_2(t)\\ \dot{x}_2(t) &= \frac{1}{M}(-k_0e^{-x_1(t)}x_1(t)-h_dx_2(t)+u(t)+w(t))\end{aligned} \tag{3.42}$$

where $M = 1$ kg is the mass of the cart, and x_1 and x_2 are the displacement and the velocity of the cart respectively, as shown in Fig. 3.2. The nonlinear spring stiffness is $k = k_0e^{-x_1} = 0.33e^{-x_1}$ N/m and the damping coefficient is $h_d = 1.1$ Ns/m. The force u applied on the cart is the control input. The air resistance force w is expressed as

$$w = -c_dx_2^2\text{sign}(x_2) \tag{3.43}$$

where c_d is the resistance coefficient satisfying $0 \leq c_d \leq 0.4$ Ns^2/m^2. The state constraints are chosen as $|x_1| < 0.5$ m and $|x_2| < 1$ m/s. Considering w as an unknown term, the control parameters are designed as $\psi(x^*) = 0.5$ and $\epsilon = 0.001$. Using the barrier avoidance based sliding mode control approach, various initial conditions are tested in the simulation without any violations of the constraints, as shown in Fig. 3.3(a). In comparison, when a standard sliding mode control is used under the same initial conditions, the barriers are reached and the constraints are violated, as shown in Fig. 3.3(b). This simulation result verifies the effectiveness of the proposed barrier avoidance scheme.

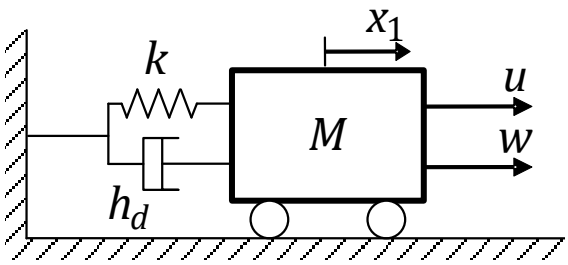

Figure 3.2: Sketch of the mechanical system

3.5 Case Study II: Backstepping Control with Barrier Avoidance

3.5.1 Control Design

Consider the following nth order nonlinear system in a strict feedback form

$$\begin{aligned}\dot{x}_i &= f_i(\bar{x}_i) + g_i(\bar{x}_i)x_{i+1}, \quad i = 1, 2, ..., n-1 \\ \dot{x}_n &= f_n(\bar{x}_n) + g_n(\bar{x}_n)u \\ y &= x_1 \end{aligned} \tag{3.44}$$

where $\bar{x}_i = [x_1, x_2, ..., x_i]^T$, and $f_i(\bar{x}_i)$, $g_i(\bar{x}_i)$ are smooth functions under the assumption $g_i \neq 0$. In this case, the safety region $\mathcal{D}$ is defined as

$$\mathcal{D} = \left\{ x \in \mathbb{R}^n \;\middle|\; |x_i| < k_i,\ i = 1, 2, ..., n \right\} \tag{3.45}$$

The control objective is to track the desired trajectory $y_d(t)$ while the states can avoid reaching the barrier $\partial\mathcal{D}$., where $|y_d| < k_1$ and its ith order derivatives ($i = 1, ..., n$) are bounded. The state transformation for each state x_i is given as

$$x_i^* = \frac{x_i}{(k_i^2 - x_i^2)^{1/2}},\ i = 1, 2, ..., n \tag{3.46}$$

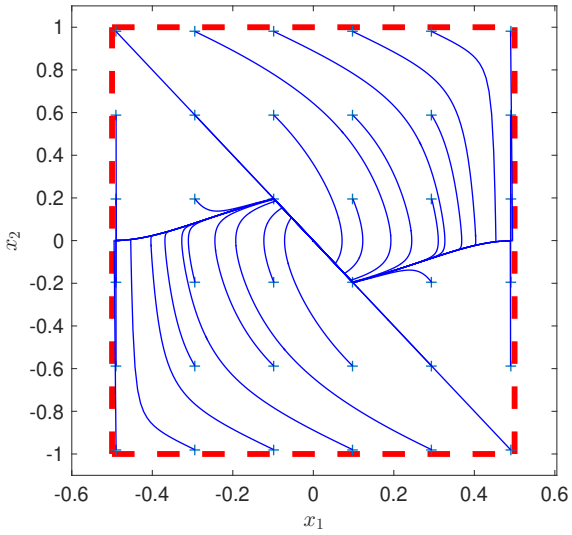

(a)

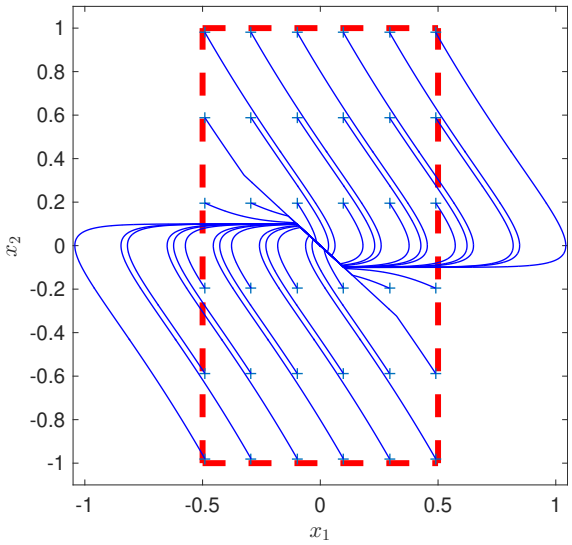

(b)

Figure 3.3: Phase portrait with various initial conditions: a) Barrier avoidance sliding mode control; b) Standard sliding mode control (Initial conditions are marked by '+'.)

In the new coordinates, (3.44) is rewritten as

$$\begin{aligned}
\dot{x}_i^* &= \frac{(1+x_i^{*2})^{3/2}}{k_i}\left(f_i^*(\bar{x}_i^*) + g_i^*(\bar{x}_i^*)\frac{k_{i+1}x_{i+1}^*}{(1+{x_{i+1}^*}^2)^{1/2}}\right), \quad i = 1, 2, ..., n-1 \\
\dot{x}_n^* &= \frac{(1+x_n^{*2})^{3/2}}{k_n}[f_n^*(\bar{x}_n^*) + g_n^*(\bar{x}_n^*)u] \\
y^* &= x_1^*
\end{aligned} \tag{3.47}$$

where $\bar{x}_i^* = [x_1^*, x_2^*, ..., x_i^*]^T$, and the identities $f_i^*(\bar{x}_i^*) = f_i(\bar{x}_i)$, $g_i^*(\bar{x}_i^*) = g_i(\bar{x}_i)$ hold. We define $y_d^* = \frac{y_d}{(k_1^2 - y_d^2)^{1/2}}$ as the desired trajectory in the new coordinates. Note that, system (3.47) is in a pure feedback form instead of a strict feedback form.

Step 1: Define $z_1^* = x_1^* - y_d^*$, $z_i^* = x_i^* - \alpha_{i-1}^*$, $i = 2, ..., n$, $\bar{z}_i^* = [z_1^*, ..., z_i^*]^T$ and $\bar{y}_{di} = [y_d, y_d^{(1)}, ..., y_d^{(i)}]^T$. Choose the Lyapunov candidate $V_1 = 1/2 z_1^{*2}$. The time-derivative of V_1 is given as

$$\dot{V}_1 = z_1^* \Big(\frac{(1 + x_1^{*2})^{3/2}}{k_1} \Big(f_1^* + g_1^* \frac{k_2 (z_2^* + \alpha_1)}{(1 + x_2^{*2})^{1/2}} \Big) - \dot{y}_d^* \Big) \tag{3.48}$$

Design the stabilizing function α_1^* as

$$\alpha_1^*(\bar{x}_2^*, z_1^*) = \frac{(1 + x_2^{*2})^{1/2}}{k_2} \frac{1}{g_1^*} \Big(- f_1^* + \frac{k_1 (\dot{y}_d^* - \kappa_1 z_1^*)}{(1 + x_1^{*2})^{3/2}} \Big) \tag{3.49}$$

where $\kappa_1 > 0$ is a constant control gain. We obtain

$$\dot{V}_1 = -\kappa_1 z_1^{*2} + \frac{(1 + x_1^{*2})^{3/2}}{k_1} \frac{k_2}{(1 + x_2^{*2})^{1/2}} g_1^* z_1^* z_2^* \tag{3.50}$$

Step i (i=2,...,n)**:** Choose the Lyapunov candidate $V_i = 1/2 z_1^{*2} + \cdots + 1/2 z_i^{*2}$. The time-derivative of V_i is given as

$$\begin{aligned} \dot{V}_i = & - \kappa_1 z_1^{*2} - \cdots - \kappa_{i-1} {z_{i-1}^*}^2 + \frac{(1 + {x_{i-1}^*}^2)^{3/2}}{k_{i-1}} \frac{k_i}{(1 + x_i^{*2})^{1/2}} g_{i-1}^* z_{i-1}^* z_i^* \\ & + z_i^* \Big(\frac{(1 + x_i^{*2})^{3/2}}{k_i} \Big(f_i^* + g_i^* \frac{k_{i+1} (z_{i+1}^* + \alpha_i^*)}{(1 + {x_{i+1}^*}^2)^{1/2}} \Big) - \dot{\alpha}_{i-1}^* \Big) \end{aligned} \tag{3.51}$$

Design the stabilizing function α_i^* as

$$\alpha_i^*(\bar{x}_{i+1}^*, \bar{z}_i^*) = \frac{(1 + {x_{i+1}^*}^2)^{1/2}}{k_{i+1}} \frac{1}{g_i^*} \Bigg(- f_i^* + \frac{\dot{\alpha}_{i-1}^* - \kappa_i z_i^* - \frac{(1 + {x_{i-1}^*}^2)^{3/2}}{k_{i-1}} \frac{k_i g_{i-1}^* z_{i-1}^*}{(1 + x_i^{*2})^{1/2}}}{k_i^{-1} (1 + x_i^{*2})^{3/2}} \Bigg) \tag{3.52}$$

where $\kappa_i > 0$ is a constant control gain. Then we have

$$\dot{V}_i = -\kappa_1 z_1^{*2} - \cdots - \kappa_i z_i^{*2} + \frac{(1+x_i^{*2})^{3/2}}{k_i} \frac{k_{i+1} g_i^* z_i^* z_{i+1}^*}{(1+{x_{i+1}^*}^2)^{1/2}} \tag{3.53}$$

Define a revised stabilizing function $\tilde{\alpha}_i^*$ as

$$\tilde{\alpha}_i^*(\bar{x}_{i+1}^*, \bar{z}_i^*) \triangleq \frac{\alpha_i^*(\bar{x}_{i+1}^*, \bar{z}_i^*)}{k_{i+1}^{-1}(1+{x_{i+1}^*}^2)^{1/2}}, \ i = 1, ..., n-1 \tag{3.54}$$

We set the control input as

$$u = \tilde{\alpha}_n^*(\bar{x}_n^*, u, \bar{z}_n^*) = \frac{1}{g_n^*} \left(-f_n^* + \frac{\dot{\alpha}_{n-1}^* - \kappa_n z_n^* - \frac{(1+{x_{n-1}^*}^2)^{3/2}}{k_{n-1}} \frac{k_n g_{n-1}^* z_{n-1}^*}{(1+x_n^{*2})^{1/2}}}{k_n^{-1}(1+x_n^{*2})^{3/2}} \right) \tag{3.55}$$

where u is affine in $\tilde{\alpha}_n^*$, since $\dot{\alpha}_{n-1}^*$ contains u affinely. Thus, we can rewrite (3.55) by

$$u = q_n(\bar{x}_n^*) u + l_n(\bar{x}_n^*, \bar{z}_n^*) \tag{3.56}$$

where

$$q_n(\bar{x}_n^*) = \frac{x_n^*}{(1+x_n^{*2})^{1/2}} \frac{\tilde{\alpha}_{n-1}^*}{k_n} + \sum_{i=2}^{n-1} \left(\left(\prod_{j=i+1}^{n} \frac{1}{1+x_j^{*2}} \right) \frac{x_i^*}{(1+x_i^{*2})^{1/2}} \frac{\tilde{\alpha}_{i-1}^*}{k_i} \right)$$

The resulting time-derivative of V_n is

$$\dot{V}_n = -\kappa_1 z_1^{*2} - \cdots - \kappa_n z_n^{*2} \tag{3.57}$$

To establish the main result of this case study, we expand the Lyapunov function V_n as

$$\begin{aligned} V_n =& \frac{1}{2}z_1^{*2} + \cdots + \frac{1}{2}z_i^{*2} + \cdots + \frac{1}{2}z_n^{*2} \\ =& \frac{1}{2}(x_1^* - y_d^*)^2 + \cdots + \frac{1+x_i^{*2}}{2k_i^2}\left(\frac{k_i x_i^*}{(1+x_i^{*2})^{1/2}} - \tilde{\alpha}_{i-1}^*(\bar{x}_i^*, \bar{z}_{i-1}^*)\right)^2 \\ &+ \cdots + \frac{1+x_n^{*2}}{2k_n^2}\left(\frac{k_n x_n^*}{(1+x_n^{*2})^{1/2}} - \tilde{\alpha}_{n-1}^*(\bar{x}_n^*, \bar{z}_{n-1}^*)\right)^2 \end{aligned} \tag{3.58}$$

First, we consider a set-point tracking problem, and the following theorem is obtained as a direct result of Theorem 2.

Theorem 4. *Consider the systems* (3.44) *and* (3.47) *under the control law* (3.55)*. Assume that* $y_d \equiv 0$ *and* $\tilde{\alpha}_i^*|_{\bar{x}_i^*=0} = 0$*. If there exist control gains* $\kappa_1, ..., \kappa_{n-1}$ *such that the following condition holds for* $x^* \in \mathbb{R}^n$

$$|\tilde{\alpha}_{i-1}^*| < \lambda_i k_i, \quad i = 2, ..., n \tag{3.59}$$

where

$$\lambda_i > 0, \quad \sum_{i=2}^{n} \lambda_i = 1$$

Then, the system (3.44) *is exponentially stable at the origin with attractive basin* $\mathcal{D}$*.*

Proof: Under the assumptions $y_d \equiv 0$ and $\tilde{\alpha}_i^*|_{\bar{x}_i^*=0} = 0$, we can choose V_n as a Lyapunov candidate for $\bar{x}^*$ with the equilibrium point $\bar{x}^* = 0$. Besides, if the condition (3.59) holds, from (3.56) we can conclude that $|q_n| < 1$ and the control input u is bounded. Also, in the second brackets of (3.58), as $x_i \to \infty$, $\frac{k_i x_i^*}{(1+x_i^{*2})^{1/2}} \to \pm k_i$ and $|\tilde{\alpha}_{i-1}^*| < \lambda_i k_i < k_i$, the Lyapunov function V_n is radially unbounded in x^* domain. ■

Nevertheless, having $|\tilde{\alpha}_{i-1}^*| < \lambda_i k_i$ for $\bar{x}_n^* \in \mathbb{R}^n$ can be too strict in many cases. Besides, the above theorem only considers a setpoint tracking problem but not a general tracking problem. To address these issues, we establish the following theorem for a general tracking problem.

Theorem 5. *Consider the systems* (3.44) *and* (3.47)*. The initial condition* $x(0) \in \mathcal{C} \subseteq \mathcal{D}$*. Let*

$$\chi \triangleq \Big\{ \bar{z}_n^* \in \mathbb{R}^n, \bar{y}_{dn} \in \mathbb{R}^{n+1} \;\Big|\; |z_i^*| \leq \sqrt{2B_v},\ |y_d| \leq B_0,\ |y_d^{(i)}| \leq B_i,\ i = 1, ..., n \Big\} \tag{3.60}$$

where $B_v = \max_{x \in \mathcal{C}} V_n$*,* $0 < B_0 < k_1$ *and* $B_i > 0$*. Define*

$$z_1 = x_1 - y_d, \quad z_i = x_i - \frac{k_i \alpha_{i-1}^*}{(1 + {\alpha_{i-1}^*}^2)^{1/2}},\ i = 2, ..., n \tag{3.61}$$

and $\bar{z}_i = [z_1, ..., z_i]^T$*. If there exist control gains* $\kappa_1, ..., \kappa_{n-1}$ *such that the following condition holds*

$$\sup_{(\bar{z}_n^*, \bar{y}_{dn}) \in \chi} |\tilde{\alpha}_{i-1}^*| < \lambda_i k_i, \quad i = 2, ..., n \tag{3.62}$$

where

$$\lambda_i > 0, \quad \sum_{i=2}^{n} \lambda_i = 1$$

then under the control law (3.55)*, the errors* $\bar{z}_n$ *are exponentially stable at the origin, while the system states* $x \in \mathcal{D}$ *for all* $t \in [0, \infty)$ *and the control input* u *is bounded.*

Proof: By (3.57) and (3.58), the errors $\bar{z}_n^*$ are exponentially stable at the origin. Due to Lemma 1 and Lemma 2, we can infer the exponential stability of $\bar{z}_n$ at the origin.

If the condition (3.62) holds, $V_n \to \infty$ if and only if $x \to \partial\mathcal{D}$. Also, since $V_n|_{t=0} < \infty$ and $\dot{V}_n \leq 0$, we have $V_n|_t < \infty$ for $t \in [0, \infty)$. Therefore, x will not reach $\partial\mathcal{D}$ and $x \in \mathcal{D}$ for all $t \in [0, \infty)$. ■

3.5.2 Simulation Results

Consider a second-order system

$$\begin{aligned}\dot{x}_1 &= 0.1x_1^2 + x_2 \\ \dot{x}_2 &= 0.1x_1x_2 - 0.2x_1 + (1 + x_1^2)u\end{aligned} \tag{3.63}$$

The state constraints are $|x_1| < 0.8$ and $|x_2| < 2.5$. For the first case, we set $y_d \equiv 0$ and choose $\kappa_1 = 1$, $\kappa_2 = 2$ and (3.62) is satisfied for $\mathcal{C} = \mathcal{D}$. Under the barrier avoidance based backstepping control, Fig. 3.4(a) shows the phase portraits starting from various initial conditions. The trajectories avoid reaching the boundary of the region (predefined barrier) and converge to the origin exponentially fast. In comparison, when standard backstepping control is used with the same initial conditions, violation of the state constraints can be observed, as shown in Fig. 3.4(b).

For the second case, we consider a tracking problem. The desired trajectory is defined as

$$y_d = 0.6\sin(0.7t) \tag{3.64}$$

We choose $\kappa_1 = 1$, $\kappa_2 = 2$ as the control gains, such that the condition (3.62) holds for $\mathcal{C} = \mathcal{D}$. As depicted in Fig. 3.5 and Fig. 3.6, x_1 and x_2 starting from different initial conditions will all converge to the desired trajectories. The transgressions of the state constraints are prevented, even for the states with intial conditions close to the boundary.

3.6 Case Study III: LPV Control with Barrier Avoidance

3.6.1 Control Design

Consider a LPV plant

$$\dot{x} = A(\rho)x + B(\rho)u \tag{3.65}$$

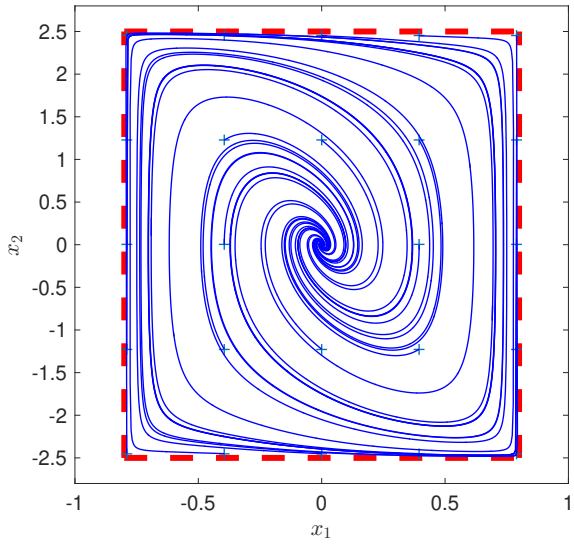

(a)

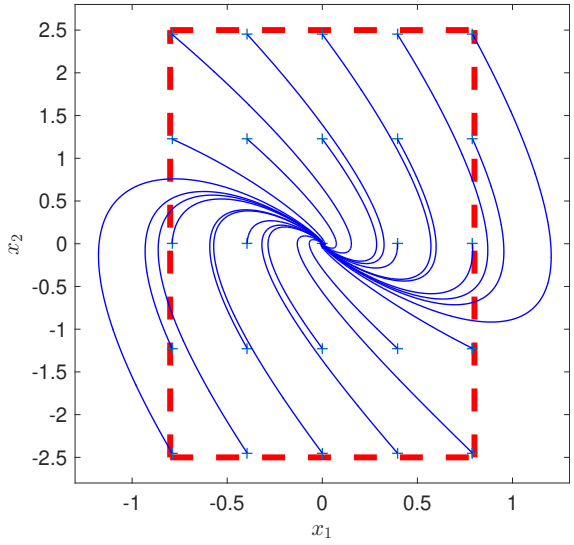

(b)

Figure 3.4: Phase portrait with various initial conditions: a) Barrier avoidance backstepping control; b) Standard backstepping control (Initial conditions are marked by '+'.)

where $x \in \mathbb{R}^n$, and ρ can be either external time-varying parameters or system states (quasi-LPV).

For $k_i > 0, i = 1, 2, ..., n$, we choose the safe region as

$$\mathcal{D} = \left\{ x \in \mathbb{R}^n \,\middle|\, |x_i| < k_i,\ i = 1, 2, ..., n \right\} \tag{3.66}$$

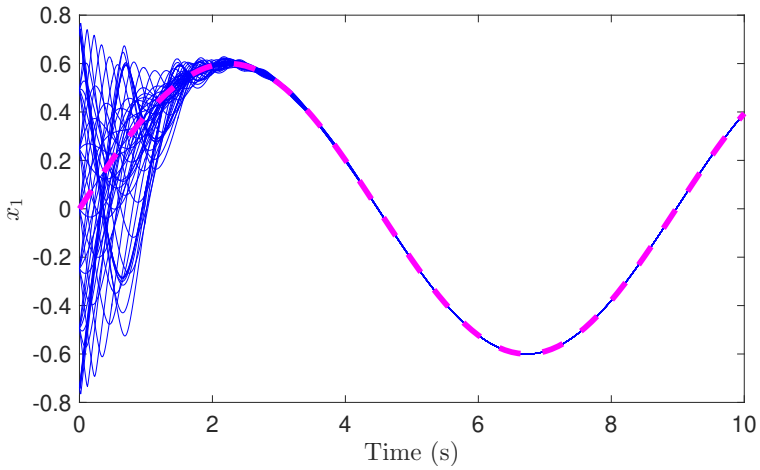

Figure 3.5: Time history of x_1 (Dashed line: desired trajectory)

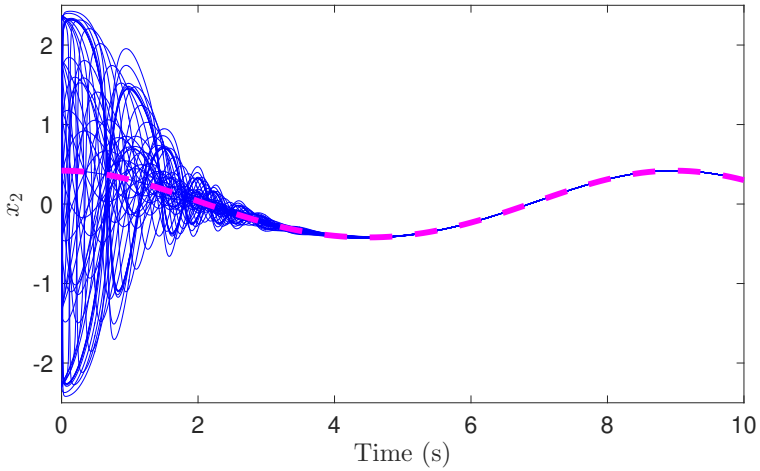

Figure 3.6: Time history of x_2 (Dashed line: desired trajectory)

We can choose the following diffeomorphic transformation

$$x_i^* = \frac{x_i}{\sqrt{k_i^2 - x_i^2}},\ i = 1, 2, ..., n \tag{3.67}$$

The converted system dynamics of (3.65) is written as

$$\dot{x}^* = \begin{bmatrix} \frac{(1+x_1^{*2})^{3/2}}{k_1} & 0 & \cdots & 0 \\ 0 & \frac{(1+x_2^{*2})^{3/2}}{k_2} & \cdots & 0 \\ \vdots & \vdots & \ddots & \vdots \\ 0 & 0 & \cdots & \frac{(1+x_n^{*2})^{3/2}}{k_n} \end{bmatrix} \hat{A}(\rho^*) \begin{bmatrix} \frac{k_1}{(1+x_1^{*2})^{1/2}} & 0 & \cdots & 0 \\ 0 & \frac{k_2}{(1+x_2^{*2})^{1/2}} & \cdots & 0 \\ \vdots & \vdots & \ddots & \vdots \\ 0 & 0 & \cdots & \frac{k_n}{(1+x_n^{*2})^{1/2}} \end{bmatrix} x^* + \begin{bmatrix} \frac{(1+x_1^{*2})^{3/2}}{k_1} & 0 & \cdots & 0 \\ 0 & \frac{(1+x_2^{*2})^{3/2}}{k_2} & \cdots & 0 \\ \vdots & \vdots & \ddots & \vdots \\ 0 & 0 & \cdots & \frac{(1+x_n^{*2})^{3/2}}{k_n} \end{bmatrix} \hat{B}(\rho^*)u \tag{3.68}$$

where $A(\rho) = \hat{A}(\rho^*)$ and $B(\rho) = \hat{B}(\rho^*)$. The equation (3.68) can be rewritten as

$$\dot{x}^* = A^*(\rho^*, x^*)x^* + B^*(\rho^*, x^*)u \tag{3.69}$$

Such system dynamics (3.69) is a quasi-LPV plant, which enables a standard LPV control design method.

Next, we will briefly introduce the LPV control design approach [85]. First, we simplified the expression of (3.69) by merging x^* into ρ^*

$$\dot{x}^* = A^*(\rho^*)x^* + B^*(\rho^*)u \tag{3.70}$$

where $|\rho_i^*| < k_{\rho_i}^*$ and $|\dot{\rho}_i^*| < k_{\dot{\rho}_i^*}$. The feedback control law is $u = E(\rho^*)x^*$. Consider the Lyapunov candidate $V = x^{*T}P(\rho^*)x^*$, where $P^T(\rho^*) = P(\rho^*)$. The closed-loop system is exponentially stable if

$$P(\rho^*)\left(A^*(\rho^*) + B^*(\rho^*)E(\rho^*)\right) + \left(A^*(\rho^*) + B^*(\rho^*)E(\rho^*)\right)^T P(\rho^*) + \dot{\rho}^* \frac{\partial P(\rho^*)}{\partial \rho^*} < 0 \tag{3.71}$$

for all $|\rho_i^*| < k_{\rho_i^*}$ and $|\dot{\rho}_i^*| < k_{\dot{\rho}_i^*}$. Then (3.71) can be transformed into a more computational

efficient form

$$\left(A^*(\rho^*) + B^*(\rho^*)E(\rho^*)\right)P^{-1}(\rho^*) + P^{-1}(\rho^*)\left(A^*(\rho^*) + B^*(\rho^*)E(\rho^*)\right)^T - \dot{\rho}^*\frac{\partial P^{-1}(\rho^*)}{\partial \rho^*} < 0 \tag{3.72}$$

Setting $Y(\rho^*) = P^{-1}(\rho^*)$ and $\tilde{E}(\rho^*) = E(\rho^*)P^{-1}(\rho^*)$, we have

$$A^*(\rho^*)Y(\rho^*) + B^*(\rho^*)\tilde{E}(\rho^*) + Y(\rho^*)A^*(\rho^*) + \tilde{E}^T(\rho^*)B^{*T}(\rho^*) - \dot{\rho}^*\frac{\partial Y(\rho^*)}{\partial \rho^*} < 0 \tag{3.73}$$

Here, the set of $Y(\rho^*)$ and $\tilde{E}(\rho^*)$ satisfying (3.73) is convex, and (3.73) is a linear matrix inequality (LMI). However, because of the dependence of ρ^*, Eq. (3.73) contains infinitely many sets of LMIs. An approch to solve this issue is discretizing the dependence parameter ρ^*. For an example with two time-varying parameters $\rho_{1,2}$, we can divide the interval $[-k_{\rho_i}, k_{\rho_i}]$ into N_i intervals of width h_i for $i = 1, 2$. Eq. (3.73) becomes a finite collection of LMIs, indexed with $m_i = 1, 2, ..., N_i$

$$\begin{aligned} &A^*_{m_1,m_2}Y_{m_1,m_2} + B^*_{m_1,m_2}\tilde{E}_{m_1,m_2} + Y_{m_1,m_2}A^*_{m_1,m_2} + \tilde{E}^T_{m_1,m_2}B^{*T}_{m_1,m_2} \\ &\pm k_{\dot{\rho}_1}\frac{Y_{m_1,m_2} - Y_{m_1-1,m_2}}{h_1} \pm k_{\dot{\rho}_2}\frac{Y_{m_1,m_2} - Y_{m_1,m_2-1}}{h_2} < 0 \end{aligned} \tag{3.74}$$

where $A^*_{m_1,m_2} = A^*([m_1h_1 - k_{\rho_1}, m_2h_2 - k_{\rho_2}]^T)$ and the subscipts have the same meaning for other matrices. It is worth noting that the rate of variation $\dot{\rho}$ enters linearly into (3.73), it is sufficient to only check the vertex points instead of all points of $\dot{\rho}$ in the region $[-k_{\dot{\rho}_1}, k_{\dot{\rho}_1}] \times [-k_{\dot{\rho}_2}, k_{\dot{\rho}_2}]$.

3.6.2 Simulation Results

Since the LPV control may only ensure the locally exponential stability instead of global stability for the converted dynamics, through Theorem 2 we know it only ensure the locally exponential stability for the original system (3.65) without any transgress of the barrier. Nevertheless, it can be demonstrated that the region of attraction (RA) is indeed enlarged by the barrier avoidance control, compared with the direct application of the same type of control, i.e. LPV control, to the original system (3.65). We will show this in the following example.

Consider a second order nonlinear system

$$\dot{x}_1 = 0.1(1 + x_1^2)x_1 + x_2$$
$$\dot{x}_2 = -2x_1 - 3x_2 + 2u \tag{3.75}$$

The constrained region is

$$\mathcal{D} = \{|x_1| < 5,\ |x_2| < 80\} \tag{3.76}$$

Using the barrier avoidance based LPV control, various initial conditions are tested in the simulation as shown in the phase portrait (Fig. 3.7(a)) and the feasibility initial map (Fig. 3.8(a)), where the region of attraction almost covers the constrained region. In comparison, using a standard LPV control under the same initial conditions, the region of attraction is in a narrow band around x_1 axis, as shown in Fig. 3.7(b) and Fig. 3.8(b). This example verifies that the region of attraction can be enlarged through the the barrier avoidance based LPV control.

3.7 Conclusions

The control design to ensure state barrier avoidance based on a diffeomorphic transformation method is proposed in this chapter. Sufficient conditions on choosing such diffeomorphic transformation are given to maintain stability under the change of coordinates, while the state constraints are not violated. Three case studies using different control strategies are discussed for different classes of nonlinear systems, illustrating the flexibility of this approach in the control design. Finally, the performance of the proposed algorithm is demonstrated through a comparison of simulation examples between the proposed barrier avoidance control methods and standard nonlinear control techniques.

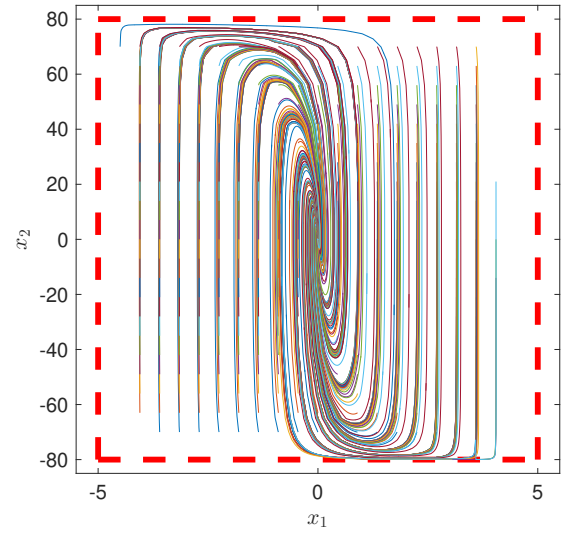

(a)

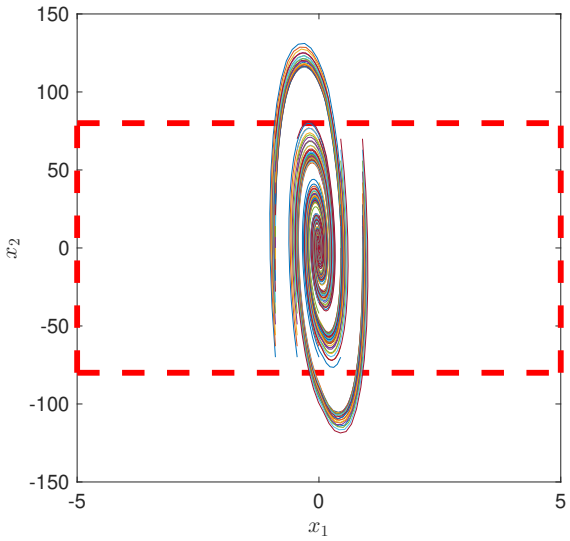

(b)

Figure 3.7: Phase portrait with various initial conditions: a) Barrier avoidance LPV control; b) Standard LPV control

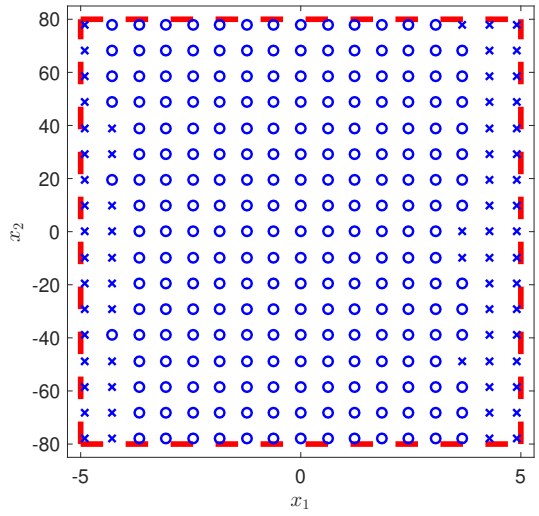

(a)

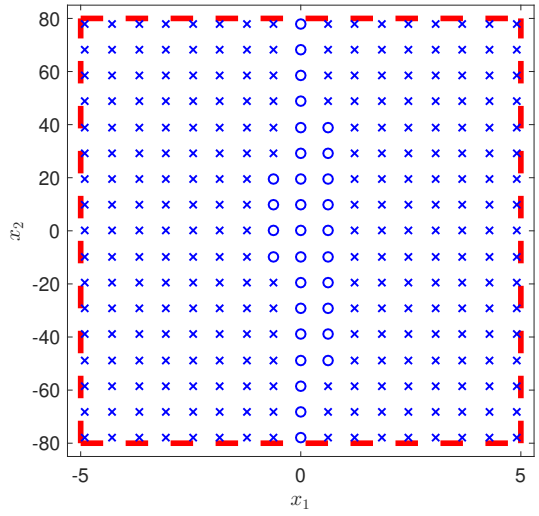

(b)

Figure 3.8: Feasibility of the solution with various initial conditions (Feasible solutions are labeled with 'o', and infeasible solutions are labeled with 'x'): a) Barrier avoidance LPV control; b) Standard LPV control

4. ADDRESSING COMPLEX STATE CONSTRAINTS IN THE DIFFEOMORPHIC TRANSFORMATION BASED BARRIER AVOIDANCE CONTROL

4.1 Introduction

Recently, the area of state-constrained control attracts a surge of research interests, and two major paths are followed to perform the state-constrained control design. One path is to formulate the state constraints as extra conditions or penalty terms, leaving the original control system unchanged. This includes the Reference Governor that modulates the control reference via an online nonlinear optimization [47], the Model Predictive Control that solves a nonlinear numerical optimization with constrained conditions in real-time [44], and the quadratic programming based approach that combines both control Lyapunov functions and control barrier functions [86]. The other path is to embed the state constraints directly into the control design, or modify the original control system into a new one, including the Barrier Lyapunov Function that assigns an infinite value to the Lyapunov candidate on the boundary of the barrier region [50, 53], the Control Lyapunov-Barrier Function that designs a level set to not only cover the barrier region but contain an attractive basin [48], and the tranformation based Barrier Avoidance Control that projects the original constrained space into an unconstrained one through diffeomorphic transformation. Ref. [87] first proposes the diffeomorphism based approach and proves its feasibility using Lyapunov based methods, and [88] shows its applicability to a general control problem including non-Lyapunov based methods through basic definition of stability. In the literature, the second path of the state-constrained control has been explored intensively in the past decade and successfully implemented to many practical applications. Most of the work only considers a hyperrectangle (or orthotope) shape of the barrier region, which can be addressed directly using a certain type of nonlinear control design such as backstepping control. However, a real-world control problem usually has a more complex shape of the state constraints rather than a simple hyperrectangle type,

and the study of control design involving complex state constraints is still limited.

In this chapter, we aim to systematically construct a state transformation for a class of complex state constraints under the framework of the diffeomorphism based barrier avoidance control scheme [88]. Firstly, complex state barriers are addressed for the first time through construction of the state transformation in a cascade manner, i.e., the ith transformation only depends on the 1st to the ith states. This enables a systematic construction of the transformation in an efficient fashion, in particular for barriers with a complex shape. Also, this structure makes the gradient matrices of the transformation and its inverse both be in lower triangular forms, which ensures the non-singularity of the matrices and therefore the diffeomorphism property of the transformation. Secondly, the first case study applies the proposed method in the sliding mode control scheme. The analysis proves that with any types of complex state barrier of n-dimension with smooth enough boundaries as described in the case study, the double integrator system can be stabilized under all initial conditions inside the barrier region. Thirdly, the other case study implements the complex state barriers into the backstepping control. We introduce the parametric model uncertainty and the adaptive control into this design, ensuring the strictly negative definite property of the time-derivative of the Lyapunov candidate, which is not established in the previous work [89].

The rest of this chapter is organized as follows. In Section 4.2, we have the state-constrained control problem formulated for a nonlinear system. Section 4.3 establishes a systematic approach to find the state transformation for a class of complex barrier regions in the high-dimension state space, and provides an analysis to prove the diffeomorphism property of this transformation. Finally, two case studies in Section 4.4 and Section 4.5 implement this method to sliding mode control design and adaptive backstepping design, demonstrating the effectiveness of the proposed algorithm.

Throughout the chapter, we define $\bar{x}_i = [x_1, x_2, ..., x_i]^T$, $\bar{z}_i = [z_1, z_2, ..., z_i]^T$, and $\bar{y}_{d_i} = [y_d, y_d^{(1)}, y_d^{(2)}, ..., y_d^{(n)}]^T$. We also denote $\|\cdot\|$ to be the Euclidean norm in $\mathbb{R}^i$, $\lambda_{\min}(\cdot)$ and $\lambda_{\max}(\cdot)$ to be the minimum and maximum eigenvalues of the matrix, and $\partial\mathcal{X}$ to be the boundary of the set $\mathcal{X}$.

4.2 Problem Formulation and Preliminaries

In this study, we consider a state-constrained control problem to design a state feedback controller $u = K(x)$ for the nonlinear system Σ_{ol}:

$$\Sigma_{ol} : \dot{x} = h_{ol}(x, u) \tag{4.1}$$

where $x \in \mathbb{R}^n$ and the initial condition $x(0) = x_0$. The closed-loop system $\Sigma : \dot{x} = h_{ol}(x, K(x)) = h(x)$ is locally Lipschitz in x, ensuring the uniqueness of the solution. Defining the safety region $\mathcal{D} \subset \mathbb{R}^n$ for the state x, the control objective is:

System Σ achieves the trajectory or setpoint tracking in $\mathcal{D}$ and the states do not cross the boundary of $\mathcal{D}$.

Under a diffeomorphism $x^* = \Phi(x)$, $x \in \Omega$, where Ω is a connected region, the closed-loop system Σ is transformed into the new coordinates. The original system and the transformed system are

$$\Sigma : \quad \dot{x} = h(x), \qquad x \in \Omega \subseteq \mathbb{R}^n \tag{4.2}$$

$$\Sigma^* : \quad \dot{x}^* = h^*(x^*), \quad x^* \in \Phi(\Omega) \subseteq \mathbb{R}^n \tag{4.3}$$

The initial conditions for Σ and Σ^* are $x_0 \in \Omega$ and $x_0^* = \Phi(x_0)$, respectively. Given the desired trajectory $x_d(t) \in \Omega$, $t \in [0, \infty)$ and $x_d^*(t) = \Phi(x_d(t)) \in \Phi(\Omega)$, the tracking errors in both the original and new coordinates are obtained as

$$z(t) = x(t) - x_d(t), \quad z^*(t) = x^*(t) - x_d^*(t) \tag{4.4}$$

To achieve the objective of state-constrained control, the diffeomorphic transformation based state barrier avoidance control method is established in the following theorem.

Theorem 6. *Consider the closed-loop system Σ and a given open set $\mathcal{D}$. The boundary $\partial\mathcal{D}$ is the*

barrier to avoid. If a diffeomorphism $x^* = \Phi(x)$ transforms the system Σ into Σ^* and satisfies:

1) The transformation $x^* = \Phi(x)$ maps $\mathcal{D}$ into $\mathbb{R}^n$ in x^*-coordinates. The boundary $\partial\mathcal{D}$ is mapped to the points at infinity.

2) Given the desired trajectory $x_d(t) \in \mathcal{D}$, $t \in [0, \infty)$ and $x_d^*(t) = \Phi(x_d(t)) \in \mathbb{R}^n$, the tracking error system z^* is asymptotically/exponentially stable at 0 for any initial condition $x_0^* \in \mathbb{R}^n$.

Whenever the initial condition $x_0 \in \mathcal{D}$, the following statements hold:

a) The state $x(t)$ stays in $\mathcal{D}$ for all $t \in [0, \infty)$, and avoids reaching the barrier $\partial\mathcal{D}$.

b) The tracking error system z is asymptotically/exponentially stable at 0.

Specially, when $x_d(t) \equiv x_e \in \mathcal{D}$ and $\Phi(x_e) = 0$ and the condition 2) is modified as

2) The system Σ^* is globally asymptotically/exponentially stable at 0.

Then the the condition b) is modified as

b) The system Σ is asymptotically/exponentially stable at $x = 0$ with the attractive region identical to $\mathcal{D}$.

Proof: The proof of the setpoint tracking case is discussed in Theorem 2 in Chapter 3. The proof of the general trajectory tracking case can be obtained in the same manner using Lemma 1 and Lemma 2 in Chapter 3. ■

Remark 3. *The barrier avoidance control method converts a state-constrained control into an unconstrained one. It allows greater flexibility in the nonlinear control design. This transformation based approach can also be extended to establishing the equivalence of other system properties, such as boundedness and ultimate boundedness, between the original and the new state spaces.*

4.3 Diffeomorphic Transformation for Complex State-Constraints

As stated in Section 4.1, most previous studies in the second path of state-constrained control only focus on the hyperrectangle shape of state barrier, where the state constraints can be generated separately in each dimension and are independent of other dimensions (for example, $|x_1| < k_1$, ..., $|x_n| < k_n$, k_i are positive constants). Following Theorem 6, the diffeomorphic transformation for such orthotope barrier shapes can also be constructed independently in each dimension, as shown in [88]. However, in pratice many state barriers are in a more complex shape rather than such simple orthotope shapes. A critical problem to address is having an efficient way to obtain a feasible transformation for these complex barriers.

In this section, we will investigate the diffeomorphic transformation for a class of complex state constraints. In the space of $\mathbb{R}^n$, the state barrier is described as

$$\begin{aligned}\mathcal{D} \triangleq \{x \in \mathbb{R}^n \,\big|\, & k_1^l < x_1 < k_1^u,\, k_2^l(x_1) < x_2 < k_2^u(x_1),\, \dots, \\ & k_i^l(\bar{x}_{i-1}) < x_i < k_i^u(\bar{x}_{i-1}),\, \dots, k_n^l(\bar{x}_{n-1}) < x_n < k_n^u(\bar{x}_{n-1})\}\end{aligned} \tag{4.5}$$

where $k_i^u(\bar{x}_{i-1})$ and $k_i^l(\bar{x}_{i-1})$ are smooth enough functions with respect to $\bar{x}_{i-1}$, denoting the upper and lower bound of x_i. The diffeomorphism is chosen in each dimension of x_i as

$$\begin{aligned} x_1^* &= \ln\Big(\frac{-k_1^l + x_1}{k_1^u - x_1}\frac{k_1^u - k_1^0}{-k_1^l + k_1^0}\Big) \\ x_i^* &= \ln\Big(\frac{-k_i^l(\bar{x}_{i-1}) + x_i}{k_i^u(\bar{x}_{i-1}) - x_i}\frac{k_i^u(\bar{x}_{i-1}) - k_i^0(\bar{x}_{i-1})}{-k_i^l(\bar{x}_{i-1}) + k_i^0(\bar{x}_{i-1})}\Big), \qquad i = 2, ..., n \end{aligned} \tag{4.6}$$

This transformation maps the upper and lower bounds $k_i^u(\bar{x}_{i-1})$ and $k_i^l(\bar{x}_{i-1})$ into ∞ and $-\infty$, respectively, in the x_i^*-dimension of the new coordinates. Also, a smooth function $k_i^0(\bar{x}_{i-1})$ satisfying $k_1^l < k_1^0 < k_1^u$ and $k_i^l(\bar{x}_{i-1}) < k_i^0(\bar{x}_{i-1}) < k_i^u(\bar{x}_{i-1})$, $i = 2, ..., n$ in x_i-domain will be mapped to 0 in the x_i^*-domain. This way the state transformation (4.6) fulfills the requirement in Theorem 6 and project the point $[k_1^{ori}, k_2^{ori}, ..., k_n^{ori}]^T$ into the origin of the new space, where $k_1^{ori} = k_1^0$ and $k_i^{ori} = k_i^0([k_1^{ori}, ..., k_{i-1}^{ori}]^T)$. This approach to define the region in each dimension

sequentially can enable an effective construction of the transformation in a cascade manner, and also be easily extended to high-dimensional state barriers.

To give an example for illustration, we first consider a two-dimension case as depicted in Fig. 4.1. The state barrier region $\widehat{ABCD}$ has a complex boundary instead of a rectangular shape. In the x_1 dimension, the bounds of x_1 can be given by two scalars k_1^u and k_1^l. Then we define a new variable $k_1^0 = (k_1^u + k_1^l)/2$, and the state transformation to get x_1^* can be written as

$$x_1^* = \ln(\frac{-k_1^l + x_1}{k_1^u - x_1}) \tag{4.7}$$

It can be verified that this will transform the boundary of x_1 (k_1^u and k_1^l) into infinity in the new space x_1^*, and k_1^0 will be transformed to the origin. Then, with x_1 being constrained, we can capture its upper and lower bounds as curves $\widehat{ADC}$ and $\widehat{ABC}$, which are described by $k_2^u(x_1)$ and $k_2^l(x_1)$. We can define a variable $k_2^0(x_1) = (k_2^u(x_1) + k_2^l(x_1))/2$ (curve $\widehat{AEC}$), and the state transformation to obtain x_2^* is

$$x_2^* = \ln(\frac{-k_2^l(x_1) + x_2}{k_2^u(x_1) - x_2}) \tag{4.8}$$

This will transform the barriers $k_2^u(x_1)$ and $k_2^l(x_1)$ of x_2 dimension into infinity, and $k_2^0(x_1)$ will be mapped to the origin in x_2^*. Next, adding one more dimension x_3, we draw the state barrier region in Fig. 4.2. Here, the barrier region is the interior of $\widehat{A_1B_1C_1D_1} - \widehat{A_3B_3C_3D_3}$. The upper and lower bounds in this dimension are the surfaces $\widehat{A_3B_3C_3D_3}$ and $\widehat{A_1B_1C_1D_1}$, denoted as $k_3^u(x_1, x_2)$ and $k_3^l(x_1, x_2)$. Then similarly $k_3^0(x_1, x_2)$ (surface $\widehat{A_2B_2C_2D_2}$) is designed as $(k_3^u(x_1, x_2) + k_3^l(x_1, x_2))/2$. The state transformation to get x_3^* is

$$x_3^* = \ln(\frac{-k_3^l(x_1, x_2) + x_3}{k_3^u(x_1, x_2) - x_3}) \tag{4.9}$$

Following the same procedure, the transformation can be constructed up to the nth dimension as well.

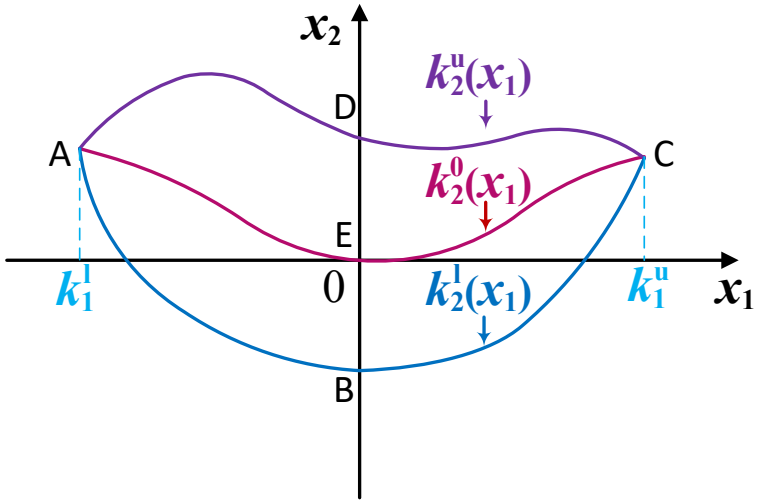

Figure 4.1: Two-dimension state barrier region

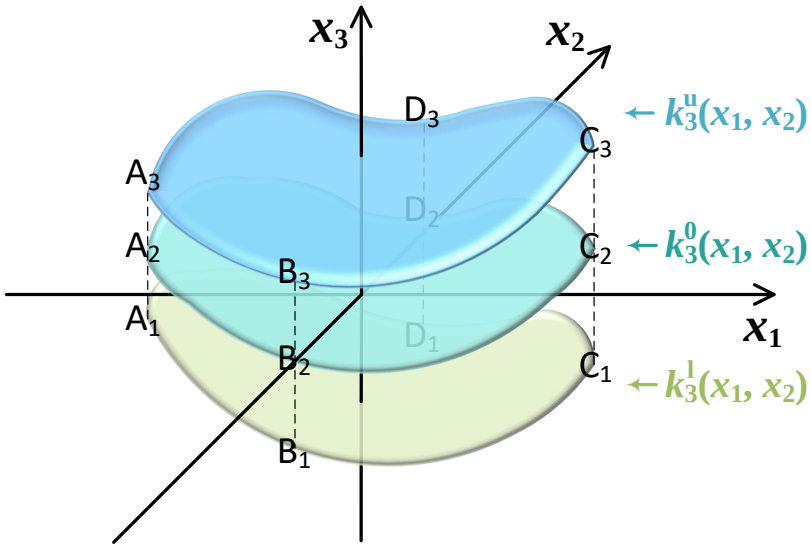

Figure 4.2: Three-dimension state barrier region

Next, we will prove the transformation defined in (4.6) is indeed a diffeomorphism. This can be verified by listing the gradient matrix of the transformation and its inverse and examining if they are non-singular. For simplicity, we will first rewrite (4.6) as

$$
\begin{aligned}
x_1^* &= \ln\Big(\frac{-k_1^l + x_1}{k_1^u - x_1}\phi_1\Big) \\
x_i^* &= \ln\Big(\frac{-k_i^l(\bar{x}_{i-1}) + x_i}{k_i^u(\bar{x}_{i-1}) - x_i}\phi_i(\bar{x}_{i-1})\Big), \qquad i = 2, ..., n
\end{aligned} \tag{4.10}
$$

where $\phi_1 = \frac{k_1^u - k_1^0}{-k_1^l + k_1^0}$ and $\phi_i(\bar{x}_{i-1}) = \frac{k_i^u(\bar{x}_{i-1}) - k_i^0(\bar{x}_{i-1})}{-k_i^l(\bar{x}_{i-1}) + k_i^0(\bar{x}_{i-1})}$. Since $k_1^l < k_1^0 < k_1^u$ and $k_i^l(\bar{x}_{i-1}) < k_i^0(\bar{x}_{i-1}) < k_i^u(\bar{x}_{i-1})$, hold, we have $\phi_1 > 0$ and $\phi_i > 0$, $i = 2, ..., n$. Also, for the inverse transformation we can obtain the expression of x_i using (4.10) as

$$
\begin{aligned}
x_1 &= \frac{e^{x_1^*}k_1^u + \phi_1 k_1^l}{e^{x_1^*} + \phi_1} \\
x_i &= \frac{e^{x_i^*}k_i^u(\bar{x}_{i-1}) + \phi_i(\bar{x}_{i-1})k_i^l(\bar{x}_{i-1})}{e^{x_i^*} + \phi_i(\bar{x}_{i-1})}, \qquad i = 2, ..., n
\end{aligned} \tag{4.11}
$$

The gradient matrix of both forward and inverse transformation are derived as

$$
\begin{bmatrix}
\frac{\partial x_1^*}{\partial x_1} & \frac{\partial x_1^*}{\partial x_2} & \cdots & \frac{\partial x_1^*}{\partial x_n} \\
\frac{\partial x_2^*}{\partial x_1} & \frac{\partial x_2^*}{\partial x_2} & \cdots & \frac{\partial x_2^*}{\partial x_n} \\
\vdots & \vdots & \ddots & \vdots \\
\frac{\partial x_n^*}{\partial x_1} & \frac{\partial x_n^*}{\partial x_2} & \cdots & \frac{\partial x_n^*}{\partial x_n}
\end{bmatrix} =
$$

$$
\begin{bmatrix}
\frac{k_1^u - k_1^l}{(-k_1^l + x_1)(k_1^u - x_1)} & 0 & \cdots & 0 \\
\frac{-\partial k_2^l/\partial x_1}{-k_2^l + x_2} - \frac{\partial k_2^u/\partial x_1}{k_2^u - x_2} + \frac{\partial \phi_2/\partial x_1}{\phi_2} & \frac{k_2^u - k_2^l}{(-k_2^l + x_2)(k_2^u - x_2)} & \cdots & 0 \\
\vdots & \vdots & \ddots & \vdots \\
\frac{-\partial k_n^l/\partial x_1}{-k_n^l + x_n} - \frac{\partial k_n^u/\partial x_1}{k_n^u - x_n} + \frac{\partial \phi_n/\partial x_1}{\phi_n} & \frac{-\partial k_n^l/\partial x_2}{-k_n^l + x_n} - \frac{\partial k_n^u/\partial x_2}{k_n^u - x_n} + \frac{\partial \phi_n/\partial x_2}{\phi_n} & \cdots & \frac{k_n^u - k_n^l}{(-k_n^l + x_n)(k_n^u - x_n)}
\end{bmatrix}
$$

(4.12)

$$\begin{bmatrix} \frac{\partial x_1}{\partial x_1^*} & \frac{\partial x_1}{\partial x_2^*} & \cdots & \frac{\partial x_1}{\partial x_n^*} \\ \frac{\partial x_2}{\partial x_1^*} & \frac{\partial x_2}{\partial x_2^*} & \cdots & \frac{\partial x_2}{\partial x_n^*} \\ \vdots & \vdots & \ddots & \vdots \\ \frac{\partial x_n}{\partial x_1^*} & \frac{\partial x_n}{\partial x_2^*} & \cdots & \frac{\partial x_n}{\partial x_n^*} \end{bmatrix} = \begin{bmatrix} \frac{\phi_1 e^{x_1^*}(k_1^u - k_1^l)}{(e^{x_1^*}+\phi_1)^2} & 0 & \cdots & 0 \\ \beta_{2,1}(x, x^*) & \frac{\phi_2 e^{x_2^*}(k_2^u - k_2^l)}{(e^{x_2^*}+\phi_2)^2} & \cdots & 0 \\ \vdots & \vdots & \ddots & \vdots \\ \beta_{n,1}(x, x^*) & \beta_{n,2}(x, x^*) & \cdots & \frac{\phi_n e^{x_n^*}(k_n^u - k_n^l)}{(e^{x_n^*}+\phi_n)^2} \end{bmatrix} \tag{4.13}$$

where

$$\begin{aligned} \beta_{i,j}(x, x^*) = & \sum_{k=j}^{i-1} \frac{\partial x_i}{\partial x_k} \frac{\partial x_k}{\partial x_j^*} = \Big(\frac{\partial k_i^l}{\partial x_j} + \frac{e^{x_i^*}}{e^{x_i^*} + \phi_i} \frac{\partial (k_i^u - k_i^l)}{\partial x_j} \Big) \frac{\phi_j e^{x_j^*} (k_j^u - k_j^l)}{(e^{x_j^*} + \phi_j)^2} \\ & + \sum_{k=j+1}^{i-1} \Big(\frac{\partial k_i^l}{\partial x_k} + \frac{e^{x_i^*}}{e^{x_i^*} + \phi_i} \frac{\partial (k_i^u - k_i^l)}{\partial x_k} \Big) \frac{\partial x_k}{\partial x_j^*} \end{aligned}$$

The gradient matrices (4.12) and (4.13) are both in lower triangular forms, and the determinants of these two gradient matrices are the product of all the diagonal elements. Since the condition $k_i^l < x_i < k_i^u$ and $\phi_i > 0$ holds for $i = 1, ..., n$, the determinants of these two matrices have non-zero values, and the gradient matrices of both forward and inverse transformation are non-singular.

One of the merits of defining the transformation in a cascade manner is that it makes the gradient matrices of the transformation and its inverse be in lower triangular forms. This makes it straightforward to verify the non-singularity of the gradient matrices, ensuring the diffeomorphic property of the transformation. Note that, the method of forming the transformation is not dependent on the structure of the system dynamics, so it can be applied to broad types of dynamic systems. In addition, the transformation requires the barriers k_i^l and k_i^u to be smooth functions. Nevertheless, even if the barriers in the practical problem are non-smooth, an approximation can be made at a price of a merely less volume of the barrier region. As long as the state can avoid the approximated barrier sufficiently close to the original barrier, the control objective will be achieved without being too conservative.

4.4 Case Study I: Sliding Mode Control with Complex State-Constraints

4.4.1 Control Design

In this case study, we design the barrier avoidance controller for a double integrator of dimension n with the state constraint being complex curves as

$$\mathcal{D} = \{x \in \mathbb{R}^n \,\big|\, k_1^l < x_1 < k_1^u,\ k_i^l(\bar{x}_{i-1}) < x_i < k_i^u(\bar{x}_{i-1}) \ \text{ for } \ i = 2, ..., n\} \tag{4.14}$$

where $k_i^u(\bar{x}_{i-1})$ and $k_i^l(\bar{x}_{i-1})$ are smooth enough functions with respect to $\bar{x}_{i-1}$. Assume $k_i^u(\bar{x}_{i-1}) - k_i^l(\bar{x}_{i-1}) < q_i$ (q_i is a positive constant). Then, consider the double integrator as

$$\begin{aligned} \dot{x} &= v \\ \dot{v} &= f(x, v) + G(x, v)E(x, v)u + \delta(t, x, v, u) \end{aligned} \tag{4.15}$$

where $x = [x_1, x_2, ..., x_n]^T$, $v = [v_1, v_2, ..., v_n]^T$ and $u = [u_1, u_2, ..., u_n]^T$. Functions $f(x, v)$, $G(x, v)$, and $E(x, v)$ are sufficiently smooth in $(x, v) \in \mathcal{D} \times \mathbb{R}^n$. The uncertainty term $\delta(t, x, v, u)$ is piecewise continuous in t and sufficiently smooth with respect to (x, v, u), where $(t, x, v, u) \in [0, \infty) \times \mathcal{D} \times \mathbb{R}^n \times \mathbb{R}^n$. Assume $f(x, v)$ and $E(x, v)$ are known, and $E(x, v)$ is a non-singular matrix. Also, $G(x, v)$ and $\delta(t, x, v, u)$ are unknown, and $G(x, v)$ is a diagonal matrix with elements $g_i(x, v) \geq g_0 > 0$.

Choosing (4.10) as the diffeomorphic transformation, we can rewrite the system (4.15) in the new coordinates as

$$\dot{x}_1^* = \frac{k_1^u - k_1^l}{(-k_1^l + x_1)(k_1^u - x_1)} v_1$$

$$\dot{x}_i^* = \sum_{k=1}^{i-1} \alpha_{i,k}(x) v_k + \frac{k_i^u(\bar{x}_{i-1}) - k_i^l(\bar{x}_{i-1})}{(-k_i^l(\bar{x}_{i-1}) + x_i)(k_i^u(\bar{x}_{i-1}) - x_i)} v_i, \qquad i = 2, ..., n \tag{4.16}$$

$$\dot{v} = f(x, v) + G(x, v)E(x, v)u + \delta(t, x, v, u) \tag{4.17}$$

where

$$\alpha_{i,j}(x) = \frac{\partial x_i^*}{\partial x_j} = -\frac{\partial k_i^l/\partial x_j}{-k_i^l + x_i} - \frac{\partial k_i^u/\partial x_j}{k_i^u - x_i} + \frac{\partial \phi_i/\partial x_j}{\phi_i}$$

Here, we denote $\dot{x}^* = \sigma(x, v)$ through (4.16). The sliding manifolds are designed as

$$\begin{aligned} s_1 &= v_1 - h_1(x, x^*) \\ s_i &= v_i - h_i(x, x^*), \qquad i = 2, ..., n \end{aligned} \tag{4.18}$$

where

$$\begin{aligned} h_1(x, x^*) &= -\kappa_1 x_1^* \\ h_i(x, x^*) &= -\frac{(-k_i^l(\bar{x}_{i-1}) + x_i)(k_i^u(\bar{x}_{i-1}) - x_i)}{k_i^u(\bar{x}_{i-1}) - k_i^l(\bar{x}_{i-1})} \sum_{k=1}^{i-1} \alpha_{i,k}(x) h_k(x, x^*) - \kappa_i x_i^* \end{aligned}$$

The positive constants κ_i are the control parameters. Denote $s = [s_1, s_2, ..., s_n]^T$ and $h(x, x^*) = [h_1, h_2, ..., h_n]^T$. On the sliding surface $s = 0$, the system dynamics (4.16) is rewritten as

$$\begin{aligned} \dot{x}_1^* &= -\frac{k_1^u - k_1^l}{(-k_1^l + x_1)(k_1^u - x_1)} \kappa_1 x_1^* \\ \dot{x}_i^* &= -\frac{k_i^u(\bar{x}_{i-1}) - k_i^l(\bar{x}_{i-1})}{(-k_i^l(\bar{x}_{i-1}) + x_i)(k_i^u(\bar{x}_{i-1}) - x_i)} \kappa_i x_i^*, \qquad i = 2, ..., n \end{aligned} \tag{4.19}$$

Since $\frac{k_i^u - k_i^l}{(-k_i^l + x_i)(k_i^u - x_i)} > \frac{2}{q_i}$, the sub-system (4.19) is globally exponentially stable at $x^* = 0$. The time-derivative of s is then obtained as

$$\dot{s} = -\Big(\frac{\partial h}{\partial x} v + \frac{\partial h}{\partial x^*} \sigma(x, v)\Big) + f(x, v) + G(x, v) E(x, v) u + \delta(t, x, v, u) \tag{4.20}$$

The control input u is designed as

$$u = E^{-1}(x, v)\Big(- \hat{G}^{-1}(x, v)\Big(- \frac{\partial h}{\partial x} v - \frac{\partial h}{\partial x^*} \sigma(x, v) + f(x, v)\Big) + w\Big) \tag{4.21}$$

where $\hat{G}^{-1}(x,v)$ is the nominal model of $G(x,v)$, and $w=[w_1,w_2,...,w_n]^T$ is the virtual control. Plugging (4.21) into (4.20), we have

$$\dot{s}_i = g_i(x,v)w_i + \Delta_i(x,v,w) \qquad i=1,...,n \tag{4.22}$$

where g_i is the ith diagonal element of G, and Δ_i is the ith component of Δ that can be expressed as

$$\Delta(x,x^*,v,w) = \Big(I - G(x,v)\hat{G}^{-1}(x,v)\Big)\Big(-\frac{\partial h}{\partial x}v - \frac{\partial h}{\partial x^*}\sigma(x,v) + f(x,v)\Big) + \delta(x,v,u)$$

To eliminate the chattering effect, the virtual control is chosen as

$$w_i = -\psi_i(x^*,v)\text{sat}\left(\frac{s_i}{\epsilon}\right) \qquad i=1,...,n \tag{4.23}$$

where sat$(\cdot)$ is the saturation function and $\psi_i(x^*,v) \geq \varrho_i(x^*,v) + \psi_0$ for $\psi_0 > 0$. Also, $\varrho_i(x^*,v)$ satisfies

$$\left|\frac{\Delta_i(x,x^*,v,w)}{g_i(x,v)}\right| \leq \varrho(x^*,v) \qquad i=1,...,n \tag{4.24}$$

Given the above control design, the objective of barrier avoidance control for a double integrator with complex state-constrained can be achieved through the following theorem.

Theorem 7. *For the system* (4.15) *with control* u *given by* (4.21)*, if the condition* (4.24) *holds globally, and* $\varrho(0,0)=0$*, then there exists* $\epsilon^* > 0$ *such that for* $0 < \epsilon < \epsilon^*$*, the origin of system* (4.16) *is globally asymptotically stable, and the equilibrium point* $x=[k_1^{ori},k_2^{ori},...,k_n^{ori}]^T$*,* $v=0$ *of system* (4.15) *is asymptotically stable with the attractive region* $(x,v) \in \mathcal{D}\times\mathbb{R}^n$*, where* $\mathcal{D}$ *is defined in* (4.14)*.*

Proof: In the region of $|s_i| > \epsilon$, we choose $V_{s_i} = 1/2 s_i^{*2}$. The time-derivative of V_{s_i} satisfies

$$\begin{aligned}\dot{V}_{s_i} = s_i \dot{s}_i &\leq -g_i(x)(s_i w + |s_i| \varrho_i(x^*, v)) \\ &\leq -g_i(x)(-|s_i| \psi_i(x^*, v) + |s_i| \varrho_i(x^*, v)) \\ &\leq -g_0 \psi_0 |s_i| < 0 \end{aligned} \tag{4.25}$$

This ensures the finite time convergence of s_i to the sliding manifold $s_i = 0$. Next, substituting v_i in (4.16) with (4.18), we obtain

$$\begin{aligned}\dot{x}_1^* &= \frac{k_1^u - k_1^l}{(-k_1^l + x_1)(k_1^u - x_1)}(s_1 - \kappa_1 x_1^*) \\ \dot{x}_i^* &= \sum_{k=1}^{i-1} \alpha_{i,k} s_i + \frac{k_i^u - k_i^l}{(-k_i^l + x_i)(k_i^u - x_i)}(s_i - \kappa_i x_i^*), \qquad i = 2, ..., n \end{aligned} \tag{4.26}$$

We can first choose $V_{x_1^*} = 1/2 x_1^{*2}$. The following condition is obtained using (4.26)

$$\dot{V}_{x_1^*} \leq -\rho_1(|x_1^*|) \qquad \forall\ |x_1^*| \geq \gamma_1(|s_1|) \tag{4.27}$$

where $\rho_1(\cdot)$ and $\gamma_1(\cdot)$ are class $\mathcal{K}$ functions. In the region $|s_1| < \epsilon$, whenever $|x_1^*| > \gamma_1(\epsilon)$, we have $\dot{V}_{x_1^*} \leq -\rho_1(\gamma_1(\epsilon))$. Thus, in a finite time, the trajectories will reach the set

$$\mathcal{P}_1 = \left\{ x^* \in \mathbb{R}^n \,\middle|\, |x_1^*| \leq \gamma_1(\epsilon) \right\} \times \left\{ s \in \mathbb{R}^n \,\middle|\, |s_1| \leq \epsilon \right\} \tag{4.28}$$

For $i = 2, ..., n$, let $V_{x_i^*} = 1/2 x_i^{*2}$ and obtain the following condition

$$\dot{V}_{x_i^*} \leq -\rho_i(|x_i^*|) \qquad \forall\ |x_i^*| \geq \gamma_i(|s_i|) \tag{4.29}$$

where $\rho_i(\cdot)$ and $\gamma_i(\cdot)$ are class $\mathcal{K}$ functions. When the state has already reached the set $\mathcal{P}_{i-1}$, if

$|s_i| < \epsilon$, we will obtain $|x_i^*| > \gamma_i(\epsilon)$ and $\dot{V}_{x_i^*} \leq -\rho_i(\gamma_i(\epsilon))$. Define the set

$$\mathcal{P}_i = \left\{ x^* \in \mathbb{R}^n \,\middle|\, |x_1^*| \leq \gamma_1(\epsilon), ..., |x_i^*| \leq \gamma_i(\epsilon) \right\} \times \left\{ s \in \mathbb{R}^n \,\middle|\, |s_1| \leq \epsilon, ..., |s_i| \leq \epsilon \right\} \tag{4.30}$$

For the scenario that the state is not in $\mathcal{P}_i$, it will reach the set $\mathcal{P}_i$ in a finite time. Finally, by applying the above process repetitively, since $V_{x_i^*}$ is radially unbounded, for any initial conditions, the system state will reach the positive invariant set $\mathcal{P}_n$ in a finite time.

Inside $\mathcal{P}_n$, the closed-loop system is expressed by (4.26) (denoted as $\dot{x}^* = f_a(x^*, s)$) as well as

$$\dot{s}_i = -g_i(x, v)\psi_i(x^*, v)\frac{s_i}{\epsilon} + \Delta_i(x, v, w) \qquad i = 1, ..., n \tag{4.31}$$

There exist a Lyapunov function $V_0 = \sum_{k=1}^{n} V_{x_k^*}$ and positive constants c_1, c_2, c_3 and c_4 such that

$$\begin{aligned} & c_1||x^*||_2^2 \leq V_0(x^*) \leq c_2||x^*||_2^2 \\ & \frac{\partial V_0}{\partial x^*} f_a(x^*, 0) \leq -c_3||x^*||_2^2 \\ & \left|\frac{\partial V_0}{\partial x^*}\right| \leq c_4||x^*||_2 \end{aligned} \tag{4.32}$$

in the neighborhood of $x^* = 0$. By the smoothness of f_a and Δ, we can choose $p_1, p_2, p_3 > 0$ such that

$$\begin{aligned} & ||f_a(x^*, s) - f_a(x^*, 0)||_2 \leq p_1||s||_2 \\ & ||\Delta||_2 \leq p_2||x^*||_2 + p_3||s||_2 \end{aligned} \tag{4.33}$$

in the neighborhood of $(x^*, s) = (0, 0)$. Choosing a Lyapunov candidate $V = V_0 + \sum_{k=1}^{n} V_{s_k}$, it is shown that

$$\dot{V} \leq -c_3||x^*||_2^2 + (c_4 p_1 + p_2)||x^*||_2||s||_2 + p_3||s||_2^2 - \frac{g_0\psi_0}{\epsilon}||s||_2^2 \leq 0 \tag{4.34}$$

holds for small enough ϵ. ■

4.4.2 Simulation Result

Consider a double integrator

$$\begin{aligned}
\dot{x}_1 &= v_1 \\
\dot{x}_2 &= v_2 \\
\dot{v}_1 &= x_1 x_2 + 9.66u_1 - 2.59u_2 + c_d v_1^2 \text{sign}(v_1) \\
\dot{v}_2 &= 0.1x_1^2 + 0.259u_1 + 0.966u_2
\end{aligned} \tag{4.35}$$

where c_d is unknown and satisfies $0 < c_d < 0.01$. The constrained region is drawn in Fig. 4.3, where the region with 'x' marks is the undesired domain of the state. The boundaries of the barrier are approximated by polynomial interpolations in x_2 dimension. The expressions of the boundaries of the state barrier are then written as

$$\begin{aligned}
k_1^l = 70, \qquad k_1^u &= 140 \\
k_2^l(x_1) &= -1.44906e^{-4}x_1^3 + 4.81590e^{-2}x_1^2 - 5.13265x_1 + 183.990 \\
k_2^u(x_1) &= -1.04798e^{-4}x_1^3 + 2.83983e^{-2}x_1^2 - 2.35943x_1 + 73.3258
\end{aligned} \tag{4.36}$$

To design the barrier avoidance based sliding mode controller, we choose $k_1^0 = (k_1^l + k_1^u)/2$ and $k_2^0(x_1) = (k_2^l(x_1) + k_2^u(x_1))/2$ for the diffeomorphism. Also, we pick

$$E = \begin{bmatrix} 0.966 & -0.259 \\ 0.259 & 0.966 \end{bmatrix}, \; G = \begin{bmatrix} 10 & 0 \\ 0 & 1 \end{bmatrix}, \; \hat{G} = \begin{bmatrix} 10.01 & 0 \\ 0 & 1 \end{bmatrix} \tag{4.37}$$

The control parameters are designed as $\psi_1 = 1000 + 0.01v_1^2$, $\psi_2 = 1000$, $\epsilon = 0.001$, and $\kappa_1 = \kappa_2 = 1$. In the simulation, the phase portrait with various initial conditions are tested using the

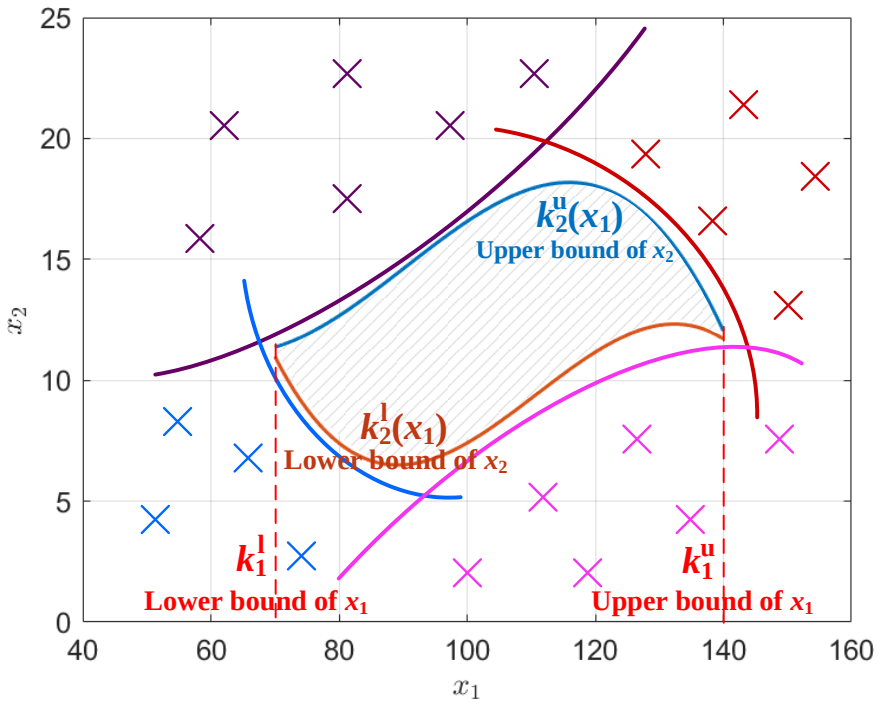

Figure 4.3: Complex state-constrained region and polynomial interpolations of its boundaries of the double integrator case study

barrier avoidance based sliding mode controller, and no violation of the constraint is observed, as shown in Fig. 4.4(a). In contrast, when the standard sliding mode controller is applied with the same initial conditions, the transgress of the state barrier will occur, as shown in Fig. 4.4(b).

4.5 Case Study II: Adaptive Backstepping Control with Complex State-Constraints

4.5.1 Control Design

Consider a strict-feedback nonlinear system in the space of $\mathbb{R}^n$ as

$$\begin{aligned} \dot{x}_i &= f_i(\bar{x}_i) + g_i(\bar{x}_i)x_{i+1}, \quad i = 1, 2, ..., n-1 \\ \dot{x}_n &= f_n(\bar{x}_n) + g_n(\bar{x}_n)u \\ y &= x_1 \end{aligned} \tag{4.38}$$

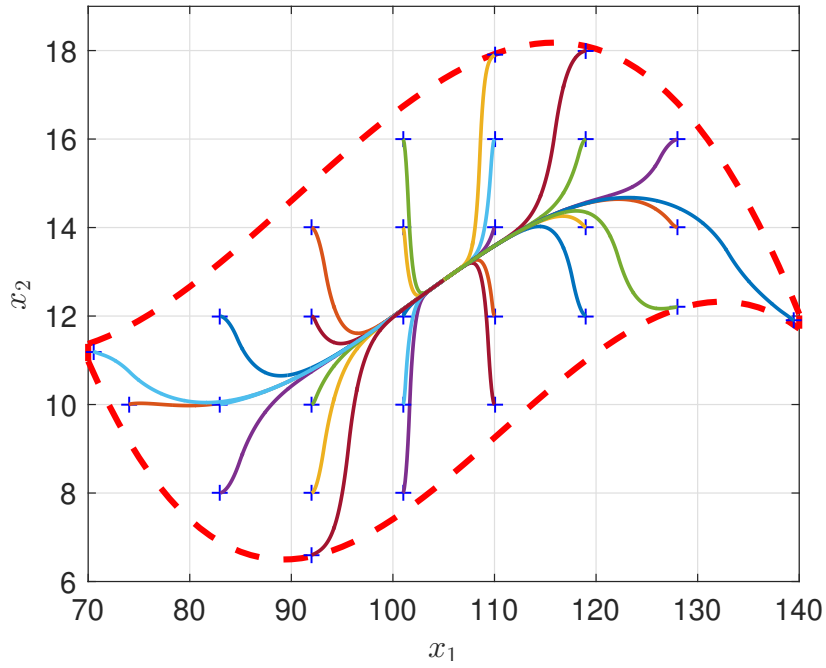

(a)

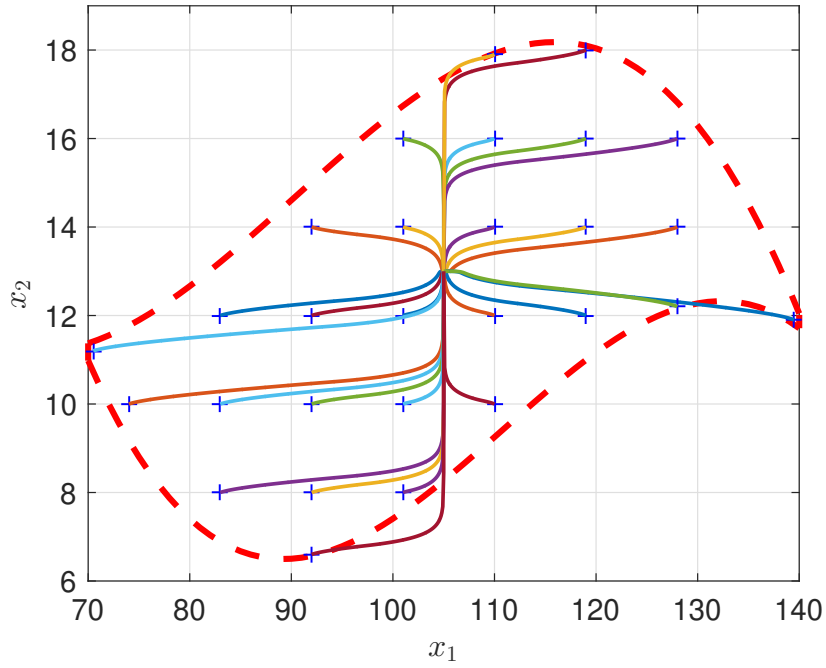

(b)

Figure 4.4: Phase portrait with diffierent initial conditions: a) Barrier avoidance sliding mode control; b) Standard sliding mode control (Initial conditions are marked by '+'.)

where $x_1, x_2, ..., x_n$ are the states, $u \in \mathbb{R}$ is the input, and $y \in \mathbb{R}$ is the output. The smooth function $f_i(\bar{x}_i)$ is linear-in-the-parameter and can be written as

$$f_i(\bar{x}_i) = \theta^T \phi_i(\bar{x}_i), \quad i = 1, 2..., n \tag{4.39}$$

where $\theta \in \mathbb{R}^m$ is an unknown constant vector of parameters and $\phi_i(\bar{x}_i) \in \mathbb{R}^m$ is a known nonlinear function vector satisfying $\|\theta\| \leq \theta_M$ for $\theta_M > 0$.

To address the complex state constraints $\mathcal{D}$ as described in (4.5), the boundary of the constraints $\partial\mathcal{D}$ is incorporated into the Lyapunov candidate. Under the diffeomorphic transformation (4.10), we choose the Lyapunov candidate in the new plane as

$$V = \sum_{i=1}^{n} \int_{\frac{1}{2}\ln(\frac{-k_i^l+\alpha}{k_i^u-\alpha})}^{x_i^*} \frac{k_i^u - k_i^l}{2} \left(\frac{e^{2\beta^*} k_i^u + k_i^l}{e^{2\beta^*}+1} - \alpha \right) d\beta^* \tag{4.40}$$

which is radially unbounded in $\mathbb{R}^n$ in the x^*-coordinates. This Lyapunov function can be further simplified. Considering each term in this (4.40), we have

$$\begin{aligned}
V_i &= \int_{\frac{1}{2}\ln(\frac{-k_i^l+\alpha}{k_i^u-\alpha})}^{x_i^*} \frac{k_i^u - k_i^l}{2} \left(\frac{e^{2\beta^*} k_i^u + k_i^l}{e^{2\beta^*}+1} - \alpha \right) d\beta^* \\
&= \int_{\frac{1}{2}\ln(\frac{-k_i^l+\alpha}{k_i^u-\alpha})}^{x_i^*} \left(\frac{k_i^u - k_i^l}{2} \right)^2 \frac{(e^{2\beta^*}+1)^2}{e^{2\beta^*}(k_i^u - k_i^l)^2} \left(\frac{e^{2\beta^*} k_i^u + k_i^l}{e^{2\beta^*}+1} - \alpha \right) \frac{2e^{2\beta^*}(k_i^u - k_i^l)}{(e^{2\beta^*}+1)^2} d\beta^* \\
&= \int_{\alpha}^{x_i} \left(\frac{k_i^u - k_i^l}{2} \right)^2 \frac{1}{(k_i^u - \beta)(\beta - k_i^l)} (\beta - \alpha) d\beta \\
&= \int_0^z \frac{\tau \left(\frac{k_i^u - k_i^l}{2} \right)^2}{(k_i^u - (\tau+\alpha))((\tau+\alpha) - k_i^l)} d\tau
\end{aligned} \tag{4.41}$$

This way we can establish the equivalence of the barrier avoidance control and the iBLF for this backstepping control problem.

Accordingly, the Lyapunov function candidate for the system (4.38) is then written as

$$V(z,\alpha,x) = V_1(z_1, y_d) + \sum_{i=2}^{n} V_i(z_i, \alpha_{i-1}, \bar{x}_{i-1}) \tag{4.42}$$

where

$$\begin{aligned}
V_1(z_1, y_d) &= W_1(z_1, y_d) + \frac{1}{2}\tilde{\theta}_1^T \Gamma^{-1} \tilde{\theta}_1 \\
V_i(z_i, \alpha_{i-1}, \bar{x}_{i-1}) &= W_i(z_i, \alpha_{i-1}, \bar{x}_{i-1}) + \frac{1}{2}\tilde{\theta}_i^T \Gamma^{-1} \tilde{\theta}_i \\
W_1(z_1, y_d) &= \int_0^{z_1} \frac{\tau \left(\frac{k_1^u - k_1^l}{2}\right)^2}{(k_1^u - (\tau + y_d))((\tau + y_d) - k_1^l)} d\tau \\
W_i(z_i, \alpha_{i-1}, \bar{x}_{i-1}) &= \int_0^{z_i} \frac{\tau \left(\frac{k_i^u(\bar{x}_{i-1}) - k_i^l(\bar{x}_{i-1})}{2}\right)^2}{(k_i^u(\bar{x}_{i-1}) - (\tau + \alpha_{i-1}))((\tau + \alpha_{i-1}) - k_i^l(\bar{x}_{i-1}))} d\tau
\end{aligned} \tag{4.43}$$

Here, $z_1 = x_1 - y_d$, $z_i = x_i - \alpha_{i-1}$, $i = 2, ..., n$, and $\Gamma = \Gamma^T > 0$ is the adaptation gain matrix. The stabilizing functions $\alpha_1, ..., \alpha_{n-1}$ are continuously differentiable. We define $\hat{\theta}_i$ to be the ith estimation of θ and let $\tilde{\theta}_i = \hat{\theta}_i - \theta$. Note that, as can be verified by (4.43), if the states approach the boundary of the constrained region, i.e. $x_i \to k_i^u$ or $x_i \to k_i^l$, the integral will reach infinity at its upper limit, and the barrier Lyapunov candidate will result in an infinitely large value. In particular, when $k_i^u = -k_i^l = c_i$ holds (c_i is a positive constant), the term W_i becomes the same type as the one used in the standard iBLF [53] for the simple barrier with hyperrectangular shape.

Lemma 3. *The term W_i defined in* (4.43) *satisfies the following condition if $k_i^l < \alpha_{i-1} < k_i^u$ holds*

$$\frac{z_i^2}{2} \leq W_i \leq \frac{(k_i^u - k_i^l)^2/4}{(k_i^u - x_i)(x_i - k_i^l)} z_i^2 \tag{4.44}$$

Proof: For the left part of the inequality, since $(k_i^u - (\tau + \alpha_{i-1}))((\tau + \alpha_{i-1}) - k_i^l) > 0$ we have

$$\frac{\left(\frac{k_i^u - k_i^l}{2}\right)^2}{(k_i^u - (\tau + \alpha_{i-1}))((\tau + \alpha_{i-1}) - k_i^l)} = \frac{\left(\frac{k_i^u - k_i^l}{2}\right)^2}{\left(\frac{k_i^u - k_i^l}{2}\right)^2 - \left(\frac{k_i^u + k_i^l}{2} - (\tau + \alpha_{i-1})\right)^2} \geq 1 \tag{4.45}$$

Thus, it can be derived that

$$W_i \geq \int_0^{z_i} \tau d\tau = \frac{z_i^2}{2} \tag{4.46}$$

Next, to prove the right part of the inequality, we first define

$$\sigma_i(\tau, \alpha_{i-1}, \bar{x}_{i-1}) = \frac{\tau \left(\frac{k_i^u - k_i^l}{2}\right)^2}{(k_i^u - (\tau + \alpha_{i-1}))((\tau + \alpha_{i-1}) - k_i^l)} \tag{4.47}$$

Then take derivative of σ_i with respect to τ

$$\frac{\partial \sigma_i}{\partial \tau} = \left(\frac{k_i^u - k_i^l}{2}\right)^2 \frac{(k_i^u - \alpha_{i-1})(\alpha_{i-1} - k_i^l)}{(k_i^u - (\tau + \alpha_{i-1}))^2((\tau + \alpha_{i-1}) - k_i^l)^2} \tag{4.48}$$

This partial derivative is positive when $k_i^l < \alpha_{i-1} < k_i^u$ holds. Therefore, σ_i is monotonically increasing with respect to τ, since $\sigma_i(0, \alpha_{i-1}) = 0$. Thus, we have

$$W_i = \int_0^{z_i} \sigma_i(\tau, \alpha_{i-1}) d\tau \leq z_i \sigma_i(z_i, \alpha_{i-1}) \tag{4.49}$$

This completes the proof of the right part of the inequality. ■

Following the backstepping scheme, a step-by-step control design is then proposed.

Step 1: In the first step, consider V_1 defined in (4.43). We write its time-derivative as

$$\begin{aligned}
\dot{V}_1 =& \frac{\partial W_1}{\partial z_1}\dot{z}_1 + \frac{\partial W_1}{\partial y_d}\dot{y}_d + \tilde{\theta}_1^T \Gamma^{-1} \dot{\hat{\theta}}_1 \\
=& \frac{z_1 (k_1^u - k_1^l)^2/4}{(k_1^u - x_1)(x_1 - k_1^l)}(f_1 + g_1 z_2 + g_1 \alpha_1 - \dot{y}_d) + \Big(\frac{(k_1^u - k_1^l)^2/4}{(k_1^u - x_1)(x_1 - k_1^l)} \\
& - \frac{k_1^u - k_1^l}{4 z_1} \ln \frac{(z_1 + y_d - k_1^l)(k_1^u - y_d)}{(k_1^u - z_1 - y_d)(y_d - k_1^l)} \Big) z_1 \dot{y}_d + \tilde{\theta}_1^T \Gamma^{-1} \dot{\hat{\theta}}_1 \\
=& \frac{z_1 (k_1^u - k_1^l)^2/4}{(k_1^u - x_1)(x_1 - k_1^l)}(f_1 + g_1 z_2 + g_1 \alpha_1) - \varrho_1(z_1, y_d) z_1 \dot{y}_d + \tilde{\theta}_1^T \Gamma^{-1} \dot{\hat{\theta}}_1
\end{aligned} \tag{4.50}$$

where

$$\varrho_1(z_1, y_d) = \frac{k_1^u - k_1^l}{4z_1} \ln \frac{(z_1 + y_d - k_1^l)(k_1^u - y_d)}{(k_1^u - z_1 - y_d)(y_d - k_1^l)} \tag{4.51}$$

Per L'Hôpital's rule, we can verify the limit of $\varrho_1(z_1, y_d)$ at $z_1 = 0$ as

$$\lim_{z_1 \to 0} \varrho_1(z_1, y_d) = \frac{(k_1^u - k_1^l)^2/4}{(k_1^u - y_d)(y_d - k_1^l)} \tag{4.52}$$

The stablizing function α_1 is chosen as

$$\alpha_1 = \frac{1}{g_1}\Big(- \hat{\theta}_1^T \phi_1 - p_1 z_1 + \frac{(k_1^u - x_1)(x_1 - k_1^l)}{(k_1^u - k_1^l)^2/4} \varrho_1 \dot{y}_d \Big) \tag{4.53}$$

where the postive constant p_1 is the control gain, yielding

$$\dot{V}_1 = \frac{(k_1^u - k_1^l)^2/4}{(k_1^u - x_1)(x_1 - k_1^l)}(-p_1 z_1^2 + g_1 z_1 z_2) + \tilde{\theta}_1^T \Big(\Gamma^{-1} \dot{\hat{\theta}}_1 - \frac{(k_1^u - k_1^l)^2/4}{(k_1^u - x_1)(x_1 - k_1^l)} z_1 \phi_1 \Big) \tag{4.54}$$

Step i (i=2,...,n-1): In the ith step, we take time-derivative of V_i and write it as

$$\begin{aligned}
\dot{V}_i =& \frac{\partial W_i}{\partial z_i} \dot{z}_i + \frac{\partial W_i}{\partial \alpha_{i-1}} \dot{\alpha}_{i-1} + \tilde{\theta}_i^T \Gamma^{-1} \dot{\hat{\theta}}_i \\
=& \frac{z_i (k_i^u - k_i^l)^2/4}{(k_i^u - x_i)(x_i - k_i^l)}(f_i + g_i z_{i+1} + g_i \alpha_i - \dot{\alpha}_{i-1}) + \Big(\frac{(k_i^u - k_i^l)^2/4}{(k_i^u - x_i)(x_i - k_i^l)} \\
& - \frac{k_i^u - k_i^l}{4 z_i} \ln \frac{(z_i + \alpha_{i-1} - k_1^l)(k_i^u - \alpha_{i-1})}{(k_i^u - z_i - \alpha_{i-1})(\alpha_{i-1} - k_i^l)} \Big) z_i \alpha_{i-1} \\
& + \sum_{j=1}^{i-1} \Big(\int_0^{z_i} \frac{\partial \sigma_i}{\partial x_j} d\tau \cdot \dot{x}_j \Big) + \tilde{\theta}_i^T \Gamma^{-1} \dot{\hat{\theta}}_i \\
=& \frac{z_i (k_i^u - k_i^l)^2/4}{(k_i^u - x_i)(x_i - k_i^l)}(f_i + g_i z_{i+1} + g_i \alpha_i) - \varrho_i(z_i, \alpha_{i-1}, \bar{x}_{i-1}) z_i \dot{\alpha}_{i-1} \\
& + z_i \sum_{j=1}^{i-1} \psi_{ij}(z_i, \alpha_{i-1}, \bar{x}_{i-1}) \dot{x}_j + \tilde{\theta}_i^T \Gamma^{-1} \dot{\hat{\theta}}_i
\end{aligned} \tag{4.55}$$

where

$$\varrho_i(z_i, \alpha_{i-1}, \bar{x}_{i-1}) = \frac{k_i^u - k_i^l}{4z_i} \ln \frac{(z_i + \alpha_{i-1} - k_i^l)(k_i^u - \alpha_{i-1})}{(k_i^u - z_i - \alpha_{i-1})(\alpha_{i-1} - k_i^l)} \tag{4.56}$$

$$\psi_{ij}(z_i, \alpha_{i-1}, \bar{x}_{i-1}) = \frac{1}{z_i} \int_0^{z_i} \frac{\partial \sigma_i(\tau, \alpha_{i-1}, \bar{x}_{i-1})}{\partial x_j} d\tau \tag{4.57}$$

$$\begin{aligned} \frac{\partial \sigma_i}{\partial x_j} = & \frac{\tau}{(k_i^u - \tau - \alpha_{i-1})^2 (\tau + \alpha_{i-1} - k_i^l)^2} \Bigg[\frac{1}{2}(k_i^u - k_i^l) \\ & \times \left(\frac{\partial k_i^u}{\partial x_j} - \frac{\partial k_i^l}{\partial x_j} \right) (k_i^u - \tau - \alpha_{i-1})(\tau + \alpha_{i-1} - k_i^l) \\ & - \left(\frac{k_i^u - k_i^l}{2} \right)^2 \Bigg(\frac{\partial k_i^u}{\partial x_j} (k_i^u - \tau - \alpha_{i-1}) - \frac{\partial k_i^l}{\partial x_j} \\ & \times (\tau + \alpha_{i-1} - k_i^l) \Bigg) \Bigg] \end{aligned} \tag{4.58}$$

The limits of $\varrho_i(z_i, \alpha_{i-1}, \bar{x}_{i-1})$ and $\psi_{ij}(z_i, \alpha_{i-1}, \bar{x}_{i-1})$ at $z_i = 0$ are given as

$$\lim_{z_i \to 0} \varrho_i(z_i, \alpha_{i-1}, \bar{x}_{i-1}) = \frac{(k_i^u - k_i^l)^2/4}{(k_i^u - \alpha_{i-1})(\alpha_{i-1} - k_i^l)} \tag{4.59}$$

$$\lim_{z_i \to 0} \psi_{ij}(z_i, \alpha_{i-1}, \bar{x}_{i-1}) = \frac{\partial \sigma_i(z_i, \alpha_{i-1}, \bar{x}_{i-1})}{\partial x_j} \tag{4.60}$$

which are both well-defined in $x \in \mathcal{D}$ and $k_i^l < \alpha_{i-1} < k_i^u$. The existence of the high order derivatives of ϱ_i and ψ_{ij} can be validated through the following Lemma.

Lemma 4. *The functions $\varrho_i(z_i, \alpha_{i-1}, \bar{x}_{i-1})$ and $\psi_{ij}(z_i, \alpha_{i-1}, \bar{x}_{i-1})$ are $\mathcal{C}^{n-i}$ in the set*

$$\begin{aligned} \Psi = \Big\{ & \bar{x}_{i-1} \in \mathbb{R}^{i-1}, \alpha_{i-1} \in \mathbb{R} \,\Big|\, k_1^l < x_1 < k_1^u,\ k_2^l(x_1) < x_2 < k_2^u(x_1),\ \dots, \\ & k_{i-1}^l(\bar{x}_{i-2}) < x_{i-1} < k_{i-1}^u(\bar{x}_{i-2}), k_i^l(\bar{x}_{i-1}) < \alpha_{i-1} < k_i^u(\bar{x}_{i-1}) \Big\} \end{aligned} \tag{4.61}$$

Proof: We will first prove $\psi_{ij}(z_i, \alpha_{i-1}, \bar{x}_{i-1})$ is $\mathcal{C}^{n-i}$, and the same procedure can be applied to $\varrho_i(z_i, \alpha_{i-1}, \bar{x}_{i-1})$.

Define $\xi_i = z_i \psi_{ij}$. We can obtain the following equality by taking partial derivative recursively

$$\begin{aligned}
\frac{\partial^k \xi_i}{\partial z_i^k} &= \frac{\partial^{k-1}}{\partial z_i^{k-1}} \left(z_i \frac{\partial \psi_{ij}}{\partial z_i} + \psi_{ij} \right) \\
&= \frac{\partial^{k-1} \psi_{ij}}{\partial z_i^{k-1}} + \frac{\partial^{k-2}}{\partial z_i^{k-2}} \left(z_i \frac{\partial^2 \psi_{ij}}{\partial z_i^2} + \frac{\partial \psi_{ij}}{\partial z_i} \right) \\
&= k \frac{\partial^{k-1} \psi_{ij}}{\partial z_i^{k-1}} + z_i \frac{\partial^k \psi_{ij}}{\partial z_i^k}
\end{aligned} \tag{4.62}$$

From (4.62), we can write the kth order partial derivative of ψ_{ij} with respect to z_i as

$$\frac{\partial^k \psi_{ij}}{\partial z_i^k} = \frac{1}{z_i} \left(\frac{\partial^k \xi_i}{\partial z_i^k} - k \frac{\partial^{k-1} \psi_{ij}}{\partial z_i^{k-1}} \right) = \frac{\eta}{z_i^{k+1}} \tag{4.63}$$

where

$$\eta = z_i^k \left(\frac{\partial^k \xi_i}{\partial z_i^k} - k \frac{\partial^{k-1} \psi_{ij}}{\partial z_i^{k-1}} \right) \tag{4.64}$$

The following limit can be obtained by L'Hôpital's rule and (4.62)

$$\begin{aligned}
\lim_{z_i \to 0} \frac{\partial^k \psi_{ij}}{\partial z_i^k} &= \lim_{z_i \to 0} \frac{1}{(k+1) z_i^k} \frac{\partial \eta}{\partial z_i} \\
&= \lim_{z_i \to 0} \frac{1}{(k+1) z_i^k} \left(k z_i^{k-1} \frac{\partial^k \xi_i}{\partial z_i^k} + z_i^k \frac{\partial^{k+1} \xi_i}{\partial z_i^{k+1}} - k^2 z_i^{k-1} \frac{\partial^{k-1} \psi_{ij}}{\partial z_i^{k-1}} - k z_i^k \frac{\partial^k \psi_{ij}}{\partial z_i^k} \right) \\
&= \lim_{z_i \to 0} \frac{1}{k+1} \frac{\partial^{k+1} \xi_i}{\partial z_i^{k+1}}
\end{aligned} \tag{4.65}$$

By (4.58), we have $\xi_i = \int_0^{z_i} (\partial \sigma_i / \partial x_j) d\tau$ to be $\mathcal{C}^\infty$ in the set Ψ. Thus, the pure partial derivative of ψ_{ij} with respect to z_i is at least $n - i$ times continuously differentiable.

Then, we consider the pure partial derivatives with respect to α_{i-1} or x_j and mixed partial derivatives of ψ_{ij}. Per Clairaut's Theorem, we can obtain any mixed partial derivative of ψ_{ij}

regardless of the drifferentiation order, given the following

$$\lim_{z_i\to 0}\frac{\partial^{k+l+m_1+\cdots+m_{i-1}}\psi_{ij}}{\partial z_i^k\partial\alpha_{i-1}^l\partial x_1^{m_1}\cdots\partial x_{i-1}^{m_{i-1}}}=\frac{\partial^{l+m_1+\cdots+m_{i-1}}}{\partial\alpha_{i-1}^l\partial x_1^{m_1}\cdots\partial x_{i-1}^{m_{i-1}}}\Big(\lim_{z_i\to 0}\frac{\partial^k\psi_{ij}}{\partial z_i^k}\Big) \tag{4.66}$$

where $(k+l+m_1+\cdots+m_{i-1})\in\{1,...,n-i\}$ and $k,l,m_1,...,m_{i-1}$ are positive integers. Due to the smoothness of k_i^u and k_i^l, the limits (4.66) exist. Thus, the pure partial derivatives with respect to α_{i-1} or x_j and mixed partial derivatives of ψ_{ij} are $\mathcal{C}^\infty$ in the set Ψ. ■

Next, the time-derivative of α_{i-1} can be expanded as

$$\dot{\alpha}_i=\sum_{j=1}^{i}\frac{\partial\alpha_i}{\partial\hat{\theta}_j}\dot{\hat{\theta}}_j+\sum_{j=1}^{i}\frac{\partial\alpha_i}{\partial x_j}\dot{x}_j+\sum_{j=1}^{i}\frac{\partial\alpha_i}{\partial y_d^{(j)}}y_d^{(j+1)} \tag{4.67}$$

Choose the stablizing function as

$$\begin{aligned}\alpha_i=&\frac{1}{g_i}\Big[-p_iz_i-\frac{(k_{i-1}^u-k_{i-1}^l)^2(k_i^u-x_i)(x_i-k_i^l)g_{i-1}z_{i-1}}{(k_i^u-k_i^l)^2(k_{i-1}^u-x_{i-1})(x_{i-1}-k_{i-1}^l)}-\hat{\theta}_i^T\Big(\phi_i-\frac{(k_i^u-x_i)(x_i-k_i^l)}{(k_i^u-k_i^l)^2/4}\\&\times\sum_{j=1}^{i-1}\Big(\frac{\partial\alpha_{i-1}}{\partial x_j}\varrho_i-\psi_{ij}\Big)\phi_j\Big)+\frac{(k_i^u-x_i)(x_i-k_i^l)}{(k_i^u-k_i^l)^2/4}\sum_{j=1}^{i-1}\Big(\Big(\frac{\partial\alpha_{i-1}}{\partial x_j}\varrho_i-\psi_{ij}\Big)g_jx_{j+1}\\&+\varrho_i\frac{\partial\alpha_{i-1}}{\partial y_d^{(j)}}y_d^{(j+1)}+\varrho_i\frac{\partial\alpha_{i-1}}{\partial\hat{\theta}_j}\dot{\hat{\theta}}_j\Big)\Big]\end{aligned} \tag{4.68}$$

Substituting (4.68) into (4.55) gives

$$\begin{aligned}\dot{V}_i=&\frac{(k_i^u-k_i^l)^2/4}{(k_i^u-x_i)(x_i-k_i^l)}(-p_iz_i^2+g_iz_iz_{i+1})-\frac{(k_{i-1}^u-k_{i-1}^l)^2/4}{(k_{i-1}^u-x_{i-1})(x_{i-1}-k_{i-1}^l)}g_{i-1}z_{i-1}z_i\\&+\tilde{\theta}_i^T\Big[\Gamma^{-1}\dot{\hat{\theta}}_i-z_i\Big(\frac{(k_i^u-k_i^l)^2/4}{(k_i^u-x_i)(x_i-k_i^l)}\phi_i-\sum_{j=1}^{i-1}\Big(\frac{\partial\alpha_{i-1}}{\partial x_j}\varrho_i-\psi_{ij}\Big)\phi_j\Big)\Big]\end{aligned} \tag{4.69}$$

Step n: The time-derivative of z_n is

$$\dot{z}_n=\dot{x}_n-\dot{\alpha}_{n-1}=f_n(\bar{x}_n)+g_n(\bar{x}_n)u-\dot{\alpha}_{n-1} \tag{4.70}$$

Use the convienient notation

$$
\begin{aligned}
h_1 &= \frac{(k_1^u - k_1^l)^2/4}{(k_1^u - x_1)(x_1 - k_1^l)} z_1 \phi_1 \\
h_i &= z_i \Big(\frac{(k_i^u - k_i^l)^2/4}{(k_i^u - x_i)(x_i - k_i^l)} \phi_i - \sum_{j=1}^{i-1} \Big(\frac{\partial \alpha_{i-1}}{\partial x_j} \varrho_i - \psi_{ij} \Big) \phi_j \Big), \qquad i = 2, ..., n
\end{aligned} \tag{4.71}
$$

Choose the input and the adaptive law as

$$
u = \alpha_n, \qquad \dot{\hat{\theta}}_i = \Gamma h_i, \qquad i = 1, ..., n \tag{4.72}
$$

We can generate the time-derivative of $V = \sum_{i=1}^n V_i$ as

$$
\begin{aligned}
\dot{V} =& \sum_{i=1}^n \dot{V}_i \\
=& - \sum_{i=1}^n \frac{(k_i^u - k_i^l)^2/4}{(k_i^u - x_i)(x_i - k_i^l)} p_i z_i^2 + \sum_{i=1}^n \tilde{\theta}_i^T (\Gamma^{-1} \dot{\hat{\theta}}_i - h_i) \\
=& - \sum_{i=1}^n \frac{(k_i^u - k_i^l)^2/4}{(k_i^u - x_i)(x_i - k_i^l)} p_i z_i^2 \\
\leq& - \rho \sum_{i=1}^n W_i
\end{aligned} \tag{4.73}
$$

where $\rho = \min\{p_i, i = 1, .., n\}$.

With the closed-loop system well formulated, the main result of this study is provided as follows.

Theorem 8. *Consider the closed-loop system* (4.38) *under the control input and the adaptive law* (4.72). *If the initial condition satisfies* $x(0) \in \mathcal{D}$ *and the condition is provided as*

$$
k_i^l(\bar{x}_{i-1}) < \alpha_{i-1} < k_i^u(\bar{x}_{i-1}), \quad i = 2, ..., n, \ \forall (\bar{z}_n, \bar{y}_{d_n}) \in \Omega \tag{4.74}
$$

where

$$\Omega = \left\{ \bar{z}_n \in \mathbb{R}^n,\, \bar{y}_{d_n} \in \mathbb{R}^{n+1} \;\middle|\; |z_i| \leq \sqrt{2V_M},\, k_1^l < y_d < k_1^u,\, |y_d^{(i)}| \leq B_i,\, i = 1, ..., n \right\} \tag{4.75}$$

$$V_M = \sum_{i=1}^{n} W_i(0) + \frac{1}{2}\lambda_{\max}(\Gamma^{-1}) \sum_{i=1}^{n} (\|\hat{\theta}_i(0)\| + \theta_M)^2 \tag{4.76}$$

Then the following properties hold.

i) The tracking error $\bar{z}_n$ and the estimator $\hat{\theta}_i$ remain in the compact set given as

$$\Omega_z = \left\{ \bar{z}_n \in \mathbb{R}^n \;\middle|\; \|\bar{z}_n\| \leq \sqrt{2V_M} \right\} \tag{4.77}$$

$$\Omega_{\hat{\theta}_i} = \left\{ \hat{\theta}_i \in \mathbb{R}^m \;\middle|\; \|\hat{\theta}_i\| \leq \theta_M + \sqrt{\frac{2V_M}{\lambda_{\min}(\Gamma^{-1})}} \right\} \tag{4.78}$$

Also, z_i and $\dot{\hat{\theta}}_i$, $i = 1, ..., n$, converge to zero.

ii) The state x stays in $\mathcal{D}$ for all $t > 0$.

iii) The stablizing functions α_i, $i = 1, ..., n-1$, and control input u are bounded for all $t > 0$.

Proof:

i) From $\dot{V}(t) \leq 0$, we have $V(t) \leq V(0)$. Also, since $\|\theta\| \leq \theta_M$, it follows that $V(0) \leq V_M$. Given Lemma 3, we obtain $(1/2)\Sigma_{i=1}^{n} z_i^2(t) \leq V(t) \leq V(0) \leq V_M$. Thus, we can show that $\|\bar{z}_n\| \leq \sqrt{2V_M}$ and $\bar{z}_n \in \Omega_z$. Furthermore, as $\lambda_{\min}(\Gamma^{-1})\|\hat{\theta}_i - \theta\|^2 \leq 2V_M$, it follows that $\hat{\theta}_i \in \Omega_{\hat{\theta}_i}$.

Let $\int_0^t (-\dot{V}(t))dt = V(0) - V(t)$. Since $V(0)$ is bounded and $\dot{V}(t) \leq 0$, we have $V(t)$ non-increasing and thus bounded. It can be shown that $\int_0^\infty (-\dot{V}(t))dt$ is bounded. Also, as $-\dot{V}(t)$ is uniformly continuous, by Barbalat's Lemma, we have $-\dot{V}(t)$ converge to zero and then $z_i \to 0$ as $t \to \infty$. By the definition of $\dot{\hat{\theta}}_i = \Gamma h_i$, it follows that $\dot{\hat{\theta}}_i \to 0$ as $t \to \infty$.

ii) By proof of contradiction, we assume that there exists a time instance $t = \bar{t}$ such that $x \in \partial\mathcal{D}$, i.e. $x_i = k_i^u$ or $x_i = k_i^l$, given the initial condition $x(0) \in \mathcal{D}$. From $\dot{V}(t) \leq 0$, we have

$V(\bar{t}) = \Sigma_{i=1}^{n} V_i(\bar{t}) \leq V(0)$ and thus $V_i(\bar{t})$ is bounded. Meanwhile, integrating $V_i(\bar{t})$ gives

$$\begin{aligned} V_i(\bar{t}) =& \frac{k_i^u - k_i^l}{4} \int_0^{z_i} \tau \Big(\frac{1}{k_i^u - (\tau + \alpha_{i-1})} + \frac{1}{(\tau + \alpha_{i-1}) - k_i^l} \Big) d\tau + \frac{1}{2} \tilde{\theta}_i^T \Gamma^{-1} \tilde{\theta}_i \\ =& \frac{k_i^u - k_i^l}{4} \Big(\int_0^{z_i} \Big(\frac{k_i^u - \alpha_{i-1}}{k_i^u - (\tau + \alpha_{i-1})} - 1 \Big) d\tau + \int_0^{z_i} \Big(\frac{-\alpha_{i-1} + k_i^1}{(\tau + \alpha_{i-1}) - k_i^l} + 1 \Big) d\tau \Big) + \frac{1}{2} \tilde{\theta}_i^T \Gamma^{-1} \tilde{\theta}_i \\ =& \frac{k_i^u - k_i^l}{4} \Big((\alpha_{i-1}(\bar{t}) - k_i^l) \ln \frac{\alpha_{i-1}(\bar{t}) - k_i^l}{x_i(\bar{t}) - k_i^l} + (k_i^u - \alpha_{i-1}(\bar{t})) \ln \frac{k_i^u - \alpha_{i-1}(\bar{t})}{k_i^u - x_i(\bar{t})} \Big) + \frac{1}{2} \tilde{\theta}_i^T \Gamma^{-1} \tilde{\theta}_i \end{aligned} \tag{4.79}$$

As the condition (4.74) holds, if $x_i = k_i^u$ or $x_i = k_i^l$, the value of $V_i(\bar{t})$ becomes unbounded, which contradicts the above discussion. Therefore, the state x will not reach $\partial\mathcal{D}$.

iii) Due to the condition (4.74), Lemma 4 holds and $\varrho_i(z_i, \alpha_{i-1}, \bar{x}_{i-1})$, $\psi_{ij}(z_i, \alpha_{i-1}, \bar{x}_{i-1})$ are $\mathcal{C}^{n-i}$. Given the definition of α_i in (4.53), (4.68) and the choice of control input $u = \alpha_n$, it is clear that the closed-loop signals of α_i and u are bounded. ■

4.5.2 Simulation Result

The simulation is performed on a second-order nonlinear system given as

$$\begin{aligned} \dot{x}_1 &= 0.1x_1^2 + x_2 \\ \dot{x}_2 &= 0.1x_1x_2 - 0.2x_1 + (1 + x_1^2)u \end{aligned} \tag{4.80}$$

where we choose the nonlinear function vectors as $\phi_1 = [0.01x_1^2, 0, 0]^T$, $\phi_2 = [0, 0.01x_1x_2, -0.02x_1]^T$, and the unknown parameter vector as $\theta = [10, 10, 10]^T$. The desired trajectory is given as

$$y_d(t) = 0.5\sin(t) \tag{4.81}$$

The state constrained region is defined in the coordinates of $x_1 - x_2$, as shown in Fig. 4.5. We

provide the expressions of the boundaries of this constrained region as

$$\begin{aligned} k_1^u &= 1 \\ k_1^l &= -1 \\ k_2^u(x_1) &= -1.102x_1^2 - 0.987x_1 + 1.270 \\ k_2^l(x_1) &= 0.897x_1^2 - 0.989x_1 - 1.270 \end{aligned} \tag{4.82}$$

To design the controller under adaptive backstepping scheme as proposed in this study, we choose the control gains as $p_1 = p_2 = 1$. Also, the parameters for adaptive laws are designed as

$$\hat{\theta}_1 = \begin{bmatrix} \vartheta_1 \\ 0 \\ 0 \end{bmatrix}, \ \hat{\theta}_2 = \begin{bmatrix} \vartheta_2 \\ \vartheta_3 \\ \vartheta_4 \end{bmatrix}, \ \Gamma = \begin{bmatrix} 5000 & 0 & 0 \\ 0 & 5000 & 0 \\ 0 & 0 & 5000 \end{bmatrix} \tag{4.83}$$

The initial conditions of the numerical test are $x_1(0) = -0.8$, $x_1(0) = 0.1$, and $\vartheta_1(0) = \vartheta_2(0) = \vartheta_3(0) = \vartheta_4(0) = 15$. In the simulation, the phase portrait of $x_1 - x_2$ is drawn in Fig. 4.5, where the trajectory of x approaches a periodic cycle that matches the desired sinusoidal trajectory without any violation of the state constaints. Also, Fig. 4.6 shows that the phase portrait of $z_1 - z_2$ appoaches to the origin, indicating the convergence of z_1 and z_2 to zero. The time history of the adaptive gain $\hat{\theta}$ is depicted in Fig. 4.7, which verifies the fact that $\dot{\hat{\theta}}$ converges to zero. Finally, the boundedness of the control input is shown in Fig. 4.8.

4.6 Conclusions

This chapter investigates a supplementary study for the barrier avoidance control approach, particularly on the construction of state transformation for a complex state-constrained region. For a class of constrained regions with complex shapes, the state transformation can be established sequentially in a cascade manner, and such a transformation is proved to be a diffeomorphism which enables the barrier avoidance control design. In the case studies, we formulate the constrained

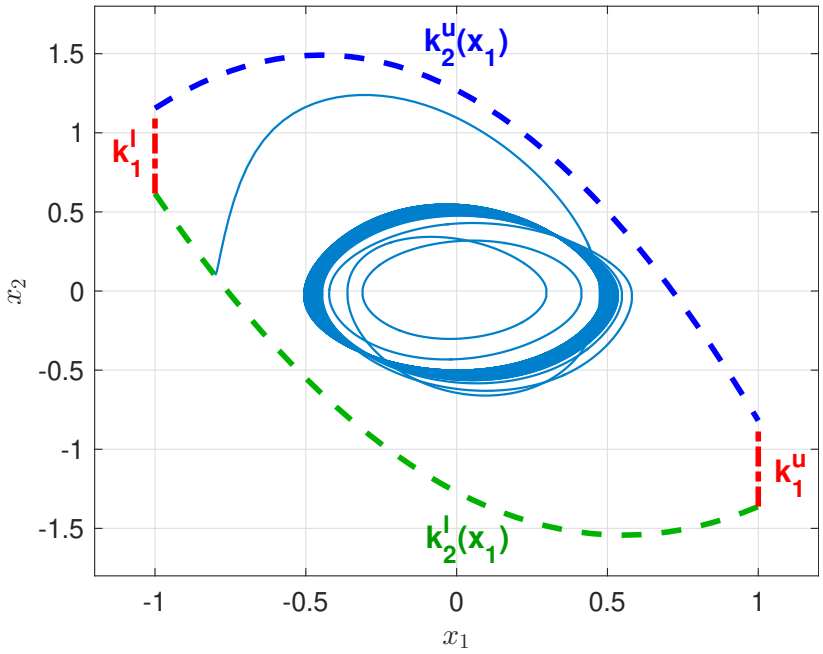

Figure 4.5: Complex state constrained region and phase portrait of $x_1 - x_2$ (boundaries denoted by dashed lines)

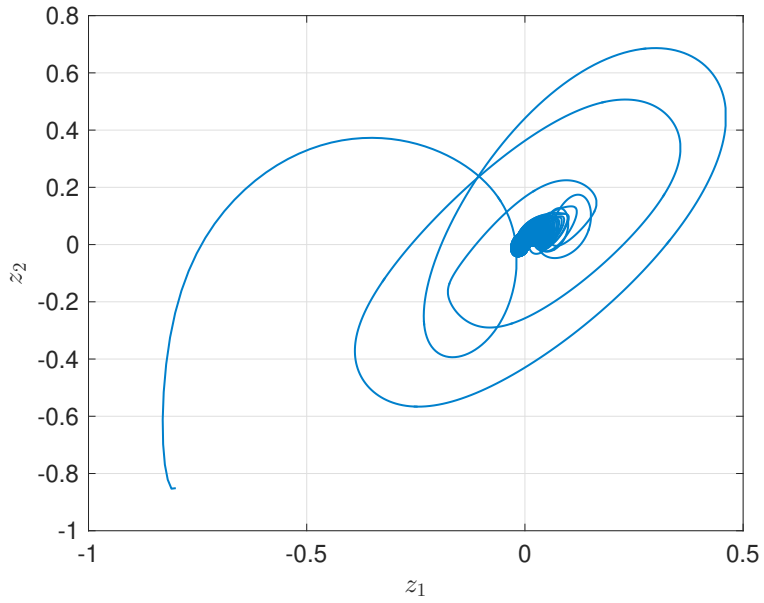

Figure 4.6: Phase portrait of $z_1 - z_2$

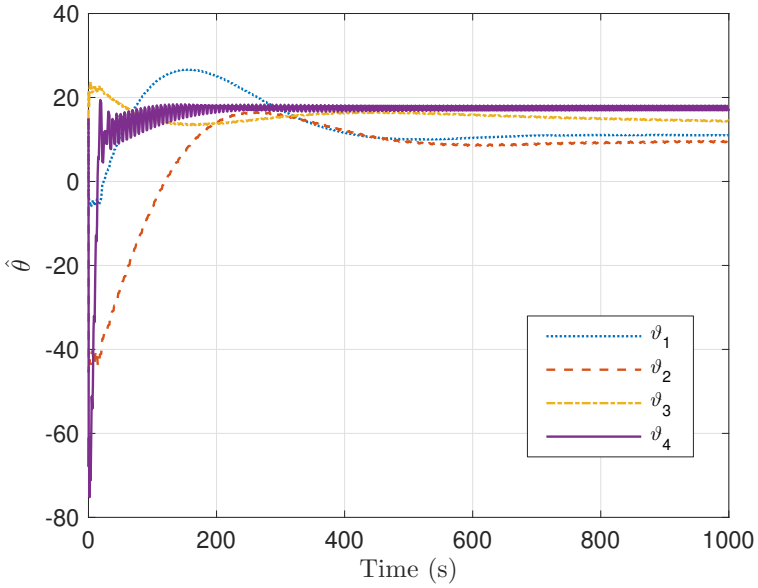

Figure 4.7: Time history of the adaptive gain $\hat{\theta}$

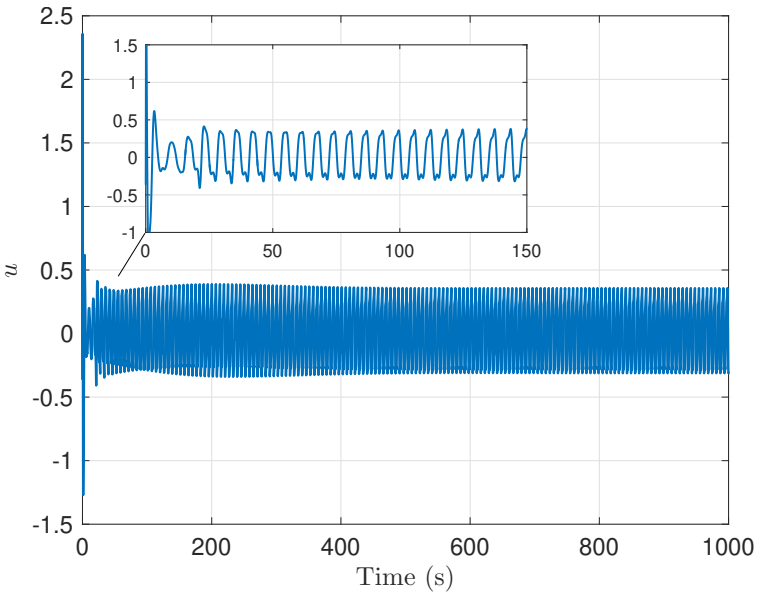

Figure 4.8: Time history of the control input u

control problem for a high-order double integrator system using sliding mode control, and then for a high-order strict feedback system using backstepping control. Numerical simulations are given

to demonstrate the effectiveness of the proposed method with a thorough performance analysis.

5. CONTROL OF A DIRECTIONAL DRILLING SYSTEM USING THE PROPOSED BARRIER AVOIDANCE CONTROL METHOD

5.1 Introduction

Downhole drilling is primarily used to create a well-bore to access natural resources underground. While mostly used in the oil gas industry in the past, the technology starts to be adopted by other important applications such as enhanced geothermal systems (EGS) [90] and robotic drilling in the space exploration [91]. In addition, the development of unconventional oil and gas reservoirs such as shale oil and gas reservoirs also urges technology advancement in down-hole drilling. One of the trends that becomes common is to have drilling be to directional, where the drilling system behaves like a flexible robot traveling through a 3D space with curved trajectory deep underground ten thousand feet away from the surface.

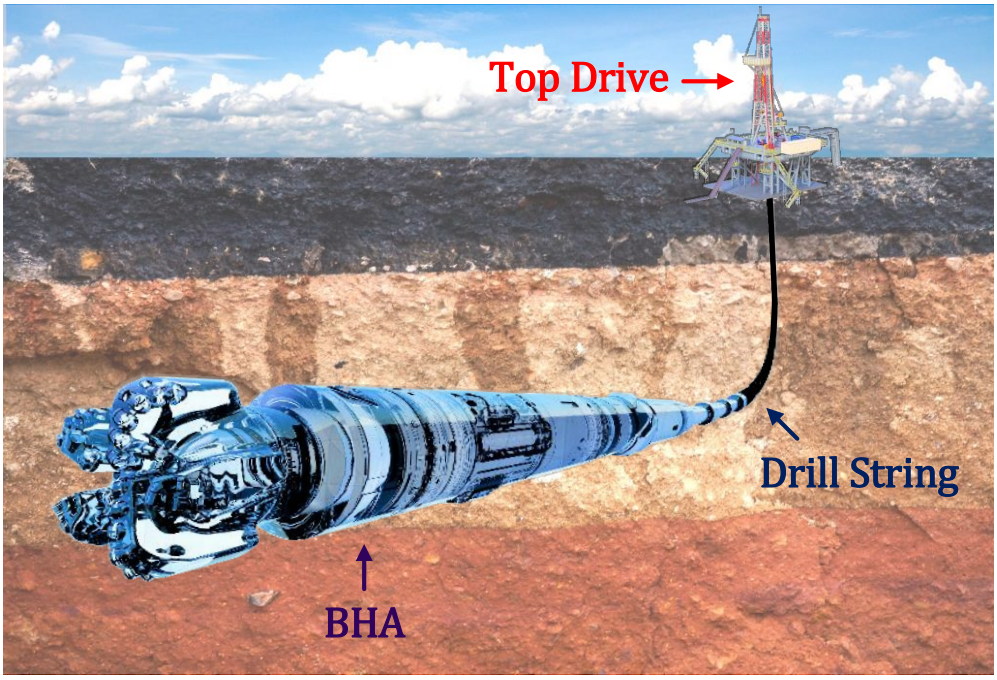

Figure 5.1: Directional drilling system

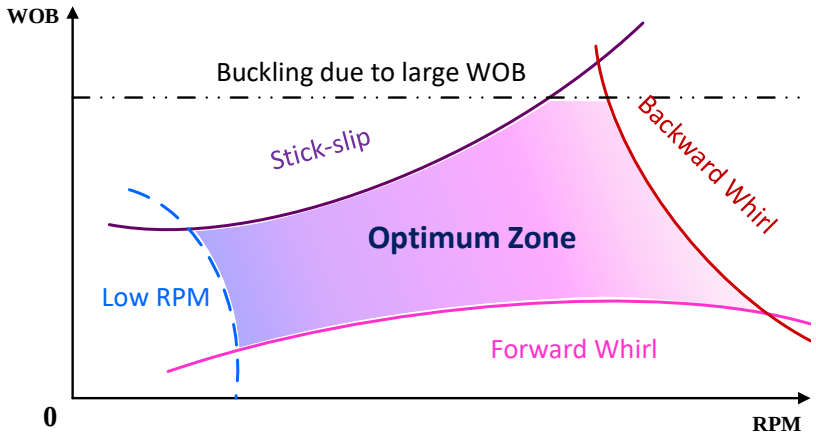

Figure 5.2: Optimum region in drilling process [1]

The majority of existing drilling control research targets vertical drilling, where a straight vertical well is drilled and the drill string is straight from top to bottom. Research in this category mainly focuses on torsional vibration mitigation, a critical vibration mode in vertical drilling [10, 11, 12, 15, 16, 17]. Compared to vertical drilling, directional drilling control is more challenging. The string dynamics modes are coupled due to the curved string geometry and the 3D drilling path. Moreover, interaction between the drilling system and wellbore formation (such as rock) can induce sharp transients in certain operating conditions. The modes coupling together with formation interaction make some regions in the state space, which correspond to particular working conditions, undesirable for operation (Fig. 5.2). For example, if the torsional velocity of the drill bit is too low while the penetration speed is high, the drilling system can be stalled, which will cause twist and vibration damaging the drill string. Thus, drilling operation needs to avoid these undesired state regimes and their barriers (Fig. 5.2), so as not to experience slowed drilling rate, significant vibration, safety problems, and drilling system failure. Avoidance is necessary for steady state, but is also critical during control transients. Some studies [92, 93] related to directional drilling are actually low-bandwidth control of the secondary actuator for local drill bit motion, but not the primary power actuator control for the overall drilling automation. There

are a few preliminary studies on applying PI, adaptive, optimal, and H-infinity control to directional drilling in the overall scale [94, 95]. Most results are based on simple lumped parameter or kinematic models, but none of these ensures barrier avoidance of the undesired state regimes.

To have states avoid the undesired regimes, in one of our previous works, we introduced the idea of using state constrained control for drilling with the integral barrier Lyapunov functionals (iBLF) (Chapter 2). The state constraints are embedded in the barrier terms of the Lyapunov function to ensure the avoidance of the undesired operating points when the control is active. However, this method has several limitations that prevent it from being applied to the directional drilling. First, the iBLF method presented is only suitable for a vertical drilling system modeled by low-order dynamics, but not for the directional drilling system, which typically requires a larger number of finite-element nodes to capture the curved geometry so a higher order dynamics model is inevitable. Second, this method can only be used to avoid barriers with rectangular shape, while the optimum zone of the directional drilling system considered has a more complex shape as shown in Fig. 5.2.

In this study, to address the aforementioned challenges, a novel state-constrained controller for directional drilling is designed using a transformation-based barrier avoidance method we recently developed. The control design is based on a high-order directional drilling model with coupled axial and torsional dynamics. To avoid undesired drilling operating conditions, we formulate those undesired operating regimes into complex state constraints. Note that the reference of complex state constraints is stated relative to straight lines used in most existing state-constrained control studies. The state constraints are then embedded in the system dynamics through a state transformation, and a state-constrained controller is then designed based on the transformed dynamics. In addition, the nonlinear drilling dynamics are represented as a Linear Parameter Varying (LPV) system by treating certain nonlinear terms as varying parameters. This enables a feasible control design for the high order directional drilling system dynamics. The main contribution of this paper is that it is the first study that presents control of a directional drilling system to avoid complex state barriers in the state space, which prevents drilling to operate at undesired and harmful conditions.

The rest of this chapter is organized as follows. In Section 5.2, we present the directional drilling system model as the coupled dynamics of both axial and torsional dimensions, including a FEM model for the curved drill string and a bit-rock interaction model as the boundary condition. Also, the shape of the state constraints is derived from the optimum region of the drilling process. In Section 5.3, we the state barrier avoidance control is formulated and designed, which embeds the state constraints into the nonlinear control synthesis for the downhole drilling system. Finally, a series of simulation tests are exhibited in Section 5.4.

5.2 Model of the Directional Drilling System

Unlike the vertical drilling system with a lumped-parameter drill string model considered in Chapter 2, the dynamic model of a directional drilling system is much more complicated. Oftentimes, the vertical drilling system is defined in a 1-dimensional space. In contrast, due to the directional drilling's geometry nature, its dynamic model is a 3-dimensional space, including axial, torsional and lateral motions. Besides, since the major portion of a vertical drill string can be straight and uniform, a low-order/DOF model is suitable for the dynamic modeling and widely used for control design. However, due to the existence of the curvature part in the directional drilling, a higher-order/DOF model is required to capture the dynamic mode and geometry of this portion. In this work, we adopt the FEM approach as the baseline for the modeling of the curved drill string, since the FEM based drill string models have been well validated with field testing data and is proved to offer high fidelity modeling result [96].

5.2.1 Model of the Drill String

As shown in Fig. 5.3, the curved drill string is discretized into N nodes. All these nodes are in the same global frame $X^gY^gZ^g$, where X^g axis is in the direction of gravity and Y^g axis is in parallel to the ground surface. To use the FEM method, we have every two adjacent nodes share a local coordinate frame $X^lY^lZ^l$. The superscript 'g' and 'l' denote 'global' and 'local', respectively. In this study, we assume that all the nodes are inside the $X^g - Y^g$ plane. In this setting, we have 4 DOF for each node i, i.e., the translational displacements x_i, y_i and the rotational displacements

α_i, β_i. The displacement vector of node i is then defined as

$$U_i = [x_i, y_i, \alpha_i, \beta_i]^T \tag{5.1}$$

In the local coordinates, these elements are denoted as the axial displacement x_i^l, the radial displacement y_i^l, the torsional angle α_i^l, and the bending angle β_i^l. Consider the nodes i and $i+1$ that share the same local frame. The dynamic equation of their local coordinates is provided as

$$M^l \ddot{U}^l_{\{i,i+1\}} + D^l \dot{U}^l_{\{i,i+1\}} + K^l U^l_{\{i,i+1\}} = F^l_{\{i,i+1\}} \tag{5.2}$$

where $U^l_{\{i,i+1\}} = [U_i^{l^T} \; U_{i+1}^{l^T}]^T$ is the local displacement vector of the nodes i and $i+1$, $F^l_{\{i,i+1\}}$ is the external force and torque vector of the nodes i and $i+1$, and M^l, K^l, D^l are the local ineria, stiffness, and damping matrices given as

$$M^l = \frac{\varrho \mathcal{A} l}{420} \begin{bmatrix} 140 & 0 & 0 & 0 & 70 & 0 & 0 & 0 \\ & 156 & 0 & 0 & 0 & 54 & 0 & 0 \\ & & \frac{140 I_x}{\mathcal{A}} & 0 & 0 & 0 & -\frac{70 I_x}{\mathcal{A}} & 0 \\ & & & 4l^2 & 0 & 0 & 0 & -3l^2 \\ & & & & 140 & 0 & 0 & 0 \\ & & & & & 156 & 0 & 0 \\ & \textit{sym.} & & & & & \frac{140 I_x}{\mathcal{A}} & 0 \\ & & & & & & & 4l^2 \end{bmatrix} \tag{5.3}$$

$$K^l = \begin{bmatrix} \frac{\mathcal{E}\mathcal{A}}{l} & 0 & 0 & 0 & -\frac{\mathcal{E}\mathcal{A}}{l} & 0 & 0 & 0 \\ & \frac{12\mathcal{E}I_z}{l^3} & 0 & 0 & 0 & -\frac{12\mathcal{E}I_z}{l^3} & 0 & 0 \\ & & \frac{\mathcal{G}J}{l} & 0 & 0 & 0 & -\frac{\mathcal{G}J}{l} & 0 \\ & & & \frac{4\mathcal{E}I_y}{l} & 0 & 0 & 0 & \frac{2\mathcal{E}I_y}{l} \\ & & & & \frac{\mathcal{E}\mathcal{A}}{l} & 0 & 0 & 0 \\ & & & & & \frac{12\mathcal{E}I_z}{l^3} & 0 & 0 \\ & \textit{sym.} & & & & & \frac{\mathcal{G}J}{l} & 0 \\ & & & & & & & \frac{4\mathcal{E}I_y}{l} \end{bmatrix} \tag{5.4}$$

$$D^l = r_a M^l + r_b K^l \tag{5.5}$$

Here, I_x, I_y and I_z are the second moment of inertia with respect to the local coordinates, ϱ is the density of the drill string, $\mathcal{A}$ is the area of the cross-section, l is the length of the frame element, $\mathcal{E}$ denotes the elastic modulus, $\mathcal{G}$ denotes the shear modules, J is the polar moment of inertia, and r_a, r_b are the Rayleigh damping coefficients.

The coordinate transformation gives the relationship of the local displacement vector and the global displacement vector as

$$U^l_{\{i,i+1\}} = R_i U^g_{\{i,i+1\}} \tag{5.6}$$

where R_i is the rotation matrix of the nodes i and $i+1$. It can be written as

$$R_i = \begin{bmatrix} T_i & 0 & 0 & 0 \\ 0 & T_i & 0 & 0 \\ 0 & 0 & T_i & 0 \\ 0 & 0 & 0 & T_i \end{bmatrix} \tag{5.7}$$

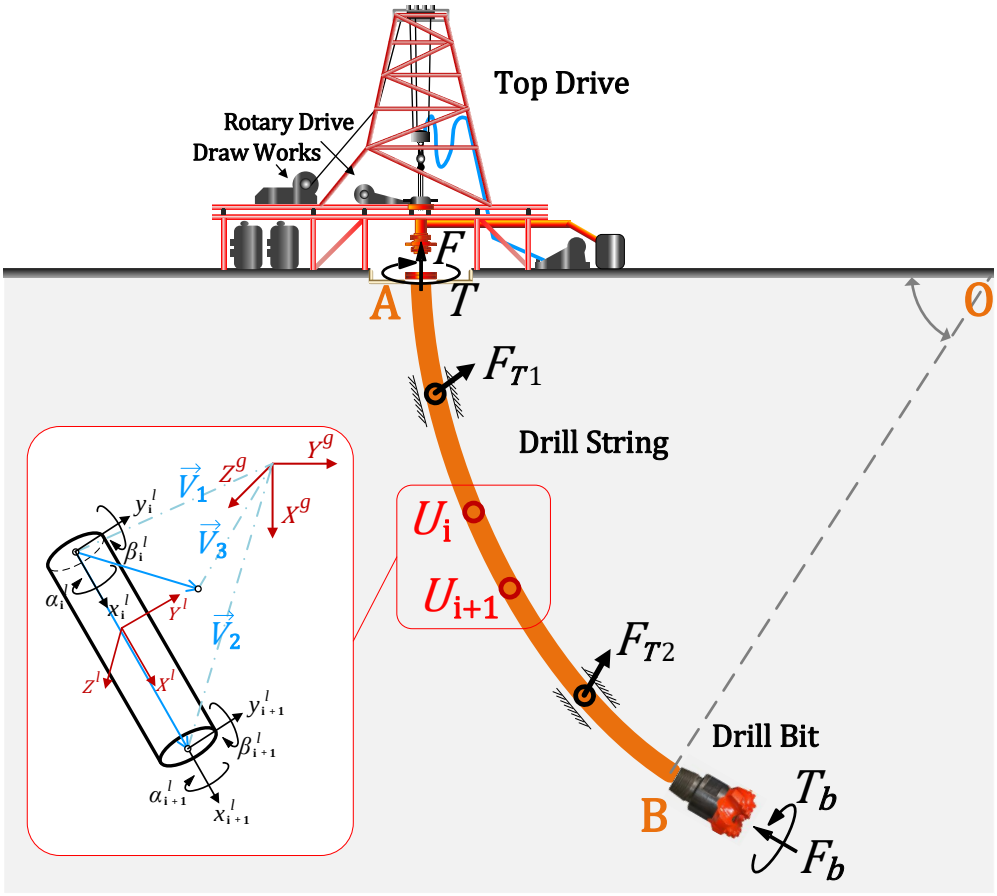

Figure 5.3: Schematic of directional drilling system

$$T_i = \begin{bmatrix} \cos(\vec{\boldsymbol{X}}^l, \vec{\boldsymbol{X}}^g) & \cos(\vec{\boldsymbol{X}}^l, \vec{\boldsymbol{Y}}^g) \\ \cos(\vec{\boldsymbol{Y}}^l, \vec{\boldsymbol{X}}^g) & \cos(\vec{\boldsymbol{Y}}^l, \vec{\boldsymbol{Y}}^g) \end{bmatrix} \tag{5.8}$$

where $\vec{\boldsymbol{X}}^l, \vec{\boldsymbol{Y}}^l, \vec{\boldsymbol{X}}^g, \vec{\boldsymbol{Y}}^g$ are the unit vectors of the axis in the local and global coordinates, respectively. The directional cosine of these vectors can be derived by three non-collinear points. For simplicity, we denote these three points by nodes 1,2 and 3. As shown in Fig. 5.3, the position

vectors $\vec{\boldsymbol{V}}_1$, $\vec{\boldsymbol{V}}_2$ and $\vec{\boldsymbol{V}}_3$ can be expressed as

$$\begin{aligned}
\vec{\boldsymbol{V}}_1 &= X_1\vec{\boldsymbol{X}}^g + Y_1\vec{\boldsymbol{Y}}^g + Z_1\vec{\boldsymbol{Z}}^g \\
\vec{\boldsymbol{V}}_2 &= X_2\vec{\boldsymbol{X}}^g + Y_2\vec{\boldsymbol{Y}}^g + Z_2\vec{\boldsymbol{Z}}^g \\
\vec{\boldsymbol{V}}_3 &= X_3\vec{\boldsymbol{X}}^g + Y_3\vec{\boldsymbol{Y}}^g + Z_3\vec{\boldsymbol{Z}}^g
\end{aligned} \tag{5.9}$$

Vectors $(\vec{\boldsymbol{V}}_2 - \vec{\boldsymbol{V}}_1)$ and $(\vec{\boldsymbol{V}}_3 - \vec{\boldsymbol{V}}_1)$ are defined as

$$\begin{aligned}
\vec{\boldsymbol{V}}_2 - \vec{\boldsymbol{V}}_1 &= X_{21}\vec{\boldsymbol{X}}^g + Y_{21}\vec{\boldsymbol{Y}}^g + Z_{21}\vec{\boldsymbol{Z}}^g \\
\vec{\boldsymbol{V}}_3 - \vec{\boldsymbol{V}}_1 &= X_{31}\vec{\boldsymbol{X}}^g + Y_{31}\vec{\boldsymbol{Y}}^g + Z_{31}\vec{\boldsymbol{Z}}^g
\end{aligned} \tag{5.10}$$

Also, we define

$$l = \sqrt{X_{21}^2 + Y_{21}^2 + Z_{21}^2} \tag{5.11}$$

$$A_{123} = \sqrt{(Y_{21}Z_{31} - Y_{31}Z_{21})^2 + (Z_{21}X_{31} - Z_{31}X_{21})^2 + (X_{21}Y_{31} - X_{31}Y_{21})^2} \tag{5.12}$$

The directional cosine is obtained as

$$\begin{aligned}
\cos(\vec{\boldsymbol{X}}^l, \vec{\boldsymbol{X}}^g) &= \frac{X_{21}}{l}, \qquad \cos(\vec{\boldsymbol{X}}^l, \vec{\boldsymbol{Y}}^g) = \frac{Y_{21}}{l} \\
\cos(\vec{\boldsymbol{Y}}^l, \vec{\boldsymbol{X}}^g) &= \frac{Z_{21}X_{31} - Z_{31}X_{21}}{A_{123}} \cdot \frac{Z_{21}}{l} + \frac{X_{21}Y_{31} - X_{31}Y_{21}}{A_{123}} \cdot \frac{Y_{21}}{l} \\
\cos(\vec{\boldsymbol{Y}}^l, \vec{\boldsymbol{Y}}^g) &= \frac{X_{21}Y_{31} - X_{31}Y_{21}}{A_{123}} \cdot \frac{X_{21}}{l} + \frac{Y_{21}Z_{31} - Y_{31}Z_{21}}{A_{123}} \cdot \frac{Z_{21}}{l}
\end{aligned} \tag{5.13}$$

With the coordinate transformation (5.6), the dynamic motion in (5.2) can be rewritten in the global coordinates as

$$(R_i^T M^l R_i)\ddot{U}^g_{\{i,i+1\}} + (R_i^T D^l R_i)\dot{U}^g_{\{i,i+1\}} + (R_i^T K^l R_i)U^g_{\{i,i+1\}} = R_i^T F^l_{\{i,i+1\}} \tag{5.14}$$

Combining the dynamics of all N nodes along the drill string gives the augmented dynamics in the

global frame as

$$M\ddot{U}^g + D\dot{U}^g + KU^g = F^{ext} \tag{5.15}$$

where $U^g = [U_1^{g^T}, U_2^{g^T}, ..., U_N^{g^T}]^T$ is the overall global state vector, $M, K, D \in \mathbb{R}^{4N\times 4N}$ are the global inertia, stiffness, and damping matrices. The external force vector F^{ext} includes several portions. The input force F and torque are actuated by the draw works and rotary drive at the top drive. The gravitational force and wellbore contact force/torque are distributed along with each element of the drill string. The bit-rock interaction force F_b and torque T_b are exerted at the bottom of the BHA. Note that, the drilling process is typically slow in the axial penetration rate and stops each time when having 10-15 meters drilled [97]. Thus, even though the validity of the system model depends on the length of the drill string, we can still assume the parameters of drilling system dynamics to be constant in certain time duration, due to this slow penetration rate.

5.2.2 Model of the Bit-Rock Interaction

The bit-rock interaction model of a PDC bit is considered in this study. Both force/weight on the bit F_b and torque on the bit T_b consist of friction component and cutting components, which are denoted as

$$F_b = F_b^f + F_b^c, \quad T_b = T_b^f + T_b^c \tag{5.16}$$

Characterized by the depth-of-cut d (i.e., the length of contact between the bit blade and rock surface to be cut), the contact force and torque have different regimes and are piecewise linear with respect to the value of d. It is modeled by a delay differential equation as [14, 13, 15]

$$d(t) = n(x_N^l(t) - x_N^l(t - \tau(t))) \tag{5.17}$$

$$2\pi/n = \alpha_N^l(t) - \alpha_N^l(t - \tau(t)) \tag{5.18}$$

where n is the number of the bit's blades, and τ is a state dependent-delay constrained by the torsional motion of the bit. In this study, to enable a feasible control design, we use an approximation of the depth-of-cut model in the control design [25], given as

$$d(t) = 2\pi \frac{\dot{x}_N^l}{\dot{\alpha}_N^l} \tag{5.19}$$

which is valid when the bit axial velocity $\dot{\alpha}_N^l$ is far beyond zero.

Consider the Phases I and II of the bit-rock interaction as discussed by [28]. In this model, both friction and cutting components increase as d rises up in Phase I, but only the cutting component increases with respect to d in Phase II. We can then list the expressions of F_b and T_b as

$$F_b = \begin{cases} R_b\sigma\kappa d(t) + R_b\zeta\epsilon d(t) & 0 < d(t) \leq d^* \\ R_b\sigma\kappa d^* + R_b\zeta\epsilon d(t) & d(t) > d^* \end{cases} \tag{5.20}$$

$$T_b = \begin{cases} 0.5R_b^2\mu\gamma\sigma\kappa d(t) + 0.5R_b^2\epsilon d(t) & 0 < d(t) \leq d^* \\ 0.5R_b^2\mu\gamma\sigma\kappa d^* + 0.5R_b^2\epsilon d(t) & d(t) > d^* \end{cases} \tag{5.21}$$

where R_b is the radius of drill bit, σ is the maximum normal contact stress, κ is the rate of variance of the contact length, ϵ stands for the intrinsic specific energy required to remove a unit volume of rock, μ is the coefficient of friction at the wear-flat, γ represents the orientation and distribution of the contact forces on the bit, ζ is a characteristic number in $[0.5, 0.8]$, and d^* is the critical depth-of-cut at the transition point of Phases I and II. Note that, when the bit stays stuck in either axial or torsional dimensions ($\dot{x}_N^l = 0$ or $\dot{\alpha}_N^l = 0$), the force F_b and torque T_b on the bit can be determined by the force/torque balance using a static/dynamic Coulomb friction model.

5.2.3 Embedding The Well-bore Geometry To The Drill String Modeling

Since the motion of the drill string is restricted within the created well-bore, this geometric restriction can be incorporated into the drill string dynamics modeling. The dynamics (5.14) can

be written in a state-space form as

$$\dot{X} = AX + H \tag{5.22}$$

where $X = [U^{g^T}\ \dot{U}^{g^T}]^T \in \mathbb{R}^{8N}$ is the state, and the matrices $A \in \mathbb{R}^{8N\times 8N}$ and $H \in \mathbb{R}^{8N\times 4N}$ are given as

$$A = \begin{bmatrix} 0 & I \\ -M^{-1}K & -M^{-1}D \end{bmatrix}, \quad H = \begin{bmatrix} 0 \\ M^{-1}F^{ext} \end{bmatrix} \tag{5.23}$$

The external force vector F^{ext} consists of the control inputs at the top end and the nonlinear bit rock interaction at the bottom end. The rest of the elements in this vector includes the gravity and wellbore contact tension and friction force that are distributed on each node across the whole drill string.

In the directional drilling settings given in Fig. 5.3, the free body diagram of a single node of the drill string is shown in Fig. 5.4. We first consider the translational motion part, whose corresponding external forces include gravity and wellbore contact tension/friction. Since the drill string is constrained in the downhole well-bore, the dynamic motion of each node is latched in the well-bore's axial direction by the contact forces, and the displacements in the global coordinates have the constraint $y_i^g = x_i^g \tan(\theta_i)$. Therefore, the external forces in the radial direction are canceled, and only the components in the axial direction remain, driving the motion of the drill string. For the rotation of the same node, the constraint $\beta_i^g = \alpha_i^g \tan(\theta_i)$ can be found through a similar analysis.

Since the constraints are set for both translational and rotational displacements, we can truncate the state vector using only half of the elements, which is given as

$$X_{tr} = \begin{bmatrix} U_{tr}^g \\ \dot{U}_{tr}^g \end{bmatrix} \tag{5.24}$$

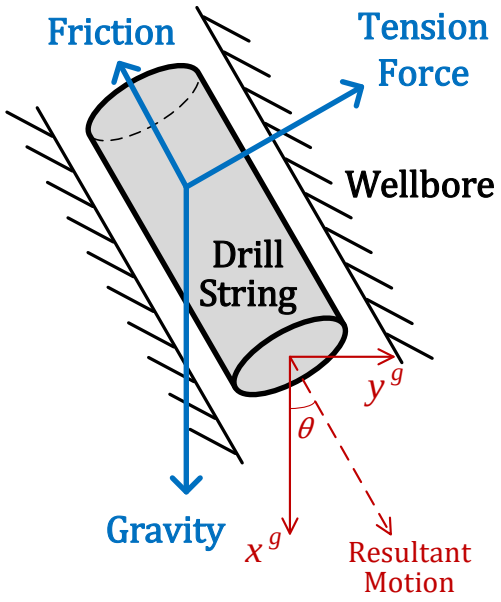

Figure 5.4: Free body diagram of a single node of the drill string

where

$$U_{tr}^g = [x_1^g, \alpha_1^g, x_2^g, \alpha_2^g, ..., x_N^g, \alpha_N^g]^T \tag{5.25}$$

The state-space system equation for this truncated state $X_{tr} \in \mathbb{R}^{4N}$ is derived from the original system equation (5.22) as

$$\dot{X}_{tr} = A_{tr} X_{tr} + H_{tr} \tag{5.26}$$

where $A_{tr} \in \mathbb{R}^{4N \times 4N}$ and $H_{tr} \in \mathbb{R}^{4N \times 1}$ can be obtained through the elementwise matrix operation of A and H. Given the elementwise definition of the matrix $P = (p_{i,j})_{n \times m}$ with $p_{i,j}$ being the element of the ith row and the jth column, we can define the matrix operators $\mathbb{F}(\cdot)$ and $\mathbb{E}(\cdot)$ as follows

$$Q = \mathbb{F}(P, d) \tag{5.27}$$

where $Q \in \mathbb{R}^{n\times m}$, $P \in \mathbb{R}^{n\times 2m}$, $d = [d_1, d_2, ..., d_m]^T$, and their elements satisfy

$$q_{i,j} = p_{i,2j-1} + p_{i,2j} d_j \tag{5.28}$$

Also, we have

$$Q = \mathbb{E}(P) \tag{5.29}$$

where $Q \in \mathbb{R}^{n\times m}$, $P \in \mathbb{R}^{2n\times m}$, and their elements satisfy

$$q_{i,j} = p_{2i-1,j} \tag{5.30}$$

Therefore, we can express A_{tr} and H_{tr} using the matrix operators as

$$\begin{aligned} A_{tr} &= \mathbb{F}(\mathbb{E}(A), d) \\ H_{tr} &= \mathbb{E}(H) \end{aligned} \tag{5.31}$$

where $d = [\tan\theta_1, \tan\theta_1, \tan\theta_2, \tan\theta_2, ..., \tan\theta_N, \tan\theta_N]^T$, and θ_i is the inclined angle of the node i. An intuitive interpretation for the elementwise operation of A is drawn in Fig. 5.5. As each node of the drill string contains 4 elements, we can divide the matrix A into 4-by-4 blocks for each node. Since the truncated state vector (5.24) only includes the elements x_i^g and α_i^g, we can eliminate every second row of the matrix A, corresponding to y_i^g and β_i^g. Moreover, due to the constraints $y_i^g = x_i^g \tan(\theta_i)$ and $\beta_i^g = \alpha_i^g \tan(\theta_i)$, the resultant coefficients of node j in the matrix A_{tr} can be derived by the operation $a_{i,j}^{tr} = a_{i,2j-1} + a_{i,2j}\tan(\theta_j)$. Under these elementwise operation, the matrices A_{tr} and H_{tr} can be denoted as

$$A_{tr} = \begin{bmatrix} 0 & I \\ -A_{km}^{tr} & -A_{dm}^{tr} \end{bmatrix}, \quad H_{tr} = \begin{bmatrix} 0 \\ H_{fm}^{tr} \end{bmatrix} \tag{5.32}$$

where $A_{km}^{tr}, A_{dm}^{tr} \in \mathbb{R}^{2N\times 2N}$ and $H_{fm}^{tr} \in \mathbb{R}^{2N\times 1}$.

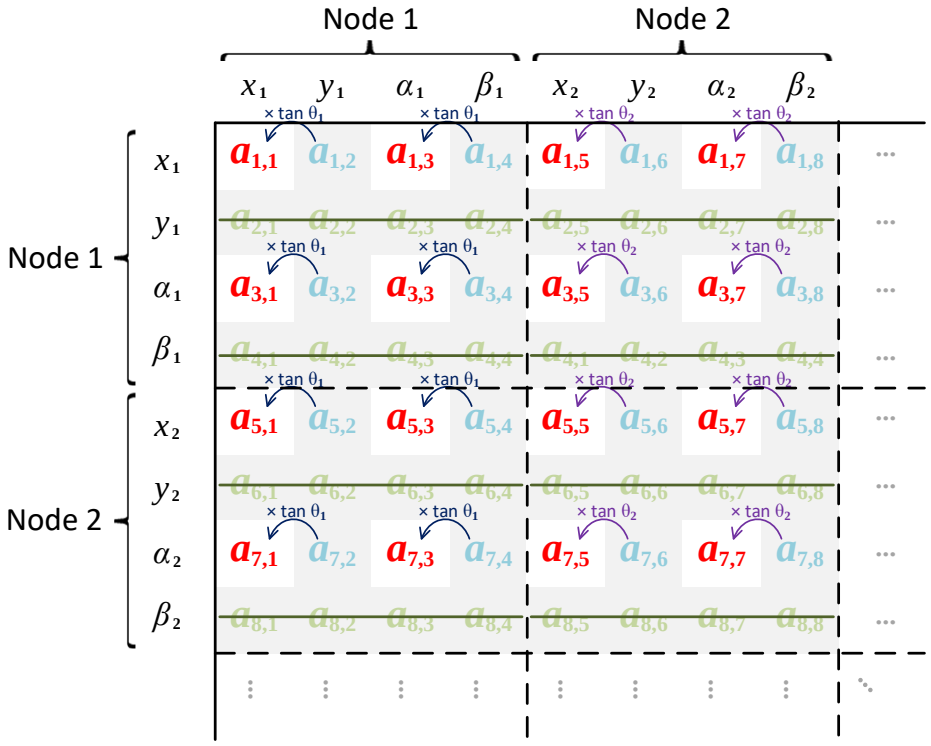

Figure 5.5: Matrix manipulation to incorporate the geometric constraint of the wellbore

With the system equation (5.26) formulated for the truncated system state X_{tr}, the feedback control through the top drive's force and torque can then be determined by the state barrier avoidance control to be shown in the next section.

5.3 Constrained Control Design of the Directional Drilling System with Complex State Constraints

Given the undesired regime of the drilling operation as discussed in Section 5.1, an advanced nonlinear control design coping with state constraints is developed in this section. Having the state constraints depicted in the space of the torsional RPM and the axial ROP, we introduce the barrier avoidance control technique to transform the error dynamics into a new space through a

diffeomorphism. The LPV control is then implemented in the transformed system to achieve the constrained control objective.

5.3.1 Constraints of the Bit-Rock Interaction

The aforementioned bit-rock interaction model (5.20) and (5.21) is only valid when the drilling is in the desired operation mode, where severe vibration modes such as axial/torsional stick-slip, bit bouncing, and lateral whirl motions do not arise. If the operating point falls into the undesired regime as discussed in Section 5.1, these harmful vibrations are likely to occur, and induce highly nonlinear and nonsmooth dynamics at the bottom of the wellbore. Therefore, in this study, we aim to integrate the state constraints into the feedback control of downhole drilling dynamics in order to eliminate these vibration modes and ensure the validity of the bit-rock interaction model.

As shown in Fig. 5.2, an optimum region of the drilling process is depicted in the plane of the axial WOB (or F_b) and the torsional RPM. To enable the formulation of the state constraints, a conversion of this optimum region from WOB-RPM coordinates to ROP-RPM coordinates (i.e., the plane of bit's axial and torsional velocities $\dot{x}_N^l$ and $\dot{\alpha}_N^l$) is needed. In this study, we use parameters of a type of PDC bit in Table 5.1, and also draw the shape of the drilling's optimum region in Fig. 5.6(a). With the expression of bit-rock interaction in (5.20) and the depth-of-cut being $d = 2\pi\dot{x}_N^l/\dot{\alpha}_N^l$, we can map the boundary of the optimum region from Fig. 5.6(a) to Fig. 5.6(b) in the dimensions of bit's velocities. Inside the optimum region, the Phases I and II of the bit-rock interaction regimes are separated by the blue dashed line in Fig. 5.6(b). Without being too conservative, we can choose the state constraints of the bit's velocities to be the region contoured by the red dashed curves in this figure. The objective in this study is to suppress the damaging vibrations in the drilling process using the active control method. Therefore, whenever the system state can stay inside the defined constrained region and avoid entering the undesired operating conditions, these harmful vibration modes will be eliminated.

Table 5.1: Parameters of Bit-Rock Interaction

Symbol	Value [Unit]	Description
ϵ	45×10^6 [Pa]	Instrinsic specific energy
μ	0.3	Friction coefficient at wearflat
γ	1	Geometry parameter of bit
ζ	0.8	Cutter face inclination
n	3	Number of blades
κ	6.06	Variance rate of contact
σ	45×10^6 [Pa]	Contact strength
R_b	0.22 [m]	Radius of drill bit
d^*	5.94×10^{-4} [m]	Critical depth-of-cut

5.3.2 State Barrier Avoidance Based LPV Control Design

Given the directional drilling system model (5.20), (5.21), and (5.26), we will formulate a state-constrained controller to avoid the operating point falling into the undesired regime. To enable the feedback control design for the setpoint tracking objective with the desired local axial and torsional velocities being v_d and w_d (in this study $v_d = 1$ mm/s, $\omega_d = 10$ rad/s), we can define the desired trajectory of the truncated system state X_{tr} as

$$X_d = \begin{bmatrix} V_d t + Y \\ V_d \end{bmatrix} \tag{5.33}$$

where $V_d = [v_d \cos(\theta_1), w_d \cos(\theta_1), v_d \cos(\theta_2), w_d \cos(\theta_2), ..., v_d \cos(\theta_N), w_d \cos(\theta_N)]^T$ is the vector of desired velocities, and Y is the initial displacement vector which will be determined later. Define the error state as

$$E = \begin{bmatrix} E_1 \\ E_2 \end{bmatrix} \tag{5.34}$$

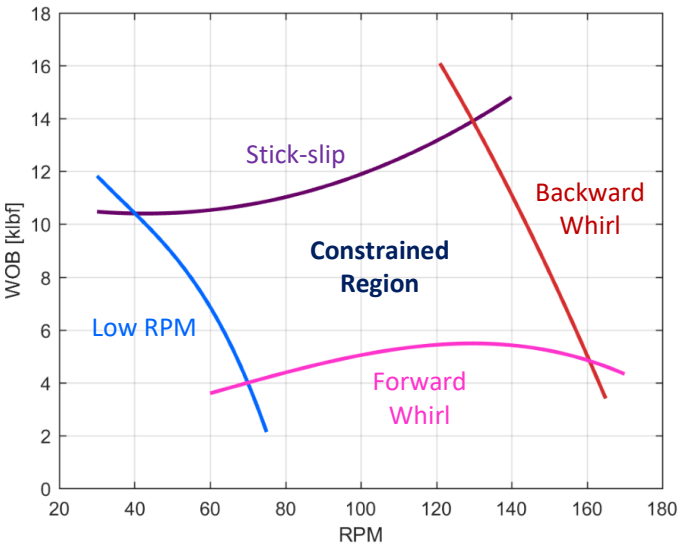

(a)

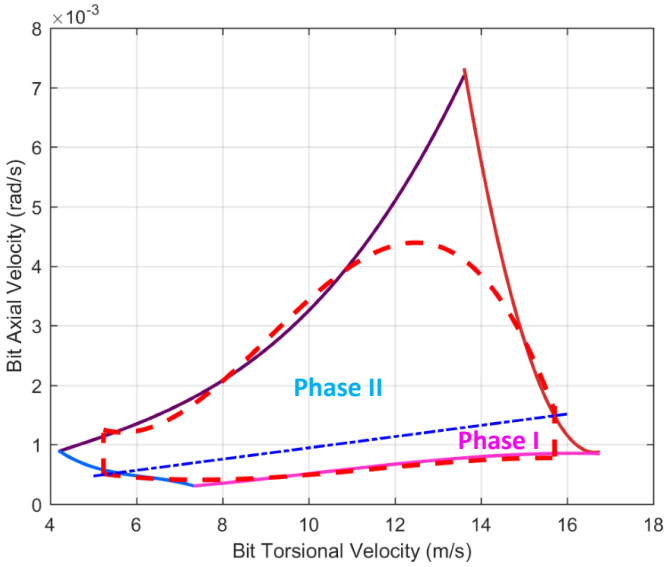

(b)

Figure 5.6: Conversion of the optimum region: a) Optimum region in WOB-RPM plane; b) Optimum region in the plane of bit's axial and torsional velocities (two of the states in drilling dynamics)

where

$$E_1 = U_{tr}^g - (V_d t + Y), \quad E_2 = \dot{U}_{tr}^g - V_d \tag{5.35}$$

Also, we can denote the entries of the error state as $E_1 = [e_1, e_2, ..., e_{2N}]$ and $E_2 = [e_{2N+1}, e_{2N+2}, ..., e_{4N}]$.

From (5.26), we can derive the error dynamics of the setpoint tracking problem as

$$\begin{aligned}
\dot{E}_1 &= E_2 \\
\dot{E}_2 &= -A_{km}^{tr} U_{tr}^g - A_{dm}^{tr} \dot{U}_{tr}^g + H_{fm}^{tr} \\
&= -A_{km}^{tr} E_1 - A_{dm}^{tr} E_2 - A_{km}^{tr}(V_d t + Y) - A_{dm}^{tr} V_d + H_{fm}^{tr} \\
&= -A_{km}^{tr} E_1 - A_{dm}^{tr} E_2 + H_{fm}^{tr} - H_d^{tr}
\end{aligned} \tag{5.36}$$

where $H_d^{tr} = \mathbb{E}(M^{-1} F_d^{ext})$, and F_d^{ext} is the desired external force vector including the desired top drive's actuations F_d and T_d, the desired bit-rock interaction forces/torques F_{bd} and T_{bd}, and an axial resultant forces/torques of the gravity and the wellbore contact. The initial displacement vector is chosen as $Y = A_{km}^{tr^{-1}}(H_d^{tr} - A_{dm}^{tr} V_d)$. Also, it can be verified that $A_{km}^{tr} V_d = 0$. The error dynamics (5.36) is then rewritten in a compact form as

$$\dot{E} = A_{tr} E + H_{tr}^e \tag{5.37}$$

Since the terms $F_b(t) - F_{bd}$ and $T_b(t) - T_{bd}$ appear in the vector $H_{tr}^e = H_{fm}^{tr} - H_d^{tr}$, we convert these two nonlinear terms into a quasi-LPV form to enable the LPV based control design. Addressing this problem in an LPV setting will make the control design for a high order dynamics system more efficient. Without loss of generality, we assume the desired depth-of-cut stays in the Phase II of the bit-rock interaction, i.e., $d_d = 2\pi v_d / \omega_d > d^*$. (If the desired depth-of-cut is located in Phase I, a similar analysis can be proceed as follows.) Using the error states of bit's axial and

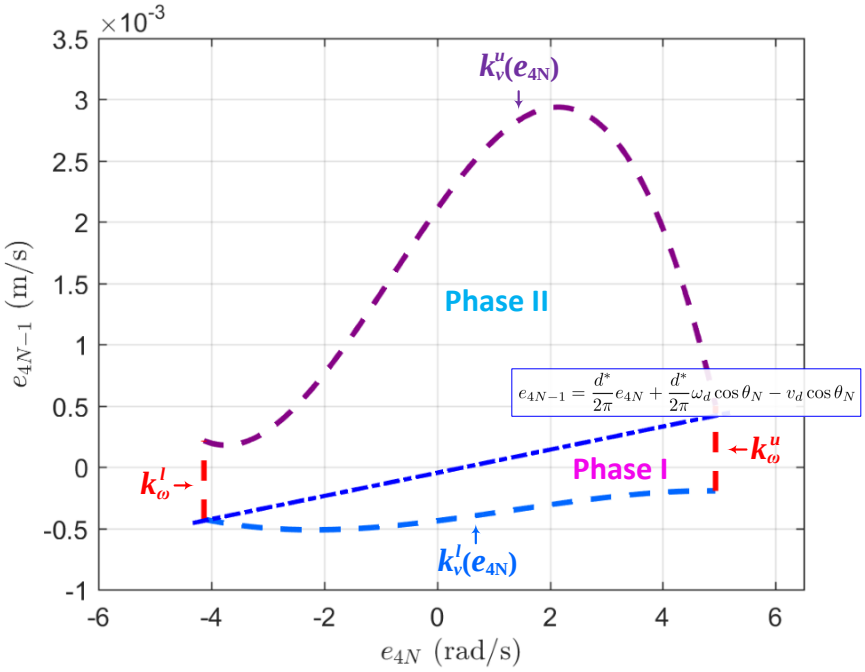

Figure 5.7: State constraints and switching of Phase I and II in $e_{4N-1} - e_{4N}$ coordinates

torsional velocities e_{4N-1} and e_{4N}, the depth-of-cut model is expressed as

$$d = 2\pi \frac{\dot{x}_N^l}{\dot{\alpha}_N^l} = 2\pi \frac{v_d + \frac{e_{4N-1}}{\cos\theta_N}}{\omega_d + \frac{e_{4N}}{\cos\theta_N}} = 2\pi \frac{v_d \cos\theta_N + e_{4N-1}}{\omega_d \cos\theta_N + e_{4N}} \tag{5.38}$$

In the plane of the error states e_{4N-1} and e_{4N} as shown in Fig. 5.7, the regimes of Phase I and II of the bit-rock interaction are divided by a switching condition, which can be found by setting $d = d^*$ in (5.38)

$$\begin{aligned} &\frac{v_d \cos\theta_N + e_{4N-1}}{\omega_d \cos\theta_N + e_{4N}} = \frac{d^*}{2\pi} \\ \Rightarrow\ & e_{4N-1} = \frac{d^*}{2\pi} e_{4N} + \frac{d^*}{2\pi} \omega_d \cos\theta_N - v_d \cos\theta_N \end{aligned} \tag{5.39}$$

For simplicity, in the bit-rock interaction model (5.20) and (5.21), we denote the coefficients as $p_1 = R_b\zeta\epsilon$, $p_2 = R_b\sigma\kappa$, $p_3 = 0.5R_b^2\epsilon$, and $p_4 = 0.5R_b^2\mu\gamma\sigma\kappa$. In Phase II, the entry $F_b(t) - F_{bd}$

can be re-organized as

$$\begin{aligned}
&\left(p_1 2\pi \frac{v_d \cos\theta_N + e_{4N-1}}{\omega_d \cos\theta_N + e_{4N}} + p_2 d^*\right) - \left(p_1 2\pi \frac{v_d}{\omega_d} + p_2 d^*\right) \\
=&p_1 2\pi \frac{\omega_d e_{4N-1} - v_d e_{4N}}{(\omega_d \cos\theta_N + e_{4N})\omega_d} \\
=&\frac{p_1 2\pi}{\omega_d \cos\theta_N + e_{4N}} e_{4N-1} + \frac{p_1 2\pi v_d}{(\omega_d \cos\theta_N + e_{4N})\omega_d} e_{4N} \\
=&\kappa_{11}(e) e_{4N-1} + \kappa_{12}(e) e_{4N} \qquad \text{(Phase II)}
\end{aligned} \tag{5.40}$$

In Phase I, the entry $F_b(t) - F_{bd}$ can be expressed as

$$\begin{aligned}
&(p_1 + p_2)\, 2\pi \frac{v_d \cos\theta_N + e_{4N-1}}{\omega_d \cos\theta_N + e_{4N}} - \left(p_1 2\pi \frac{v_d}{\omega_d} + p_2 d^*\right) \\
=&p_1 2\pi \frac{\omega_d e_{4N-1} - v_d e_{4N}}{(\omega_d \cos\theta_N + e_{4N})\omega_d} + p_2 \frac{2\pi \frac{v_d \cos\theta_N + e_{4N-1}}{\omega_d \cos\theta_N + e_{4N}} - d^*}{e_{4N-1} - \frac{d^*}{2\pi} e_{4N}} \left(e_{4N-1} - \frac{d^*}{2\pi} e_{4N}\right) \\
=&\left(\frac{p_1 2\pi}{\omega_d \cos\theta_N + e_{4N}} + p_2 \frac{2\pi \frac{v_d \cos\theta_N + e_{4N-1}}{\omega_d \cos\theta_N + e_{4N}} - d^*}{e_{4N-1} - \frac{d^*}{2\pi} e_{4N}}\right) e_{4N-1} \\
&+ \left(\frac{p_1 2\pi v_d}{(\omega_d \cos\theta_N + e_{4N})\omega_d} - p_2 \frac{2\pi \frac{v_d \cos\theta_N + e_{4N-1}}{\omega_d \cos\theta_N + e_{4N}} - d^*}{e_{4N-1} - \frac{d^*}{2\pi} e_{4N}} \frac{d^*}{2\pi}\right) e_{4N} \\
=&\kappa_{21}(e) e_{4N-1} + \kappa_{22}(e) e_{4N} \qquad \text{(Phase I)}
\end{aligned} \tag{5.41}$$

The terms κ_{21} and κ_{22} are non-singular, since their denominators satisfy the condition $e_{4N-1} - \frac{d^*}{2\pi} e_{4N} < \frac{d^*}{2\pi}\omega_d - v_d < 0$ in Phase I. Then under the same derivation, the entry $T_b(t) - T_{bd}$ can be written as

$$\begin{aligned}
&\kappa_{31}(e) e_{4N-1} + \kappa_{32}(e) e_{4N}, \quad \text{(Phase II)} \\
&\kappa_{41}(e) e_{4N-1} + \kappa_{42}(e) e_{4N}, \quad \text{(Phase I)}
\end{aligned} \tag{5.42}$$

Inserting the nonlinear terms to the A_{tr} matrix using the expressions (5.40), (5.41), and (5.42), we

can rewrite the error dynamics (5.37) into a quasi-LPV form as

$$\dot{E} = \tilde{A}_{tr}(E)E + B_{tr}u \tag{5.43}$$

where $\tilde{A}_{tr}(E)$ contains the error state E in its elements, B_{tr} is a scalar matrix, and the control input $u = [F - F_d, T - T_d]^T$.

Since the numerical value of the axial and torsional dimensions are typically $y \sim 0.001$ m and $\phi \sim 1$ rad, a scaling factor $\nu \sim 1000$ is introduced to the axial's error dynamics. Applying this scaling factor, we choose the scaled state vector as $\bar{E} = [\nu e_1, e_2, \nu e_3, e_4, ..., \nu e_{4N-1}, e_{4N}]^T$. The error dynamics in the quasi-LPV form (5.43) can be revised accordingly as

$$\dot{\bar{E}} = \bar{A}_{tr}(\bar{E})\bar{E} + \bar{B}_{tr}u \tag{5.44}$$

Next, we will adopt the transformation based barrier avoidance control method as proposed in Chapter 3 to the directional drilling application. As shown in Fig. 3.1, the key idea of the method is to transform the original state space (left) to a new space (right). The barrier will be mapped to infinity or a region far from the origin of the new space. In the new space, as long as we can design a controller ensuring stability in the radially bounded region, the control will ensure avoidance of the barrier in the new space and therefore the same can be achieved in the original space. In other words, the barrier avoidance control is translated into a regular asymptotic stabilizer design in the new space.

The main theorem of the barrier avoidance control is provided as follows.

Theorem 9. *Consider the closed-loop system $\Sigma : \dot{x} = h(x)$ and a given open set $\mathcal{D}$. The boundary of $\mathcal{D}$ is noted as $\partial\mathcal{D}$ is the barrier to avoid. If a diffeomorphism $x^* = \Phi(x)$ transforms the system Σ into $\Sigma^* : \dot{x}^* = h^*(x^*)$ and satisfies:*

1) The diffeomorphism $x^* = \Phi(x)$ maps $\mathcal{D}$ into $\mathbb{R}^n$. The boundary $\partial\mathcal{D}$ is mapped to the points at infinity, and the origin $x = 0$ is mapped to the origin $x^* = 0$.

2) The system Σ^* is globally stable (globally asymptotically/exponentially stable) at $x^* = 0$.

The following statements hold:

a) The set $\mathcal{D}$ is forward invariant for the system Σ.

b) The system Σ is stable (asymptotically/exponentially stable with the attractive region identical to $\mathcal{D}$) at $x = 0$.

Specially, when the condition 2) is modified as

2) The system Σ^* is locally stable (locally asymptotically/exponentially stable) at $x^* = 0$.

Then the following statements hold:

a) The state $x(t)$ stay in $\mathcal{D}$ for all $t \in [0, \infty)$.

b) The system Σ is locally stable (locally asymptotically/exponentially stable) at $x = 0$.

Proof: The scheme of the proof follows Theorem 2 in Chapter 3. Here, the local stability and global stability cases are both considered. ■

The diffeomorphism defined in Theorem 9 will map the constrained region $\mathcal{D}$ into the whole real plane $\mathbb{R}^n$, and convert a state constrained control problem into an unconstrained one, which can enable more flexibility in the options of nonlinear control design tools. In our design, by choosing $\mathcal{D}$ as the optimum region in the Fig. 5.6(b) and obtaining the diffeomorphism to transform the scaled error dynamics (5.44) into a new system equation, we can then implement the LPV control to achieve the constrained control objective.

To apply this method, a diffeomorphism needs to be found for the directional drilling system as required in Theorem 9. In Fig. 5.7, the constrained region is contoured by the dashed curves in the $e_{4N-1} - e_{4N}$ coordinates to prevent the state from falling into the undesired operating conditions. This region can be expressed as

$$\mathcal{D} = \left\{ E \in \mathbb{R}^{4N} \,\middle|\, k_\omega^l < e_{4N} < k_\omega^u,\, k_v^l(e_{4N}) < e_{4N-1} < k_v^u(e_{4N}) \right\} \tag{5.45}$$

where the upper and lower bounds in the e_{4N-1} and e_{4N} dimensions are chosen as

$$\begin{aligned} k_\omega^l &= -4.13094, \qquad k_\omega^u = 4.91902 \\ k_v^l(e_{4N}) &= -1.84101 \times 10^{-6} e_{4N}^3 + 7.29018 \times 10^{-6} e_{4N}^2 + 5.84175 \times 10^{-5} e_{4N} - 4.38985 \times 10^{-4} \\ k_v^u(e_{4N}) &= -2.69561 \times 10^{-5} e_{4N}^3 - 6.44755 \times 10^{-5} e_{4N}^2 + 6.50835 \times 10^{-4} e_{4N} + 2.10445 \times 10^{-3} \end{aligned} \tag{5.46}$$

The diffeomorphism satisfying the condition of Theorem 9 is provided as

$$\begin{aligned} e_{4N}^* &= \frac{e_{4N}}{(k_\omega^u - e_{4N})^{\frac{1}{2}}(e_{4N} - k_\omega^l)^{\frac{1}{2}}} \\ e_{4N-1}^* &= \frac{e_{4N-1}}{(k_v^u - e_{4N-1})^{\frac{1}{2}}(e_{4N-1} - k_v^l)^{\frac{1}{2}}} \end{aligned} \tag{5.47}$$

If $k_\omega^l < 0 < k_\omega^u$ and $k_\omega^l < 0 < k_\omega^u$ hold, it can be verified that $e_{4N} \to k_\omega^l \Rightarrow e_{4N}^* \to -\infty$, $e_{4N} \to k_\omega^u \Rightarrow e_{4N}^* \to \infty$, $e_{4N-1} \to k_v^l \Rightarrow e_{4N-1}^* \to -\infty$, and $e_{4N-1} \to k_v^u \Rightarrow e_{4N-1}^* \to \infty$. Thus, the diffeomorphism (5.47) maps $\mathcal{D}$ into $\mathbb{R}^{4N}$.

Defining the state vector in the new space as $E^* = [\nu e_1, e_2, \nu e_3, e_4, ..., \nu e_{4N-3}, e_{4N-2}, e_{4N-1}^*, e_{4N}^*]^T$, we can obtain the system equation in the E^*-coordinates as

$$\dot{E}^* = A^*(E)E^* + B^*(E)u \tag{5.48}$$

where

$$A^*(E) = \begin{bmatrix} 1 & 0 & \cdots & 0 & 0 \\ 0 & 1 & \cdots & 0 & 0 \\ \vdots & \vdots & \ddots & \vdots & \vdots \\ 0 & 0 & \cdots & \frac{k_v^u(e_{4N-1}-k_v^l)-k_v^l(k_v^u-e_{4N-1})}{2(k_v^u-e_{4N-1})^{\frac{3}{2}}(e_{4N-1}-k_v^l)^{\frac{3}{2}}} & -\frac{e_{4N-1}\left(\frac{\partial k_v^u}{\partial e_{4N}}(e_{4N-1}-k_v^l)-\frac{\partial k_v^l}{\partial e_{4N}}(k_v^u-e_{4N-1})\right)}{2(k_v^u-e_{4N-1})^{\frac{3}{2}}(e_{4N-1}-k_v^l)^{\frac{3}{2}}} \\ 0 & 0 & \cdots & 0 & \frac{k_\omega^u(e_{4N}-k_\omega^l)-k_\omega^l(k_\omega^u-e_{4N})}{2(k_\omega^u-e_{4N})^{\frac{3}{2}}(e_{4N}-k_\omega^l)^{\frac{3}{2}}} \end{bmatrix} A_{tr}(E) \tag{5.49}$$

$$\times \begin{bmatrix} 1 & 0 & \cdots & 0 & 0 \\ 0 & 1 & \cdots & 0 & 0 \\ \vdots & \vdots & \ddots & \vdots & \vdots \\ 0 & 0 & \cdots & (k_v^u - e_{4N-1})^{\frac{1}{2}}(e_{4N-1} - k_v^l)^{\frac{1}{2}} & 0 \\ 0 & 0 & \cdots & 0 & (k_\omega^u - e_{4N})^{\frac{1}{2}}(e_{4N} - k_\omega^l)^{\frac{1}{2}} \end{bmatrix}$$

$$B^*(E) = \begin{bmatrix} 1 & 0 & \cdots & 0 & 0 \\ 0 & 1 & \cdots & 0 & 0 \\ \vdots & \vdots & \ddots & \vdots & \vdots \\ 0 & 0 & \cdots & \frac{k_v^u(e_{4N-1}-k_v^l)-k_v^l(k_v^u-e_{4N-1})}{2(k_v^u-e_{4N-1})^{\frac{3}{2}}(e_{4N-1}-k_v^l)^{\frac{3}{2}}} & -\frac{e_{4N-1}\left(\frac{\partial k_v^u}{\partial e_{4N}}(e_{4N-1}-k_v^l)-\frac{\partial k_v^l}{\partial e_{4N}}(k_v^u-e_{4N-1})\right)}{2(k_v^u-e_{4N-1})^{\frac{3}{2}}(e_{4N-1}-k_v^l)^{\frac{3}{2}}} \\ 0 & 0 & \cdots & 0 & \frac{k_\omega^u(e_{4N}-k_\omega^l)-k_\omega^l(k_\omega^u-e_{4N})}{2(k_\omega^u-e_{4N})^{\frac{3}{2}}(e_{4N}-k_\omega^l)^{\frac{3}{2}}} \end{bmatrix} B_{tr}^*(E) \tag{5.50}$$

System (5.48) is in a quasi-LPV form, and enables using a standard LPV design framework. According to Theorem 9, if the closed-loop system of (5.48) is exponentially stabilized by the LPV controller, then applying the same amount of control back to the original error dynamic equation (5.37) ensures the exponential stability of the tracking error E and the avoidance of the state constraints.

Next, we will briefly introduce the sketch of a standard LPV control method [85]. In the matrices $A^*(E)$ and $B^*(E)$ of (5.48), we treat E as a time-varying variable and denote it as ρ for clarity in the following control synthesis. The system equation (5.48) can be rewritten as

$$\dot{E}^* = A^*(\rho)E^* + B^*(\rho)u \tag{5.51}$$

Also, we assume $|\rho_i| < k_{\rho_i}$ and $|\dot{\rho}_i| < k_{\dot{\rho}_i}$ hold. The feedback control law is chosen as $u = K(\rho)E^*$. Consider the Lyapunov candidate $V = E^{*T}P(\rho)E^*$, where $P^T(\rho) = P(\rho)$. The closed-

loop system is exponentially stable if

$$P(\rho)\left(A^*(\rho)+B^*(\rho)K(\rho)\right)+\left(A^*(\rho)+B^*(\rho)K(\rho)\right)^T P(\rho)+\dot{\rho}\frac{\partial P(\rho)}{\partial \rho}<0 \tag{5.52}$$

for all $|\rho_i|<k_{\rho_i}$ and $|\dot{\rho}_i|<k_{\dot{\rho}_i}$. Then (5.52) can be transformed into a computationally efficient form as

$$\left(A^*(\rho)+B^*(\rho)K(\rho)\right)P^{-1}(\rho)+P^{-1}(\rho)\left(A^*(\rho)+B^*(\rho)K(\rho)\right)^T-\dot{\rho}\frac{\partial P^{-1}(\rho)}{\partial \rho}<0 \tag{5.53}$$

Setting $Q(\rho)=P^{-1}(\rho)$ and $\tilde{K}(\rho)=K(\rho)P^{-1}(\rho)$, we have

$$A^*(\rho)Q(\rho)+B^*(\rho)\tilde{K}(\rho)+Q(\rho)A^*(\rho)+\tilde{K}^T(\rho)B^{*T}(\rho)-\dot{\rho}\frac{\partial K(\rho)}{\partial \rho}<0 \tag{5.54}$$

Here, the set of $Q(\rho)$ and $\tilde{K}(\rho)$ satisfying (5.54) is convex, and thus (5.54) is an LMI. However, because of the dependence of ρ^*, the condition (5.54) contains infinitely many sets of LMIs. A remedy to this issue is to discretize the dependence parameter ρ^*, and to solve an finite number of LMIs.

In the quasi-LPV system (5.51), having two time-varying parameters denoted as $\rho_1=e_{4N-1}$ and $\rho_2=e_{4N}$, we can divide the interval $[-k_{\rho_i},k_{\rho_i}]$ into N_i segments with width h_i for $i=1,2$. Then (5.54) becomes a finite collection of LMIs, indexed with $n_i=1,2,...,N_i$ as

$$\begin{aligned}&A^*_{(n_1,n_2)}Y_{(n_1,n_2)}+B^*_{(n_1,n_2)}\tilde{K}_{(n_1,n_2)}+Q_{(n_1,n_2)}A^*_{(n_1,n_2)}+\tilde{K}^T_{(n_1,n_2)}B^{*T}_{(n_1,n_2)}\\&\pm k_{\dot{\rho}_1}\frac{Q_{(n_1,n_2)}-Q_{(n_1-1,n_2)}}{h_1}\pm k_{\dot{\rho}_2}\frac{Q_{(n_1,n_2)}-Q_{(n_1,n_2-1)}}{h_2}<0\end{aligned} \tag{5.55}$$

where $A^*_{(n_1,n_2)}=A^*([n_1h_1-k_{\rho_1},n_2h_2-k_{\rho_2}]^T)$ and the subscipts (n_1,n_2) have the same meaning for other matrices. It is worth noting that the rate of variation $\dot{\rho}_i$ enters linearly into (5.54), so it is sufficient to only check the LMIs of the vertex points instead of all points of $\dot{\rho}_i$ in the region $[-k_{\dot{\rho}_1},k_{\dot{\rho}_1}]\times[-k_{\dot{\rho}_2},k_{\dot{\rho}_2}]$.

To implement the designed LPV controller on the error dynamics (5.48), we create a 2-dimensional mesh grid in the $e^*_{4N-1} - e^*_{4N}$ coordinates and numerically solve the solution of the LMI at each grid point. Note that, since the switching condition of Phase I and II of the bit-rock interaction only occurs in the $e^*_{4N-1} - e^*_{4N-1}$ plane and is formulated inside the matrix A^*, it can be integrated into this discretization based quasi-LPV approach, by solving the LMI at each grid point with the corresponding A^* and B^* matrices.

5.4 Simulation Results

To validate the effectiveness of the novel state barrier avoidance based LPV approach, we perform a series of simulations in this section. Firstly, the open-loop responses are provided by applying constant actuation on the top drive, under both full-order model and reduced-order model settings. Closed-loop results are then examed with different initial conditions using the proposed method given in Section 5.3.2. Finally, we conduct a comparison of the standard LPV and the barrier avoidance based LPV approaches, and also check the robustness of the proposed controller under parameter perturbation.

Throughout the simulations in this section, the geometry setting of the directional drilling system is displayed in Fig. 5.3. We set the curved drill string $\widehat{AB}$ as an arc with the center O, and its central angle is 30 degrees. The drill string is evenly discretized in the FEM model. The parameter of the drill string's model is listed in Table 5.2. Besides, the parameter of the bit-rock interaction model is provided in Table 5.1.

5.4.1 Stick-slip and Bit-bouncing Behavior in the Open-loop Control

For the first simulation, we set the initial values of each node of the directional drill string to be the desired axial and torsional velocities $v_d = 1$ mm/s and $\omega_d = 10$ rad/s, and feed the constant input force and torque into top drive's motors, which can be calculated using the force/torque balance of the system. This way the velocities of each node will follow the desired value due to the top drive's actuation. The time history of the bit's velocities under this open-loop control is displayed in Fig. 5.8, under both 20-node (40-DOF) FEM model and 5-node (10-DOF) FEM model

Table 5.2: Parameters of Drill String FEM Model

Symbol	Value [Unit]	Description
D_o	0.12 [m]	Drill string outer diameter
D_i	0.06 [m]	Drill string inner diameter
ϱ	7850 [kg/m^3]	Drill string density
$\mathcal{A}$	0.0085 [m^2]	Cross-section area
L	1047.2 [m]	Length of arc AB
N	5	Number of nodes
$\mathcal{E}$	2.1×10^{11} [Pa]	Young's modulus
$\mathcal{G}$	8.08×10^{10} [Pa]	Shear modulus
J	1.72×10^{-5} [Pa]	Polar moment of inertia
r_a	0.005 [m]	Rayleigh damping coefficient
r_b	0.001 [m]	Rayleigh damping coefficient
θ	30 [°]	Central angle of arc AB

settings. The axial bit-bouncing and the torsional stick-slip can be observed in each dimension. As depicted in the figure, the velocities drop down to zero and the bit gets stuck while the energy is accumulating. The release of the energy can force the bit to a high speed, and the peak values of the velocities in this simulation are four times of its desired value in the torsional dimension, and over ten times in the axial one. Since the system has no feedback control using the downhole measurement, the energy will dissipate and cause the bit to stick again. Such vibration modes stimulate periodic responses in both axial and torsional motions, namely bit-bouncing and stick-slip behaviors. Also, from Fig. 5.8 we notice that the response of the 5-node model can line up well with the 20-node model with minor discrepancies. The matching result demonstrates that the bandwidth of the reduced-order model is suitable for capturing complex nonlinearities such as bit-bouncing and stick-slip. Thus, in the rest of simulation results, we will use a 5-node model for the controller design, while setting the 20-node model as the drilling system's physical plant.

5.4.2 Closed-loop Control Using Barrier Avoidance Based LPV method

To address the harmful vibrations arising in the responses of the open-loop control, we integrate the state constraints into the closed-loop control using the barrier avoidance based LPV method as discussed in Section 5.3.2. Considering the target axial and torsional velocities $v_d = 1$ mm/s and

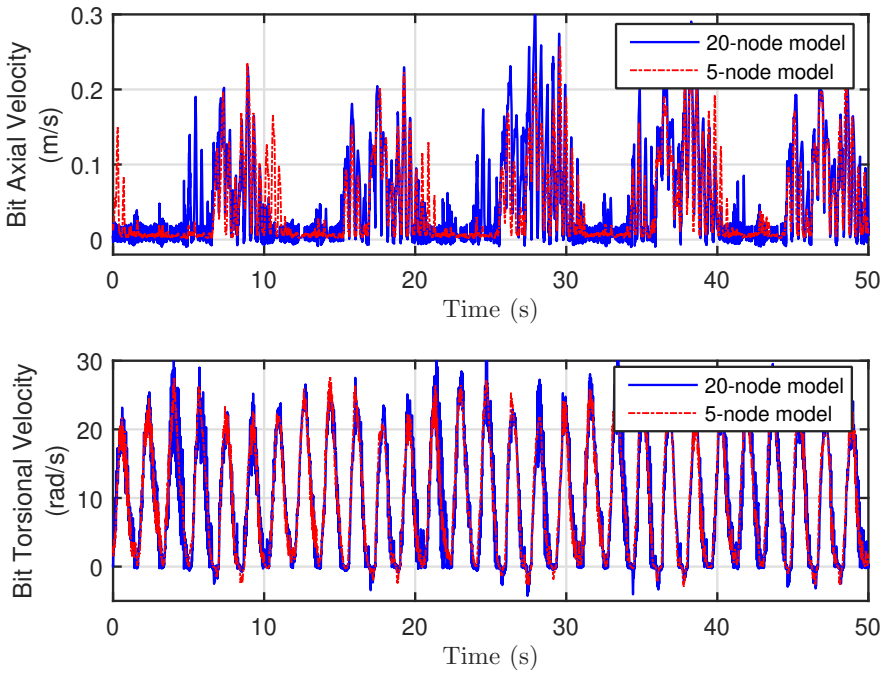

Figure 5.8: Stick-slip and bit-bouncing behavior of the bit under constant top drive's control inputs

$\omega_d = 10$ rad/s, we choose the shape of the constraints as shown in Fig. 5.7 in the space of bit's axial and torsional velocities to avoid the undesired operating regimes. The numerical expression of the state barrier is given in (5.46), which enables the diffeomorphic transformation to convert the system dynamics into the new coordinates. In the $e_{4N-1} - e_{4N}$ plane, we choose a 2-dimension mesh grid with evenly distributed 40×40 grid points inside the intervals $[-10, 10] \times [-10, 10]$. In the simulation, we choose a number of initial conditions inside this state barrier region, and the phase portraits of 4 different cases are drawn in Fig. 5.9. The responses of the bit's velocities converge to the desired values without any violation of the state barriers during the transient, even starting from an initial state close to the boundary. By constraining the state in the desired operating regime, the oscillation modes such as bit-bouncing and stick-slip are indeed eliminated in the simulation. Also, the time history of the input force F and torque T is plotted in Fig. 5.10, which can prove the feasibility of the proposed control.

To verify the barrier avoidance base method can outperform other unconstrained control strate-

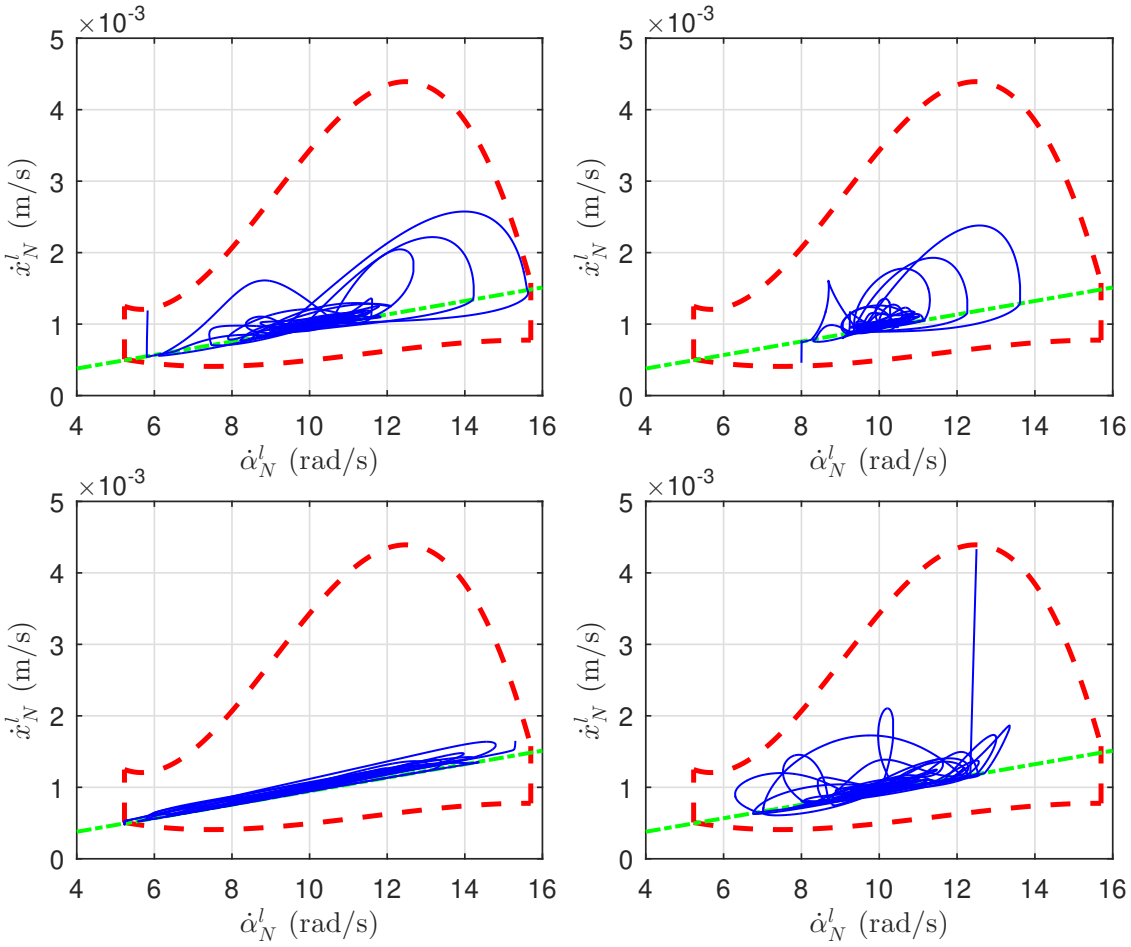

Figure 5.9: Phase portraits of the bit's torsional velocity $\dot{\alpha}_N^l$ and axial velocity $\dot{x}_N^l$ with 4 different initial conditions under barrier avoidance control

gies, we compare our approach with a standard LPV method (without the barrier avoidance). Under the same initial conditon, the time history of the bit's velocities is tested with both barrier avoidance LPV and standard LPV approaches. The phase portraits is plot in Fig. 5.11, in which major oscillations and barrier violation will occur. As shown in Fig. 5.12, severe vibrations still arise in both axial and torsional dimensions using a standard LPV controller, while the proposed controller can significantly shrink the magnitude of the velocities and eliminate the oscillations.

Next, we will exam the robustness of this control strategy under parameter perturbation. A significant uncertainty can arise in the system modeling due to the complex downhole environment. One major factor causing the uncertainty is the variation of the rock formation, which affects the

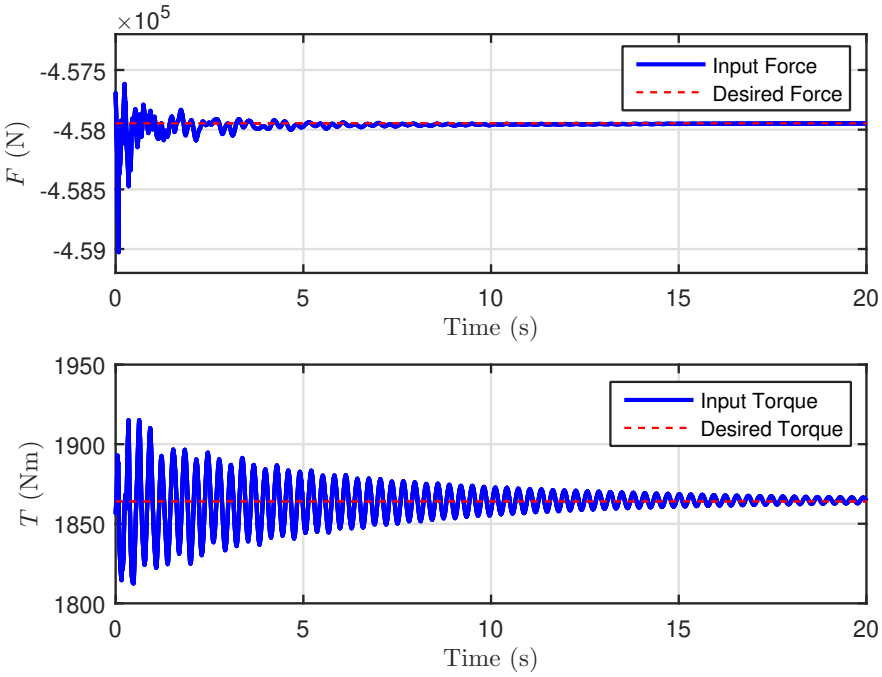

Figure 5.10: Time history of top drive's force F and torque T

intrinsic specific energy parameter ϵ in the bit-rock interaction. In this simulation, we will check the control performance under a perturbation of the parameter ϵ. In Fig. 5.13(a) and Fig. 5.13(b), the bit's velocities are depicted in the range 70% to 150% of the nominal value 45 MPa, where the state constraints are not violated under the variance of the perturbed parameter ϵ.

To conclude, the closed-loop control using the barrier avoidance based LPV control not only stabilize the drilling process for the setpoint tracking problem, but also integrates the complex state constraints into the state-space to prevent the undesired operating regimes. As highlighted by the responses of the numerical simulations, the severe vibrations are indeed suppressed, and the control performance and robustness are validated.

5.5 Conclusion

In this work, the state constrained control technique is applied to the directional drilling system. To capture the curved drill string's dynamic modes, we apply the FEM method to the system modeling. Having the empirical optimal region of the drilling operation depicted, we formulate the

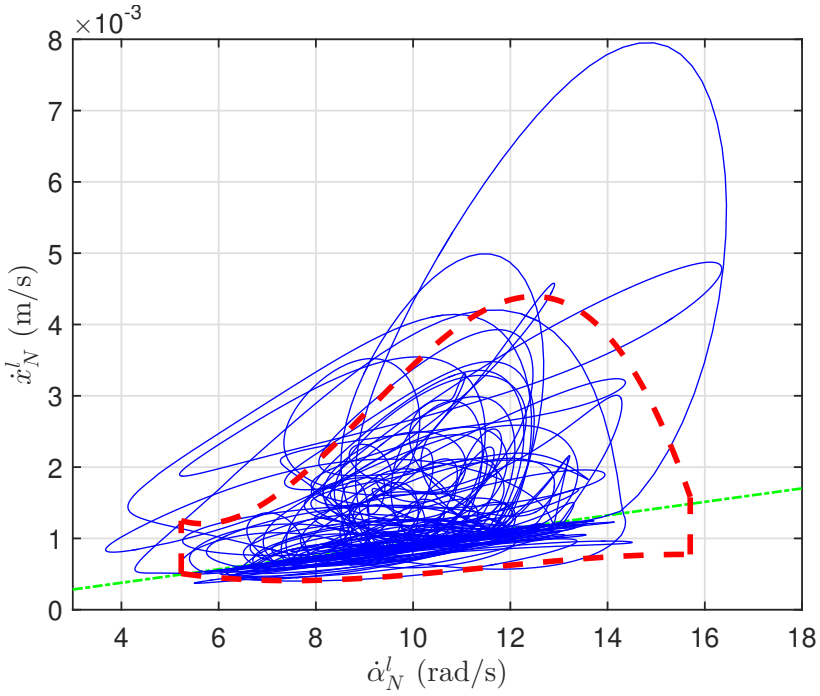

Figure 5.11: Phase portraits of the bit's torsional velocity $\dot{\alpha}_N^l$ and axial velocity $\dot{x}_N^l$ under standard LPV control

state constraints in the bit's dynamics with a complex shape. The novel barrier avoidance control technique is then implemented to this directional drilling system, embedding the state constraints into the LPV control design. To the end, the simulation case studies validates the effectiveness of the proposed constrained control design, through a comparison of open-loop, standard LPV control, and barrier avoidance based LPV control methods.

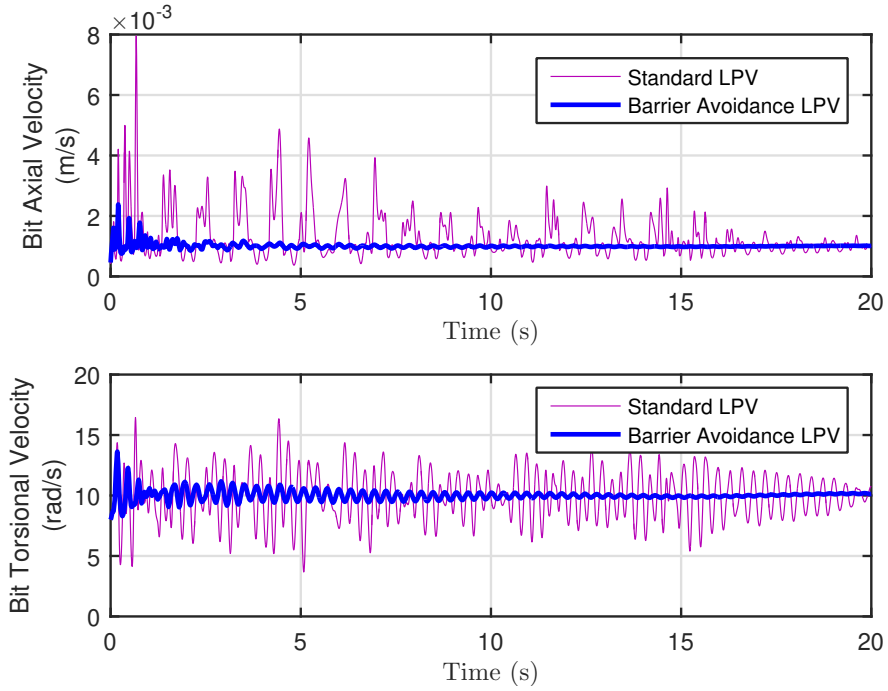

Figure 5.12: Comparison of the responses using standard LPV and barrier avoidance based LPV

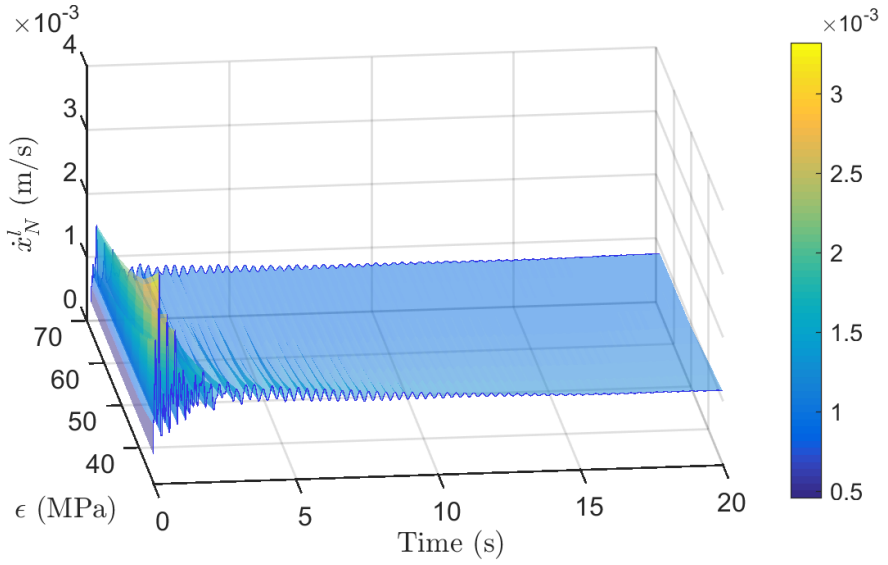

(a)

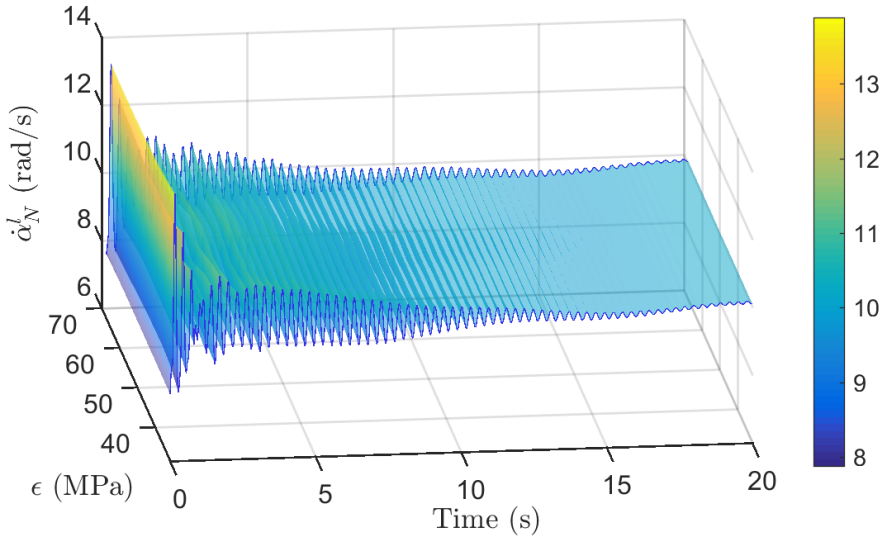

(b)

Figure 5.13: Robustness test under parameter perturbance of the instrinsic specific energy ϵ (70% to 150%): a) Responses of bit's axial velocity $\dot{x}_N^l$; b) Responses of bit's torsional velocity $\dot{\alpha}_N^l$

6. VALIDATION OF BARRIER AVOIDANCE BASED DRILLING CONTROL IN A LAB-SCALE DRILL RIG USING HARDWARE-IN-THE-LOOP SYSTEM

6.1 Introduction

In the practice of oil & gas production, drilling rigs are commonly built on-site after the geology exploration of the reservoirs. In order to complete the well, human drillers are often required to monitor and pilot the drilling, especially in directional and horizontal settings. However, this process largely depends on the driller's skills and experience, and a failure operation can result in severe vibration modes and drilling tool damage. This will significantly decrease the drilling efficiency and increase the non-production time, which can cause economic loss. To address this limitation, an automated drilling system has been intensively studied and developed in recent years. Based on the downhole data measurement through LWD and MWD [98], the automated drilling system can optimize the drilling parameter and make decisions in real-time, where the design of the control system is involved.

To validate the performance of drilling control, a drilling testbed is needed for both theoretical proof-of-concept and experimental validation. Nevertheless, it is not feasible to implement the control algorithm to a full-scale drill rig that comprises of a drill pipe of over ten thousand feet long. Also, an actual size PDC bit is critical in the experimental tests, since it can endure different major dynamic modes through the bit-rock interaction. Employing a PDC bit to the drilling requires powerful and complex machinery, which is challenging for a lab-scale implementation. In the previous work, many efforts have been put into the experimental study of the down-hole drilling [99, 100, 101, 102, 103]. However, most of them only consider a scaled size of both drill bit and drill string in a vertical setting, which can lose validity in modeling a full-size drill rig. In this work, we adopt the hardware-in-the-loop (HIL) technique to overcome this challenge. HIL provides a platform to replace a portion of the physical system with numerical simulations. This way, the complexity of building up a full-scale system can be tremendously reduced. In our experimental

testbed, we combine a physical system consisting of the bottom drill string and a full-size PDC bit, with a real-time simulation that models the directional drill string with FEM nodes, as shown in Fig. 6.1. This setup ensures a proper size of the device that can fit in the laboratory room and retains major dynamic modes of the system with a physical bit-rock contact, which enables a solid testing condition for the drilling control synthesis.

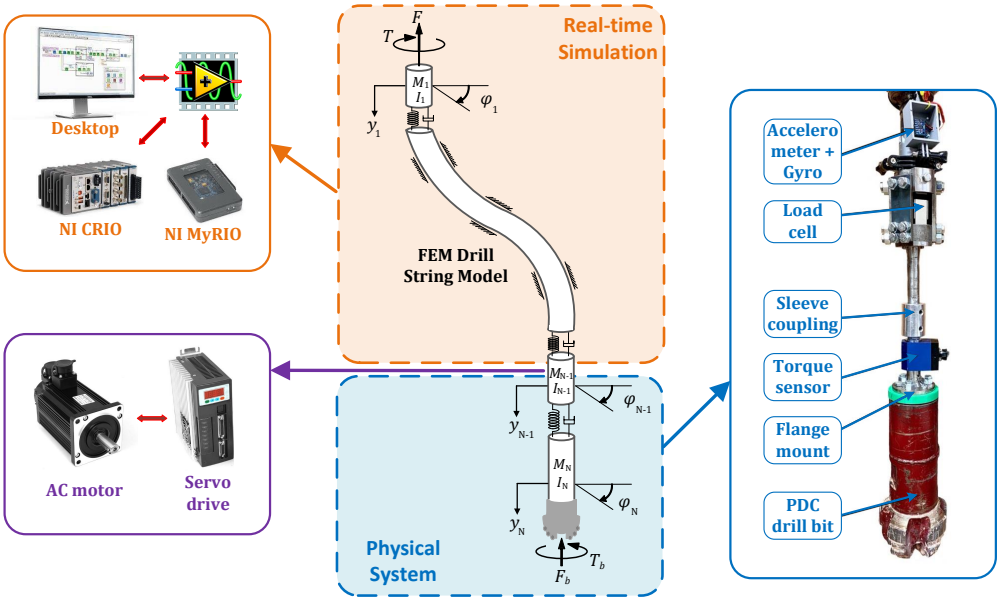

Figure 6.1: Schematic of the lab-scale drill rig

To mitigate the harmful vibration modes, we introduce a novel state-constrained control technique named barrier avoidance control. The constraint is formulated in the bit's velocities to enforce the drilling to stay inside the desired operating region, serving as a performance guarantee using active control. Due to the dynamic nature of this HIL system through FEM modeling and system identification, we embed the barrier avoidance control into the LPV method, to enable the feedback control of the high-order nonlinear system of the drilling. Considering the model uncertainties and downhole disturbances, we also integrate the H_∞ control to the design for disturbance rejection.

The outline of this chapter is given as follows. In Section 6.2, we first introduce each component of the hardware/mechanical setup of the physical system, including motors and sensors along the drill string, and then present the embedded environment that arranges the feedback control and real-time simulation. Section 6.3 states the framework of the HIL system, containing a FEM model-based virtual drill string, a lumped-parameter model of the physical system obtained by system identification, and an observer that estimates the system states. In Section 6.4, the barrier avoidance control approach is embedded in an LPV based control synthesis to enable the state-constrained control of the drilling system for vibration mitigation purposes. Finally, a series of experimental tests are exhibited in Section 6.5.

6.2 System Configuration

As depicted in Fig. 6.1, the experimental setup of a lab-scale drill rig has two major portions, a physical drilling machine that houses a PDC drill bit, and a real-time simulation in the NI LabVIEW software simulates the dynamic behavior of the long drill string. The reason of simulating the drill string using a dynamic model is because the drill string is the longest portion in a drilling system and is impractical to house physically in a lab environment. Yet, the dynamics of drill string are well studied based on beam theory and can be accurately modeled using methods such as finite element method (FEM) validated with a number of experiment based studies [96]. In contrast, the interaction of the drill bit and rock is typically nontrivial to model, so a physical drill it is incorporated in the HIL to ensure high fidelity. The simulation of the drill string dynamics generates real-time speed and torque/force of the lower portion of the drill string connected to the drill bit, and then two servo motors (one axial and one torsional) on top of the drill bit will generate the same force/torque to drive the drill bit at the bottom of the rig. The physical portion of the HIL testbed is shown in Fig. 6.2. There are four subsystems for controls setup: AC motors with servo drives, sensors, data acquisition devices, and an embedded control system.

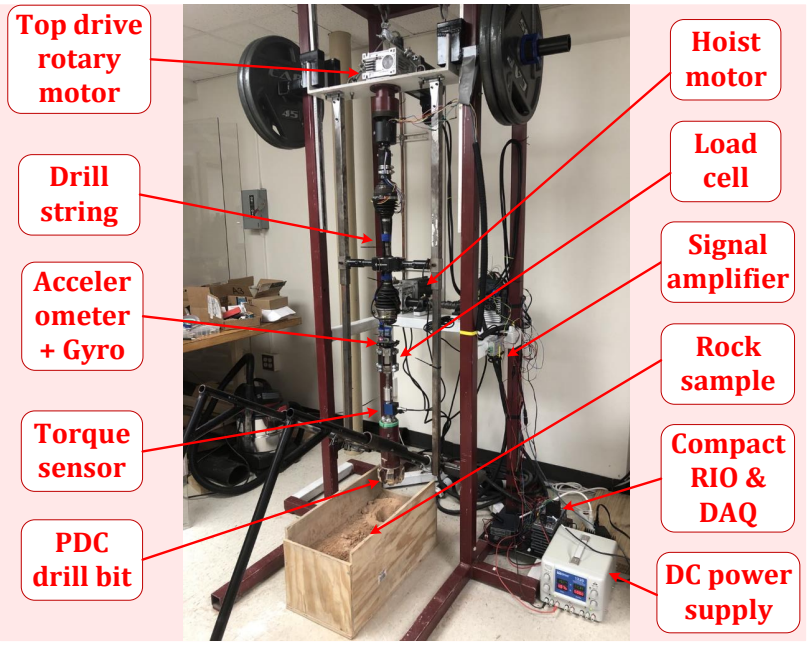

Figure 6.2: Photograph of the lab-scale drill rig

6.2.1 AC Motors with Servo Drives

To meet the rated power to penetrate the rock sample, we choose AC motors (ToAuto 1.8KW 6NM AC Servo Motor NEMA42) integrated with servo drives (KRS series) for the experimental setup. The speed reducers (NMRV050 30:1 Worm-Gear Reducer) are mounted at the output shaft of the AC motors, serving as the top rotary drive and the hoist drive to actuate torsional and axial motions, respectively. The motor drive is set to the speed mode, taking analog DC voltage input to control the speed, and it provides built-in position, velocity, and current feedback for a swift servo tracking performance.

6.2.2 Sensors

Different types of sensors are installed along the drill string to collect real-time measurements, enabling the system identification and the feedback control design. Incremental encoders are attached to the rotors of the AC motors, providing position/velocity readings in both axial and torsional dimensions. Besides, an IMU sensor board, including an integrated accelerometer and gyro-

scope module (Adafruit 9-DOF IMU Fusion - BNO055), is located at the drill bit, which measures the motion of the bit. Also, a load cell (Optima OP-312 1klb) and a dynamic torque sensor (WTQ 1050A 25Nm) are mounted at the shaft of the bottom drill string. These measurements are sent to the data acquisition devices for further data processing.

6.2.3 Data Acquisition Devices

Due to measurement noise, electromagnetic noise, and signal scaling, we use data acquisition devices to obtain accessible and reliable sensor measurements before sending them to the embedded control system. As shown in Fig. 6.3, the NI MyRIO board acquires all the sensors' signals after a low-pass filter circuit. Encoder data with two channels of pulses is sent to the FPGA ports of the MyRIO board. IMU sensor readings are converted into analog signals using a D/A converter (Adafruit 12-Bit DAC - MCP4725). The analog outputs of the load cell and torque sensor are amplified through a signal amplifier and then sent to the MyRIO board with proper scales.

6.2.4 Embedded Control System

The control system of this experimental drill rig is employed in the NI LabVIEW embedded environment. This environment includes the desktop PC, and two real-time operating systems (RTOS), i.e., MyRIO and CompactRIO (CRIO), and the data can transmit among these three devices in real-time. The signal flow is drawn in Fig. 6.3. After acquiring sensor measurements, the MyRIO board will forward the data to the embedded environment. The desktop PC then runs a real-time simulation to process this data through feedback control design. The voltage value for the speed control mode is calculated in the simulation and sent to the CompactRIO, which generates analog signals connected to the servo motor's drive. This way, we can construct the HIL framework of a drill string through the embedded control environment.

6.3 Hardware-in-the-loop System Design

As depicted in Fig. 6.1, a torsional rotary motor and an axial hoist motor can drive a physical drill rig to contact and penetrate the rock sample through the PDC drill bit. As we consider this physical system as only the lower portion of the drill string, a real-time simulation through a

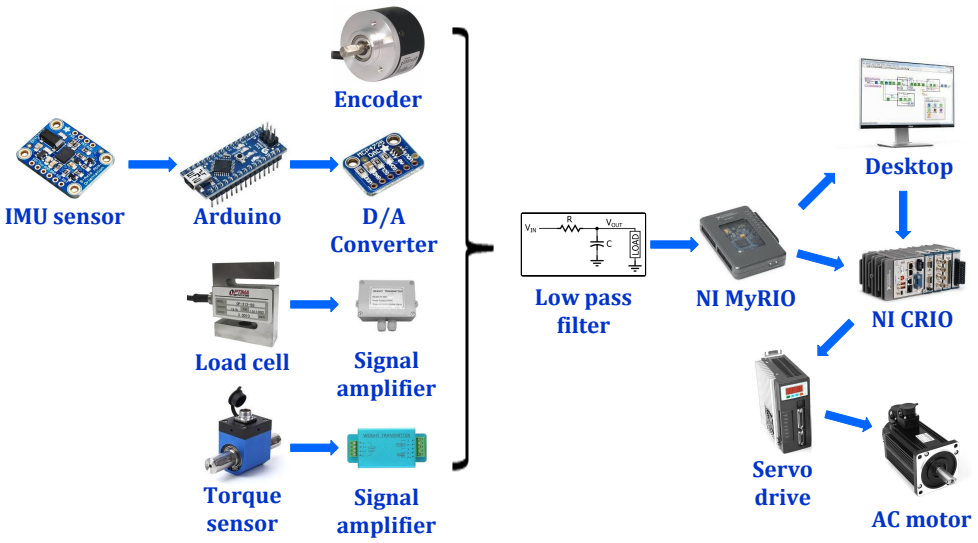

Figure 6.3: Data transmission signal flow graph

sophisticated mathematical model becomes the upper portion of the drill string. Based on this setup, the full-scale downhole drilling system is constructed in a HIL fashion, as shown in Fig. 6.4. The feedback control framework is drawn in the figure, where the virtual control inputs, i.e., force F and torque T on the top drive of the simulation model, actuate the dynamic motion of the drill string, and generate the velocities of the axial and torsional motors in the real-time, as the outputs of the simulations. These velocities are then fed into the servo drive as reference speeds of the motors, serving as the inputs to the physical system. When the drill bit penetrates the rock sample, the real-time measurements from the encoder, accelerometer, and gyro are collected. Finally, these state feedback signals are fed into the controller. This way, the feedback control loop is formulated with given reference positions and speeds, as shown in Fig. 6.4.

6.3.1 Mathematical Model of the Real-time Simulation

Typically, a full-scale drill rig in the field can have a drill string over ten thousand feet long. Thus, developing an experimental system under such a large size in the real drilling condition is not feasible. In this work, a large portion of the drilling string is simulated in the software, and connected to a physical drill bit.

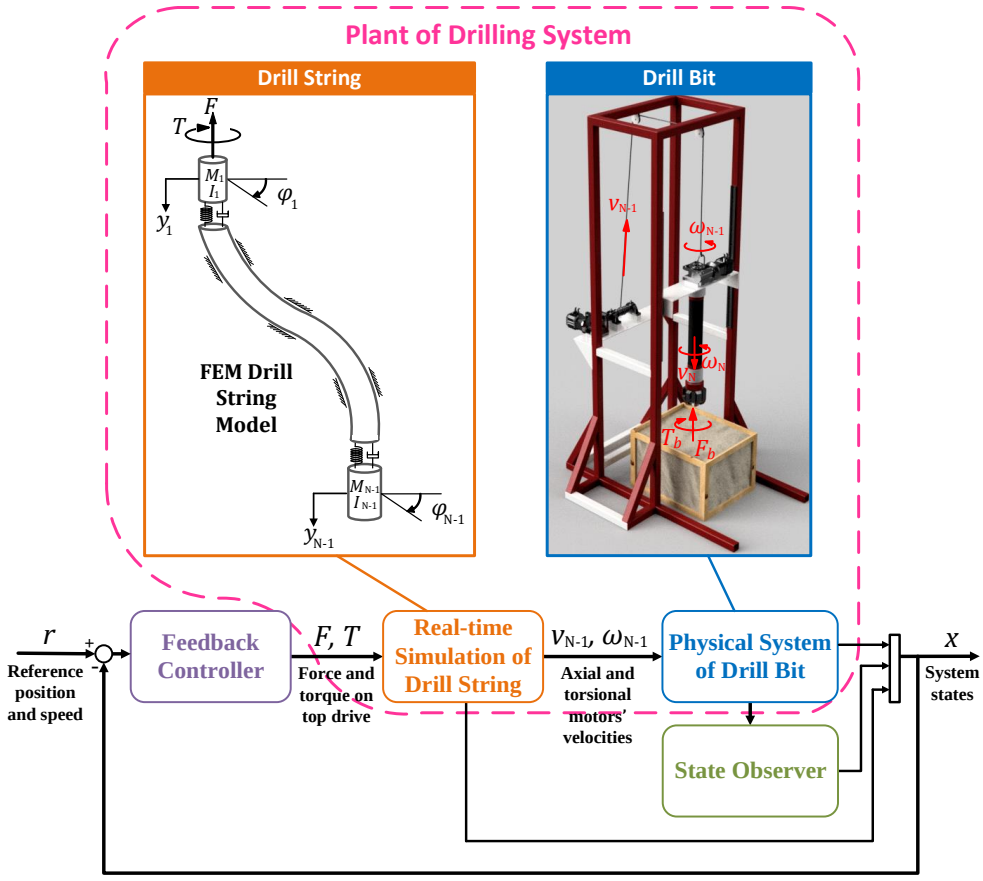

Figure 6.4: Hardware-in-the-loop based closed-loop control system

As shown in Fig. 6.4, the geometry of the drilling system is in a directional setting, where the drill string is discretized into N nodes. In the numerical simulation, we adopt a FEM approach to model the curved drill string for the first $N-1$ nodes, following the scheme in Chapter 5. The global frame is denoted by $X^gY^gZ^g$, where X^g axis is in the direction of gravity, and Y^g axis is in parallel to the ground surface. Every two adjacent nodes share a local coordinate frame, namely $X^lY^lZ^l$. The displacement vector of node i has four elements, denoted as

$$U_i^l = [x_i^l, y_i^l, \phi_i^l, \beta_i^l]^T \tag{6.1}$$

where x_i^l is the axial displacement, y_i^l is the radial displacement, ϕ_i^l is the torsional angle, and β_i^l is

the bending angle. The dynamic motion of the two adjacent nodes i and $i+1$ can be written as

$$M^l\ddot{U}^l_{\{i,i+1\}} + D^l\dot{U}^l_{\{i,i+1\}} + K^lU^l_{\{i,i+1\}} = F^l_{\{i,i+1\}} \tag{6.2}$$

where $U^l_{\{i,i+1\}} = [U_i^{l^T}\ U_{i+1}^{l^T}]^T$ is the local vector of the nodes i and $i+1$, M^l, K^l, D^l are the local ineria, stiffness, and damping matrices, and $F^l_{\{i,i+1\}}$ is the external force vector. Under the coordinate transformation between global and local frames $U^l_{\{i,i+1\}} = R_iU^g_{\{i,i+1\}}$, we express the dynamics in the global coordinates as

$$(R_i^TM^lR_i)\ddot{U}^g_{\{i,i+1\}} + (R_i^TD^lR_i)\dot{U}^g_{\{i,i+1\}} + (R_i^TK^lR_i)U^g_{\{i,i+1\}} = R_i^TF^l_{\{i,i+1\}} \tag{6.3}$$

Augmenting the motion equations of all the finte element nodes gives the overall dynamics as

$$M\ddot{U}^g + D\dot{U}^g + KU^g = F^{ext} \tag{6.4}$$

where $U^g = [U_1^{g^T}, U_2^{g^T}, ..., U_{N-1}^{g^T}]^T$ is the global state vector, M, K, D are the global inertia, stiffness, and damping matrices.

The dynamics (6.4) can be written in a state-space form as

$$\dot{X}_0 = A_0X_0 + H_0 \tag{6.5}$$

where $X_0 = [U^{g^T}\ \dot{U}^{g^T}]^T$ is the state, and the system matrices A_0 and H_0 are given as

$$A_0 = \begin{bmatrix} 0 & I \\ -M^{-1}K & -M^{-1}D \end{bmatrix}, \quad H_0 = \begin{bmatrix} 0 \\ M^{-1}F^{ext} \end{bmatrix} \tag{6.6}$$

The external force vector F^{ext} contains the input force F and torque T at the top end, the gravitational force, and the distributed wellbore contact tension and friction force/torque along with each FEM node. As constrained in the downhole drill pipes, the drill string's dynamic motion is latched

in the drill pipe's axial direction, through the wellbore contact force/torque. Thus, assuming the resultant motion is lined up with the drill pipe at an inclined angle θ_i, we will have the constraints in both axial and torsional dimensions as

$$y_i^g = x_i^g \tan(\theta_i), \quad \beta_i^g = \phi_i^g \tan(\theta_i) \tag{6.7}$$

We can then trancate the state vector using half of the state variables, given as

$$X_{tr} = \begin{bmatrix} U_{tr}^g \\ \dot{U}_{tr}^g \end{bmatrix} \tag{6.8}$$

where

$$U_{tr}^g = [x_1^g, \phi_1^g, x_2^g, \phi_2^g, ..., x_{N-1}^g, \phi_{N-1}^g]^T \tag{6.9}$$

For clarity, we can also denote

$$\dot{U}_{tr}^g = [v_1^g, \omega_1^g, v_2^g, \omega_2^g, ..., v_{N-1}^g, \omega_{N-1}^g]^T \tag{6.10}$$

The state-space system equation for the truncated state X_{tr} is then derived from the original system equation (6.5) as

$$\dot{X}_{tr} = A_{tr} X_{tr} + H_{tr} \tag{6.11}$$

where the system matrices A_{tr} and H_{tr} can be obtained using the procedures given in Chapter 5.

The numerical calculation of the FEM nodes is implemented in the NI LabVIEW software environment in real-time. As shown in Fig. 6.5, a Mathscript block contains the system matrices of the FEM nodes, and calculates the system states $\dot{X}_{tr}$ in real-time. In this block, we choose the Runge-Kutta 4th Order Method with a 0.02 sec time step, to ensure the numerical stability of the

simulation. The outputs of this Mathscript block are the vertical/angular velocities of the $N-1$th node, which are fed into the motor dive as the reference speeds.

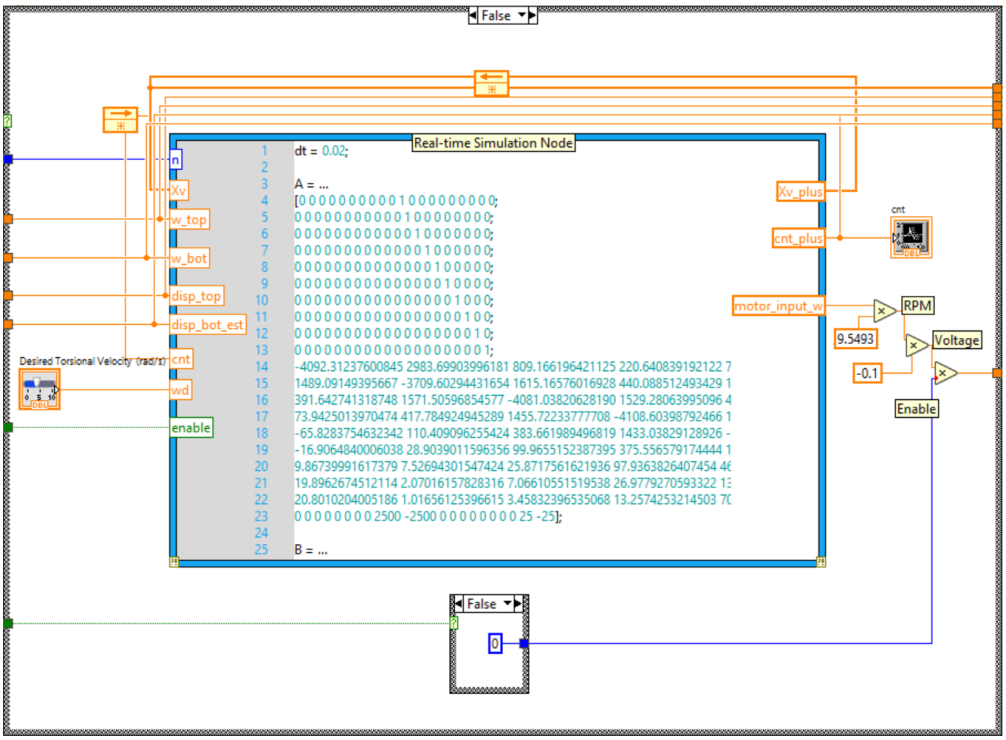

Figure 6.5: Math node for real-time simulation in LabVIEW

6.3.2 Model Identification of the Physical System

The bottom portion of the drill string is implemented in a physical experimental setup. As shown in the photograph of the lab-scale drill rig in Fig. 6.2, two AC motors in both axial and torsional dimensions drive the vertical drill string to penetrate the rock sample through the contact of the drill bit, while the sensors' measurements are logged in the real-time. We assume this physical system includes the drill string's last two nodes, i.e., $N-1$ and N, attaching to the PDC drill bit. To enable the feedback control of the drilling system in a HIL setting, we will first perform the system identification to obtain the coefficients of the two nodes $N-1$ and N in a lumped-parameter setting, and then to find the coefficients of the bit-rock interaction model. In the

rest of this section, we will discuss the system identification procedure in the torsional dynamics, and the axial one can be performed in the same manner.

The system identification of the lumped-parameter dynamics is performed, with the bottom of the drill string being a free end, i.e., the drill bit not in contact with the rock. The system equation of the Nth node can be written as

$$I_N \ddot{\phi}_N = -c_t(\dot{\phi}_N - \dot{\phi}_{N-1}) - k_t(\phi_N - \phi_{N-1}) \tag{6.12}$$

where I_N is the moment of inertia of the node N, and c_t and k_t are the damping and stiffness coefficients between the nodes $N-1$ and N. The transfer function of this SISO model is given as

$$\frac{\Phi_N(s)}{\Phi_{N-1}(s)} = \frac{\frac{c_t}{I_N}s + \frac{k_t}{I_N}}{s^2 + \frac{c_t}{I_N}s + \frac{k_t}{I_N}} \tag{6.13}$$

Feeding a chirp signal (in a 0.1-3 Hz frequency range) into the motor's reference speed $\dot{\phi}_{N-1}$, we can log the bit's speed $\dot{\phi}_N$ from the gyroscope's readings. The estimation of the coefficients is performed using the MATLAB System Identification Toolbox. The responses of both numerical model and physical plant are compared in Fig. 6.6. In this figure, we can observe that, except for some discrepancies in the high-frequency portion, the response of the numerical model matches well with the bottom drill string subsystem. In this setting, the coefficients of (6.13) are found as

$$\frac{c_t}{I_N} = 25, \quad \frac{k_t}{I_N} = 2500 \tag{6.14}$$

Besides, we can estimate the moment of inertia $I_N = 0.005$ from the dimension and density of the drill string and drill bit.

Next, to obtain the coefficients of the bit-rock interaction model, we set the velocities of torsional and axial motors to be constants, and let the bit contact with the rock sample and break the rock smoothly. The bit-rock interaction torque T_b is obtained from the torque sensor mounted at the drill string's shaft above the drill bit, as shown in Fig. 6.1. Its numerical model is given as

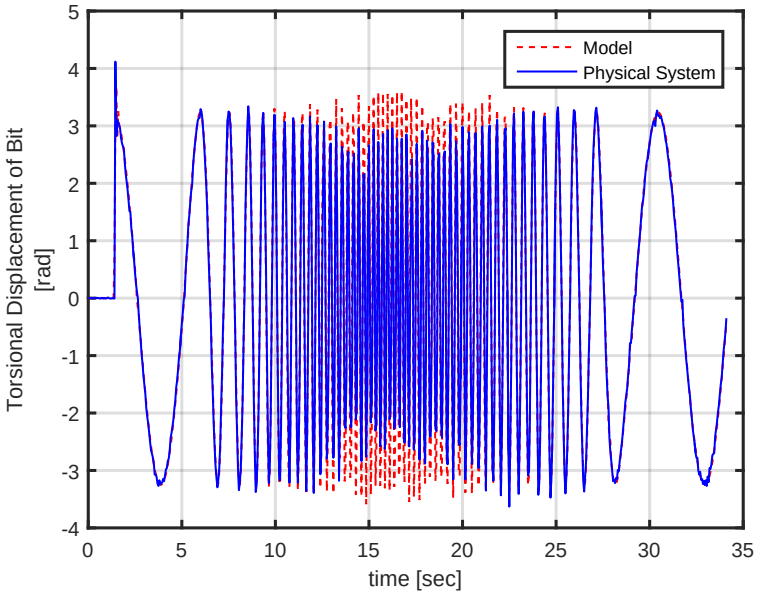

Figure 6.6: Responses of numerical model and physical plant

$T_b = l_b d$, where $d = 2\pi v_N/\omega_N$ is the depth-of-cut. The coefficient l_b can be derived by applying linear regression to the expression of T_b.

6.3.3 State Observer Design

Closed-loop control using state feedback requires precise real-time measurements from the sensors. For the torsional motion, the incremental encoder attached to the AC motor provides accurate angular speed ω_{N-1} and displacement ϕ_{N-1} values. The gyroscope located at the drill bit can generate angular speed readings ω_N. However, the integral of this speed becoming the bit's angular displacement ϕ_N will lose its validity due to the unpredictable zero offset of the gyroscope and the high-frequency measurement noise, when following a ramp signal. Therefore, we can design a state-observer to estimate the angular displacement ϕ_N at the bottom, using the torque sensor's measurement, as shown in Fig. 6.7.

The system equation of the node N with the bit-rock contact can be expressed as

$$I_N\ddot{\phi}_N = -c_t(\dot{\phi}_N - \dot{\phi}_{N-1}) - k_t(\phi_N - \phi_{N-1}) - T_b \tag{6.15}$$

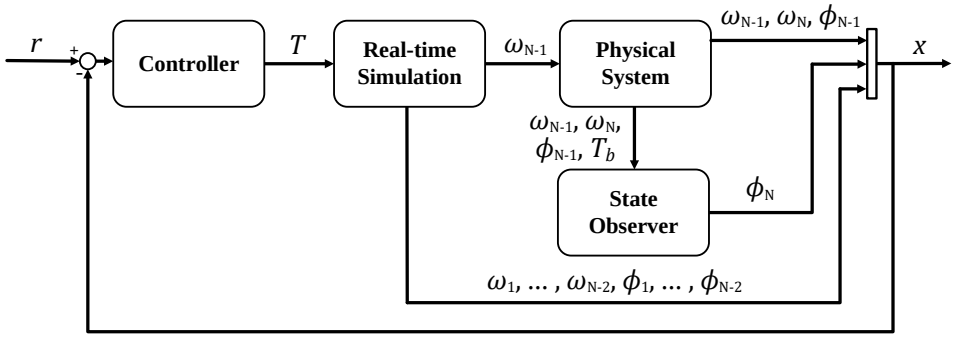

Figure 6.7: Block diagram of the torsional hardware-in-the-loop control system

Choosing $x_1 = \phi_N$ and $x_2 = \dot{\phi}_N$, we can convert (6.15) into a state-space model as

$$\begin{aligned} \dot{x}_1 &= x_2 \\ \dot{x}_2 &= -\frac{k_t}{I_N}x_1 - \frac{c_t}{I_N}x_2 + \frac{c_t}{I_N}\omega_N + \frac{k_t}{I_N}\phi_N - \frac{T_b}{I_N} \end{aligned} \tag{6.16}$$

where the term $c_t/I_N \cdot \omega_N + k_t/I_N \cdot \phi_N - T_b/I_N$ is accessible in the real time, and we assume it is the input u to the system. Thus, the system equation (6.15) becomes

$$\begin{aligned} \dot{x} &= A_N x + B_N u \\ y &= C_N x \end{aligned} \tag{6.17}$$

where

$$A_N = \begin{bmatrix} 0 & 1 \\ -\frac{k_t}{I_N} & -\frac{c_t}{I_N} \end{bmatrix}, \quad B_N = \begin{bmatrix} 0 \\ 1 \end{bmatrix}, \quad C_N = \begin{bmatrix} 1 & 0 \end{bmatrix} \tag{6.18}$$

The state observer is then designed as

$$\dot{\hat{x}} = A_N\hat{x} + B_N u + L(y - \hat{y})$$
$$\hat{y} = C_N\hat{x} \tag{6.19}$$

The observer gain L is chosen to place the eigenvalues of $A_N - LC_N$ 3 times away from the origin than the eigenvalues of the matrix A_N. Therefore, the estimated displacement of the bit is available for the feedback control design.

6.4 Barrier Avoidance Control Design

In this work, assuming the axial dynamics have constant velocities at each FEM node, we introduce the barrier avoidance control method for the torsional dynamics of the drilling system in the HIL setting. This state-constrained control technique can prevent the drilling from falling into the undesired operating regime, and thus can mitigate harmful vibrations such as stick-slip [83]. Since the drilling system contains higher-order nonlinear dynamics, we will embed the barrier avoidance control method in an LPV control scheme to enable a nonlinear feedback design for such a high-order system. Thus, we will next find the system equations' error dynamics and convert them into an LPV plant.

Combining the torsional dyamics of the virtual system (6.11) and the physical system (6.15), we obtain the system equation of N nodes as

$$\dot{X} = AX + H \tag{6.20}$$

where $X = [\Phi, \Omega]^T = [\phi_1, \phi_2, ..., \phi_N, \omega_1, \omega_2, ..., \omega_N]^T$ (Since all the elements of X are in global frame, we omit the notation g). The system matrices $A \in \mathbb{R}^{2N\times 2N}$, $H \in \mathbb{R}^{2N\times 1}$ are written as

$$A = \begin{bmatrix} 0 & I \\ -A_{km} & -A_{dm} \end{bmatrix}, \quad H = \begin{bmatrix} 0 \\ H_{fm} \end{bmatrix} \tag{6.21}$$

Given the desired torsional velocity to be ω_d in the local coordinates, we choose the desired state vector as

$$X_d = \begin{bmatrix} \Omega_d t + \Phi_{ic} \\ \Omega_d \end{bmatrix} \tag{6.22}$$

where $\Omega_d = [w_d \cos(\theta_1), w_d \cos(\theta_2), ..., w_d \cos(\theta_N)]^T$. Therefore, we can define the error state as

$$E = \begin{bmatrix} E_1 \\ E_2 \end{bmatrix} \tag{6.23}$$

where $E_1 = \Phi - (\Omega_d t + \Phi_{ic})$ and $E_2 = \Omega - \Omega_d$. The entries of the error state are defined as $E_1 = [e_1, e_2, ..., e_N]$ and $E_2 = [e_{N+1}, e_{N+2}, ..., e_{2N}]$. The error dynamics can be then derived from (6.20) as

$$\begin{aligned} \dot{E}_1 &= E_2 \\ \dot{E}_2 &= -A_{km}\Phi - A_{dm}\Omega + H_{fm} \\ &= -A_{km}E_1 - A_{dm}E_2 - A_{km}(\Omega_d t + \Phi_{ic}) - A_{dm}\Omega_d + H_{fm} \\ &= -A_{km}E_1 - A_{dm}E_2 + H_{fm} - H_d \end{aligned} \tag{6.24}$$

where H_d is the desired external torque vector including the desired top drive's torque T_d and the desired bit-rock interaction torque T_{bd}. The term $A_{km}\Omega_d$ is close to zero with a large number N of the FEM nodes. Also, the initial condition of the torsional displacement is given as $\Phi_{ic} = A_{km}^{-1}(H_d - A_{dm}\Omega_d)$. The error dynamics (6.24) can be simplified as

$$\dot{E} = AE + H_e \tag{6.25}$$

where the vector H_e contains the term $T_b - T_{bd}$, and can be converted into a quasi-LPV form.

Under a smooth drilling condition, the torque of the bit T_b is calculated using a depth-of-cut model

$$T_b = l_b 2\pi \frac{v_N}{\omega_N} + \delta_T \tag{6.26}$$

where v_N and ω_N are the axial and torsional velocities of the bit, l_b is a positive constant, and δ_T stands for the model uncertainty and disturbance. Given the desired axial velocity v_d, we can express the nonlinear term $T_b - T_{bd}$ as

$$\begin{aligned} T_b - T_{bd} &= l_b 2\pi \left(\frac{v_d + \delta_v}{\omega_d + (e_{2N}/\cos(\theta_N))} - \frac{v_d}{\omega_d}\right) + \delta_T \\ &= -\frac{l_b 2\pi e_{2N}}{\omega_d \cos(\theta_N)(\omega_d + (e_{2N}/\cos(\theta_N)))} + \Delta \end{aligned} \tag{6.27}$$

Plugging (4) into the error dynamics (6.25) gives the quasi-LPV form as

$$\dot{E} = \tilde{A}(e_{2N})E + Bu + W\Delta \tag{6.28}$$

where $\tilde{A}(e_{2N})$ contains the error state e_{2N} in its elements, the control input $u = T - T_b d$, and the overall disturbance Δ.

Next, the state constraint is chosen as $\omega_d - k_\omega < \omega_N < \omega_d + k_\omega$ (or $|e_{2N}| < k_\omega \cos\theta_N$), where $0 < k_\omega < \omega_d$, to avoid the bit's torsional speed droping below zero. The state-constrained control is then performed by combining barrier avoidance control with LPV method.

The principle of the barrier avoidance control is briefly summarized as follows (Theorem 2 in Chapter 3):

1) Choose a diffeomorphic transformation that projects the boundary of the state constraints to the points at infinity.

2) Convert the original system equation to a new one using this diffeomorphic transformation.

3) Design the state feedback controller that can stabilize the new system equation, and apply the same amount of control back to the original system to achieve the state-constrained control.

Given state constraint $|e_{2N}| < k_\omega \cos\theta_N$, we choose the diffeomorphic transformation as

$$e^*_{2N} = \frac{e_{2N}}{(k^2_\omega \cos^2\theta_N - e^2_{2N})^{1/2}} \tag{6.29}$$

Let $E^* = [e_1, ..., e_{2N-1}, e^*_{2N}]^T$. The system equation in the new coordinates of E^* is written as

$$\begin{aligned}\dot{E}^* =& \text{diag}\{_{1,\cdots,1,\frac{(1+{e^*_{2N}}^2)^{3/2}}{k_\omega \cos\theta_N}}\}\tilde{A}(e_{2N})\,\text{diag}\{_{1,\cdots,1,\frac{k_\omega\cos\theta_N}{(1+{e^*_{2N}}^2)^{1/2}}}\}E^* \\ &+ \text{diag}\{_{1,\cdots,1,\frac{(1+{e^*_{2N}}^2)^{3/2}}{k_\omega \cos\theta_N}}\}Bu + \text{diag}\{_{1,\cdots,1,\frac{(1+{e^*_{2N}}^2)^{3/2}}{k_\omega \cos\theta_N}}\}W\Delta \\ =& A^*(E^*)E^* + B^*(E^*)u + W^*(E^*)\Delta\end{aligned} \tag{6.30}$$

Also, we consider the bit angular displacement to be the output $z = CE^*$. The objective is to find the state feedback control $u = K_c E^*$, so that we can mitigate the effect of the disturbance to the output. This can be achieved by minimizing η, such that the L_2 gain is bounded, given as

$$\sup_{\|\Delta\|_2=1} \|z\|_2 = \sup_{\|\Delta\|_2\neq 0} \frac{\|z\|_2}{\|\Delta\|_2} \leq \eta \tag{6.31}$$

The above condition is equivalent to the follow LMI [36, 104]

$$\begin{bmatrix} A^*Q + Q^TA^* + B^*Y + Y^TB^{*T} + W^*W^{*T} & Q^TC^T \\ CQ & -\eta^2 I \end{bmatrix} \leq 0 \tag{6.32}$$

where $Q = P^{-1}$, and the Lyapunov candidate is chosen as $V = E^{*T}PE^*$. The state feedback gain is derived by $K_c = YQ^{-1}$. Together with (6.32), two additional LMIs are provided to enforce the input constraint $|u| \leq \eta$ [105]

$$\begin{bmatrix} 1 & E^*(0)^T \\ E^*(0) & Q \end{bmatrix} \geq 0\ , \quad \begin{bmatrix} Q & Y^T \\ Y & \eta^2 I \end{bmatrix} \geq 0 \tag{6.33}$$

To implement an LPV control scheme for the new system equation (6.30), we can solve the

above set of LMIs in finite points of the discretized interval of the time-varying parameter e_{2N}^*. The efficient computer software, such as Matlab LMI toolbox [106] and Sedumi [107], can calculate the control gains K_c in each mesh grid. Then the state feedback control is performed in real-time using a lookup table with the pre-set controller gains.

Remark 4. *Note that, due to the unknown axial speed of the bit, the uncertainty term of the bit-rock interaction is not neglectable, and can greatly degrade the control performance. Thus, unlike the LPV plant in Chapter 5, the uncertainty term Δ in this HIL system model enters the system equation* (6.30)*. We then introduce an L_2 induced norm to eliminate the effect of this unknown term by solving the augmented LMIs in* (6.32) *and* (6.33)*.*

6.5 Experimental Results

In the experimental study, we integrate the proposed barrier avoidance control of Section 6.4 into our lab-scale drill rig in a HIL setting. The value of the control gains K_c are arranged in the LabVIEW embedded environment. In the simulation of the upper drill string, the geometry of the directional drill string is depicted as Fig. 6.8, where AB and BC are two arcs with centers O and O'. The parameters of this FEM model are listed in Table 6.1. Note that the drill string parameters are chosen in scaled dimensions, and it can model a full-size drill string if converted into a proper scale.

In the axial dimension, given the reference speed as 0.05 mm/s, the motion is actuated by the hoist motor in the physical system. For the torsional dynamics, we first performed three tests using open-loop control, standard LPV control, and barrier avoidance based LPV control, respectively.

The open-loop control sets the top drive's actuation to track a constant speed, and this so-called 'Speed Mode' is commonly used in practice. Given the reference speed as 2 rad/s, we observed severe vibrations of the bit while contacting the rock sample. The time history of the bit's angular speed and the torque on the bit are drawn in Fig. 6.9. In this figure, inside each cycle of the oscillations, the speed drops down to zero and enters the 'stick' phase, while the energy accumulates and the torque rises up to a high value. After the energy exceeds a certain threshold, the bit enters the 'slip' phase, and the speed can increase and form a peak in the time response.

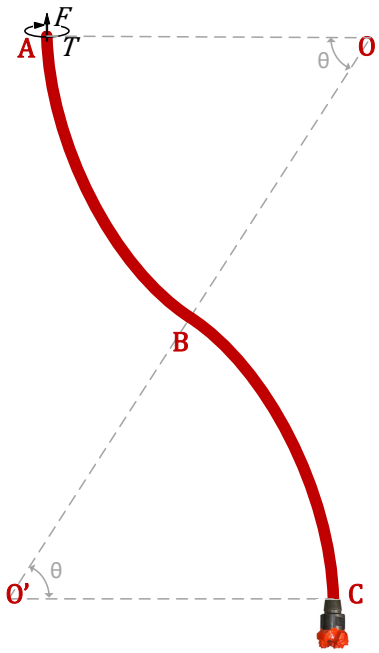

Figure 6.8: Geometry of the directional drill string using FEM model

This way, the stick-slip behavior can generate harmful vibration and spread along the drill string. Also, the torque on the bit lines up with this stick-slip behavior.

Next, we apply the standard LPV control without barrier avoidance to the torsional dynamics. The stick-slip behavior is eliminated, and the responses of the bit's angular speed are controlled within a certain range, as shown in Fig. 6.10. However, significant fluctuation still arises under the disturbance of bit-rock interaction, resulting in a poor performance of the HIL control system.

In comparison, we finally implement the barrier avoidance control to this experimental setup, by choosing $k_\omega = 0.7\omega_d$. As shown in Fig. 6.11, the vibrations are greatly suppressed, and the constraints are not violated. The bit's speed tracks the 2 rad/s references with a smooth steady-state, proving the effectiveness of the proposed barrier avoidance method.

Next, we perform a series of tests, letting the drilling system track different setpoint speeds using barrier avoidance control. Again, we set the axial reference speed to be 0.05 mm/s for all the tests. In Fig. 6.12, the torsional velocities of the bit, the midpoint of the drill string, and the top drive are logged, given the reference speeds as 3 rad/s, 4 rad/s, 5 rad/s, and 6 rad/s. As

Table 6.1: Parameters of Drill String FEM Model

Symbol	Value [Unit]	Description
D_o	0.075 [m]	Drill string outer diameter
D_i	0 [m]	Drill string inner diameter
ρ	7850 [kg/m^3]	Drill string density
$\mathcal{A}$	0.0044 [m^2]	Cross-section area
N	10	Number of nodes
$\mathcal{E}$	2×10^6 [Pa]	Young's modulus
$\mathcal{G}$	7.69×10^5 [Pa]	Shear modulus
J	1.55×10^{-6} [Pa]	Polar moment of inertia
r_a	0.001 [m]	Rayleigh damping coefficient
r_b	0.01 [m]	Rayleigh damping coefficient
θ	10 [°]	Central angle of arc AB and BC

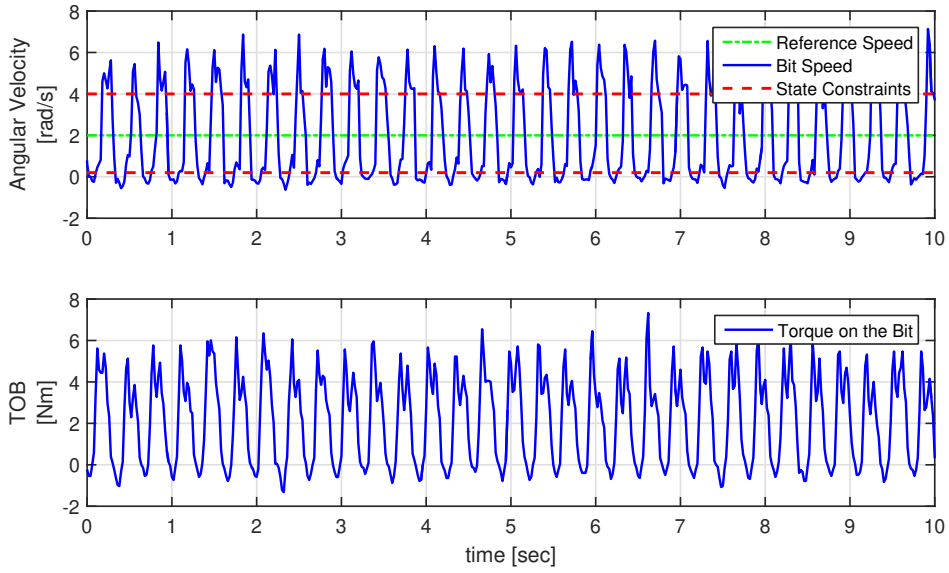

Figure 6.9: Bit angular velocity and torque under speed mode of the top drive with reference speed 2 rad/s

being verified in these figures, the state-constrained controller can effectively suppress the severe vibration modes, even when the system endures large disturbances at the drill bit. These results demonstrate the performance and the robustness of our feedback control design using the barrier avoidance control.

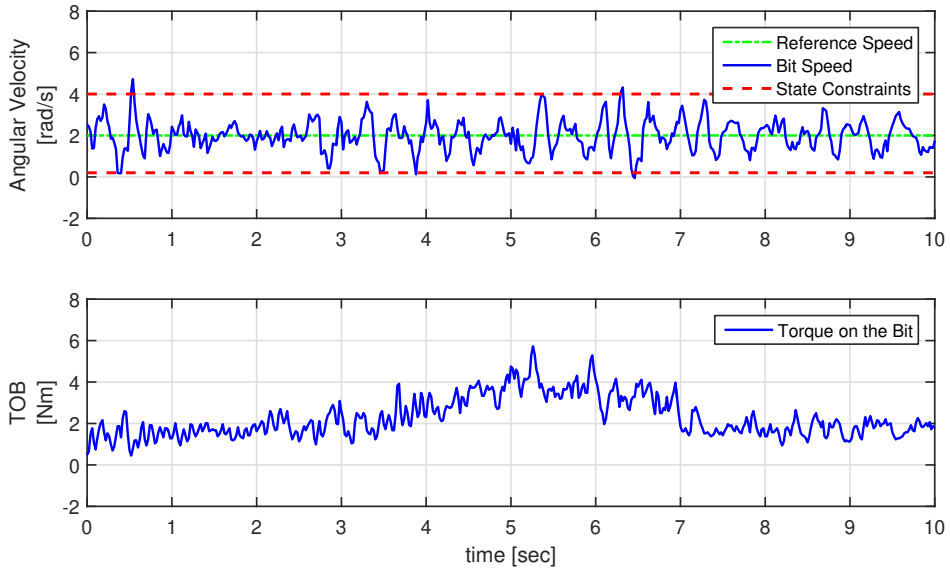

Figure 6.10: Bit angular velocity and torque under standard LPV control with reference speed 2 rad/s

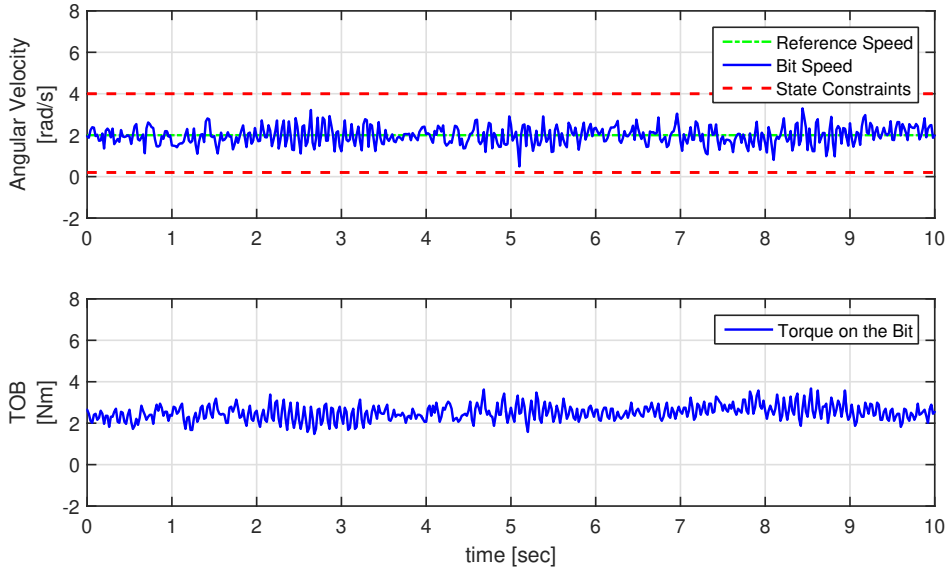

Figure 6.11: Bit angular velocity and torque under barrier avoidance control with reference speed 2 rad/s

6.6 Conclusion

In this chapter, we present the control of a lab-scale drill rig under the HIL scheme. All components in the hardware setup, including the actuation system, sensors, and data acquisition devices, are explained in detail, contributing to the physical system's construction. The directional drilling system model is captured using the FEM method for the real-time simulation and system identification for the physical dynamics. A novel state-constrained control scheme named barrier avoidance control is proposed using the H_∞ control based LPV approach. Responses of the experimental results are performed with a variety of reference velocities, and the efficacy of the proposed control design is validated through the comparison of the open-loop and closed-loop control.

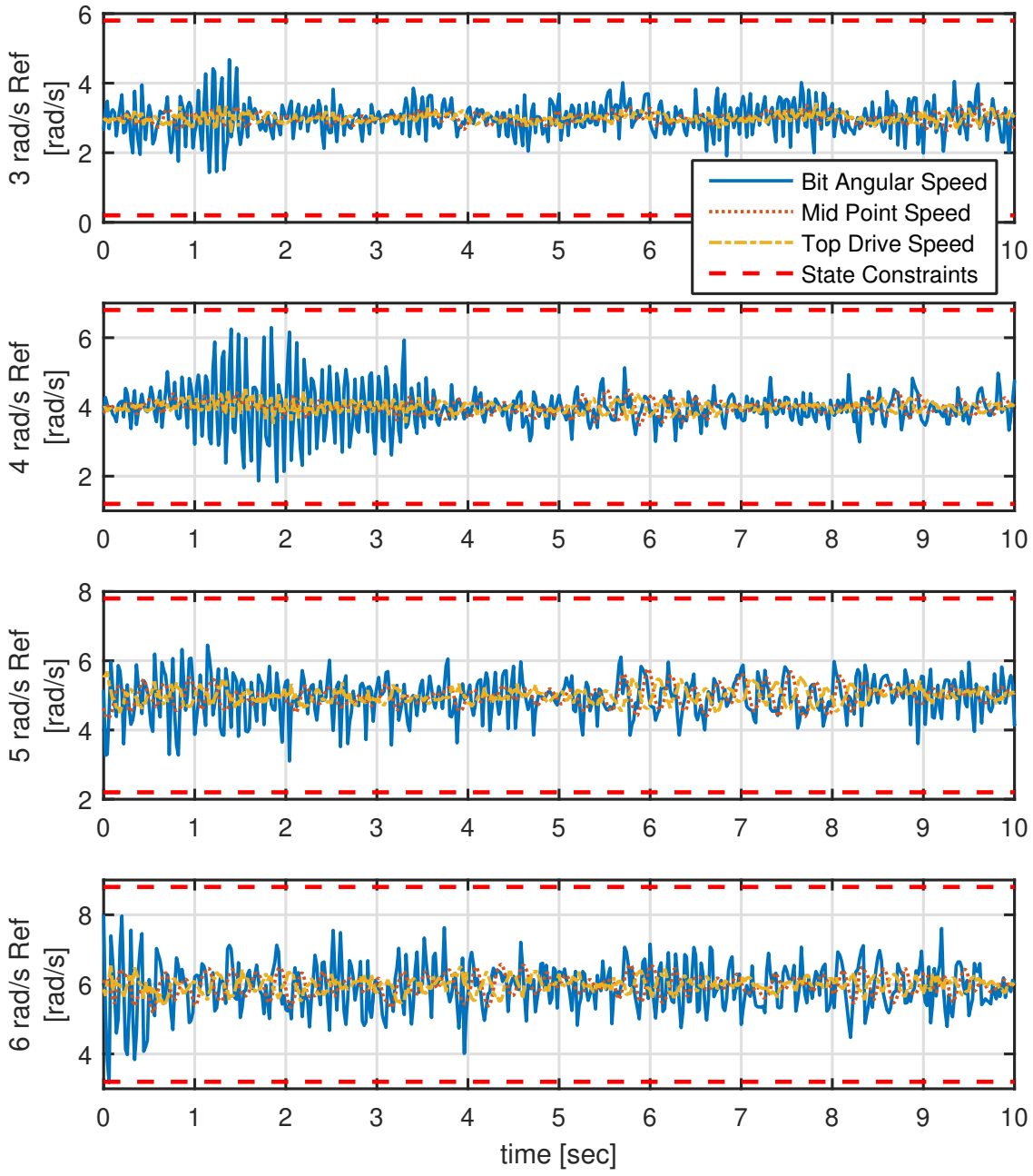

Figure 6.12: Angular velocities of bit, drill string midpoint, and top drive under barrier avoidance control with reference speeds: 3 rad/s, 4 rad/s, 5 rad/s, and 6 rad/s

7. SUMMARY

7.1 Summary

This dissertation discusses the barrier avoidance control method, as a novel state-contrained control technique, and applies this method to a down-hole drilling system for vibration mitigation. Both theoritical investigation and its application to the drilling are presents in this thesis. In the theoretical study, barrier avoidance control is proposed to enlarge the flexibility for a state-constrained control problem. In the study of the drilling control, the barrier avoidance method is implemented to both vertical and directional drilling systems, and is validated by the testing results of a lab-scale drill rig in HIL settings.

7.1.1 Theoretical Study

The main theory of the barrier avoidance control is proposed in Chapter 3, where a diffeomorphic tranformation can project the constrained region in the original plane into the new radially unbounded plane, and the system dynamics are converted accordingly. By designing any types of controllers that can stablilize the new system, the state-contrained control is achieved in the original system, which enables any well-established nonlinear control to be used. However, even though it can be directly implemented to the state constraint with a hyperrectangle shape as proven in the cases studies, its application to a complex shape of the state constraint is non-trivial and required further investigation. In Chapter 4, we propose a systematic way to integrate the complex constraint into the barrier avoidance control, and this routine can effectively solve the constrained-control problem in many physical systems.

7.1.2 Application to Drilling System

The early study introducing the concept pf state-constrained control to a drilling system is discussed in Chapter 2. The iBLF approach is brought into the down-hole drilling system for the first time. Nevertheless, it can only be implemented to a low-order lumped-parameter system with 2 nodes, due to the requirement of the strict-feedback form. Also, in Chapter 2, the state barrier

region is in a rectangle shape of the bit's velocities, which can be conservative compared with the empirical field testing results in a complex barrier shape. Since a higher-order system dynamics model is capable of capturing vibration modes of higher frequencies, and also is a foundation of the directional drilling's modeling, in Chapter 5 we make two improvements to the drilling control design, i.e., using high-order FEM to model the directional drill string, and choosing a complex barrier shape for the drill bit. Finally, in Chapter 6 the constrained control algorithm is programed in a HIL experimental setup of a lab-scale drill rig, whose feasbility and performance are proven by the real testing results

REFERENCES

[1] X. Wu, L. C. Paez, U. T. Partin, and M. Agnihotri, "Decoupling stick/slip and whirl to achieve breakthrough in drilling performance," in *IADC/SPE Drilling Conference and Exhibition*, pp. 966–978, Feb 2010.

[2] S. Dalvi, *Fundamentals of Oil & Gas Industry for Beginners*. Chennai, India: Notion Press, 2015.

[3] H. U. Vogel, "The great well of China," *Scientific American*, vol. 268, no. 6, pp. 116–121, 1993.

[4] L. S. Russell, *A heritage of light: Lamps and lighting in the early Canadian home*. Toronto, Canada: University of Toronto Press, 1968.

[5] R. Mitchell, S. Miska, *et al.*, *Fundamentals of drilling engineering*. Richardson, TX: Society of Petroleum Engineers, 2011.

[6] T. Vromen, *Control of stick-slip vibrations in drilling systems*. PhD thesis, Eindhoven University of Technology, 2015.

[7] J. G. Speight, *Deep shale oil and gas*. Cambridge, MA: Gulf Professional Publishing, 2016.

[8] A. R. Brandt, "Testing hubbert," *Energy Policy*, vol. 35, no. 5, pp. 3074–3088, 2007.

[9] E. M. Navarro-López and D. Cortés, "Avoiding harmful oscillations in a drillstring through dynamical analysis," *Journal of Sound and Vibration*, vol. 307, no. 1–2, pp. 152–171, 2007.

[10] E. M. Navarro-López and E. Licéaga-Castro, "Non-desired transitions and sliding-mode control of a multi-dof mechanical system with stick-slip oscillations," *Chaos, Solitons & Fractals*, vol. 41, no. 4, pp. 2035–2044, 2009.

[11] A. S. Yigit and A. P. Christoforou, "Stick-slip and bit-bounce interaction in oil-well drillstrings," *Journal of Energy Resources Technology*, vol. 128, no. 4, pp. 268–274, 2006.

[12] N. Mihajlovic, A. Van Veggel, N. Van De Wouw, and H. Nijmeijer, "Analysis of friction-induced limit cycling in an experimental drill-string system," *Journal of Dynamic Systems, Measurement, and Control*, vol. 126, no. 4, pp. 709–720, 2004.

[13] B. Besselink, N. Van De Wouw, and H. Nijmeijer, "Model-based analysis and control of axial and torsional stick-slip oscillations in drilling systems," in *IEEE International Conference on Control Applications*, pp. 495–500, Sept 2011.

[14] B. Besselink, N. Van De Wouw, and H. Nijmeijer, "A semi-analytical study of stick-slip oscillations in drilling systems," *Journal of Computational and Nonlinear Dynamics*, vol. 6, no. 2, p. 021006, 2011.

[15] B. Besselink, T. Vromen, N. Kremers, and N. Van De Wouw, "Analysis and control of stick-slip oscillations in drilling systems," *IEEE Transactions on Control Systems Technology*, vol. 24, pp. 1582–1593, Sept 2016.

[16] T. Richard, C. Germay, and E. Detournay, "Self-excited stick-slip oscillations of drill bits," *Comptes Rendus MECANIQUE*, vol. 332, no. 8, pp. 619–626, 2004.

[17] K. Nandakumar and M. Wiercigroch, "Stability analysis of a state dependent delayed, coupled two DOF model of drill-string vibration," *Journal of Sound and Vibration*, vol. 332, no. 10, pp. 2575–2592, 2013.

[18] T. Richard, C. Germay, and E. Detournay, "A simplified model to explore the root cause of stick-slip vibrations in drilling systems with drag bits," *Journal of Sound and Vibration*, vol. 305, no. 3, pp. 432–456, 2007.

[19] H. Melakhessou, A. Berlioz, and G. Ferraris, "A nonlinear well-drillstring interaction model," *Journal of Vibration and Acoustics*, vol. 125, no. 1, pp. 46–52, 2003.

[20] C. Ke and X. Song, "Computationally efficient down-hole drilling system dynamics modeling integrating finite element and transfer matrix," *Journal of Dynamic Systems, Measurement, and Control*, vol. 139, no. 12, p. 121003, 2017.

[21] H. A. Alnaser, *Finite element dynamic analysis of drillstring*. PhD thesis, King Fahd University of Petroleum and Minerals (Saudi Arabia), 2002.

[22] Y. Khulief, F. Al-Sulaiman, and S. Bashmal, "Vibration analysis of drillstrings with string-borehole interaction," *Proceedings of the Institution of Mechanical Engineers, Part C: Journal of Mechanical Engineering Science*, vol. 222, no. 11, pp. 2099–2110, 2008.

[23] T. Feng, M. Vadali, Z. Ma, D. Chen, and J. Dykstra, "A finite element method with full bit-force modeling to analyze drillstring vibration," *Journal of Dynamic Systems, Measurement, and Control*, vol. 139, no. 9, p. 091016, 2017.

[24] A. Christoforou and A. Yigit, "Fully coupled vibrations of actively controlled drillstrings," *Journal of Sound and Vibration*, vol. 267, no. 5, pp. 1029–1045, 2003.

[25] E. Detournay and P. Defourny, "A phenomenological model for the drilling action of drag bits," *International Journal of Rock Mechanics and Mining Sciences & Geomechanics Abstracts*, vol. 29, no. 1, pp. 13–23, 1992.

[26] C. Fairhurst and W. Lacabanne, "Some principles and developments in hard rock drilling techniques," in *6th Annual Drilling & Blasting Symposium (University of Minnesota)*, pp. 15–25, Oct 1956.

[27] D. A. Glowka, "Use of single-cutter data in the analysis of PDC bit designs: part 1-development of a PDC cutting force model," *Journal of Petroleum Technology*, vol. 41, no. 08, pp. 797–849, 1989.

[28] E. Detournay, T. Richard, and M. Shepherd, "Drilling response of drag bits: Theory and experiment," *International Journal of Rock Mechanics and Mining Sciences*, vol. 45, no. 8, pp. 1347–1360, 2008.

[29] X. Liu, N. Vlajic, X. Long, G. Meng, and B. Balachandran, "Coupled axial-torsional dynamics in rotary drilling with state-dependent delay: stability and control," *Nonlinear Dynamics*, vol. 78, no. 3, pp. 1891–1906, 2014.

[30] X. Liu, X. Long, X. Zheng, G. Meng, and B. Balachandran, "Spatial-temporal dynamics of a drill string with complex time-delay effects: bit bounce and stick-slip oscillations," *International Journal of Mechanical Sciences*, vol. 170, p. 105338, 2020.

[31] X. Zheng, V. Agarwal, X. Liu, and B. Balachandran, "Nonlinear instabilities and control of drill-string stick-slip vibrations with consideration of state-dependent delay," *Journal of Sound and Vibration*, vol. 473, p. 115235, 2020.

[32] X. Zhu, L. Tang, and Q. Yang, "A literature review of approaches for stick-slip vibration suppression in oilwell drillstring," *Advances in Mechanical Engineering*, vol. 6, p. 967952, 2014.

[33] J. D. Jansen and L. Van Den Steen, "Active damping of self-excited torsional vibrations in oil well drillstrings," *Journal of Sound and Vibration*, vol. 179, no. 4, pp. 647–668, 1995.

[34] A. Serrarens, M. Van De Molengraft, J. Kok, and L. Van Den Steen, "H_∞ control for suppressing stick-slip in oil well drillstrings," *IEEE Control Systems Magazine*, vol. 18, no. 2, pp. 19–30, 1998.

[35] M. Karkoub, M. Zribi, L. Elchaar, and L. Lamont, "Robust μ-synthesis controllers for suppressing stick-slip induced vibrations in oil well drill strings," *Multibody System Dynamics*, vol. 23, no. 2, pp. 191–207, 2010.

[36] M. W. Harris, B. Açıkmeşe, and E. Van Oort, "LMI based control of stick-slip oscillations in drilling," in *ASME 2014 Dynamic Systems and Control Conference*, pp. V001T09A004–V001T09A004, American Society of Mechanical Engineers, 2014.

[37] C. Ke and X. Song, "Drilling control system using an equivalent input disturbance-based control with a neutral-type axial-torsional coupled dynamics model," *Journal of Dynamic Systems, Measurement, and Control*, vol. 141, no. 12, 2019.

[38] P. J. Nessjøen, Å. Kyllingstad, P. D'Ambrosio, I. S. Fonseca, A. Garcia, and B. Levy, "Field experience with an active stick-slip prevention system," in *SPE/IADC Drilling Conference and Exhibition*, 2011.

[39] M. Ghasemi and X. Song, "Trajectory tracking and rate of penetration control of downhole vertical drilling system," *Journal of Dynamic Systems, Measurement, and Control*, vol. 140, no. 9, p. 091003, 2018.

[40] F. Abdulgalil and H. Siguerdidjane, "Backstepping design for controlling rotary drilling system," in *IEEE Conference on Control Applications*, pp. 120–124, 2005.

[41] C. Mendil, M. Kidouche, and M. Doghmane, "Hybrid backstepping sliding mode controller for stick–slip vibrations mitigation in rotary drilling systems," *IETE Journal of Research*, pp. 1–11, 2021.

[42] M. Karkoub, Y. Abdel-Magid, B. Balachandran, *et al.*, "Drill-string torsional vibration suppression using GA optimized controllers," *Journal of Canadian Petroleum Technology*, vol. 48, no. 12, pp. 32–38, 2009.

[43] T. Feng, H. Zhang, and D. Chen, "Dynamic programming based controllers to suppress stick-slip in a drilling system," in *American Control Conference*, pp. 1302–1307, 2017.

[44] D. Q. Mayne, J. B. Rawlings, C. V. Rao, and P. O. Scokaert, "Constrained model predictive control: Stability and optimality," *Automatica*, vol. 36, no. 6, pp. 789–814, 2000.

[45] F. Allgöwer and A. Zheng, *Nonlinear Model Predictive Control*. Progress in Systems and Control Theory, Basel, Switzerland: Birkhäuser, 2012.

[46] A. Bemporad, A. Casavola, and E. Mosca, "Nonlinear control of constrained linear systems via predictive reference management," *IEEE Transactions on Automatic Control*, vol. 42, pp. 340–349, March 1997.

[47] A. Bemporad, "Reference governor for constrained nonlinear systems," *IEEE Transactions on Automatic Control*, vol. 43, pp. 415–419, March 1998.

[48] M. Z. Romdlony and B. Jayawardhana, "Stabilization with guaranteed safety using control Lyapunov–barrier function," *Automatica*, vol. 66, pp. 39–47, 2016.

[49] K. B. Ngo, R. Mahony, and Z.-P. Jiang, "Integrator backstepping using barrier functions for systems with multiple state constraints," in *44th IEEE Conference on Decision and Control*, pp. 8306–8312, Dec 2005.

[50] K. P. Tee, S. S. Ge, and E. H. Tay, "Barrier Lyapunov functions for the control of output-constrained nonlinear systems," *Automatica*, vol. 45, no. 4, pp. 918–927, 2009.

[51] K. P. Tee and S. S. Ge, "Control of nonlinear systems with full state constraint using a barrier Lyapunov function," in *48h IEEE Conference on Decision and Control*, pp. 8618–8623, Dec 2009.

[52] K. P. Tee and S. S. Ge, "Control of nonlinear systems with partial state constraints using a barrier lyapunov function," *International Journal of Control*, vol. 84, no. 12, pp. 2008–2023, 2011.

[53] K. P. Tee and S. S. Ge, "Control of state-constrained nonlinear systems using integral barrier Lyapunov functionals," in *51st IEEE Conference on Decision and Control*, pp. 3239–3244, Dec 2012.

[54] Z. L. Tang, K. P. Tee, and W. He, "Tangent barrier Lyapunov functions for the control of output-constrained nonlinear systems," *IFAC Proceedings Volumes*, vol. 46, no. 20, pp. 449–455, 2013. 3rd IFAC Conference on Intelligent Control and Automation Science.

[55] B. Ren, S. S. Ge, K. P. Tee, and T. H. Lee, "Adaptive neural control for output feedback nonlinear systems using a barrier Lyapunov function," *IEEE Transactions on Neural Networks*, vol. 21, no. 8, pp. 1339–1345, 2010.

[56] B. Niu and J. Zhao, "Barrier Lyapunov functions for the output tracking control of constrained nonlinear switched systems," *Systems & Control Letters*, vol. 62, no. 10, pp. 963–971, 2013.

[57] Y. Liu and S. Tong, "Barrier Lyapunov functions-based adaptive control for a class of nonlinear pure-feedback systems with full state constraints," *Automatica*, vol. 64, pp. 70–75, 2016.

[58] Y. J. Liu and S. Tong, "Barrier Lyapunov functions for nussbaum gain adaptive control of full state constrained nonlinear systems," *Automatica*, vol. 76, pp. 143–152, 2017.

[59] D. Li, G. Ma, C. Li, W. He, J. Mei, and S. S. Ge, "Distributed attitude coordinated control of multiple spacecraft with attitude constraints," *IEEE Transactions on Aerospace and Electronic Systems*, vol. 54, no. 5, pp. 2233–2245, 2018.

[60] W. He, S. Zhang, and S. S. Ge, "Adaptive control of a flexible crane system with the boundary output constraint," *IEEE Transactions on Industrial Electronics*, vol. 61, pp. 4126–4133, Aug 2014.

[61] W. He, S. S. Ge, B. V. E. How, Y. S. Choo, and K. S. Hong, "Robust adaptive boundary control of a flexible marine riser with vessel dynamics," *Automatica*, vol. 47, no. 4, pp. 722–732, 2011.

[62] D. Tian and X. Song, "Control of a downhole drilling system using an integral barrier Lyapunov function based method," *International Journal of Control*, pp. 1–14, 2021.

[63] J. Cheng, M. Wu, C. Lu, L. Chen, X. Chen, W. Cao, and X. Lai, "A stick-slip vibration suppression method for the drillstring system based on neutral type model," in *11th Asian Control Conference*, pp. 2837–2842, 2017.

[64] C. Ke and X. Song, "Control of down-hole drilling process using a computationally efficient dynamic programming method," *Journal of Dynamic Systems, Measurement, and Control*, vol. 140, no. 10, p. 101010, 2018.

[65] B. Saldivar, S. Mondié, J. Loiseau, and V. Rasvan, "Stick-slip oscillations in oillwell drilstrings: Distributed parameter and neutral type retarded model approaches," *IFAC Proceedings Volumes*, vol. 44, no. 1, pp. 284–289, 2011. 18th IFAC World Congress.

[66] B. Saldivar and S. Mondié, "Drilling vibration reduction via attractive ellipsoid method," *Journal of the Franklin Institute*, vol. 350, no. 3, pp. 485–502, 2013.

[67] C. Germay, V. Denoël, and E. Detournay, "Multiple mode analysis of the self-excited vibrations of rotary drilling systems," *Journal of Sound and Vibration*, vol. 325, no. 1, pp. 362–381, 2009.

[68] M. A. Henson and D. E. Seborg, *Nonlinear Process Control*. Upper Saddle River, NJ: Prentice Hall PTR, 1997.

[69] S. Hovda, H. Wolter, G. O. Kaasa, and T. S. Olberg, "Potential of ultra high-speed drill string telemetry in future improvements of the drilling process control," in *IADC/SPE Asia Pacific Drilling Technology Conference and Exhibition*, no. SPE-115196-MS, Aug 2008.

[70] D. Tian and X. Song, "Observer design for a wellbore drilling system with downhole measurement feedback," *Journal of Dynamic Systems, Measurement, and Control*, vol. 140, no. 7, p. 071012, 2018.

[71] A. Filippov, *Differential Equations with Discontinuous Righthand Sides: Control Systems*, vol. 18. Dordrecht, Netherlands: Springer Science & Business Media, 1988.

[72] A. E. Taylor, "L'Hôpital's rule," *The American Mathematical Monthly*, vol. 59, no. 1, pp. 20–24, 1952.

[73] D. Shevitz and B. Paden, "Lyapunov stability theory of nonsmooth systems," *IEEE Transactions on Automatic Control*, vol. 39, pp. 1910–1914, Sept 1994.

[74] J. J. E. Slotine and W. Li, *Applied Nonlinear Control*, vol. 199. Englewood Cliffs, NJ: Prentice Hall, 1991.

[75] M. Vidyasagar, "Decomposition techniques for large-scale systems with nonadditive interactions: Stability and stabilizability," *IEEE Transactions on Automatic Control*, vol. 25, pp. 773–779, August 1980.

[76] H. Khalil, *Nonlinear Systems*. Englewood Cliffs, NJ: Prentice Hall, 2nd ed., 1996.

[77] E. M. Navarro-López, "An alternative characterization of bit-sticking phenomena in a multi-degree-of-freedom controlled drillstring," *Nonlinear Analysis: Real World Applications*, vol. 10, no. 5, pp. 3162 – 3174, 2009.

[78] J. M. Kamel and A. S. Yigit, "Modeling and analysis of stick-slip and bit bounce in oil well drillstrings equipped with drag bits," *Journal of Sound and Vibration*, vol. 333, no. 25, pp. 6885–6899, 2014.

[79] T. Insperger, G. Stépán, and J. Turi, "State-dependent delay in regenerative turning processes," *Nonlinear Dynamics*, vol. 47, no. 1-3, pp. 275–283, 2007.

[80] T. Insperger, D. Lehotzky, and G. Stépán, "Regenerative delay, parametric forcing and machine tool chatter: A review," *IFAC-PapersOnLine*, vol. 48, no. 12, pp. 322 – 327, 2015. 12th IFAC Workshop on Time Delay Systems.

[81] Z. L. Tang, S. S. Ge, K. P. Tee, and W. He, "Adaptive neural control for an uncertain robotic manipulator with joint space constraints," *International Journal of Control*, vol. 89, no. 7, pp. 1428–1446, 2016.

[82] K. P. Tee, S. S. Ge, and F. E. H. Tay, "Adaptive control of electrostatic microactuators with bidirectional drive," *IEEE Transactions on Control Systems Technology*, vol. 17, pp. 340–352, March 2009.

[83] D. Tian and X. Song, "Control of a downhole drilling system using integral barrier Lyapunov functionals," in *American Control Conference*, pp. 1349–1354, 2019.

[84] M. Rubagotti and A. Ferrara, "Second order sliding mode control of a perturbed double integrator with state constraints," in *American Control Conference*, pp. 985–990, June 2010.

[85] W. J. Rugh and J. S. Shamma, "Research on gain scheduling," *Automatica*, vol. 36, no. 10, pp. 1401–1425, 2000.

[86] A. D. Ames, X. Xu, J. W. Grizzle, and P. Tabuada, "Control barrier function based quadratic programs for safety critical systems," *IEEE Transactions on Automatic Control*, vol. 62, pp. 3861–3876, Aug 2017.

[87] J. Á. Acosta, A. Dòria-Cerezo, and E. Fossas, "Stabilisation of state-and-input constrained nonlinear systems via diffeomorphisms: A Sontag's formula approach with an actual application," *International Journal of Robust and Nonlinear Control*, vol. 28, no. 13, pp. 4032–4044, 2018.

[88] D. Tian, C. Ke, and X. Song, "State barrier avoidance control design using a diffeomorphic transformation based method," in *American Control Conference*, pp. 854–857, 2020.

[89] D. J. Li, J. Li, and S. Li, "Adaptive control of nonlinear systems with full state constraints using integral barrier Lyapunov functionals," *Neurocomputing*, vol. 186, pp. 90–96, 2016.

[90] A. Jelacic, R. Fortuna, R. LaSala, J. Nathwani, G. Nix, C. Visser, B. Green, J. Renner, D. Blankenship, M. Kennedy, *et al.*, "An evaluation of enhanced geothermal systems technology," tech. rep., Office of Energy Efficiency and Renewable Energy (EERE), Washington, DC, 2008.

[91] F. Tavares, "NASA is testing a drill to search for life on mars – On its own." `https://www.nasa.gov/feature/ames/arads-drill`, accessed 2019-09-19.

[92] J. Kim and H. Myung, "Development of a novel hybrid-type rotary steerable system for directional drilling," *IEEE Access*, vol. 5, pp. 24678–24687, 2017.

[93] Y. Zhao, U. Zalluhoglu, J. Marck, N. Demirer, and M. Morari, "Model predictive control for mud motor operation in directional drilling," in *American Control Conference*, pp. 5197–5202, 2019.

[94] N. Demirer, U. Zalluhoglu, J. Marck, R. Darbe, and M. Morari, "Autonomous directional drilling with rotary steerable systems," in *American Control Conference*, pp. 5203–5208, IEEE, 2019.

[95] N. Panchal, M. T. Bayliss, and J. F. Whidborne, "Attitude control system for directional drilling bottom hole assemblies," *IET Control Theory & Applications*, vol. 6, no. 7, pp. 884–892, 2012.

[96] A. Wu, G. Hareland, and M. Fazaelizadeh, "Torque & drag analysis using finite element method," *Modern Applied Science*, vol. 5, no. 6, p. 13, 2011.

[97] R. B. Jijón, C. Canudas-de-Wit, S. I. Niculescu, and J. Dumon, "Adaptive observer design under low data rate transmission with applications to oil well drill-string," in *American Control Conference*, pp. 1973–1978, June 2010.

[98] S. Prensky, "Recent advances in LWD/MWD and formation evaluation," *World Oil*, vol. 227, no. 3, p. 69, 2006.

[99] M. Kapitaniak, V. Vaziri, J. P. Chávez, and M. Wiercigroch, "Experimental studies of forward and backward whirls of drill-string," *Mechanical Systems and Signal Processing*, vol. 100, pp. 454–465, 2018.

[100] Y. Khulief and F. Al-Sulaiman, "Laboratory investigation of drillstring vibrations," *Proceedings of the Institution of Mechanical Engineers, Part C: Journal of Mechanical Engineering Science*, vol. 223, no. 10, pp. 2249–2262, 2009.

[101] C. Liao, B. Balachandran, M. Karkoub, and Y. L. Abdel-Magid, "Drill-string dynamics: reduced-order models and experimental studies," *Journal of Vibration and Acoustics*, vol. 133, no. 4, 2011.

[102] Y. Liu and D. Gao, "A nonlinear dynamic model for characterizing downhole motions of drill-string in a deviated well," *Journal of Natural Gas Science and Engineering*, vol. 38, pp. 466–474, 2017.

[103] P. A. Patil and C. Teodoriu, "A comparative review of modelling and controlling torsional vibrations and experimentation using laboratory setups," *Journal of Petroleum Science and Engineering*, vol. 112, pp. 227–238, 2013.

[104] F. Wu, X. H. Yang, A. Packard, and G. Becker, "Induced L2-norm control for LPV systems with bounded parameter variation rates," *International Journal of Robust and Nonlinear Control*, vol. 6, no. 9-10, pp. 983–998, 1996.

[105] S. Boyd, L. El Ghaoui, E. Feron, and V. Balakrishnan, *Linear Matrix Inequalities in System and Control Theory*. Philadelphia, PA: SIAM Studies in Applied Mathematics, 1994.

[106] P. Gahinet, A. Nemirovskii, A. J. Laub, and M. Chilali, "The LMI control toolbox," in *33rd IEEE Conference on Decision and Control*, vol. 3, pp. 2038–2041, 1994.

[107] J. F. Sturm, "Using SeDuMi 1.02, a MATLAB toolbox for optimization over symmetric cones," *Optimization Methods and Software*, vol. 11, no. 1-4, pp. 625–653, 1999.